UNIVERSIDADE DE LISBOA
FACULDADE DE CIÊNCIAS
DEPARTAMENTO DE QUÍMICA E BIOQUÍMICA

A MASS SPECTROMETRY STUDY OF COMPOUNDS WITH ENVIRONMENTAL AND BIOLOGICAL INTEREST

Tese orientada por
Professora Doutora Maria Helena Ferreira da Silva Florêncio

Paulo Jorge Amorim Madeira

DOUTORAMENTO EM QUÍMICA
(Química Analítica)

2010

The work presented in this thesis was performed in the Environmental and Biological Mass Spectrometry Group, Departamento de Química e Bioquímica da Faculdade de Ciências da Universidade de Lisboa, with the financial support of Fundação para a Ciência e a Tecnologia (SFRH/BD/27614/2006)

To my parents

To my sister

To my darling wife

To my grand-parents

Acknowledgements

Throughout the years many people have contributed, directly or indirectly, to the successful completion of my work.

First I would like to express my deepest gratitude to Professor Helena Florêncio. Her guidance and counseling together with the challenges she offered me during this past 4 years made this work possible and helped me to grow as an individual as well as a scientist.

Professor Tereza opened my eyes, together with Professor João Paulo, to the fabulous world of Gas-Phase Thermochemistry during my MSc work. And the bug has never left. All the teachings that you shared with me helped me to successfully complete this step and for that I thank you. Professor Tereza needs an extra big thank you; she always has shown great interest in my work, and every time I needed an advice she was there to give me one.

Professor Filomena and Professor Carlos I would like to thank you for all the friendship you shown ever since I started to work in the Environmental and Biological Mass Spectrometry Group.

To all these persons, thanks for the trust that you deposited on to me ever since I started in this research group.

I would like to thank Doctor Pedro Vaz for the theoretical calculations and Doctor Ana Mourato for the electrochemical measurements.

Now is time to thank the FCUL friends; the guys and girls that every single day are there to either help us or bug us with requests of accurate masses (I mean you synthesis fellows, ☺):

From the Mass Spectrometry Group: Ana Luísa, Narciso and Pedro Alves.

From the Chromatography Group, our neighbours: NunoNeng, Fátima and Rita.

From the Adsorption Group: Ana Mestre and Marta Andrade.

From the Carbohydrate Chemistry Group: Susana and Nuno Xavier (my Scientific Brother).

From the Organometallic Chemistry: Pedro Florindo and Tânia.

From the Inorganic and Theoretical Chemistry Group: Paulo Costa.

Ana Luísa deserves a special attention. I have known her ever since I started to work in Mass Spectrometry and the friendship has grown. I miss you in the lab and I miss our long conversations, but I know you are happy and that is enough. Thanks for the friendship.

To the *monthly dinner, bike rides, tennis matches and eternal "goofing of"* group who kept me **reasonably** sane in these past months. João and Lena my closest friends, we know each other for what seems to be ages, thanks for the big friendship. Jorge, Sara, Nuno and Sandrina (and of course little Lea, the youngest addition to the Quirino clan), a special thanks is needed for you all!!!!!

The family should always come first, nevertheless in these acknowledgements I decided to save the best for last.

I would like to thank my parents for all the support and efforts that they have made in order to make this academic step possible. They wanted us to have all the opportunities that they didn't have and, with a huge effort, they succeeded. The person and, I dare to say, scientist that I am today I owe it to you. To my sister, the youngest of the clan

Madeira, thanks for everything, you make us all proud. To my father and mother-in-law, you gave me permission to marry your daughter and for that I thank you. I also would like to thank you for all the support you gave me in all the years we know each other.

To my grand-father, he lived with us for a long time, ever since my grand-mother sadly past away. In 2003 he left this world to engage on the ultimate adventure. Even though he didn't know how to read and write he was probably the cleverest person I ever knew. When he left us at the tender age of 87 he left a big void that slowly was filled with all the fond memories we have of him. Thanks grandpa, you are always in my mind.

To my darling wife, the exceptional woman that is the beacon that safely brings me back to land. We know each other for almost 14 years and you always stood by my side. You are indeed the love of my life and I am extremely happy to share it with you.

Resumo

Este trabalho tem como domínio comum a aplicação da Espectrometria de Massa ao estudo de vários compostos com interesse ambiental e biológico. Foram realizados estudos que envolvem o desenvolvimento e optimização de metodologias eficientes de análise; foi investigado o comportamento dos compostos em estudo usando várias técnicas de espectrometria de massa e foram realizados estudos de natureza fundamental, a maioria dos quais complementados por cálculos semi-empíricos. Concretamente:

Ionização/desorção laser assistida por matriz (MALDI) é uma técnica de ionização muito usada na análise de moléculas com massas moleculares elevadas. No entanto, a sua capacidade de ionizar de um modo suave e eficiente compostos não voláteis e termicamente instáveis levou-nos a investigar a sua aplicabilidade à análise de moléculas pequenas. Para tal, comparou-se a performance da fase anatase do TiO_2 com a de matrizes orgânicas convencionais na ionização de vários compostos cobrindo várias classes. Um dos compostos em particular, um flavonóide, formou iões agregados com a matriz orgânica, o que nos levou a aprofundar o estudo deste comportamento. Conclui-se que a estrutura do flavonóide influencia a formação dos iões agregados.

Derivados de anilina têm uma grande importância a nível industrial e os derivados halogenados, em particular, constituem um grupo de poluentes bastante significativo. Assim, estudou-se o comportamento em fase gasosa de halo- e nitroanilinas com o intuito de estabelecer mecanismos de fragmentação e metodologias que permitam a identificação de isómeros. Para a identificação de isómeros recorreu-se

a fragmentações competitivas de heterodímeros ligados por protão. Também são apresentados e discutidos resultados preliminares sobre o comportamento de derivados de anilina quando expostos a condições de dissociação por captura de electrões.

O comportamento de cinco isoflavonas foi estudado no modo positivo e recorrendo à espectrometria de massa com ionização por electrospray. Foram propostos mecanismos de fragmentação tendo em conta experiências de espectrometria de massa tandem, medições de massa exacta e cálculos semi-empíricos. Algumas das fragmentações observadas são dependentes do anel B e dos seus substituintes e, como tal, os iões originados por estas fragmentações podem ser considerados como iões diagnóstico.

Várias γ-lactonas fundidas ou ligadas a açúcares, compostos recentemente sintetizados, foram estudadas com o intuito de estabelecer mecanismos de fragmentação. Tal foi feito tendo em conta dados de espectrometria de massa tandem e cálculos semi-empíricos.

Palavras-Chave

FTICR-MS

ESI

MALDI

Mecanismos de Fragmentação

Dissociação Induzida por Colisão

Abstract

The leading thread of this work is the application of Mass Spectrometry to the study of environmental and biological relevant compounds. Several studies were performed involving the development and optimization of efficient analysis methodologies, the behaviour of the compounds under study was investigated using various mass spectrometry techniques and fundamental studies were carried out, most of them complemented with semi-empirical calculations.

Matrix-Assisted Laser Desorption/Ionization (MALDI) has been extensively used for the analysis of large molecules. Nevertheless, since the technique provides soft and efficient ionization of thermolabile and non-volatile organic compounds, we decided to investigate its application to small molecules as an alternative ionization method. For that we compared the performance of nanosized TiO_2 anatase as matrix with that of common organic matrices. The formation of organic matrix-flavonoid cluster ions was also investigated and it was found to be dependent of the structure of the flavonoid.

Aniline derivatives are of great industrial importance and several constitute a significant group of pollutants. The gas-phase behaviour of halo- and nitroanilines under electrospray ionization mass spectrometry conditions was studied. Isomer identification methodologies are proposed using for that purpose competitive fragmentations of proton-bound heterodimers. Preliminary results on the behaviour of the aniline derivatives when subjected to electron capture dissociation conditions are presented and discussed.

The behaviour of five isoflavones was studied under electrospray ionization mass spectrometry in the positive ion mode. The fragmentation mechanisms were proposed taking into account MS^n experiments, accurate mass measurements and semi-empirical calculations. Some of the fragmentations were found to be dependent on the substitution pattern of the B-ring and the ions afforded by these fragmentations can be considered as diagnostic ions.

Several newly synthesized γ-lactones, fused or C-C linked to sugar rings, were studied. Their fragmentation mechanisms were proposed taking into account MS^n experiments and semi-empirical calculations.

Keywords

FTICR-MS

ESI

MALDI

Fragmentation Mechanisms

Collision Induced Dissociation

General Contents

Figure List

Chapter 1

Chapter 3

Chapter 4

Chapter 5

Chapter 6

Appendix

Table List

Chapter 5

Chapter 6

Abbreviations and Symbols

2,5-DHB	2,5-dihydroxybenzoic acid
4-HCCA	α-cyano-4-hydroxycinnamic acid
A	ampere (unit of electrical current)
ac	alternating current
AM1	Austin model 1
APCI	atmospheric pressure chemical ionization
APPI	atmospheric pressure photoionization
B	magnetic field
CE	capillary electrophoresis
CEL	collision energy level
CI	chemical ionization
CID	collision induced dissociation
cm^2	square centimetre (area unit)
CRM	charge residue model
d	distance from the electrospray capillary to the counter-electrode
Da	dalton
DESI	desorption electrospray ionization
DFT	density functional theory
DMSO	dimethyl sulfoxide
E^0	redox potential
E_c	electric field at the electrospray capillary tip
ECD	electron capture dissociation
EDD	electron detachment dissociation

EED	electronic excitation dissociation
EI	electron ionization
EID	electron induced dissociation
EIEIO	electron induced excitation of ions from organics
ESI	electrospray ionization
eV	electronvolt
f	fundamental RF frequency of the ion trap
FAB	fast atom bombardment
FD	field desorption
FI	field ionization
FT	Fourier transform
FT-ICR	Fourier transform ion cyclotron resonance
GB	gas-phase basicity
GC-MS	gas chromatography-mass spectrometry
h	Planck's constant
HPA	3-hydroxypicolinic acid
HPLC	high performance liquid chromatography
Hz	Hertz (frequency unit)
I	electrical current
ICP	inductively coupled plasma
ICR	ion cyclotron resonance
IE	ionization energy
IEM	ion evaporation model
IR	infrared
Kaem	kaempferol
$\mathbf{k_B}$	Boltzmann's constant
$\mathbf{k_i}$	rate constant for ion emission from charged droplets
kJ mol^{-1}	kilojoule per mole

kV	kilovolt (Electric potential unit)
L min^{-1}	liter per minute
LAMMA	laser microprobe mass analyzer
LC-MS	liquid chromatography-mass spectrometry
LC-MS/MS	liquid chromatography-tandem mass spectrometry
LIT	linear ion trap
LTOF	linear time-of-flight
M	Molarity (concentration unit)
Lut	luteolin
m/z	mass-to-charge ratio
MALDI	matrix assisted laser desorption/ionization
mbar	millibar (Pressure unit)
MEP	molecular electrostatic potential
mg mL^{-1}	milligram per milliliter
min	minute (time unit)
mM	millimolar (concentration unit)
MS	mass spectrometry
ms	millisecond
MS/MS	tandem mass spectrometry
MS^n	multiple stage mass spectrometry
mV s^{-1}	millivolt per second
Myr	myricetin
NADH	reduced form of NAD (nicotinamide adenine dinucleotide)
nm	nanometer
NMR	nuclear magnetic resonance
ns	nanosecond
oa-TOF	orthogonal acceleration time-of-flight

ºC	degree Celsius (Temperature unit)
PA	proton affinity
Pa	Pascal (pressure unit)
PD	plasma desorption
PEG200	polyethyleneglycol
PM6	Latest parameterization of the MNDO model
pmol	picomole
ppm	part-per-million
QET	quasi equilibrium theory
QIT	quadrupole ion trap
Q_r	excess charge on the droplet of radius r
Quer	quercetin
R	gas constant
r_c	electrospray capillary radius
r_D	droplet radius
RF	radiofrequency potential
r_J	jet radius
ROS	reactive oxygen species
RRKM	Rice-Ramsperger-Kassel-Marcus theory
SF_6	Sulfur hexafluoride
SIMS	secondary ion mass spectrometry
SORI-CAD	Sustained Off-Resonance Irradiation Collision Activated Dissociation
SPME	solid phase micro-extraction
SWIFT	stored waveform inverse Fourier transform
T	temperature
T	tesla (Magnetic field unit)
TBATFB	tetrabutylammonium tetrafluoroborate

$\mathbf{T_{eff}}$	effective temperature
TOF	time-of-flight
torr	torr (Pressure unit)
TSP	thermospray
UV	ultraviolet
V	Volt (Electric potential unit)
$\mathbf{V_c}$	voltage applied to the electrospray capillary
$\mathbf{V_{on}}$	potential required for the onset of electrospray
$\mathbf{v_{xy}}$	velocity on the xy plane
$\mathbf{Z_{av}}$	average observed charge state
ZPE	zero point energy
γ	surface tension of the solvent
$\Delta G^{\neq}$	Gibbs activation energy
ΔH_f	heat of formation
$\Delta_r H$	reaction enthalpy
ε^0	permittivity of vacuum
θ	half-angle of the Taylor cone
λ	wavelength
μJ	microjoule
$\mu L\ h^{-1}$	microliter per hour
μm	micrometer
ω_c	cyclotron frequency

Aims of the Thesis

The aim of this thesis is to explore various applications of Mass Spectrometry to the analysis of small molecules.

After an Introduction section (Chapter 1) and the description of the experimental methods used (Chapter 2), the work here presented is organized in four chapters (Chapters 3 to 6). Chapter 3 deals with two aspects of MALDI analysis of small molecules. The first aspect addressed is the ability of inorganic matrices to efficiently ionise small molecules and the second one discusses the matrix-flavonoids cluster ion formation. Chapter 4 addresses the gas-phase behaviour of aniline derivatives and methodologies to differentiate isomers of these environmentally relevant compounds. In Chapters 5 and 6 the fragmentation mechanisms of various organic compounds with biological interest are addressed. Chapter 5 deals with isoflavones while Chapter 6 deals with newly synthesized γ-lactones fused or C-C linked to sugar rings.

The main contents of Chapters 3 and 6 have already been published:

- *"TiO_2 anatase as matrix for MALDI analysis of small molecules"*, Ana L. Castro, Paulo J. Amorim Madeira, Manuel R. Nunes, Fernanda M. Costa, M. Helena Florêncio, Rapid Communications in Mass Spectrometry, 2008, 22, 3761-3766.

- *"Flavonoid-Matrix cluster ions in MALDI Mass Spectrometry"*, Paulo J. Amorim Madeira, M. Helena Florêncio, Journal of Mass Spectrometry, 2009, 44, 1105-1113.

- *"Electrospray ionization mass spectrometric analysis of newly synthesized a,β-unsaturated γ-lactones fused to sugars"*, Paulo J. Amorim Madeira, Ana Margarida Rosa, Nuno M. Xavier, Amélia P. Rauter, M. Helena Florêncio, Rapid Communications in Mass Spectrometry, 2010, 24, 1049-1058.

- *"Furanose C-C-linked γ-lactones: a combined ESI FT-ICR MS and semi-empirical calculations study"*, Paulo J. Amorim Madeira, Nuno M. Xavier, Amélia P. Rauter, M. Helena Florêncio, accepted for publication in Journal of Mass Spectrometry.

A paper concerning the work presented in Chapter 5 has been submitted to Rapid Communications in Mass Spectrometry with the title *"Electrospray FTICR Mass Spectrometry of five isoflavone aglycones: Some new insights"*.

Furthermore a paper concerned with Chapter 4 is being prepared for submission with the title *"Gas-phase behaviour of aniline derivatives: New features"*.

This thesis also includes Conclusions and Future Work sections in the last chapter (Chapter 7).

Chapter 1
Introduction

1. Mass Spectrometry: An Introduction

The first and most important question that arises in someone's head is: What is mass spectrometry?

> *The basic principle of mass spectrometry (MS) is to generate ions from either inorganic or organic compounds by any suitable method, to separate these ions by their mass-to-charge ratio (m/z) and to detect them qualitatively and quantitatively by their respective m/z and abundance. The analyte may be ionized thermally, by electric fields or by impacting energetic electrons, ions or photons. The ... ions can be single ionized atoms, clusters, molecules or their fragments or associates. Ion separation is effected by static or dynamic electric or magnetic fields.*[1]

Although this definition dates back to 1968, when mass spectrometry was at its childhood, it is still valid. Nevertheless, two additions should be made. These concern the fact that besides electrons, (atomic) ions or photons, energetic neutral atoms and heavy cluster ions can also be used to ionize the analyte. Secondly, ion separation by *m/z* can be effected in field free regions, as effectively demonstrated by the time-of-flight analyser, provided the ions possess a well-defined kinetic energy at the entrance of the flight path.

From the 1950s to the present, mass spectrometry has evolved tremendously. The pioneering mass spectrometrist had a home-built naked instrument, typically a magnetic sector instrument with electron

ionization. Nowadays, highly automated commercial systems, able to produce thousands of spectra per day, are now concealed in a "black box", a nicely designed and beautifully coloured unit resembling more an espresso machine or tumble dryer than a mass spectrometer.

Mass spectrometry (MS) is probably the most versatile and comprehensive analytical technique currently available in the chemists and biochemists arsenal. Mass spectrometry precisely measures the molecular masses of individual compounds by converting them into charged ions and analysing them in what is called a mass analyser. This is the simplest, but somewhat reductionist, definition of mass spectrometry. The days of the simple determination of the m/z ratio of an organic compound are over, today mass spectrometry can be used to determine molecular structures, to study reaction dynamics and ion chemistry, provides thermochemical and physical properties such as ionization energy, appearance energy, reaction enthalpies, proton and ion affinities, gas-phase acidities, and so on.

Mass spectrometry is so versatile that even several areas of physics, pharmaceutical sciences, archaeology, forensic and environmental sciences, just to state a few, have benefited from the advances in this instrumental technique.

1.1 Mass Spectrometry History and Basic concepts (sample introduction, ionization, mass analysis, detectors)

The history of mass spectrometry starts in 1898 with the work of Wien, who demonstrated that canal rays could be deflected by passing them through superimposed parallel electric and magnetic fields. Nevertheless, its birth can be credited to Sir J. J. Thomson, Cavendish Laboratory of University of Cambridge, through his work on the analysis of negatively and positively charged cathode rays with a parabola mass spectrograph, the great grand-father of the modern mass spectrometers.[2, 3] In the next two decades, the developments of mass spectrometry continued in the hands of renowned physicists like Aston,[4] Dempster,[5] Bainbridge,[6, 7] and Nier.[8, 9]

In the 1940s, chemists recognized the great potential of mass spectrometry as an analytical tool, and applied it to monitor petroleum refinement processes. The first commercial mass spectrometer became available in 1943 through the Consolidated Engineering Corporation. The principles of time-of-flight (TOF) and ion cyclotron resonance (ICR) were introduced in 1946 and 1949, respectively.[10, 11]

Applications to organic chemistry started to appear in the 1950s and exploded during the 1960s and 1970s. Double-focusing high-resolution mass spectrometers, which became available in the early 1950s, paved the way for accurate mass measurements. The quadrupole mass analyser and the ion traps were described by Wolfgang Paul and co-workers in 1953.[12] The development of the GC/MS in the 1960s marked the beginning of the analysis of seemingly complex mixtures by

mass spectrometry.[13, 14] The 1960s also witnessed the development of tandem mass spectrometry and collision-induced decompositions,[15] being a high point in the field of structural analysis, in unambiguous quantification by mass spectrometry, as well as in the development of soft ionization techniques such as chemical ionization.[16]

By the 1960s, mass spectrometry had become a standard analytical tool in the analysis of organic compounds. Its application to the biosciences, however, was lacking due to the inexistence of suitable methods to ionize fragile and non-volatile compounds of biological origin. During the 1980s the mass spectrometry range of applications increased "exponentially" with the development of softer ionization methods. These included fast atom bombardment (FAB) in 1981,[17] electrospray ionization (ESI) in 1984-1988,[18] and matrix-assisted laser desorption/ionization (MALDI) in 1988.[19] With the development of the last two methods, ESI and MALDI, the upper mass range was extended beyond 100kDa and had an enormous impact on the use of mass spectrometry in biology and life sciences. This impact was recognized in 2002 when John Fenn (for his work on ESI) and Koichi Tanaka (for demonstrating that high molecular mass proteins could be ionized using laser desorption) won the Nobel Prize in Chemistry.

Concurrent with the ionization methods development, several innovations in mass analyser technology, such as the introduction of high-field and superfast magnets, as well as the improvements in the TOF and Fourier transform ion cyclotron resonance (FTICR) enhanced the sensitivity and the upper mass range. The new millennium brought us two new types of ion traps, the orbitrap in 2000 by the hands of

Alexander Makarov[20] and the linear quadrupole ion trap (LIT) in 2002 by James W. Hager.[21]

The coupling of high-performance liquid chromatography (HPLC) with mass spectrometry was first demonstrated in the 1970s [22], nevertheless, it was with the development and commercialization of atmospheric pressure ionization sources (ESI, APCI) that for the first time the combination of liquid chromatography and mass spectrometry entered the realm of routine analysis.[23-26] A mass spectrometry chronology is presented in Table 1.1.

Table 1.1: Mass Spectrometry chronology 1886-2004.[27]

1886	**E. Goldstein** discovers anode rays (positive gas-phase ions) in gas discharge.
1897	**J. J. Thomson** discovers the electron and determines its mass-to-charge ratio. *Nobel Prize in 1906*.
1898	**W. Wien** analyses anode rays by magnetic deflection and then establishes that these rays carried a positive charge. *Nobel Prize in 1911*.
1901	**W. Kaufmann** analyses cathodic rays using parallel electric and magnetic fields.
1909	**R. A. Millikan** and **H. Fletcher** determine the elementary unit of charge.
1912	**J. J. Thomson** constructs the first mass spectrometer (then called a parabola spectrograph). He obtains mass spectra of O_2, N_2, CO, CO_2 and $COCl_2$. He observes negative and multiply charged ions. He discovers metastable ions. In 1913, he discovers isotopes 20 and 22 of neon.
1918	**A. J. Dempster** develops the electron ionization source and the first spectrometer with a sector-shaped magnet (180°) with direction focusing.
1919	**F. W. Aston** develops the first mass spectrometer with velocity focusing. *Nobel Prize in 1922*. He measures mass defects in 1923.
1932	**K. T. Bainbridge** proves the mass–energy equivalence postulated by Einstein.
1934	**R. Conrad** applies mass spectrometry to organic chemistry. **W. R. Smythe**, **L. H. Rumbaugh** and **S. S. West** succeed in the first preparative isotope separation.
1940	**A. O. Nier** isolates uranium-235.

Table 1.1 (*cont.*)

1945	First recognition of the metastable peaks by **J. A. Hipple** and **E. U. Condon**.
1948	**A. E. Cameron** and **D. F. Eggers** publish design and mass spectra for a linear time-of-flight (LTOF) mass spectrometer. **W. Stephens** proposed the concept of this analyser in 1946.
1949	**H. Sommer**, **H. A. Thomas** and **J. A. Hipple** describe the first application in mass spectrometry of ion cyclotron resonance (ICR).
1952	Theories of quasi-equilibrium (QET) and RRKM explain the monomolecular fragmentation of ions. **R. A. Marcus** receives the *Nobel Prize in 1992*. **E. G. Johnson** and **A. O. Nier** develop double-focusing instruments.
1953	**W. Paul** and **H. S. Steinwedel** describe the quadrupole analyser and the ion trap or quistor (quadrupole ion storage trap) in a patent. **W. Paul**, **H. P. Reinhard** and **U. Von Zahn**, of Bonn University, describe the quadrupole spectrometer in *Zeitschrift für Physik* in 1958. **Paul** and **Dehmelt** receive the *Nobel Prize in 1989*.
1955	**W. L. Wiley** and **I. H. McLaren**, of Bendix Corporation, make key advances in LTOF design.
1956	**J. Beynon** shows the analytical usefulness of high-resolution and exact mass determinations of the elementary composition of ions. First spectrometers coupled with a gas chromatograph by **F. W. McLafferty** and **R. S. Gohlke**.
1957	Kratos introduces the first commercial mass spectrometer with double focusing.
1958	Bendix introduces the first commercial LTOF instrument.
1966	**M. S. B. Munson** and **F. H. Field** discover chemical ionization (CI).
1967	**F. W. McLafferty** and **K. R. Jennings** introduce the collision induced dissociation (CID) procedure.
1968	Finnigan introduces the first commercial quadrupole mass spectrometer. First mass spectrometers coupled with data processing units.
1969	**H. D. Beckey** demonstrates field desorption (FD) mass spectrometry of organic molecules.
1972	**V. I. Karatev**, **B. A. Mamyrim** and **D. V. Smikk** introduce the reflectron that corrects the kinetic energy distribution of the ions in a TOF mass spectrometer.
1973	**R. G. Cooks**, **J. H. Beynon**, **R. M. Caprioli** and **G. R. Lester** publish the book *Metastable Ions*, a landmark in tandem mass spectrometry.

Table 1.1 (*cont.*)

	E. C. Horning, **D. I. Carroll**, **I. Dzidic**, **K. D. Haegele**, **M. D. Horning** and **R. N. Stillwell** discover atmospheric pressure chemical ionization (APCI).
1974	First spectrometers coupled with a high-performance liquid chromatograph by **P. J. Arpino**, **M. A. Baldwin** and **F. W. McLafferty**. **M. D. Comisarov** and **A. G. Marshall** develop Fourier transformed ICR (FTICR) mass spectrometry.
1975	First commercial gas chromatography/mass spectrometry (GC/MS) instruments with capillary columns.
1976	**R. D. Macfarlane** and **D. F. Torgesson** introduce the plasma desorption (PD) source.
1977	**R. G. Cooks** and **T. L. Kruger** propose the kinetic method for thermochemical determination based on measurement of the rates of competitive fragmentations of cluster ions.
1978	**R. A. Yost** and **C. G. Enke** build the first triple quadrupole mass spectrometer, one of the most popular types of tandem instrument. Introduction of lamellar and high-field magnets.
1980	**R. S. Houk**, **V. A. Fassel**, **G. D. Flesch**, **A. L. Gray** and **E. Taylor** demonstrate the potential of inductively coupled plasma (ICP) mass spectrometry.
1981	**M. Barber**, **R. S. Bordoli**, **R. D. Sedgwick** and **A. H. Tyler** describe the fast atom bombardment (FAB) source.
1982	First complete spectrum of insulin (5750 Da) by FAB and PD. Finnigan and Sciex introduce the first commercial triple quadrupole mass spectrometers.
1983	**C. R. Blakney** and **M. L. Vestal** describe the thermospray (TSP). **G. C. Stafford**, **P. E. Kelly**, **J. E. Syka**, **W. E. Reynolds** and **J. F. J. Todd** describe the development of a gas chromatography detector based on an ion trap and commercialized by Finnigan under the name Ion Trap.
1987	**M. Guilhaus** and **A. F. Dodonov** describe the orthogonal acceleration time-of-flight (oa-TOF) mass spectrometer. The concept of this technique was initially proposed in 1964 by **G. J. O'Halloran** of Bendix Corporation. **M. Karas**, **D. Bachmann**, **U. Bahr** and **F. Hillenkamp** discover matrix-assisted laser desorption/ionization (MALDI). **K. Tanaka** and co-workers demonstrate the feasibility of ionization of molecules up to m/z 100 000 and receives the *Nobel Prize in 2002*. **R. D. Smith** describes the coupling of capillary electrophoresis (CE) with mass spectrometry.

Table 1.1 (*cont.*)

1988	**J. Fenn** develops the electrospray (ESI). First spectra of proteins above 20 000 Da. He demonstrated the electrospray's potential as a mass spectrometric technique for small molecules in 1984. The concept of this source was proposed in 1968 by **M. Dole**. **Fenn** receives the *Nobel Prize in 2002*.
1991	**V. Katta** and **B. T. Chait** and **B. Gamen**, **Y. T. Li** and **J. D. Henion** demonstrate that specific non-covalent complexes could be detected by mass spectrometry. **B. Spengler**, **D. Kirsch** and **R. Kaufmann** obtain structural information with reflectron TOF mass spectrometry (MALDI post-source decay).
1993	**R. K. Julian** and **R. G. Cooks** develop broadband excitation of ions using the stored-waveform inverse Fourier transform (SWIFT).
1994	**M. Wilm** and **M. Mann** describe the nanoelectrospray source (then called microelectrospray source).
2000	**A. A. Makarov** describes a new type of mass analyser: the orbitrap. The orbitrap is a high-performance ion trap using an electrostatic quadro-logarithmic field.
2002	**J. W. Hager** describes the Linear Ion Trap (LIT).
2004	**R. G. Cooks** and co-workers described the Desorption Electrospray Ionization (DESI)[28]

Generally, a mass spectrometer is composed of five components (Figure 1.1): inlet system, ion source, mass analyser, ion detector and data system.

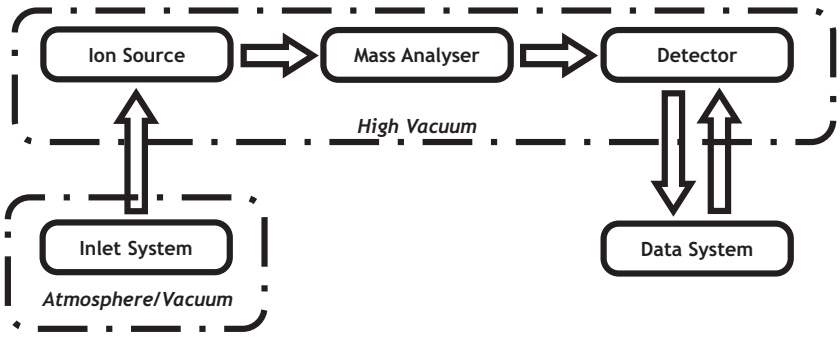

Figure 1.1. Diagram of the major components common to all typical modern mass spectrometers.

Samples are introduced in the mass spectrometer and transferred into the gas phase through the inlet system that could be at atmospheric pressure or under vacuum. In the ion source, the gas phase analytes are ionized and transferred into the mass analyser where they are separated according to their mass-to-charge ratios (m/z). Ion detection can be accomplished by electron multiplier systems that enable m/z and abundance to be measured and displayed by means of an electric signal perceived by the data system, which also controls the equipment. All mass spectrometers are equipped with a vacuum system in order to maintain the low pressure (high vacuum) required for operation. This high vacuum is necessary to allow ions to reach the detector without undergoing collisions with other gaseous molecules. In fact, collisions would produce a deviation of the trajectory and the ion would lose its charge against the walls of the instrument. On the other hand, a relatively high pressure environment could facilitate the occurrence of ion-molecule reactions that would increase the complexity of the spectrum. In some experiments the pressure in the source region or in a part of the mass spectrometer is intentionally increased to study ion-molecule reactions or to perform collision induced dissociations. The high vacuum is maintained using mechanical pumps in conjunction with turbomolecular, diffusion or cryogenic pumps. The mechanical pumps allow a vacuum of about 10^{-3} torr to be obtained. Once this vacuum is achieved the operation of the remainder of the vacuum system allows a vacuum as high as 10^{-10} torr to be reached.

Two types of ion sources and two types of mass analysers, the ones used in the studies reported in this thesis, will be described in the following sections. Electrospray Ionization (ESI) and Matrix Assisted

Laser/Desorption Ionization (MALDI) will be dealt in section 1.2, Quadrupole Ion Traps (QIT) and Fourier Transform Ion Cyclotron Resonance (FT-ICR) will be dealt in section 1.3.

1.2 Ionization Sources: ESI and MALDI

One of the crucial steps in mass spectrometry is the formation and transfer of ions from a sample to the gas-phase. This can be done by a variety of available ionization techniques. In order to make a correct choice, it is necessary to take into account the internal energy transferred during the ionization process and the physico-chemical properties of the analyte.[27] Some ionization techniques are very energetic and cause extensive fragmentation. Other techniques are softer and only produce ion of the molecular species. Electron ionization, chemical ionization and field ionization are only suitable for gas-phase ionization and thus their use is limited to compounds sufficiently volatile and thermally stable. There is, however, a large number of compounds that are either thermally labile or do not have sufficient vapour pressure. For these compounds to be analysed, they must be directly extracted from the condensed phase to the gas-phase.[27]

There are three groups of methods for the formation of gas-phase ions:[29]

i. Volatile materials are generally ionized by interaction of their vapours with electrons (Electron Ionization - EI), with ions (Chemical Ionization - CI), or with strong electric fields (Field Ionization - FI);
ii. Nonvolatile and thermally labile materials can be desorbed into the gas-phase via bombardment with fast atoms (Fast Atom Bombardment - FAB), ions (Secondary Ion Mass Spectrometry - SIMS and Liquid SIMS), laser photons (Matrix Assisted Laser Desorption/Ionization - MALDI) or electrosprayed solvent (DESI)[28];
iii. Liquid solutions of the analyte may directly be converted to gas-phase ions via spray techniques (Electrospray Ionization - ESI, Atmospheric Pressure Chemical Ionization - APCI, Atmospheric Pressure Photoionization - APPI).

The next two subsections will address Electrospray Ionization (ESI) and Matrix Assisted Laser Desorption/Ionization.

1.2.1 Electrospray Ionization (ESI)

The electrical atomization of liquids was first observed by Georg Mathias Bose in 1745. In 1882 Lord Rayleigh determined an instability criterion for the charged liquid droplets. Between 1914 and 1920,

Zeleny [30-32] studied the droplet shape as a function of the applied voltage and established a criterion for the instability of an electrified liquid at the end of a capillary tube.[33, 34]

The development of electrospray by Fenn and co-workers [18, 35] was largely ignored by the mass spectrometry community until, before a small audience at the 1988 ASMS meeting, they showed that multiply charged ions could be obtained from proteins, allowing their molecular weight to be determined in instruments for which the mass range was limited to as low as 2000 Da. At the beginning, ESI was considered to be an ionization source dedicated to protein analysis; nevertheless its use was extended not only to other polymers and biopolymers, but also to the analysis of small polar molecules. In fact, one of the first papers published by Fenn and co-workers was indeed about the use of electrospray with small molecules.[36]

ESI principles and biological applications have been extensively reviewed in the literature [37-39], and several books either on this subject or that addressed this topic appeared over the years.[1, 22, 27, 34, 40-42]

There are three major steps in the production of gas-phase ions by electrospray:

i. Production of charged droplets at the electrospray capillary tip (The Electrophoretic Mechanism);
ii. Shrinkage of the charged droplets by solvent evaporation and repeated droplet disintegrations (fissions), leading to very small highly charged droplets;

iii. The actual mechanism by which gas-phase ions are produced from very small and highly charged droplets.

Production of charged droplets at the electrospray capillary tip (The Electrophoretic Mechanism)

As shown in the schematic representation of the charged droplet formation (Figure 1.2) a voltage, V_c, of 2-3kV is applied to the metal capillary, usually located at 1-3 cm from the counter electrode (in ESI-MS this counter electrode has an orifice leading to the mass spectrometric sampling system). Because the capillary tip is very narrow, the electric field, E_c, at the capillary tip is very high ($E_c \approx 10^6$ V/m).

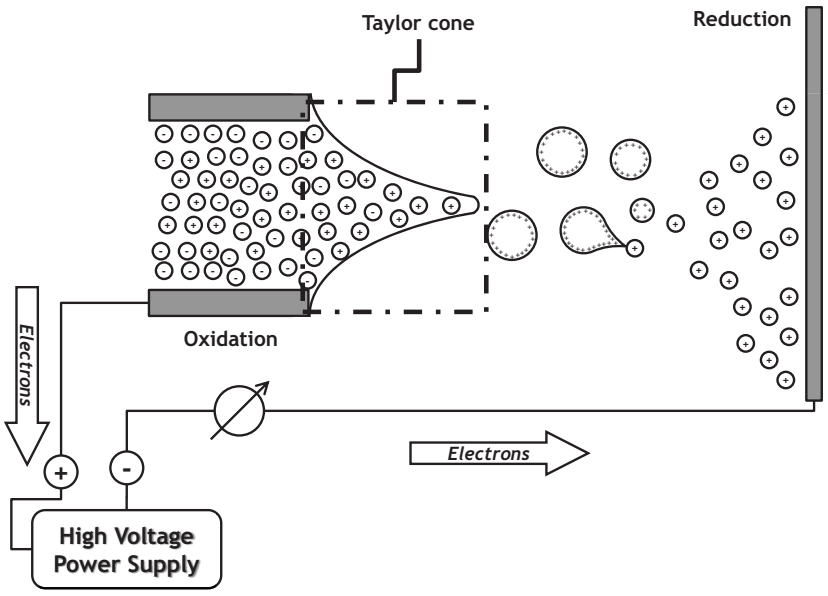

Figure 1.2. Schematic representation of the electrospray events occurring at atmospheric pressure.

When the capillary of radius r_c is located at a distance d from the planar counter electrode, the magnitude of E_c for a given potential V_c can be estimated using the approximate relationship:[43]

$$E_c = \frac{2V_c}{r_c ln\left(\frac{4d}{r_c}\right)} \qquad \text{(Equation 1.1)}$$

Where V_c is the applied potential, r_c is the capillary outer radius and d is the distance from the capillary tip to the counter-electrode. E_c, is proportional to V_c. E_c is essentially inversely proportional to r_c and it decreases slowly with the electrode separation d due to the logarithmic dependence on d.[44, 45]

The typical solution used in ESI-MS consists of using a polar solvent in which the analyte is soluble. Because ESI-MS is a very sensitive method, very low concentrations, 10^{-7}-10^{-3} mol/L (M), of analyte can be used. Methanol or methanol-water, acetonitrile or acetonitrile-water are often used as solvent, nevertheless, since electrolyte concentrations as low as 10^{-7} M are sufficient for ESI to function, other solvents such as toluene (that have a very low solubility for electrolytes) can also be used.[45]

The imposed field, E_c, will also partially penetrate the liquid at the capillary tip. When the capillary is the positive electrode (positive ion mode) some positive ions will drift toward the liquid surface and some negative ions will drift away from it until the imposed field inside the liquid is removed by charge redistribution. The accumulated positive charge at the surface leads to its destabilization since the positive ions

are drawn down-field but cannot escape from the liquid. The surface is then drawn down-field in such a way that a liquid cone is formed. This is called the Taylor cone, named after Sir Geofrey Taylor who was one of the first to investigate the conditions under which a stable liquid cone can exist with the competing forces of an electric field and the surface tension of the liquid.[46]

At a sufficiently high field, E_c, the cone is not stable and a liquid filament with a diameter of a few micrometers and a surface rich in positive ions, is emitted from the Taylor cone tip. At some distance downstream, the liquid filament becomes unstable and forms separate droplets which are charged with an excess of positive electrolyte ions, the cone jet mode (Figure 1.3a). The described cone jet mode is one of the possible and the best characterized modes in electrospray literature. The length of the unbroken liquid filament decreases if the field E_c is increased. At higher fields, a multispray condition is reached in which the central cone disappears and droplet emission occurs from a crown of four to six short liquid tips formed at the rim of the capillary (Figure 1.3b-c).[47, 48] The most commonly observed spray modes have been defined by Jaworek [49], however, many of these exhibit pulsating characteristics which translate into a periodical variation of the droplet characteristics. [50, 51] Furthermore the different spray modes generate droplets with different size and charge distribution.[52-54] Nevertheless the most effective spray mode for producing droplets suitable for ESI-MS is the cone jet spray mode [45, 46] in which a stable non-pulsating Taylor cone is formed.[52, 55, 56]

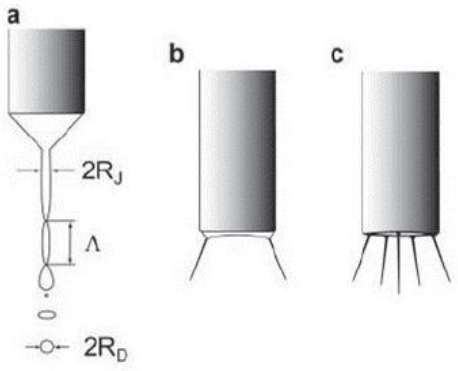

Figure 1.3. Different forms of electrospray at the tip of the capillary: a) Cone jet mode (the tip of the cone is extended into a liquid jet, R_j= jet radius, R_D= droplet radius); b) and c) multi-jet modes (multiple jet modes are observed when voltage is increased from *a* → *b* → *c*).

Due to an excess of positive electrolyte ions at the surface of the cone and cone jet, the droplets are positively charged. These charged droplets drift downfield through the air towards the opposing electrode. Solvent evaporation at constant charge leads to droplet shrinkage and an increase of the electric field normal to the surface of the droplets. At a given radius the repulsion between the charges overcomes the surface tension of the droplet which causes a coulomb fission of the droplet (coulomb explosion).[45] This droplet fission occurs via formation of a cone and cone jet that split into a number of small progeny droplets in a process that bears close resemblance with the cone jet formation at the capillary tip. [57] Further evaporation of the parent droplet leads to repeated fissions and these progeny droplets can also evaporate and undergo fissions. Very small charged droplets result, that lead ultimately to gas-phase ions, by processes that will be described in the following sections.

The ion separation mechanism which is called the electrophoretic mechanism is also most plausible on energetic grounds. Electrical double layers are already formed at low fields in electrolyte solutions. The resulting positive-negative ion redistribution reduces or completely removes the imposed field and therefore suppresses other forms of ionization such as field ionization which requires very high electric fields.[44, 45] Another way to show that electrospray results from electrophoretic charging is to deionize the solvent. Experiments involving deionized methanol and the addition of SF_6 to the atmospheric gas (in order to prevent electric discharges) showed an intermittent electrospray current attributed to the absence of electrolytes to sustain a stable electrospray operation.[48]

If the charge separation is electrophoretic, at a steady state the positive droplet emission will continuously carry off the positive ions. Considering the requirements for charge balance in such a continuous electric current device, and that only electrons can flow through the metal wire supplying the electric potential to the electrodes (Figure 1.2) it is clear that the electrospray process should involve an electrochemical conversion of ions to electrons. As such, the electrospray source can be viewed as a special type of electrolytic cell in which part of the ion transport does not occur through an uninterrupted solution, but as charged droplets and later as gas-phase ions.[44, 45] Thus, in the positive ion mode where positively charged droplets and later positive gas-phase ions are the charge carriers, a conventional electrochemical oxidation reaction should be occurring at the liquid/metal interface of the spray capillary. This reaction supplies the extra positive ions to the solution that prevent the build-up of a charge imbalance. The nature of

these ions depends on the experimental conditions. If the spray capillary is made of metal, metal ions could be entering the solution causing a release of electrons to the metal electrode (Equation 1.2). The alternative for producing extra positive ions is the removal of negative ions present in solution by an oxidation reaction (Equation 1.3).

$$M_{(s)} \rightarrow M^{2+}{}_{(aq)} + 2e^{-}{}_{\text{(on metal surface)}} \qquad \text{(Equation 1.2)}$$

$$4OH^{-}{}_{\text{(aq)}} \rightarrow O_{2\,(g)} + 2H_2O + 4e^{-}{}_{\text{(on metal surface)}} \qquad \text{(Equation 1.3)}$$

One expects that the reaction with the lowest oxidation potential will dominate, and that such reaction will be dependent on the material of the metal electrode, the ions present in solution and the nature of the solvent. In fact, proof of the occurrence of an electrochemical oxidation at the metal capillary was provided in 1991 by Kebarle's group.[58] Van Berkel and co-workers examined the consequences to ESI-MS of the electrochemical processes, from the formation of radical cations [59-61] and dications [62, 63] to the influence of hydrogen ions (produced by electrolysis) in the mass spectra of non-denatured proteins.[64] In 1986 David Smith [65] was able to derive an approximate equation for the potential, V_{on}, required for the onset of electrospray (Equation 1.4):

$$V_{on} \approx \left(\frac{r_c \gamma \cos\theta}{2\varepsilon_0}\right)^{1/2} ln\left(\frac{4d}{r_c}\right) \qquad \text{(Equation 1.4)}$$

Where γ is the surface tension of the solvent, ε_0 is the permittivity of vacuum, r_c is the capillary radius, and θ is the half-angle of the Taylor

cone. Substituting the values ε_0 = 8.8x10^{-12} J^{-1}C^2 and θ = 49.3° (see reference [46]) we obtain (Equation 1.5, where γ must be substituted in N/m and r_c in m to obtain V_{on} in volts.

$$V_{on} = 2 \times 10^5 (r_c \gamma)^{1/2} ln\left(\frac{4d}{r_c}\right) \qquad \text{(Equation 1.5)}$$

The surface tensions and calculated onset potentials for r_c = 0.1 mm and d = 40 mm are shown in Table 1.2. The solvent with the highest surface tension (H_2O) has the highest onset potential, V_{on}, which means that its surface is the hardest to stretch into a cone jet.[45] Nevertheless, for a stable electrospray operation one must go a few hundred volts higher than the required onset potential. [45]

Table 1.2. Required onset voltages (V_{on}), calculated for a spray tip of 0.1 mm radius at a distance of 4 cm from the negative electrode, for common ESI solvents with different surface tensions.

Solvent	CH_3OH	CH_3CN	$(CH3)_2SO$	H_2O
γ (N/m)	0.0226	0.030	0.043	0.073
V_{on} (V)	2200	2500	3000	4000

The experimental verification of (Equation 1.4 has been provided by Smith [65] and Kebarle's group. [66, 67] Use of neat water as solvent can lead to the initiation of an electric discharge from the spray capillary tip, particularly in the negative ion mode (i.e. when the capillary tip is negative). The onset potential is the same for both the positive and negative ion modes; however, the electric discharge onset is lower when the capillary electrode is negative and metallic, [66, 67] which might be due to the emission of electrons from the capillary tip. The occurrence of an electric discharge leads to an increase of the capillary current, *I*

(currents above 10^{-6} A are usually due to the presence of an electric discharge) or even to the appearance of discharge-characteristic ions in the mass spectrum. For example, in the positive ion mode the appearance of protonated solvent clusters, such as $H_3O^+(H_2O)_n$ from water or $CH_3OH_2^+(CH_3OH)_n$ from methanol indicates the presence of electric discharges.[66] Nevertheless, these protonated solvent clusters can be produced, in the absence of an electric discharge, with a relatively high abundance when the solvent has been acidified, i.e. when H_3O^+ and $CH_3OH_2^+$ are present in solution.[45] The presence of electric discharges degrades the ESI-MS performance, particularly at high discharge currents. [66, 67]

Trace amounts of gases with electron affinities and electron capture cross sections higher than O_2 (e.g. SF_6 and polychlorinated hydrocarbons) will lead to electron capture, suppressing the electric breakdown even when neat water is used as solvent.[66] Nevertheless, the use of such trace amount additives can introduce foreign ions in the mass spectrum, for example F^- ions can be observed when SF_6 is used as additive, but due to its low m/z there is no significant interference with analyte ions.

Shrinkage of the charged droplets by solvent evaporation and repeated droplet disintegrations (fissions)

As the solvent evaporates from charged droplets, usually with assistance of resistive heating, the size of the droplets becomes smaller while the charge that they carry remains constant.[68] The assumption that the charge remains constant is reasonable since the emission of ions

from solution to the gas-phase is a highly endoergic process (Equation 1.6) [45]; furthermore it has been shown in the literature that droplets within the micrometer range or larger do not emit gas-phase ions.[53]

$$Na^{+}_{(aq)} \rightarrow Na^{+}_{(g)}$$
$$-\Delta G^{0}_{sol} = 410\ kJ\ mol^{-1} \qquad \text{(Equation 1.6)}$$
$$-\Delta H^{0}_{sol} = 444\ kJ\ mol^{-1}$$

This results in increasing electrostatic stress near the surface of a given droplet. When the force of electrostatic repulsion between like charges becomes equal to the surface tension holding the droplet together, the so-called "Rayleigh stability limit" has been reached as defined by the Rayleigh equation (Equation 1.7) [45, 68, 69] where Q_R is the excess charge on the droplet of radius R, γ is the surface tension and ε_0 is the permittivity of vacuum.

$$\boldsymbol{Q_R = 8\pi(\varepsilon_0 \gamma R^3)^{1/2}} \qquad \text{(Equation 1.7)}$$

Just prior to reaching the Rayleigh stability limit, droplets undergo what is referred to as "Coulomb fission", a process which leads to the production of smaller progeny droplets (Figure 1.4). According to the literature, droplets with sizes in the 1 μm range, undergo fission at approximately 80% of the Rayleigh limit. [53, 70] The droplet will then shrink again, due to solvent evaporation, at constant charge until, once again, near the Rayleigh stability limit, fission occurs. The droplet does not split evenly into two smaller droplets of approximately equal mass

and charge. Charged droplets are not static entities, but rather they may distort from spherical into oblate or prolate shapes.[44, 53] Shape irregularities of these types stimulate disruptions in which a stream of much smaller droplets is emitted in what was originally termed "uneven fission" [70] and nowadays is known as "droplet-jet fission".[44, 69] Figure 1.5 shows two shadowgraphs in which this disruption is clearly seen. This disruption pattern is similar to the disruption at the tip of the Taylor cone. The emitted stream of progeny droplets carries off only about 2% of the mass of the parent droplet, but about 15% of the parent's charge. The progeny droplets, which are quite monodisperse, have a radius of about 1/10 of the parent's radius. [53]

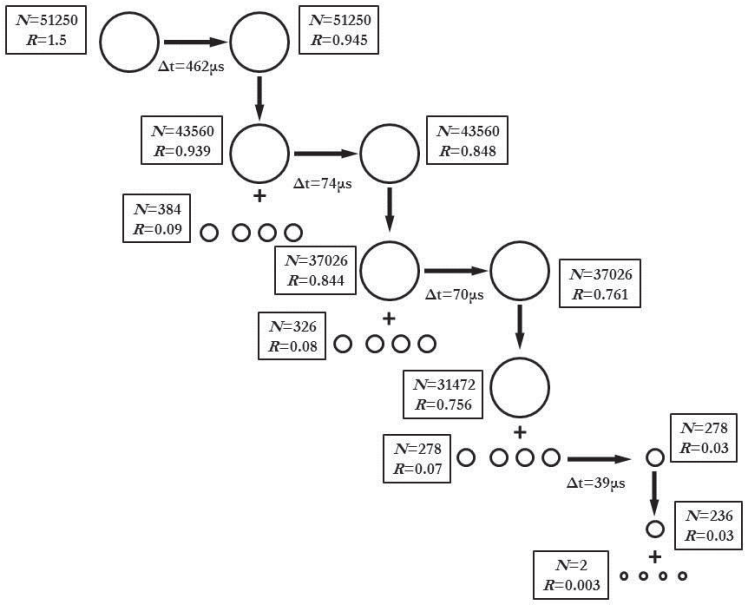

Figure 1.4. Schematic representation of the time history of parent and progeny droplets, *N* = number of elementary charges on the droplet, *R* = radius of the droplet in μm (image taken from reference [44]).

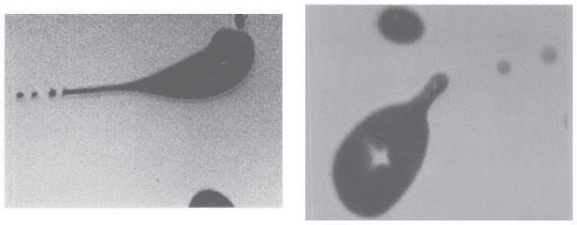

Figure 1.5. Flash shadowgraphs showing droplets undergoing Coulomb fission (images taken from reference [68]).

The charge-to-mass ratio is thus increased in the progeny droplets relative to the parent droplet from which they have been produce, but the overall repulsive force of like charges near the surface is attenuated because the charge is spread over a larger total surface area.[68] The droplet-jet fission process may repeat itself a second, and perhaps a third, time upon further shrinkage of the offspring droplets.[68]

Formation of gas-phase ions from charged droplets: ion evaporation model (IEM) and charge residue model (CRM)

There are mainly two possible mechanisms for the production of gas-phase ions in electrospray: the charge residue model (CRM) proposed by Dole et al.[71] and the ion evaporation model (IEM) proposed by Iribarne and Thomson.[72, 73] Both these models are feasible, although under different conditions. The ion evaporation model typically prevails for relatively small ions ($m/z < 3300$),[74, 75] whereas the charge residue model seems to be valid for larger multiply charges species.[76] Nevertheless, it can be considered that these models describe the two extremes of the same general process. These will be described in the following sections.

Ion Evaporation Model

Iribarne and Thomson, who worked with small ionic analytes such as Na^+ and Cl^-, proposed the ion evaporation mechanism (IEM).[72, 73] The model predicts that direct ion emission from the droplets will occur after their radius shrink to less than 10 nm. Hence, the ion evaporation process replaces Coulomb fission as a way to remove charge from the droplet (Figure 1.6).[45]

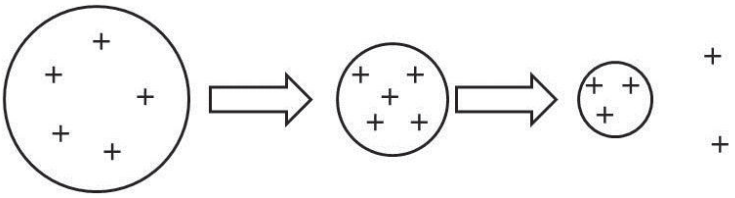

Figure 1.6. Gas-phase ion formation via ion evaporation model.

This model is supported by experimental [72] and theoretical [73] results. The experimental results involved measurements of the relative abundance of the ions produced by ESI of solutions containing NaCl as the only solute. The authors found that there was a large number of ion aggregates of the type $[(NaCl)_n(Na)_m]^{m+}$ the abundance of which decreased rapidly as *n* decreases. Nevertheless, the lowest mass ion in that series, Na^+ (n = 0 and m = 1), and the hydrated species $Na(H_2O)_k^+$ (k = 1-3) had the highest abundances.[72, 73] This observation led the authors to conclude that while large aggregate ions are probably due to a Charged Residue Mechanism (CRM) type process, the abundant Na^+ and Na^+ hydrates must be formed through a different mechanism where Na^+ ions escape directly from the droplet's surface.[45]

Iribarne and Thomson derived an equation, based on transition state theory, that provided detailed predictions for the rate of ion emission from charged droplets (Equation 1.8).[72]

$$k_I = \frac{k_B T}{h} e^{-\Delta G^{\neq}/k_B T} \quad \text{(Equation 1.8)}$$

Where k_B is the Boltzman constant, T is the temperature of the droplet and h is Planck's constant. The Gibbs energy of activation, $\Delta G^{\neq}$, was evaluated on the basis of the model shown in Figure 1.7.

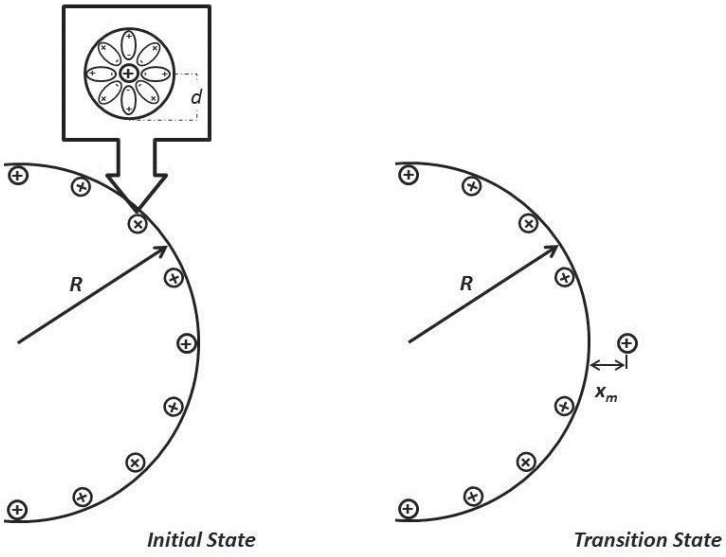

Figure 1.7. Iribarne-Thomson model for ion evaporation. (Adapted from references [44, 69])

In particular, this equation predicts the dependence of the rates on the chemical properties of the ions. Observed differences between the gas-phase ion intensities I_A and I_B of ions A^+ and B^+, present at equal concentrations in the sprayed solutions, were compared with

Iribarne and Thomson's theory [73] predictions and subsequently with data of other researchers.[18, 58, 77] In general, a qualitative agreement between experiment and theory was found, which provided support to the theory, on the assumption that the observed selectivity cannot be explained by the charge residue mechanism theory proposed by Dole.[71] Nevertheless, an expanded charge residue theory is also capable of predicting qualitatively the experimentally observed selectivities.[69]

Recently, molecular dynamics simulations helped in the understanding of the formation of gas-phase ions from charged droplets.[78, 79] Vertes and co-workers simulated the behaviour of analyte ions in water nanodroplets and concluded that the analyte ions evaporated from the nanodroplets (close to the Rayleigh limit) with a solvation shell of approximately 10 water molecules.[78]

Charge Residue Model

The charge residue mechanism was proposed by Dole,[71] who was then interested in the determination of the molecular masses of polystyrenes. For such macromolecules, Dole assumed that some of the droplets formed would contain one analyte molecule, as well as the ionic charges at the surface. Solvent evaporation from these droplets will lead to a gas-phase ion which charge has its origins from the surface charges of the parent droplet (Figure 1.8). [45].

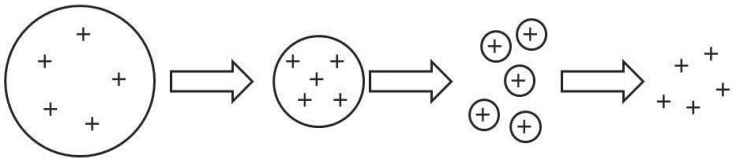

Figure 1.8. Formation of gas-phase ions via charge residue model.

Up to now, only small ions were considered and, an unequivocal decision, as to whether the gas-phase ions were produced by ion evaporation, or the charged-residue mechanism could not be attained. In fact, many of the observed results in mass spectrometric experiments can be explained by both mechanisms.

The status of the ion evaporation and charge residue theories for macroions (particularly the analytically important large polyprotonated and polydeprotonated proteins and nucleic acids) is different. The ion evaporation theory (see previous section) was derived as a model for small ions, but the extension of its equations to macroions is available. A qualitative extension of the ion evaporation model which deals with multiply charged macroions has been proposed by Fenn.[80]

When dealing with macromolecules, proteins for example, one must take into account their large size and their behaviour regarding the solvent. With the exception of the locations that carry polar and charged residues, the protein is on the whole solvophobic in the typical polar solvents used. This solvophobic behaviour, together with the repulsion of the other charges on the surface, assists the escape of the protein and its proton charges from the droplet. Nevertheless, this process cannot be expected to be fast, and may not compete with the rapid evaporation of solvent from the droplet, which may lead to Rayleigh fission or even to the formation of a charged residue.

The charged-residue theory does not require any significant modifications for macromolecules, and becomes the more natural mechanism for these entities. If the charged-residue model holds, it would statistically be expected to observe multimers as a result of more than one protein molecule being present in the final droplet. Richard Smith and co-workers [81] observed multiply charged monomers as well as low intensity dimmers and trimers. Smith et al. found an empirical correlation (Equation 1.9) between the molecular mass (M) and the average observed charge state (Z_{av}) of ions formed from starburst dendrimers (these are multi-branched alkyl-amine polymers with relatively rigid structures and close to spherical form, i.e. they resemble globular proteins), where a and b are constants and b=0.53 led to the best fit.[45]

$$\boldsymbol{Z_{av} = aM^{b}} \qquad \text{(Equation 1.9)}$$

A similar relationship was found by Standing and co-workers where the value of b was between 0.52 and 0.55.[45]

Using literature data, Fernandez de la Mora showed that (Equation **1.9)** holds and that it could be derived from the Charge Residue Mechanism.[76] This variation of the CRM received a wide acceptance. Samalikova and Grandori questioned the validity of the model, [82-84] but their conclusions were, however, questioned by Nesatyy and Suter.[85]

The Charge Residue Mechanism allowed quantitative predictions of the protein charge state in the gas-phase using a simple empirical

correlation between charge state and protein mass. Recently, Gross and co-workers[86] suggested a modification of the CRM in which CRM is preceded by IEM.

1.2.2 Matrix-Assisted Laser Desorption/Ionization (MALDI)

Matrix-Assisted Laser Desorption/Ionization (MALDI) is one of the two soft ionization techniques besides electrospray ionization (ESI) that allow for the sensitive detection of large, non-volatile and labile molecules by mass spectrometry.

The original notion was that molecules with masses in excess of 500-1000 Da could not be isolated of their natural (e.g. aqueous) environment and, even less, be charged for an analysis in the vacuum of a mass spectrometer without excessive and unspecific fragmentation. To overcome these faults, several desorption techniques were developed. Field Desorption (FD) was introduced in the late 1960's by Beckey, thus paving the road to the application of mass spectrometry to biomolecules.[87] In 1974 plasma desorption was introduced by Macfarlane[87] and the analytical potential of this technique was later (in 1986) improved by the groups of Sundqvist and Roepstorff with the addition of nitrocellulose.[88] Secondary ion mass spectrometry (SIMS) was introduced in 1975 by Benninghoven.[87] Fast atom bombardment (FAB) view the daylight in 1981 by the hands of Michael Barber and with it the concept of a matrix as a means of facilitating and enhancing ion yield was born.[87]

The first papers on the use of lasers for ion generation in mass spectrometric analysis appeared in the literature only a few years after the discovery of the laser principle.[89, 90] Over the years several groups continued to pursue this line of research, mainly R. Cotter at Johns Hopkins University (USA) and P. Kistemaker at the FOM Institute in Amsterdam (Netherlands). For a long time the Amsterdam group held the high mass record for a bioorganic analyte with a spectrum of the sodiated digitonin (m/z 1251 Da).[91]

Independently and in parallel to these groups, Hillenkamp and Kaufmann developed the laser microprobe mass analyser (LAMMA).[87] The laser was focused to a spot of <1 μm diameter to probe thin tissue sections for inorganic and trace atomic ions such as Na, K and Fe.[87] The sensitivity-limiting "noise" of the LAMMA spectra were signals that were identified as coming from the organic polymer used to embed the tissue sections, as well as other organic tissue constituents.[87] Interestingly, it was this background noise which triggered the search for a systematic analysis of organic samples that eventually led to the discovery of the MALDI principle. The principle and its acronym were published in 1985.[92]

ESI and MALDI were developed independently but concurrently, and at the time of the discovery of their potential to desorb non-volatile, fragile molecules (e.g. biomolecules), the mass spectrometry community was mostly impressed by their ability to access the high mass range. FAB- and PD-MS had already generated spectra of trypsin (23 kDa) and other high mass proteins. Nevertheless what made the difference, for biologists in particular, was the stunning sensitivity which made MS compatible with sample preparation techniques used in life sciences. For

MALDI, the minimum amount of sample (e.g. protein) needed for a high quality spectrum was reduced from 1 pmol in 1988 to a few femtomoles only a year later and, at present, the amount of sample can be in the order of the low attomole range (even though in favourable cases). Many other developments, either instrumental or specific sample preparation techniques, contributed over the decades following to make MALDI-MS an indispensable tool not only in the life sciences but also in polymer analysis. It is interesting to note that today, despite the big attention to high molecular mass analytes, the majority of applications of MALDI (as well as ESI) deal with the analysis of small and medium-sized peptides.[93]

The use of a chemical matrix (a small, laser absorbing organic molecule) in large excess over the analyte is the core of the MALDI principle. Several developments for laser desorption schemes took place in parallel to and after the publication of the MALDI principle. These attempted to replace the chemical matrix by a more easy-to-handle physical matrix or a simpler combination of the two. The most famous of these is the system of Tanaka and co-workers[94] for which Tanaka received the Nobel Prize in Chemistry in 2002 (on this particular subject see box below).

Who invented MALDI?

In 2002 Koichi Tanaka of Shimadzu Corp. (Japan) shared the Nobel Prize in Chemistry with Fenn "for their development of soft desorption ionization methods for mass spectrometric analysis of biological macromolecules." Fenn's inclusion was for his work on ESI; Tanaka was recognized for his laser desorption method of protein ionization. (...) Although Tanaka's method uses another approach for soft desorption ionization, it is often erroneously referred to as MALDI. (...) For many reasons, including its higher sensitivity compared with the Tanaka method, MALDI was the method that the MS community embraced. "The reality of it is, the techniques that [Karas and Hillenkamp] described and developed are the ones that everybody uses today," says Grayson. Mann agrees and says that it is important for the field to recognize the importance of the MALDI work, even if the Nobel committee did not.[95]

Ion formation in MALDI

Despite the broad applications of MALDI in many fields and its strong impact in the field of proteomics, a discussion of its fundamental processes was not engaged for a rather long time. Some of its important features such as the absorption of the laser energy, are easily understood; nevertheless, the overall process of desorption and ionization has not yet been fully described, more than 20 years after its discovery.[87] As a result, instead of an understanding of the overall process, the MALDI practitioners possess a set of empirical protocols for sample handling, pre-treatment, and preparation, that depend on the class of analyte to be investigated.[93]

MALDI "models" are still crude and far away from having predictive power. There was a common agreement on the key functions of the matrix: [96-98]

- Incorporating and isolating the analyte molecules in the host matrix;
- Release of the analyte molecule into the vacuum upon disintegration of the matrix-analyte solid after laser energy deposition;
- Ionization of the analyte by ion-molecule reactions in the laser plume.

The matrix transforms the laser energy into excitation energy for the sample which leads to sputtering of the analyte and matrix from the surface of the mixture. The energy transfer is efficient, nevertheless, the sample molecules are spared from excessive energy which could lead to their decomposition.[99] The process of modern-day MALDI is remarkably similar to the early experiments of Hillenkamp and Karas and can be split into distinct stages: Sample preparation, desorption by laser irradiation and ion formation (Figure 1.9).[26]

Sample preparation in MALDI involves mixing a sample solution with a matrix suspension (with a concentration of *ca.* 10 mg/mL). A few μL of this suspension is then deposited onto a MALDI plate (an electrically conducting plate) and left to dry allowing for the co-crystallization of the analyte and the matrix. This methodology is often referred to as the dried droplet method and is the original and preferred method for MALDI sample preparation today.[93, 100]

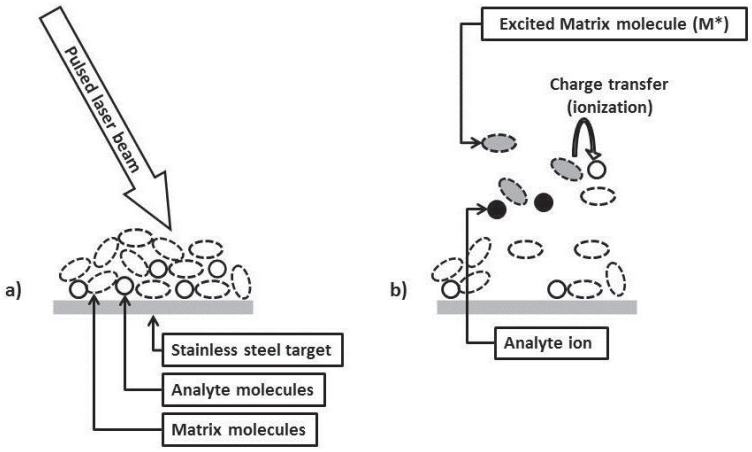

Figure 1.9: Basic schematic representation of the MALDI process: a) irradiation of the analyte-matrix mixture with a pulsed laser and b) sputtering and ionization of the analyte molecules. (Adapted from reference [26])

Desorption by laser irradiation and ion formation (Figure 1.9) occurs under vacuum conditions inside the ion source. This desorption/ionization process is initiated with short pulses of a laser beam, usually Ultraviolet lasers are employed (nitrogen or Nd:YAG), which induce the ablation of bulk portions of the analyte-doped matrix crystals. The exact mechanism of the MALDI process is not completely elucidated; nevertheless, irradiation by the laser induces rapid heating of the crystals through the excitation of the matrix molecules. The rapid heating causes localized sublimation of the crystals, ablation of the crystal surface and expansion of the matrix into the gas-phase, entraining intact analyte in the expanding matrix plume.[27, 101] The ionization reactions can occur under vacuum conditions at any time during this process but, as before mentioned, the origin of ions produced in MALDI, is still not fully understood. Many different chemical and physical ionization pathways have been suggested for MALDI [93, 102, 103] and the widely accepted current view is that

ionization in MALDI is a two-step process: a primary ionization event followed by in-plume secondary ion-molecule reactions (secondary ionization event).[102]

Primary ionization refers to the generation of ions from neutral molecules in the sample and these are often matrix-derived species. There are a few primary ionization processes, multiphoton ionization, excited state proton transfer, desorption of preformed ions, among others, which were reviewed in 1998 by Zenobi and Knochenmuss.[102]

Secondary ionization mechanisms are those that lead to ions that are not directly generated by primary ionization processes, analyte ions in particular. The most important secondary reactions are those leading to protonated and cationized analyte, *i.e.* proton-transfer, cationization and electron-transfer reactions.[102]

Proton-transfer reactions lead to the appearance of singly-charged protonated molecules, which are the most commonly observed ions in MALDI. Karas and co-workers[104] proposed that in the MALDI plume there are many multiply-charged species that are being neutralized by electrons and reduced to singly-charged species. The neutralization probability strongly increases with the charge state and singly charged ions have sufficiently low neutralization cross-sections to survive.[104] Knochenmuss and co-workers[105] proposed that these singly-charged species are formed from secondary ion-molecule reactions that can be predicted by thermodynamics.

Neutral analytes, let us consider peptides and proteins, have proton affinities (PAs) usually greater than the ones of common matrices.[103] It is therefore expected that plume proton-transfer

reactions of the primary protonated matrix, MH^+, with analyte, are efficient (Equation 1.10).

$$\boldsymbol{MH^+ + A \rightarrow M + AH^+ \quad PA(A) > PA(M)} \qquad \text{(Equation 1.10)}$$

Adducts of analyte with various cations can either be a nuisance when other signals are already strong (e.g. protonated species) or very useful when they are weak.[103] For the particular case of synthetic polymers, cations are often intentionally added in order to enhance the signal.

Cation affinities are much lower than proton affinities; hence, the first question regarding cationized species in MALDI is, why do they give the dominant signal in certain cases? Cationization is important for analytes with proton affinities lower than that of the matrix. In these cases, the analyte cannot compete with the neutral matrix for available protons and cationization becomes the ionization route of last resort.[103]

Ion-molecule reactions involving electron-transfer (Equation 1.11) and the appearance of singly-charged radical ions are rare.

$$\boldsymbol{M^+ + A \rightarrow M + A^+ \quad \Delta H = \mathrm{IP}(A) - IP(M)} \qquad \text{(Equation 1.11)}$$

For this reaction to occur, the ionization potential (IP) of the matrix must be greater than that of the analyte. That is not usually the case; nevertheless, these reactions have been used to enhance the signal of low ionization potential analytes.[96]

A detailed description of desorption/ionization steps in MALDI can be found in a number of reviews available in the literature.[93, 101-103]

1.3 Mass Analysers: Quadrupole Ion Trap and FTICR

There are numerous types of mass analysers; nevertheless, the main purpose is the same for all: to separate ions according to their mass-to-charge (m/z) ratios.

The mass analysers can be divided into:

- Sector instruments: a combination of magnetic and electrostatic sectors separates the ions according to their masses and focus the ion beam in terms of kinetic energy;
- Quadrupoles and Ion traps: a radiofrequency electric field allow the separation of the ions according to their m/z ratios;
- Time-of-Flight (TOF): the ions are accelerated and the time necessary to travel a specific distance (the length of the flight tube) can be used to determine the m/z ratio.
- Ion Cyclotron Resonance (ICR): a high magnetic field induces in the ions cyclotron motion and the frequency of this motion can be related to their m/z ratios.

The next two subsections will address Quadrupole Ion Trap (QIT) and Fourier Transform Ion Cyclotron Resonance (FTICR).

1.3.1 Quadrupole Ion Trap (QIT)

Unlike beam instruments, mass separation in quadrupole ion traps is achieved by storing ions in the trapping space and by manipulating their motion in time, rather than in space. This task is accomplished with an oscillating electric field created within the boundaries of the trap.

The development of the quadrupole ion trap can be divided into three ages: mass-selective detection, mass-selective storage and mass-selective axial ejection.[106, 107] Wolfang Paul and Helmut Steinwedel were the first to disclose a method for mass analysis, by trapping a range of ion masses in the quadrupole ion trap and employing means to detect and measure the ions while stored.[108-110] Their work can be seen as the age of ion trap mass-selective detection.

The second age, mass-selective storage, took place during the late 1960s to the early 1980s. Scientists like P. H. Dawson, N. R. Whetten, John F. Todd and Raymond E. March were leaders in this age. This second scanning method involved producing a range of ion masses, but by operating the quadrupole storage field so as to store a single mass in the ion trap at a time. This single ion mass is then ejected from the trap for detection by an external electron multiplier. The process is repeated rapidly until a complete mass spectrum is generated.[106] This method was extended further by interposing a mass analyser between the trap and the detector to give a tandem arrangement that permitted the external mass analysis of stored ions.[107]

The third age is called mass-selective axial ejection and its development started in 1979 by George Stafford Jr., John E. P. Syka,

Walter E. Reynolds and Paul E. Kelley from Finnigan Corporation (nowadays Thermo Scientific).[111] It was this mode of operation that led to the dramatically increase of interest in ion trap instruments.

The quadrupole ion trap (Figure 1.10) consists of two hyperbolic electrodes serving as end caps and a doughnut-shaped ring electrode.[1]

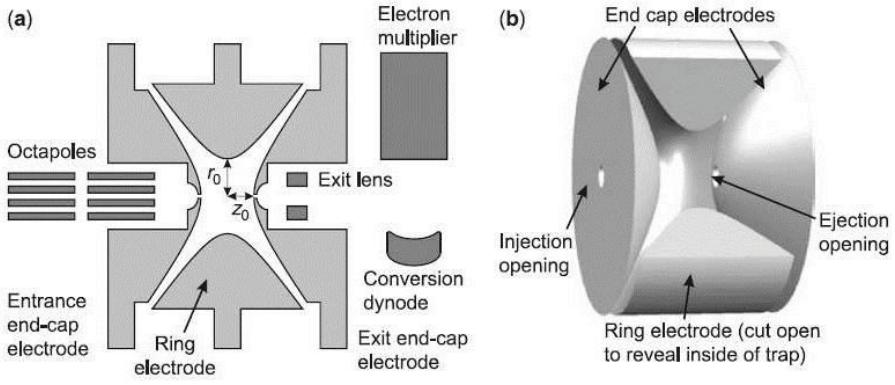

Figure 1.10: (a) Cross-section of a quadrupole ion trap; (b) three-dimensional perspective view of a quadrupole ion trap. (Image taken from reference [112])

The three-dimensional quadrupole field is created by applying a potential to the ring electrode and maintaining the end-cap electrodes at ground potential.[22, 113]

The working principle of the quadrupole ion trap is based on creating stable trajectories for ions of a certain m/z or m/z range while removing unwanted ions by colliding them with the walls, or by axial ejection from the trap due their unstable trajectories.

For the ion trap, the electric field has to be considered in three dimensions. The complete derivation and solving of the Mathieu type equations that describe the motion of the ions within the ion trap is outside the scope of this thesis and can easily be found in the

literature.[1, 27, 107, 113, 114] The trapping parameters, or Mathieu parameters, a_z (Equation 1.12) and q_z (Equation 1.13) are used as coordinates of the stability regions and can be used to construct the stability diagram of the quadrupole ion trap (Figure 1.11). In these equations $\omega=2\pi f$ where f is the fundamental RF frequency of the trap (≈1 MHz).

$$a_z = -2a_r = -\frac{16eU}{m_i r_0^2 \omega^2} \qquad \text{(Equation 1.12)}$$

$$q_z = -2q_r = -\frac{8eV}{m_i r_0^2 \omega^2} \qquad \text{(Equation 1.13)}$$

For an ion to remain stored within the volume of the trap it has to be simultaneously stable in the r and z directions (circled regions A and B in Figure 1.11a). The region A, the closest to the origin, shown in expanded form in Figure 1.11b, is of great importance for the operation of the ion trap. Region B, on the other hand, remains to be explored. In Figure 1.11b, the $\beta_z=1$ stability boundary intersects the q_z axis at $q_z=0.908$; this working point is that of the ion of lowest m/z ratio that can be stored in the ion trap for a given set of instrumental conditions; *i.e.* the low-mass cutoff.

A three-dimensional representation of an ion trajectory in the ion trap is depicted in Figure 1.12 and shows the general appearance of a Lissajous curve or figure-of-eight composed of two fundamental frequency components.

A complete description of the quadrupole ion trap theory is available in the literature, for example, the book entitled *Quadrupole Ion Trap Mass Spectrometry* by Raymond E. March and John F. J. Todd covers all theoretical aspects of the ion trap.[107]

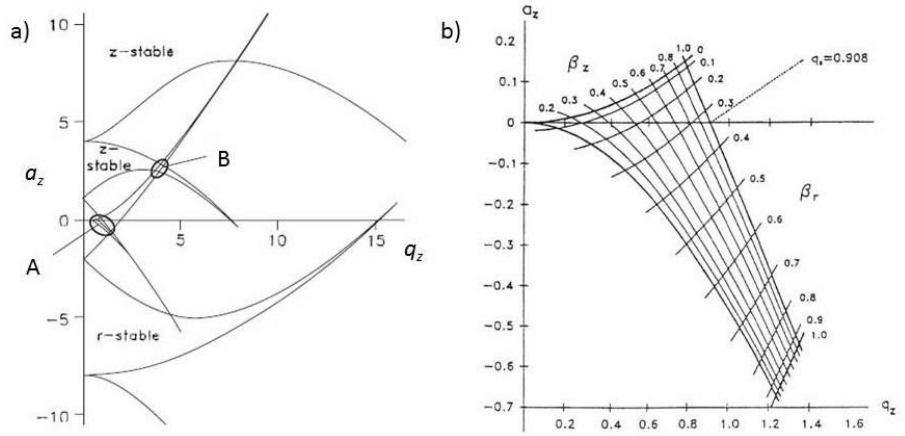

Figure 1.11: a) Stability diagram in (a_z, q_z) space for the quadrupole ion trap in the *r*- and *z*-directions (A and B are regions of simultaneous stability); b) expansion of region of simultaneous stability closest to the origin (region A) for the quadrupole ion trap in the *r*- and *z*-directions. (Image taken from reference [22])

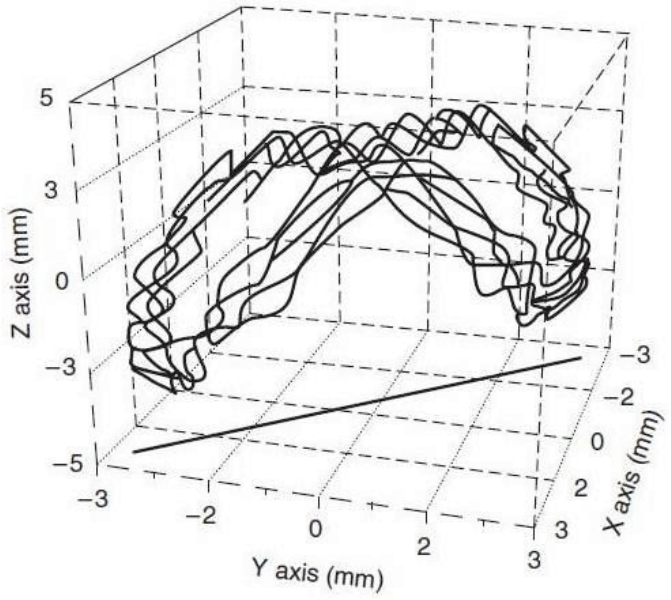

Figure 1.12: Trajectory of a trapped ion of *m*/*z* 105. The projection onto the *x*-*y* plane illustrates planar motion in three-dimensional space. (Taken from reference [107])

1.3.2 Fourier Transform Ion Cyclotron Resonance (FTICR)

The theory of cyclotron resonance was developed in the 1930s by Ernest Lawrence (Nobel Prize in Physics in 1951). Lawrence built the first cyclotron accelerator to study the fundamental properties of the atom. Subsequently, Penning devised the first trap for charged particles by using a combination of static electric and magnetic fields to confine electrons.[115] In the 1950s the principle of ion cyclotron resonance was first incorporated into a mass spectrometer, called the omegatron, by Sommer and co-workers, who successfully applied the concept of cyclotron resonance to determine the charge-to-mass ratio of the proton.[11] Major improvements in ICR awaited McIver's introduction of the trapped ion cell. Unlike the conventional drift cell, the trapped ion cell allowed for ion formation, manipulation and detection to occur within the same volume in space. The trapped ion cell differed from previous ICR cell designs by the inclusion of "trapping" electrodes. By applying small voltages to these electrodes, McIver was able to trap ions for 1-2 ms (approximately 100 times that of the drift cell). These advantages led to much greater dynamic range, sensitivity and mass resolution. More importantly, the extended trapping capability of the McIver cell was a prerequisite for the FTICR detection technique invented by Comisarow and Marshall later that decade. In the second half of the 1970s, Comisarow and Marshall adapted Fourier transform methods to ICR spectrometry and built the first FTICR-MS instrument.[116, 117] Since then, FTICR-MS has matured into a state-of-the-art high-resolution mass spectrometry instrument for the analysis of a wide variety of compounds (biological or not).

All FTICR-MS systems have in common four main components: a magnet (nowadays is usually a superconducting magnet); analyser cell (placed in the strong magnetic field created by the magnet); ultra-high vacuum system; and a sophisticated data system (many of the components in the data system are similar to those used in NMR). In this section, we shall put aside the magnet, vacuum and data systems and concentrate our attention in the ICR cell.

The ICR cell is the heart of the FTICR-MS instrument, it is where ions are stored, mass analysed and detected. Over the years several cell designs were developed (Figure 1.13).

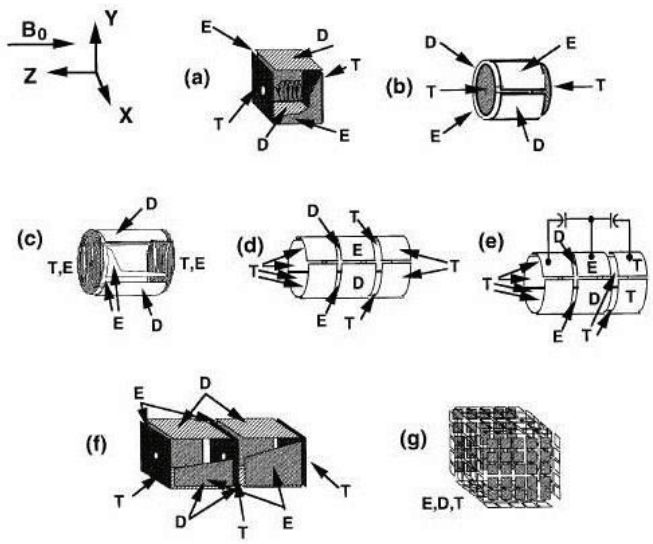

Figure 1.13: ICR ion trap configurations. E=excitation; D=detection; T=end cap ("trapping"). (a) cubic; (b) cylindrical; (c) end caps segmented to linearize excitation potential ("infinity" trap); (d) and (e) open-ended; (f) dual; and (g) "matrix-shimmed". (Image taken from reference [118])

Many fundamental aspects of FTICR can be understood from very simple idealized models:

- Ion cyclotron frequency, radius, velocity and energy, as a function of ion mass, ion charge and magnetic field strength, follow directly from the motion of an ion in a spatially uniform static magnetic field.
- Ion cyclotron motion may be rendered coherent (and thus observable) by the application of a spatially uniform *RF* electric field (excitation) at the same frequency as the ion cyclotron frequency. The ICR signal results from induction of an oscillating "image" charge on two conductive infinitely extended opposed parallel electrodes. A frequency-domain spectrum is obtained by Fourier transformation of the digitized ICR signal.
- Confinement of ions by application of a three-dimensional axial quadrupolar *dc* electric field shifts the ion cyclotron frequency, whereas excitation and detection remain essentially linear, but with a reduced proportionality constant.
- Collisions broaden the ICR signal in a simple way, and actually make it possible to cool and compress an ion packet for improved detection.
- Although FTICR-MS has been coupled to virtually every type of ion source, most ion sources work best outside the magnet. Thus, several methods have been developed to

guide the externally generated ions into the ion trap inside a high-field magnet.

- The above features may be combined in various experimental "event sequences" to perform tandem-in-time mass spectrometry (MS/MS or MS^n).

The complete derivation of the equations that describe the motion of an ion within an ICR cell is outside the scope of this thesis. Several reviews on this subject are available in the literature, for example the one by Marshall published in *Mass Spectrometry Reviews* in 1998.[118]

An ion moving in the presence of a uniform magnetic field, *B*, is subjected to a Lorentz force. If the ion maintains constant speed (i.e. no collisions), then the magnetic field bends the ion path into a circle of radius *r*, the cyclotron motion (Figure 1.14).

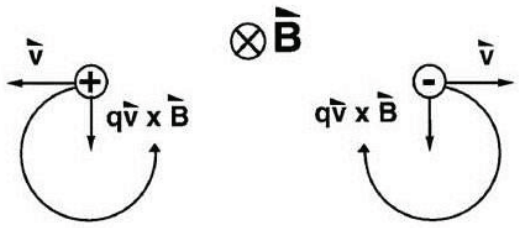

Figure 1.14: Ion cyclotron motion for a positive or negative ion due to the presence of a magnetic field (B) perpendicular to the plane of the paper. (Image taken from reference [118])

This cyclotron motion has a cyclotron frequency, ω_c, which is given by (Equation **1.14**, also called the cyclotron equation, where z is the charge of the ion, m is its mass and B is the magnetic field applied.

$$\omega_c = \frac{zB}{m} \qquad \text{(Equation 1.14)}$$

A remarkable feature of the cyclotron equation is that all ions of a given m/z ratio have the same ICR frequency, independent of their velocity. Thus, the precise determination of the m/z ratio does not require a kinetic energy "focusing".

The ion cyclotron orbital radius is given by (Equation **1.15**, where v_{xy} is the velocity on the *xy* plane.

$$r = \frac{mv_{xy}}{zB} \qquad \text{(Equation 1.15)}$$

This equation is useful to show that ions formed from large molecules are confined by the magnetic field to conveniently small orbital radii for ICR excitation and detection. For example, a singly-charged ion of m/z 100 in a magnetic field of 3 T has an ICR orbital radius of *ca.* 0.08 mm, a singly charged ion of m/z 10 000 has an ICR orbital radius of *ca.* 0.8 mm, and a singly charged ion of m/z 50 000 has an ICR orbital radius of *ca.* 1 cm.

The static magnetic field effectively confines ions in the *xy* plane; nevertheless, ions are still free to escape along the *z*-axis. To prevent this, a small electrostatic potential is applied to the trapping electrodes. This trapping potential induces a second ion motion termed trapping oscillation. The combination of the magnetic field and the radial component of the electric field created by the trapping potential induce a third motion: the magnetron rotation. The three natural ion motions (cyclotron rotation, magnetron rotation and trapping oscillation) are

depicted in Figure 1.15. The magnetron and trapping frequencies are usually much smaller than the cyclotron frequency and generally are not detected.

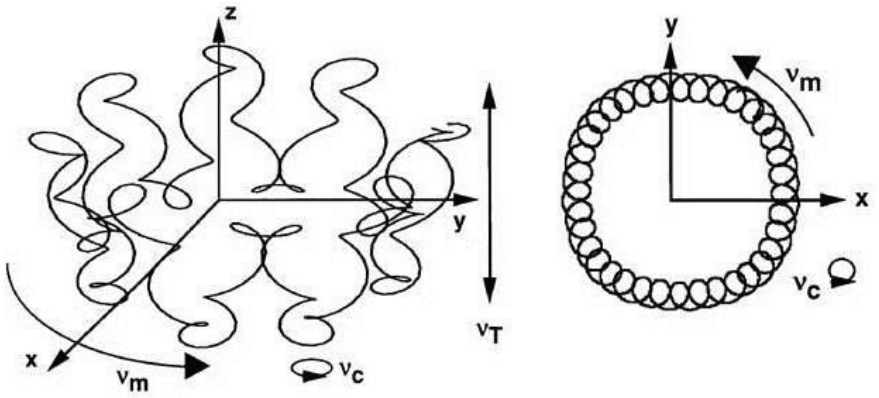

Figure 1.15: Schematic representation of the three natural motions of an ion confined in an ICR cell (m-magnetron rotation; c-cyclotron rotation; T-trapping oscillation). (Image taken from reference [118])

Ion cyclotron motion does not by itself generate an observable electric signal. Therefore, virtually all applications are based on excitation produced by applying a spatially uniform electric field oscillating at or near the cyclotron frequency of ions of a particular m/z range.

Excitation is used in three ways in FTICR-MS:

- To accelerate ions coherently to a larger (and thus detectable) orbital radius;
- To increase ion kinetic energy above the threshold for ion dissociation and/or ion-molecule reaction;

- To accelerate ions to a cyclotron radius larger than the radius of the ion trap, so that ions are removed from the instrument.

We shall examine the detection; the other two ways of using excitation will not be addressed in this thesis. Nevertheless, more information can be obtained in a review by Marshall and co-workers.[118]

The detection of the ions occurs as the ion packets pass two detector plates. As the ion packets have past these plates, charge moves within the detection circuit to counteract the proximity of the ions. The potential change (voltage) between the detection plates can be measured as a function of time and it is from here that the raw data is obtained. It should be noted that the ions repeatedly pass the detector plates for the duration of the acquisition, as non-destructive detections is employed. The magnitude of the signal is proportional to the total charge and to the proximity of the ions to the detection plates (orbital radius), and is independent of magnetic field strength. The raw data will represent the detections of all the ions at the same time, with their different cyclotron frequencies. It is therefore necessary to extract data concerning the different ion packets. This is done through the usage of a mathematical procedure known as Fourier transform (FT) where frequency information is obtained from time-domain data. Figure 1.16 illustrates the process of obtaining a mass spectrum from the time-domain data through Fourier transform and conversion to m/z and calibration.

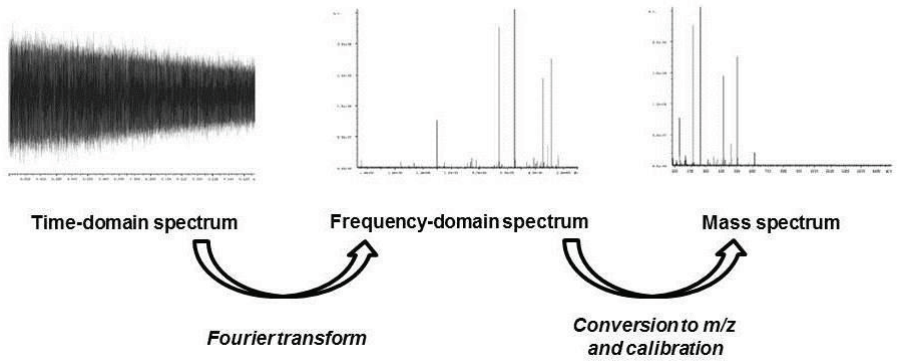

Figure 1.16: Illustration of the processing raw data. A Fourier transform is performed on time-domain data to convert it to the frequency-domain, and the resulting spectrum is then calibrated to m/z values.

When ions enter the FTICR analyser cell, the radii of the cyclotron orbits are too small to be detectable. The ions must be excited to detectable radii and this occurs through the application of a radiofrequency (RF) potential to two excitation plates. The frequency of the applied RF potential is resonant to that of the ions and the excitation additionally results in coherence of the ion packets. Figure 1.17 shows a representation of a cross section of an FTICR analyser cell where ions are being excited by the RF potential applied to the excitation plates. Ions of different m/z values are excited to orbits of the same radius, though their cyclotron frequencies differ.

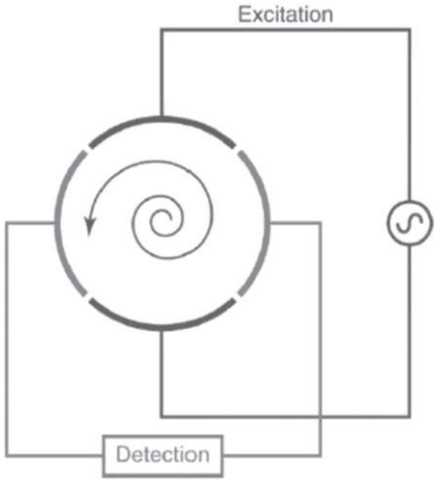

Figure 1.17: Cross section of a cylindrical cell depicting the excitation of the ions through the application of an RF potential to the excitation plates. Once the ions have been excited to a suitable radius, the image current of the orbiting ions can be detected on the detection plates. (Image taken from reference [119])

Unlike other mass spectrometers (e.g. sector instruments, time-of-flight, quadrupole) where mass analysis and ion detection are spatially separated events, in FTICR all analytical steps are separated in time. Figure 1.18 shows a typical sequence of events for a tandem mass spectrometry experiment performed in a FTICR mass spectrometer. Before ion introduction, the ICR cell is emptied with a quench pulse. After the ions have been introduced into the cell a significant amount of time is required for the ion selection, dissociation, excitation, detection, time-domain data storage and Fourier transformation events before the next experiment (i.e. sequence) is started. The time involved in the events that follow ion introduction, greatly depends on the instrument used and on the type of experiment (for example, the acquisition of a normal full scan mass spectrum will take less time than other mass

spectra since the ion selection and dissociation steps will not be performed).[120]

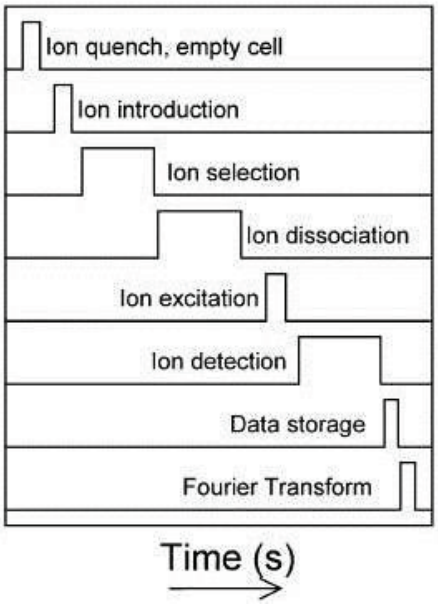

Figure 1.18: Example for a tandem mass spectrometry sequence performed in a FTICR mass spectrometer. The sequence shows the order of the different time-separated analytical steps. (Image taken from reference [120])

1.4 References

1. Gross, J.H., *Mass Spectrometry: A Textbook*. 1st ed. 2004, Berlin: Springer-Verlag.
2. Thomson, J.J., *Cathode Rays*. Phylosophical Magazine, 1897. **44**: p. 293.
3. Thomson, J.J., *On Rays of Positive Electricity*. Philosophical Magazine Series 6, 1907. **13**(77): p. 561-575.
4. Aston, F.W., *LXXIV. A positive ray spectrograph*. Philosophical Magazine Series 6, 1919. **38**(228): p. 707-714.
5. Dempster, A.J., *A new Method of Positive Ray Analysis*. Physical Review, 1918. **11**(4): p. 316-325.
6. Bainbridge, K.T., *The Isotopic Weight of H_2*. Physical Review, 1932. **42**(1): p. 1-10.
7. Bainbridge, K.T. and E.B. Jordan, *Mass Spectrum Analysis 1. The Mass Spectrograph. 2. The Existence of Isobars of Adjacent Elements*. Physical Review, 1936. **50**(4): p. 282-296.
8. Nier, A.O., *A Mass Spectrometer for Routine Isotope Abundance Measurements*. Review of Scientific Instruments, 1940. **11**(7): p. 212-216.
9. Johnson, E.G. and A.O. Nier, *Angular Aberrations in Sector Shaped Electromagnetic Lenses for Focusing Beams of Charged Particles*. Physical Review, 1953. **91**(1): p. 10-17.
10. Wolff, M.M. and W.E. Stephens, *A Pulsed Mass Spectrometer with Time Dispersion*. Review of Scientific Instruments, 1953. **24**(8): p. 616-617.

11. Sommer, H., H.A. Thomas, and J.A. Hipple, *The Measurement of e/M by Cyclotron Resonance.* Physical Review, 1951. **82**(5): p. 697-702.
12. Paul, W., *Electromagnetic traps for charged and neutral particles.* Reviews of Modern Physics, 1990. **62**(3): p. 531-540.
13. Watson, J.T. and K. Biemann, *Direct Recording of High Resolution Mass Spectra of Gas Chromatographic Effluents.* Analytical Chemistry, 2002. **37**(7): p. 844-851.
14. Ryhage, R., *Use of a Mass Spectrometer as a Detector and Analyzer for Effluent Emerging from High Temperature Gas Liquid Chromatography Columns.* Analytical Chemistry, 2002. **36**(4): p. 759-764.
15. Jennings, K.R., *Collision-induced decompositions of aromatic molecular ions.* International Journal of Mass Spectrometry and Ion Physics, 1968. **1**(3): p. 227-235.
16. Munson, M.S.B. and F.H. Field, *Chemical Ionization Mass Spectrometry. I. General Introduction.* Journal of the American Chemical Society, 2002. **88**(12): p. 2621-2630.
17. Barber, M., et al., *Fast atom bombardment of solids (F.A.B.): a new ion source for mass spectrometry.* Journal of the Chemical Society, Chemical Communications 1981(7): p. 325-327.
18. Fenn, J.B., et al., *Electrospray ionization for mass spectrometry of large biomolecules.* Science, 1989. **246**(4926): p. 64-71.
19. Karas, M. and F. Hillenkamp, *Laser desorption ionization of proteins with molecular masses exceeding 10,000 daltons.* Analytical Chemistry, 2002. **60**(20): p. 2299-2301.

20. Makarov, A., *Electrostatic Axially Harmonic Orbital Trapping: A High-Performance Technique of Mass Analysis.* Analytical Chemistry, 2000. **72**(6): p. 1156-1162.

21. Hager, J.W., *A new linear ion trap mass spectrometer.* Rapid Communications in Mass Spectrometry, 2002. **16**(6): p. 512-526.

22. Dass, C., *Fundamentals of Contemporary Mass Spectrometry*. 1st ed. 2007, Hoboken, New Jersey: John Wiley & Sons.

23. Whitehouse, C.M., et al., *Electrospray interface for liquid chromatographs and mass spectrometers.* Analytical Chemistry, 2002. **57**(3): p. 675-679.

24. Covey, T.R., E.C. Huang, and J.D. Henion, *Structural characterization of protein tryptic peptides via liquid chromatography/mass spectrometry and collision-induced dissociation of their doubly charged molecular ions.* Analytical Chemistry, 2002. **63**(13): p. 1193-1200.

25. Voyksner, R.D., *Combining Liquid Chromatography with Electrospray Mass Spectrometry*, in *Electrospray Ionization Mass Spectrometry: Fundamentals, Instrumentation, and Applications*, R.B. Cole, Editor. 1997, John Wiley & Sons: New York. p. 323-342.

26. Rodrigues, J.A., et al., *Mass Spectrometry of Carbohydrates: Newer Aspects*, in *Advances in Carbohydrate Chemistry and Biochemistry*, D. Horton, Editor. 2007, Academic Press: London. p. 59-141.

27. Hoffmann, E.d. and V. Stroobant, *Mass spectrometry: Principles and Applications*. 3rd ed. 2007, Chichester: John Wiley & Sons.

28. Takats, Z., et al., *Mass Spectrometry Sampling Under Ambient Conditions with Desorption Electrospray Ionization.* Science, 2004. **306**(5695): p. 471-473.

29. Polce, M.J. and C. Wesdemiotis, *Introduction to Mass Spectrometry of Polymers*, in *Mass Spectrometry of Polymers*, G. Montaudo and R.P. Latimer, Editors. 2002, CRC Press: Boca Raton. p. 1-39.

30. Zeleny, J., *The Electrical Discharge from Liquid Points, and a Hydrostatic Method of Measuring the Electric Intensity at Their Surfaces.* Physical Review, 1914. **3**(2): p. 69.

31. Zeleny, J., *Instability of Electrified Liquid Surfaces.* Physical Review, 1917. **10**(1): p. 1.

32. Zeleny, J., *Electrical Discharges from Pointed Conductors.* Physical Review, 1920. **16**(2): p. 102.

33. Hiraoka, K., et al., *Development of probe electrospray using a solid needle.* Rapid Communications in Mass Spectrometry, 2007. **21**(18): p. 3139-3144.

34. Cody, R.R., *Electrospray Ionization Mass Spectrometry: History, Theory, and Instrumentation*, in *Applied Electrospray Mass Spectrometry*, B.N. Pramanik, A.K. Ganguly, and M.L. Gross, Editors. 2002, Marcel Dekker: New York. p. 1-104.

35. Mann, M., C.K. Meng, and J.B. Fenn, *Interpreting mass spectra of multiply charged ions.* Analytical Chemistry, 2002. **61**(15): p. 1702-1708.

36. Yamashita, M. and J.B. Fenn, *Electrospray ion source. Another variation on the free-jet theme.* Journal of Physical Chemistry, 2002. **88**(20): p. 4451-4459.

37. Mora, J.F.d.l., et al., *Electrochemical processes in electrospray ionization mass spectrometry.* Journal of Mass Spectrometry, 2000. **35**(8): p. 939-952.

38. Cech, N.B. and C.G. Enke, *Practical implications of some recent studies in electrospray ionization fundamentals*. Mass Spectrometry Reviews, 2001. **20**(6): p. 362-387.

39. Rohner, T.C., N. Lion, and H.H. Girault, *Electrochemical and theoretical aspects of electrospray ionisation*. Physical Chemistry Chemical Physics, 2004. **6**(12): p. 3056-3068.

40. Cole, R.B., ed. *Electrospray Ionization Mass Spectrometry: Fundamentals, Instrumentation, and Applications*. 1st ed. 1997, John Wiley & Sons, Inc.: New York.

41. Herbert, C.G. and R.A.W. Johnstone, *Mass spectrometry basics*. 1st ed. 2002, Boca Raton: CRC Press.

42. Rossi, D.T. and M.W. Sinz, eds. *Mass Spectrometry in Drug Discovery*. 1st ed. 2002, Marcel Dekker: New York.

43. Loeb, L.B., et al., *Pulses in Negative Point-to-Plane Corona*. Physical Review, 1941. **60**(10): p. 714.

44. Kebarle, P. and L. Tang, *From ions in solution to ions in the gas phase - the mechanism of electrospray mass spectrometry*. Analytical Chemistry, 1993. **65**(22): p. 972A-986A.

45. Kebarle, P. and U.H. Verkerk, *Electrospray: From ions in solution to ions in the gas phase, what we know now*. Mass Spectrometry Reviews, 2009. **28**(6): p. 898-917.

46. Taylor, G., *Disintegration of Water Drops in an Electric Field*. Proceedings of the Royal Society of London. Series A. Mathematical and Physical Sciences, 1964. **280**(1382): p. 383-397.

47. Ikonomou, M.G., A.T. Blades, and P. Kebarle, *Investigations of the electrospray interface for liquid chromatography/mass spectrometry.* Analytical Chemistry, 1990. **62**(9): p. 957-967.

48. Ikonomou, M.G., A.T. Blades, and P. Kebarle, *Electrospray-ion spray: a comparison of mechanisms and performance.* Analytical Chemistry, 1991. **63**(18): p. 1989-1998.

49. Jaworek, A. and A. Krupa, *Classification of the modes of EHD spraying.* Journal of Aerosol Science, 1999. **30**(7): p. 873-893.

50. Juraschek, R. and F.W. Röllgen, *Pulsation phenomena during electrospray ionization.* International Journal of Mass Spectrometry, 1998. **177**(1): p. 1-15.

51. Wei, J., et al., *Naturally and externally pulsed electrospray.* Mass Spectrometry Reviews, 2002. **21**(3): p. 148-162.

52. Tang, K. and A. Gomez, *On the structure of an electrostatic spray of monodisperse droplets.* Physics of Fluids, 1994. **6**(7): p. 2317-2332.

53. Gomez, A. and K. Tang, *Charge and fission of droplets in electrostatic sprays.* Physics of Fluids, 1994. **6**(1): p. 404-414.

54. Olumee, Z., J.H. Callahan, and A. Vertes, *Droplet Dynamics Changes in Electrostatic Sprays of Methanol-Water Mixtures.* Journal of Physical Chemistry A, 1998. **102**(46): p. 9154-9160.

55. Valaskovic, G.A., J.P. Murphy, and M.S. Lee, *Automated orthogonal control system for electrospray ionization.* Journal of the American Society for Mass Spectrometry, 2004. **15**(8): p. 1201-1215.

56. Tang, K. and A. Gomez, *Generation of Monodisperse Water Droplets from Electrosprays in a Corona-Assisted Cone-Jet Mode.* Journal of Colloid and Interface Science, 1995. **175**(2): p. 326-332.

57. Mora, J.F.d.l., *The Fluid Dynamics of Taylor Cones.* Annual Review of Fluid Mechanics, 2007. **39**(1): p. 217-243.

58. Blades, A.T., M.G. Ikonomou, and P. Kebarle, *Mechanism of electrospray mass spectrometry. Electrospray as an electrolysis cell.* Analytical Chemistry, 1991. **63**(19): p. 2109-2114.

59. Van Berkel, G.J., S.A. McLuckey, and G.L. Glish, *Electrochemical origin of radical cations observed in electrospray ionization mass spectra.* Analytical Chemistry, 1992. **64**(14): p. 1586-1593.

60. Van Berkel, G.J. and F. Zhou, *Chemical Electron-Transfer Reactions in Electrospray Mass Spectrometry: Effective Oxidation Potentials of Electron-Transfer Reagents in Methylene Chloride.* Analytical Chemistry, 1994. **66**(20): p. 3408-3415.

61. Van Berkel, G.J. and F. Zhou, *Electrospray as a Controlled-Current Electrolytic Cell: Electrochemical Ionization of Neutral Analytes for Detection by Electrospray Mass Spectrometry.* Analytical Chemistry, 1995. **67**(21): p. 3958-3964.

62. Van Berkel, G.J., K.G. Asano, and S.A. McLuckey, *Observation of gas-phase molecular dications formed from neutral organics in solution via chemical electron-transfer reactions by using electrospray ionization mass spectrometry.* Journal of the American Society for Mass Spectrometry, 1994. **5**(7): p. 689-692.

63. Van Berkel, G.J. and F. Zhou, *Observation of gas-phase molecular dications formed from neutral organics in solution via the controlled-current electrolytic process inherent to electrospray.* Journal of the American Society for Mass Spectrometry, 1996. **7**(2): p. 157-162.

64. Van Berkel, G.J., F. Zhou, and J.T. Aronson, *Changes in bulk solution pH caused by the inherent controlled-current electrolytic process of*

an electrospray ion source. International Journal of Mass Spectrometry and Ion Processes, 1997. **162**(1-3): p. 55-67.

65. Smith, D.P.H., *The Electrohydrodynamic Atomization of Liquids*. IEEE Transactions on Industry Applications, 1986. **IA-22**(3): p. 527-535.
66. Ikonomou, M.G., A.T. Blades, and P. Kebarle, *Electrospray mass spectrometry of methanol and water solutions suppression of electric discharge with SF6 gas*. Journal of the American Society for Mass Spectrometry, 1991. **2**(6): p. 497-505.
67. Wampler, F.M., A.T. Blades, and P. Kebarle, *Negative ion electrospray mass spectrometry of nucleotides: ionization from water solution with SF6 discharge suppression*. Journal of the American Society for Mass Spectrometry, 1993. **4**(4): p. 289-295.
68. Cole, R.B., *Some tenets pertaining to electrospray ionization mass spectrometry*. Journal of Mass Spectrometry, 2000. **35**(7): p. 763-772.
69. Kebarle, P. and Y. Ho, *On the mechanism of Electrospray Mass Spectrometry*, in *Electrospray Ionization Mass Spectrometry: Fundamentals, Instrumentation, and Applications*, R.B. Cole, Editor. 1997, John Wiley & Sons, Inc.: New York. p. 3-63.
70. Taflin, D.C., T.L. Ward, and E.J. Davis, *Electrified droplet fission and the Rayleigh limit*. Langmuir, 1989. **5**(2): p. 376-384.
71. Dole, M., et al., *Molecular Beams of Macroions*. Journal of Chemical Physics, 1968. **49**(5): p. 2240-2249.
72. Iribarne, J.V. and B.A. Thomson, *On the evaporation of small ions from charged droplets*. Journal of Chemical Physics, 1976. **64**(6): p. 2287-2294.

73. Thomson, B.A. and J.V. Iribarne, *Field induced ion evaporation from liquid surfaces at atmospheric pressure.* Journal of Chemical Physics, 1979. **71**(11): p. 4451-4463.

74. Gamero-Castaño, M. and J.F.d.l. Mora, *Kinetics of small ion evaporation from the charge and mass distribution of multiply charged clusters in electrosprays.* Journal of Mass Spectrometry, 2000. **35**(7): p. 790-803.

75. Gamero-Castano, M. and J.F.d.l. Mora, *Direct measurement of ion evaporation kinetics from electrified liquid surfaces.* Journal of Chemical Physics, 2000. **113**(2): p. 815-832.

76. Fernandez de la Mora, J., *Electrospray ionization of large multiply charged species proceeds via Dole's charged residue mechanism.* Analytica Chimica Acta, 2000. **406**(1): p. 93-104.

77. Sakairi, M., et al., *Electrospray Mass Spectrometry: Protonated Molecule Intensities versus Hydration Free Energies in Amino Acids.* Analytical Sciences, 1991. **7**(2): p. 199-202.

78. Znamenskiy, V., I. Marginean, and A. Vertes, *Solvated Ion Evaporation from Charged Water Nanodroplets.* The Journal of Physical Chemistry A, 2003. **107**(38): p. 7406-7412.

79. Marginean, I., V. Znamenskiy, and A. Vertes, *Charge Reduction in Electrosprays: Slender Nanojets as Intermediates.* Journal of Physical Chemistry B, 2006. **110**(12): p. 6397-6404.

80. Fenn, J.B., *Ion formation from charged droplets: roles of geometry, energy, and time.* Journal of the American Society for Mass Spectrometry, 1993. **4**(7): p. 524-535.

81. Winger, B.E., et al., *Observation and implications of high mass-to-charge ratio ions from electrospray ionization mass spectrometry*. Journal of the American Society for Mass Spectrometry, 1993. **4**(7): p. 536-545.

82. Samalikova, M. and R. Grandori, *Protein Charge-State Distributions in Electrospray-Ionization Mass Spectrometry Do Not Appear To Be Limited by the Surface Tension of the Solvent*. Journal of the American Chemical Society, 2003. **125**(44): p. 13352-13353.

83. Samalikova, M. and R. Grandori, *Testing the role of solvent surface tension in protein ionization by electrospray*. Journal of Mass Spectrometry, 2005. **40**(4): p. 503-510.

84. Grandori, R., *Origin of the conformation dependence of protein charge-state distributions in electrospray ionization mass spectrometry*. Journal of Mass Spectrometry, 2003. **38**(1): p. 11-15.

85. Nesatyy, V.J. and M.J.F. Suter, *On the conformation-dependent neutralization theory and charging of individual proteins and their non-covalent complexes in the gas phase*. Journal of Mass Spectrometry, 2004. **39**(1): p. 93-97.

86. Hogan, C.J., et al., *Charge Carrier Field Emission Determines the Number of Charges on Native State Proteins in Electrospray Ionization*. Journal of the American Chemical Society, 2008. **130**(22): p. 6926-6927.

87. Hillenkamp, F. and M. Karas, *The MALDI Process and Method*, in *MALDI MS: A Practical Guide to Instrumentation, Methods and Applications*, F. Hillenkamp and J. Peter-Katalinic, Editors. 2007, Wiley-VCH: Weinheim. p. 1-28.

88. Jonsson, G.P., et al., *Plasma desorption mass spectrometry of peptides and proteins adsorbed on nitrocellulose.* Analytical Chemistry, 1986. **58**(6): p. 1084-1087.

89. Honig, R.E. and J.R. Woolston, *Laser-induced emission of electrons, ions, and neutral atoms from solid surfaces.* Applied Physics Letters, 1963. **2**(7): p. 138-139.

90. Fenner, N.C. and N.R. Daly, *Laser Used for Mass Analysis.* Review of Scientific Instruments, 1966. **37**(8): p. 1068-1070.

91. Posthumus, M.A., et al., *Laser desorption-mass spectrometry of polar nonvolatile bio-organic molecules.* Analytical Chemistry, 1978. **50**(7): p. 985-991.

92. Karas, M., D. Bachmann, and F. Hillenkamp, *Influence of the wavelength in high-irradiance ultraviolet laser desorption mass spectrometry of organic molecules.* Analytical Chemistry, 1985. **57**(14): p. 2935-2939.

93. Karas, M. and R. Kruger, *Ion Formation in MALDI: The Cluster Ionization Mechanism.* Chemical Reviews, 2003. **103**(2): p. 427-440.

94. Tanaka, K., et al., *Protein and polymer analyses up to m/z 100 000 by laser ionization time-of-flight mass spectrometry.* Rapid Communications in Mass Spectrometry, 1988. **2**(8): p. 151-153.

95. Griffiths, J., *A Brief History of Mass Spectrometry.* Analytical Chemistry, 2008. **80**(15): p. 5678-5683.

96. Macha, S.F., T.D. McCarley, and P.A. Limbach, *Influence of ionization energy on charge-transfer ionization in matrix-assisted laser desorption/ionization mass spectrometry.* Analytica Chimica Acta, 1999. **397**(1-3): p. 235-245.

97. Niu, S., W. Zhang, and B.T. Chait, *Direct comparison of infrared and ultraviolet wavelength matrix-assisted laser desorption/ ionization mass spectrometry of proteins*. Journal of the American Society for Mass Spectrometry, 1998. **9**(1): p. 1-7.

98. Kinsel, G.R., R.D. Edmondson, and D.H. Russell, *Profile and Flight Time Analysis of Bovine Insulin Clusters as a Probe of Matrix-assisted Laser Desorption/Ionization Ion Formation Dynamics*. Journal of Mass Spectrometry, 1997. **32**(7): p. 714-722.

99. Ashcroft, A.E., *Ionization Methods in Organic Mass Spectrometry*. 1997, Cambridge, UK: The Royal Society of Chemistry.

100. Karas, M. and F. Hillenkamp, *Laser desorption ionization of proteins with molecular masses exceeding 10,000 daltons*. Analytical Chemistry, 1988. **60**(20): p. 2299-2301.

101. Dreisewerd, K., *The Desorption Process in MALDI*. Chemical Reviews, 2003. **103**(2): p. 395-426.

102. Zenobi, R. and R. Knochenmuss, *Ion formation in MALDI mass spectrometry*. Mass Spectrometry Reviews, 1998. **17**(5): p. 337-366.

103. Knochenmuss, R. and R. Zenobi, *MALDI Ionization: The Role of In-Plume Processes*. Chemical Reviews, 2003. **103**(2): p. 441-452.

104. Karas, M., M. Glückmann, and J. Schäfer, *Ionization in matrix-assisted laser desorption/ionization: singly charged molecular ions are the lucky survivors*. Journal of Mass Spectrometry, 2000. **35**(1): p. 1-12.

105. Knochenmuss, R., et al., *Secondary ion-molecule reactions in matrix-assisted laser desorption/ionization*. Journal of Mass Spectrometry, 2000. **35**(11): p. 1237-1245.

106. Stafford Jr, G.C., *Ion trap mass spectrometry: a personal perspective*. Journal of the American Society for Mass Spectrometry, 2002. **13**(6): p. 589-596.

107. March, R.E. and J.F.J. Todd, *Quadrupole Ion Trap Mass Spectrometry*. 2nd ed. Chemical Analysis, ed. J.D. Winefordner. 2005, Hoboken, New Jersey: John Wiley & Sons.

108. Paul, W. and H. Steinwedel, *A new mass spectrometer without a magnetic field*. Zeitschrift fur Naturforschung A: Journal of Physical Sciences, 1953. **8a**: p. 448-450.

109. Paul, W. and H. Steinwedel, *Apparatus for separating charged particles of different specific charges*. 1956: German Patent.

110. Paul, W. and H. Steinwedel, *Apparatus for separating charged particles of different specific charges*. 1960: US Patent.

111. Stafford Jr, G.C., et al., *Recent improvements in and analytical applications of advanced ion trap technology*. International Journal of Mass Spectrometry and Ion Processes, 1984. **60**(1): p. 85-98.

112. Ekman, R., et al., *Mass Spectrometry: Instrumentation, Interpretation, and Applications*. Mass Spectrometry. 2009, Hoboken, New Jersey: John Wiley & Sons.

113. March, R.E., *An Introduction to Quadrupole Ion Trap Mass Spectrometry*. Journal of Mass Spectrometry, 1997. **32**(4): p. 351-369.

114. March, R.E., *Ion trap mass spectrometry*. International Journal of Mass Spectrometry and Ion Processes, 1992. **118-119**: p. 71-135.

115. Vartanian, V.H., J.S. Anderson, and D.A. Laude, *Advances in trapped ion cells for Fourier transform ion cyclotron resonance mass spectrometry*. Mass Spectrometry Reviews, 1995. **14**(1): p. 1-19.

116. Comisarow, M.B. and A.G. Marshall, *Fourier transform ion cyclotron resonance spectroscopy*. Chemical Physics Letters, 1974. **25**(2): p. 282-283.

117. Marshall, A.G., M.B. Comisarow, and G. Parisod, *Relaxation and spectral line shape in Fourier transform ion resonance spectroscopy*. Journal of Chemical Physics, 1979. **71**(11): p. 4434-4444.

118. Marshall, A.G., C.L. Hendrickson, and G.S. Jackson, *Fourier transform ion cyclotron resonance mass spectrometry: A primer*. Mass Spectrometry Reviews, 1998. **17**(1): p. 1-35.

119. Barrow, M.P., W.I. Burkitt, and P.J. Derrick, *Principles of Fourier transform ion cyclotron resonance mass spectrometry and its application in structural biology*. Analyst, 2005. **130**(1): p. 18-28.

120. Heeren, R.M.A., et al., *A mini-review of mass spectrometry using high-performance FTICR-MS methods*. Analytical and Bioanalytical Chemistry, 2004. **378**(4): p. 1048-1058.

Chapter 2
Experimental Section

2 Experimental

2.1 MALDI (Chapter 3)

2.1.1 TiO_2 anatase as matrix for MALDI analysis of small molecules

Materials and Reagents

All reagents were of analytical grade and used without further purification. 2-Chloroaniline (2CA), Quercetin (Quer) and poly(ethylene glycol), PEG200, were purchased from Sigma-Aldrich (Milwaukee, WI, USA). Caffeine was purchased from Fluka (Milwaukee, WI, USA). The organic matrices, trans-cinnamic acid and 2,5-dihydroxybenzoic acid (DHB), were purchased from Fluka (Milwaukee, WI, USA). Titanium dioxide Degussa P25, a known mixture of approximately 70% anatase and 30% rutile, was kindly supplied by Degussa (Frankfurt am Main, Germany). Nanosized TiO_2 anatase was synthesized according to our preparation method.[1] TiO_2 rutile was obtained by the calcination (1000 ºC during 6 h) of the before mentioned TiO_2 anatase sample.

The water used was purified using a Milli-Q water system from Milipore (Billerica, MA, USA) and methanol HPLC grade was obtained from Merck (Darmstadt, Germany).

Mass Spectrometry

All MS experiments were performed on a Bruker Daltonics APEX Ultra FTICR mass spectrometer (Billerica, MA, USA), equipped

with a 7.0 Tesla actively shielded superconducting magnet. The vacuum was maintained by means of mechanical vacuum pumps followed by turbomolecular pumps in two different regions: ion source (maintained ~6.0×10^{-6} mbar) and cell region (maintained ~4.0×10^{-10} mbar). The ions were generated from an external Apollo II Dual ESI/MALDI source, Bruker Daltonics (Billerica, MA, USA), equipped with a N_2 laser (λ = 337 nm), in the positive ion mode. The laser energy at the target position was 80-100 μJ and the laser pulse length was 4ns. The laser power was adjusted to obtain satisfactory resolution (> 60 000) and signal-to-noise ratio. The spectra shown are the average of 32 spectra with 20 laser shots per spectrum. The MALDI plate used was a MTP AnchorChip™ 400/384 T F from Bruker Daltonics (Billerica, MA, USA).

Electrochemical Measurements

Solutions containing 1 mM of monomer ((2- chloroaniline, 3-chloroaniline, 4-chloroaniline, benzidine, 4-fluoroaniline, 4-bromoaniline, 4-aminobifenil, 2-nitroaniline, 3-nitroaniline, 4-nitroaniline and caffeine) in 10 mM tetrabutylammonium tetrafluoroborate (TBATFB, Acros Organics, 95%) and dimethyl sulfoxide (DMSO) were prepared to evaluate the oxidation potential of the monomer. The monomer oxidation was assessed by sweeping the potential from -0.20 V to E_f, at a scan rate of 50 mV/s.

A polycrystalline Pt electrode (A= 0.196 cm^2) was used as a working electrode whereas a saturated calomel electrode (SCE) and a Pt foil (2 cm^2) were used as reference and counter electrode, respectively, in a conventional three-compartment glass cell, with a glass frit

separating the working and the counter electrodes compartments. Before each experiment, a mirror-finishing Pt surface was generated by hand-polishing the electrode in an aqueous suspension of successively finer grades of alumina (down to 0.05 μm). Prior to the experiments, the solutions were deoxygenated with N_2 for 15 min.

A CHI Electrochemical Analyzer – 620A Model controlled by a computer was used in the electrochemical experiments.

Sample preparation

Particle matrix suspensions were prepared by dispersing the TiO_2 samples in deionized water at a concentration of 10 mg/mL. Stock solutions were obtained from organic matrices dissolved in deionized water (10 mg/mL). The analytes were used as standard solutions prepared in methanol with molar concentrations of approximately 10^{-2} M.

A known volume of standard analyte solution was added to an equal volume of matrix solution (50:50). A 2 μL aliquot was pipetted to the stainless steel target plate and allowed to dry before analysis.

2.1.2 Flavonoid-Matrix cluster ions in MALDI Mass Spectrometry

Materials and Reagents

All reagents were of analytical grade and used without further purification. Quercetin (Quer), myricetin (Myr), luteolin (Lut) and kaempferol (Kaem), structures depicted in Scheme 2.1, were acquired from Sigma-Aldrich (St. Louis, MO, USA). The MALDI matrix 2,5-

dihydroxybenzoic acid (2,5-DHB) was purchased from Fluka (Seelze, Germany). The water used was purified using a Milli-Q water purification system from Millipore (Billerica, MA, USA) and methanol HPLC grade was obtained from Panreac (Barcelona, Spain). The matrix was used as a 10 mg/mL suspension in H_2O, acidified with 0.1% (V/V) formic acid acquired from Fluka (Seelze, Germany), and the flavonoids solutions were prepared in methanol at a concentration of 10 mg/mL.

Equal volumes of matrix suspension and flavonoid solution were added. A 1 μL aliquot of each flavonoids+matrix mixture was spotted on to the MALDI plate.

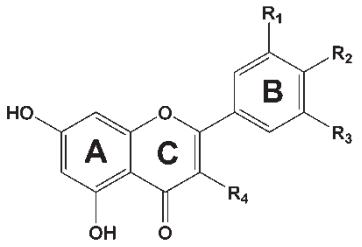

Trivial name	R_1	R_2	R_3	R_4
Quercetin	OH	OH	H	OH
Myricetin	OH	OH	OH	OH
Luteolin	OH	OH	H	H
Kaempferol	H	OH	H	OH

Scheme 2.1: Structures of the flavonoids studied.

Mass Spectrometry

All MS experiments were performed on a Bruker Daltonics APEX Ultra FTICR mass spectrometer (Billerica, MA, USA), equipped with a 7.0 tesla actively shielded superconducting magnet. The vacuum was maintained by means of mechanical vacuum pumps followed by turbomolecular pumps in two different regions: ion source (maintained ~6.0×10^{-6} mbar) and cell region (maintained ~4.0×10^{-10} mbar). The ions

were generated from an external Apollo II Scout MTP source from Bruker Daltonics (Billerica, MA, USA), equipped with a N_2 laser (λ = 337 nm), in the positive ion mode. The laser energy was kept at 80% of the maximum value (typically 80-100 μJ at the target position) and the laser pulse length was 4 ns. The ion source optics, collision cell and Ion Cyclotron Resonance (ICR) cell parameters were optimized to ensure the highest abundance possible for the ions of interest. The ions were accumulated in the collision cell during 1.0 s prior to their transfer to the ICR cell. The spectra shown are the average of 8 spectra with 20 laser shots per spectrum. The MALDI plate used was a MTP 384 target plate polished steel T F from Bruker Daltonics (Billerica, MA, USA).

The MS^2 experiments were performed using Argon, acquired from Praxair (Danbury, CT, USA), as collision gas at a flow rate of 0.30 L s^{-1}. The collision cell voltage was varied for each compound in order to find the appropriate value. An acquisition size of 512k was used throughout the experiments and all the experiments were performed in the mass range *m/z* 150-1000.

2.2 Aromatic Amines (Chapter 4)

Materials and Reagents

The aromatic amines under study comprised all isomers of fluoro, chloro, bromo, iodo and nitroanilines (Scheme 2.2) and were all used without further purification (more information on these reagents is presented in Table 2.1.

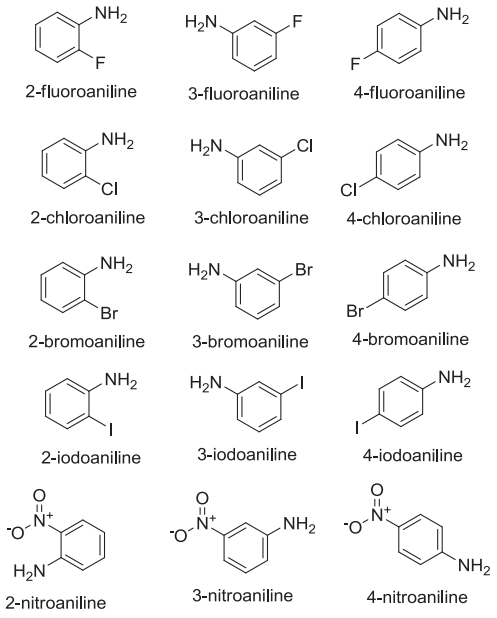

Scheme 2.2: Structures of the aniline derivatives under study.

Stock solutions in a concentration range of 90 - 140 μM were prepared in HPLC grade methanol (Panreac; Barcelona, Spain). The fragmentation studies were performed using 10-fold diluted solutions in methanol acidified with 0.2% (V/V) formic acid (Fluka; Seelze, Germany), resulting in a concentration range of 9 – 14 μM.

For the isomer distinction experiments, mixtures of 100 μL of haloaniline (stock solution), 100 μL 4-nitroaniline (stock solution), 898 μL HPLC grade methanol and 2 μL of formic acid were prepared and analysed in the mass spectrometer.

Table 2.1. Information on the aniline derivatives studied.

Analyte	Supplier	
2-fluoroaniline (L) (CAS# 348-54-9)	Acros Organics	Purity >99% d=1.151 MW=111.12
3-fluoroaniline (L) (CAS# 372-19-0)	Acros Organics	Purity >98% d=1.150 MW=111.12
4-fluoroaniline (L) (CAS# 371-40-4)	Sigma-Aldrich	Purity = 99% d=1.157 MW=111.12
2-chloroaniline (L) (CAS# 95-51-2)	Sigma-Aldrich	Purity ≥ 99.5% d=1.157 MW=127.57
3-chloroaniline (L) (CAS# 108-42-9)	Sigma-Aldrich	Purity = 99% d=1.215 MW=127.57
4-chloroaniline (S) (CAS# 106-47-8)	Sigma-Aldrich	Purity = 98% MW=127.57
2-bromoaniline (S) (CAS# 615-36-1)	Acros Organics	Purity = 98% MW=172.02
3-bromoaniline (L) (CAS# 591-19-5)	Acros Organics	Purity = 98% d=1.580 MW=172.02
4-bromoaniline (S) (CAS# 106-40-1)	Sigma-Aldrich	Purity = 97% MW=172.02
2-iodoaniline (S) (CAS# 615-43-0)	Acros Organics	Purity = 98% MW=219.02
3-iodoaniline (L) (CAS# 626-01-7)	Acros Organics	Purity = 98% d=1.820 MW=219.02
4-iodoaniline (S) (CAS# 540-37-4)	Acros Organics	Purity = 99% MW=219.02
2-nitroaniline (S) (CAS# 88-74-4)	Sigma-Aldrich	Purity = 98% MW=138.12
3-nitroaniline (S) (CAS# 99-09-2)	Sigma-Aldrich	Purity = 98% MW=138.12
4-nitroaniline (S) (CAS# 100-01-6)	Sigma-Aldrich	Purity ≥ 99% MW=138.12

Mass Spectrometry

Two mass spectrometry systems were used in this work. The low resolution LCQ Duo LCQ Duo ion trap mass spectrometer from Thermo Scientific (San Jose, CA, USA) equipped with an ESI source. Samples were introduced, via a syringe pump (flow rate of 5 μL min^{-1}), into the stainless steel capillary of the ESI source. The applied spray voltage in the source was 4.5 kV, the capillary voltage was 10 V and the capillary temperature was 220 ºC. All the mass spectrometer parameters were adjusted in order to optimize the signal-to-noise ratios for the ions of interest. Nitrogen was used as nebulising and auxiliary gas in the source. The pressure measured during the experiments at the skimmer cone, with a convectron gauge, was normally 1.25×10^{2} Pa. The base pressure in the ion trap with helium added was typically 1.59×10^{-3} Pa.

All mass spectrometry data were acquired in the positive and negative ion modes, the full scan spectra were recorded in the range m/z 50–500 and three micro-scans were averaged. CID and MS/MS experiments were performed with helium as collision gas. The ions of interest were activated by applying a percentage of a supplementary a.c. potential in the range of 0.75-1.75 Vp-p (peak-to-peak) to the end caps of the ion trap at the resonance frequency of the selected ion (referred to as Collision Energy Level, CEL). The CEL was gradually increased until the precursor and the product ions could both be observed in the MS/MS spectrum. Injection times were 50 ms in a full scan and 200 ms in an MS/MS scan. XcaliburTM software, from Thermo Scientific (San Jose, CA, USA), was used to acquire and process the data.

The high resolution mass spectra were acquired in a Bruker Daltonics APEX Ultra FTICR mass spectrometer (Billerica, MA, USA),

equipped with a 7.0 Tesla actively shielded superconducting magnet. Ions were generated from an external Apollo II Dual ESI/MALDI source, Bruker Daltonics (Billerica, MA, USA). Samples were introduced, by means of an infusion pump from KD Scientific (Holliston, MA, USA), with a flow rate of 120 μL h^{-1}. Mass spectra were acquired in the positive ion mode, with an acquisition size of 512k, in the mass range of m/z 50-500. The nebulizer gas flow rate was set to 2.5 L/min, the dry gas flow rate was set to 4.0 L min^{-1} at a temperature of 220 ºC. The capillary voltage was set to 5000 V and the spray shield voltage was set to 4500 V. The ion source optics, collision cell and ICR cell parameters were optimized to ensure the highest abundance possible for the ions of interest. All mass spectra presented are the average of 18 mass spectra. The ions were accumulated in the collision cell during 1.0 s prior to their transfer to the ICR cell. The MS^2 experiments were performed using argon, acquired from Praxair (Porto, Portugal), as collision gas at a flow rate of 0.60 L s^{-1}. The collision cell voltage was varied for each compound in order to find the appropriate value. The MS^3 experiments were performed by isolating the desired ion in the ICR cell and fragmenting it by SORI-CAD at a frequency offset of 400 Hz and with a pulse length of 0.25 s. The SORI power was adjusted for each isolated ion in order to find the appropriate value. The collision gas employed in the SORI-CAD experiments was argon, acquired from Praxair (Porto, Portugal), at a pressure of approximately 8 mbar.

Semi-empirical Calculations

Heats of formation (ΔH_f) were calculated for the neutral and the various protonated forms of each compound, using the semi-empirical PM6,[2] as implemented in MOPAC2009.[3] The changes in protonation reaction enthalpy, $\Delta_r H$, were computed to access the most probable protonation. This assessment took into account the optimized ion structure and the resulting energy.

DFT Calculations

DFT calculations[4] were performed using the Gaussian 03 program, revision C02,[5] with the MPW1PW91 hybrid functional as implemented by Adamo and Barone, which includes a mixture of Hartree-Fock exchange with DFT exchange-correlation given by the Perdew and Wang's 1991 exchange functional as modified by Adamo and Barone, with the Perdew and Wang's 1991 gradient-corrected correlation functional.[6-8]

Pople's 6-311G(2d,2p) basis set was used on all atoms.[9-15]

The geometries of aniline derivatives, and respective protonated were optimized without any geometry constrains at the MPW1PW91/6-311++G(2d,2p) level of theory as mentioned above, and carried out under tight convergence criteria for both the optimization and SCF items. The Ultrafine option for the integration grid was concomitantly adopted. Conformational analyses were accomplished as unrelaxed scans of the coordinates of interest using the Scan keyword as implemented in Gaussian 03.

Harmonic second derivatives were calculated to evaluate the nature of minima and to estimate values for Zero Point Energy (ZPE)

and thermal correction to enthalpy. The enthalpies at 298 K were obtained from Equation 2.1,

$$H=E^{0}+ ZPE+H_{trans}+H_{rot}+H_{vib}+ RT \qquad \text{(Equation 2.1)}$$

where E^0 is the electronic energy, ZPE is the zero-point energy, and H_{trans}, H_{rot}, and H_{vib} are the translational, rotational, and vibrational contributions. H_{trans} and H_{rot} are 3/2RT for a nonlinear molecule; H_{vib} (thermal correction to enthalpy) is extracted directly from the Gaussian 03 frequency calculation output. The last term, RT, stands for the pV work.

2.3 Isoflavones (Chapter 5)

Materials and Reagents

The compounds under study consisted of five isoflavones (Scheme 2.3) and were purchased from Extrasynthése (Genay, France). Sample solutions, with concentrations *ca.* 100 μM, were prepared in HPLC grade methanol acquired from Panreac (Barcelona, Spain) acidified with 0.1% (V/V) of formic acid acquired from Fluka (Seelze, Germany).

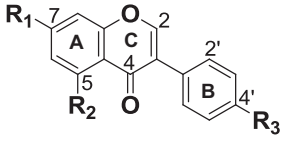

	R_1	R_2	R_3
Daidzein	OH	H	OH
Genistein	OH	OH	OH
Prunetin	OCH_3	OH	OH
Formononetin	OH	H	OCH_3
Biochanin A	OH	OH	OCH_3

Scheme 2.3: Structure of the isoflavones under study.

Mass Spectrometry

All experiments were performed on a Bruker Daltonics APEX Ultra FTICR mass spectrometer (Billerica, MA, USA), equipped with a 7.0 Tesla actively shielded superconducting magnet. The ions were generated from an external Apollo II Dual ESI/MALDI source, Bruker Daltonics (Billerica, MA, USA). The samples were introduced, by means of an infusion pump from KD Scientific (Holliston, MA, USA), with a flow rate of 120 $\mu L\ h^{-1}$. The mass spectra were acquired in the positive ion broadband mode, with an acquisition size of 512k, in the mass range of m/z 50-500. The nebulizer gas flow rate was set to 2.5 L min^{-1}, the dry gas flow rate was set to 4.0 L min^{-1} at a temperature of 220 ºC. The capillary voltage was set to 5000 V and the spray shield voltage was set to 4500 V. The ion source optics, collision cell and ICR cell parameters were optimized to ensure the highest abundance possible for the ions of interest. All mass spectra presented are the average of 32 mass spectra. The ions were accumulated in the collision cell during 1.0 s prior to their transfer to the ICR cell. The MS^2 experiments were performed using Argon, acquired from Praxair (Porto, Portugal), as collision gas at a flow rate of 0.60 L s^{-1}. The collision cell voltage was varied for each compound in order to find the appropriate value. The MS^3 experiments were performed by isolating the desired ion in the ICR cell and fragmenting it by Sustained Off Resonance Irradiation – Collision Activated Dissociation (SORI-CAD) at a frequency offset of 400 Hz and with a pulse length of 0.25 s. The SORI power was adjusted for each isolated ion in order to find the appropriate value. The collision gas employed in the SORI-CAD experiments was argon, acquired from Praxair (Porto, Portugal), at a pressure of approximately 8 mbar.

Semi-empirical calculations

To determine the most probable protonation site, Molecular Electrostatic Potential (MEP) surfaces and heats of formation were calculated for the neutral and the various protonated forms of each compound. Heats of formation were calculated using PM6 method [2] as implemented in MOPAC2009.[3] The MEP surfaces were calculated using the AM1 method [16] (the parametric molecular electrostatic potential of Wang and Ford [17, 18] has only been parameterized for the AM1 method; for more details see MOPAC2009 Manual[3]).

2.4 Lactones linked and fused to sugars (Chapter 6)

2.4.1 Electrospray Ionization Mass Spectrometry analysis of newly synthesized α,β-unsaturated γ-lactones fused to sugars

Materials and Reagents

The compounds under study (Scheme 2.4) were synthesized according to Xavier et al.[19, 20] These compounds consist of sugar fused butenolides, such as 3-deoxy-2-O,3-C-(1-oxoethan-1-yl-2-ylidene)-D-erythro-pentopyranose (compound **1**), 3-deoxy-2-O,3-C-(1-oxoethan-1-yl-2-ylidene)-D-ribo-hexopyranose (compound **2**), 3-deoxy-2-O,3-C-(1-oxoethan-1-yl-2-ylidene)-6-O-pivaloyl-D-ribo-hexopyranose (compound **3**), 1,4,6-tri-O-acetyl-3-deoxy-2-O,3-C-(1-oxoethan-1-yl-2-ylidene)-D-ribo-hexopyranose (compound **4**) and 1,2,6-tri-O-acetyl-3-deoxy-4-O,3-C-(1-oxoethan-1-yl-2-ylidene)-D-ribo-hexopyranose (compound **5**), depicted in Scheme 2.4. Sample solutions in HPLC grade methanol acquired from Panreac (Barcelona, Spain) were prepared and

acidified, in order to facilitate protonation, with 0.1%(v/v) of formic acid acquired from Fluka (Seelze, Germany).

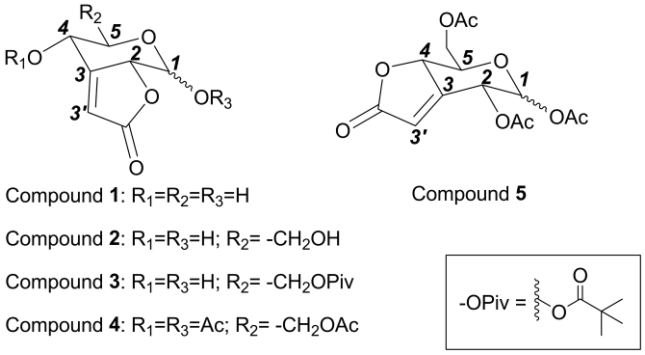

Scheme 2.4: Structure of the α,β-unsaturated γ-lactones fused to sugars, compounds under study.

Mass Spectrometry

All experiments were performed using a LCQ Duo ion trap mass spectrometer from Thermo Scientific (San Jose, CA, USA) equipped with an ESI source. Samples were introduced, via a syringe pump (flow rate of 5 μL/min), into the stainless steel capillary of the ESI source. The applied spray voltage in the source was 4.5 kV, the capillary voltage was 10 V and the capillary temperature was 220ºC. All the mass spectrometer parameters were adjusted in order to optimize the signal-to-noise ratios for the ions of interest. Nitrogen was used as nebulising and auxiliary gas in the source. The pressure measured during the experiments at the skimmer cone, with a convectron gauge, was normally 1.25×10^{2} Pa. The base pressure in the ion trap with helium added was typically 1.59×10^{-3} Pa.

All mass spectrometry data were acquired in the positive and negative ion modes, the full scan spectra were recorded in the range m/z 50–500 and three micro-scans were averaged. CID and MS/MS

experiments were performed with helium as collision gas. The ions of interest were activated by applying a percentage of a supplementary a.c. potential in the range of 0.75-1.75 Vp-p (peak-to-peak) to the end caps of the ion trap at the resonance frequency of the selected ion (referred to as Collision Energy Level, CEL). The CEL was gradually increased until the precursor and the product ions could both be observed in the MS/MS spectrum. Injection times were 50 ms in a full scan and 200 ms in an MS/MS scan. XcaliburTM software, from Thermo Scientific (San Jose, CA, USA), was used to acquire and process the data.

Semi-empirical calculations

Heats of formation were calculated using the semi-empirical PM6 [2] method implemented in MOPAC2009.[3] The changes in heat of formation, ΔH_f, were computed in order to assess whether a fragmentation pathway prevails or not over another. This assessment was done taking into account the resulting energy and the optimized ion structure.

2.4.2 Furanose C-C-linked γ-lactones: a combined ESIFT-ICR MS and semi-empirical calculations study

Materials and Reagents

The compounds under study consist of the sugar-linked butenolides (Scheme 2.5), 4-(3-*O*-allyl-1,2-*O*-isopropylidene-α-D-ribofuranos-4-yl)furan-2(5*H*)-one (compound **1**) and 4-(3-*O*-benzyl-1,2-*O*-isopropylidene-α-D-ribofuranos-4-yl)furan-2(5*H*)-one (compound **2**), and their β-hydroxy γ-lactone counterparts, namely (4*R*)-4-(3-*O*-allyl-

1,2-*O*-isopropylidene-α-D-xylofuranos-4-yl)-4-hydroxydihydrofuran-2(3*H*)-one (compound **3**) and (4*R*)-4-(3-*O*-benzyl-1,2-*O*-isopropylidene-α-D-xylofuranos-4-yl)-4-hydroxydihydrofuran-2(3*H*)-one (compound **4**), synthesized according to Xavier *et al.*[20] Sample solutions in methanol HPLC grade acquired from Panreac (Barcelona, Spain) were prepared and acidified with 0.1% (V/V) of formic acid acquired from Fluka (Seelze, Germany).

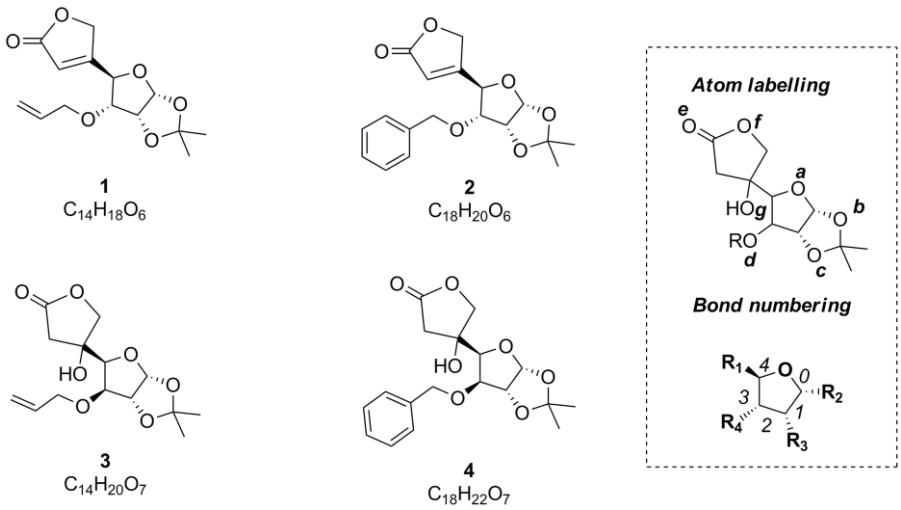

Scheme 2.5: Structure of compounds **1-4**, atom labeling and bond numbering used.

Mass Spectrometry

All experiments were performed on a Bruker Daltonics APEX Ultra FTICR mass spectrometer (Billerica, MA, USA) equipped with a 7.0 Tesla actively shielded superconducting magnet. Ions were generated from an external Apollo II Dual ESI/MALDI source, Bruker Daltonics (Billerica, MA, USA). Samples were introduced by means of an infusion pump from KD Scientific (Holliston, MA, USA), with a flow rate of 120

μL/h. Mass spectra were acquired in the positive ion mode, with an acquisition size of 512k, in the mass range of 50-500. The nebulizer gas flow rate was set to 2.5 L/min, the dry gas flow rate was set to 4.0 L/min at a temperature of 220ºC. The capillary voltage was set to 5000 V and the spray shield voltage was set to 4500 V. The ion source optics, collision cell and ICR cell parameters were optimized to ensure the highest abundance possible for the ions of interest. All mass spectra presented are the average of 32 mass spectra. The ions were accumulated in the collision cell during 1.0 s prior to their transfer to the ICR cell. The MS^2 experiments were performed using argon, acquired from Praxair (Porto, Portugal), as collision gas at a flow rate of 0.60 L/s. The collision cell voltage was varied for each compound in order to find the appropriate value. The MS^3 experiments were performed by isolating the desired ion in the ICR cell and fragmenting it by SORI-CAD at a frequency offset of 400Hz and with a pulse length of 0.25 s. The SORI power was adjusted for each isolated ion in order to find the appropriate value. The collision gas employed in the SORI-CAD experiments was argon, acquired from Praxair (Porto, Portugal), at a pressure of approximately 8 mbar.

Semi-empirical calculations

Marvin and Calculator Plugins, version 5.3.1, 2010, Chemaxon (http://www.chemaxon.com) were used for drawing and initial structure calculation in the framework of a Dreiding-type molecular mechanics force field. Heats of formation (ΔH_f) were calculated for the neutral and the various protonated forms of each compound, using the semi-empirical PM6[2] as implemented in MOPAC2009[3] using the

least energy conformer obtained with the Marvin software. The changes in reaction enthalpy (either protonation/cationization or fragmentation), $\Delta_r H$, were computed to access the most probable protonation/cationization site and whether one fragmentation pathway prevails over another. This assessment took into account the optimized ion structure and the resulting energy.

2.5 References

1. Castro, A.L., et al., *Synthesis of anatase TiO_2 nanoparticles with high temperature stability and photocatalytic activity*. Solid State Sciences, 2008. **10**(5): p. 602-606.
2. Stewart, J., *Optimization of parameters for semiempirical methods V: Modification of NDDO approximations and application to 70 elements*. Journal of Molecular Modeling, 2007. **13**(12): p. 1173-1213.
3. Stewart, J.J.P., *MOPAC2009*. 2009, Stewart Computational Chemistry: Colorado Springs, CO, USA.
4. Parr, R.G. and W. Yang, *Density-Functional Theory of Atoms and Molecules*. 1989, Oxford: Oxford University Press.
5. Frisch, M.J., et al., *Gaussian 03, Revision C.02*. 2004, Gaussian, Inc.: Wallingford CT.
6. Burke, K., J.P. Perdew, and Y. Wang, *Derivation of a generalized gradient approximation: The PW91 density functional* in *Electronic Density Functional Theory: Recent Progress and New Directions*, J.F. Dobson, G. Vignale, and M.P. Das, Editors. 1998, Plenum: New York.
7. Adamo, C. and V. Barone, *Exchange functionals with improved long-range behavior and adiabatic connection methods without adjustable parameters: The mPW and mPW1PW models*. The Journal of Chemical Physics, 1998. **108**(2): p. 664-675.
8. Adamo, C. and V. Barone, *Toward reliable adiabatic connection models free from adjustable parameters*. Chemical Physics Letters, 1997. **274**(1-3): p. 242-250.

9. McLean, A.D. and G.S. Chandler, *Contracted Gaussian basis sets for molecular calculations. I. Second row atoms, Z=11--18*. The Journal of Chemical Physics, 1980. **72**(10): p. 5639-5648.
10. Krishnan, R., et al., *Self-consistent molecular orbital methods. XX. A basis set for correlated wave functions*. The Journal of Chemical Physics, 1980. **72**(1): p. 650-654.
11. Wachters, A.J.H., *Gaussian Basis Set for Molecular Wavefunctions Containing Third-Row Atoms*. The Journal of Chemical Physics, 1970. **52**(3): p. 1033-1036.
12. Hay, P.J., *Gaussian basis sets for molecular calculations. The representation of 3d orbitals in transition-metal atoms*. The Journal of Chemical Physics, 1977. **66**(10): p. 4377-4384.
13. Raghavachari, K. and G.W. Trucks, *Highly correlated systems. Excitation energies of first row transition metals Sc--Cu*. The Journal of Chemical Physics, 1989. **91**(2): p. 1062-1065.
14. Curtiss, L.A., et al., *Extension of Gaussian-2 theory to molecules containing third-row atoms Ga--Kr*. The Journal of Chemical Physics, 1995. **103**(14): p. 6104-6113.
15. McGrath, M.P. and L. Radom, *Extension of Gaussian-1 (G1) theory to bromine-containing molecules*. The Journal of Chemical Physics, 1991. **94**(1): p. 511-516.
16. Dewar, M.J.S., et al., *Development and use of quantum mechanical molecular models. 76. AM1: a new general purpose quantum mechanical molecular model*. Journal of the American Chemical Society, 1985. **107**(13): p. 3902-3909.
17. Ford, G.P. and B. Wang, *New approach to the rapid semiempirical calculation of molecular electrostatic potentials based on the AM1 wave*

function: Comparison with ab initio HF/6-31G results.* Journal of Computational Chemistry, 1993. **14**(9): p. 1101-1111.

18. Wang, B. and G.P. Ford, *Atomic charges derived from a fast and accurate method for electrostatic potentials based on modified AM1 calculations.* Journal of Computational Chemistry, 1994. **15**(2): p. 200-207.
19. Xavier, N.M. and A.P. Rauter, *Easy and Stereoselective Approach to α,β-Unsaturated γ-Lactones Fused to Pyranoses from Furanose Scaffolds.* Organic Letters, 2007. **9**(17): p. 3339-3341.
20. Xavier, N.M., et al., *Synthesis and Biological Evaluation of Sugars Containing α,β-Unsaturated γ-Lactones.* European Journal of Organic Chemistry, 2008. **2008**(36): p. 6134-6143.

Chapter 3
MALDI

Matrix-Assisted Laser Desorption/Ionization (MALDI) has been extensively used for the analysis of large molecules. Nevertheless, since the technique provides soft and efficient ionization of thermolabile and non-volatile organic compounds, we decided to investigate its application to small molecules as an alternative ionization method (Section 3.1). During this study, we found evidence for the formation of cluster ions when 2,5-DHB was used as matrix. This led us to investigate the nature of such cluster ions and the influence of the flavonoid studied on their formation (Section 3.2).

This chapter was based on two publications:

- *TiO_2 anatase as matrix for MALDI analysis of small molecules*, Ana L. Castro, Paulo J. Amorim Madeira, Manuel R. Nunes, Fernanda M. Costa, M. Helena Florêncio, Rapid Communications in Mass Spectrometry 2008, 22, 3761-3766.
- *Flavonoid-Matrix cluster ions in MALDI Mass Spectrometry*, Paulo J. Amorim Madeira, M. Helena Florêncio, Journal of Mass Spectrometry, 2009, 44, 1105-1113.

3. Matrix Assisted Laser Desorption/Ionization (MALDI)

3.1. TiO_2 anatase as matrix for MALDI analysis of small molecules

3.1.1. Introduction

Matrix-assisted laser desorption/ionization (MALDI) technique has been used extensively for the mass spectrometric analysis of biomolecules such as peptides, proteins, oligonucleotides and oligosaccharides. It provides soft and efficient ionization of thermolabile and non-volatile organic compounds. [1]

Successful MALDI measurements depend strongly on the matrix performance, which plays a key role in the use of the MALDI technique. The matrix absorbs the laser light energy (UV or IR pulsed laser), causing substrate vaporization and allowing an easier analyte ionization. For such purpose, high UV absorbance (typically for a 337 nm nitrogen laser), solubility in solvents and long lifetime under vacuum conditions, are some of the properties required for a good matrix.[2] Nevertheless, co-desorption and ionization of the matrix molecules, during analyte desorption, inevitably introduce intense background matrix peaks in the low-mass region, in consequence of matrix fragmentation and ion cluster formation.[3] As a result, the use of MALDI to study small molecules (<500 Da) is considered inadequate when commonly organic MALDI matrices are used, due to interfering matrix peaks in the low mass region. The organic matrices most

commonly employed are sinapinic acid and some related cinnamic acid derivatives, 2,5-dihydroxybenzoic acid (2,5-DHB), α-cyano-4-hydroxycinnamic acid (4-HCCA), 3-hydroxypicolinic acid (HPA), and di- and triacetophenones.[2]

Inorganic matrices are being considered as an alternative approach to the use of conventional organic matrices. This approach was originally introduced by Tanaka *et al.*[4] in 1988, where fine cobalt powder, (30 nm), suspended in glycerol, was used as matrix for the analysis of polymers and proteins. Sunner *et al.*[5] and Dale *et al.*[6] have investigated the use of micro-particles of 2-150 μm diameter, of graphite and silicon dispersed in glycerol, to ionize large compounds including peptides and proteins, oligosaccharides, synthetic polymers and anionic analytes, respectively.

More recently, Kinumi *et al.* [7] described the development of a laser desorption/ionization technique for the analysis of poly(ethylene glycol), PEG200, and methyl stearate, using commercially available metal and metal oxide powder (Al, Mn, Mo, Si, Sn, SnO_2, TiO_2, W, WO_3, Zn and ZnO), suspended in glycerol or liquid paraffin. Among the tested materials, TiO_2 powder showed to be a promising medium for detection of small molecules, because of its strong absorption in the UV range.

Up to now, a variety of inorganic materials including porous silicon [8-11], carbon nanotubes [12-15], and mesoporous materials [16-18] have been reported as MALDI matrices with different degrees of success.

The good results found in the literature [7, 19, 20] when TiO_2 was used as MALDI matrix, led us to explore even further the use of these materials.

Titanium dioxide (TiO_2) is an important nontoxic material widely used in photocatalysis, sensor technology, optical coatings and pigments.[21] The three naturally occurring polymorphs of TiO_2, anatase, brookite and rutile, have different physical properties, such as refractive index, chemical reactivity and photochemical activity. With such wide variety of properties, it should be possible to tailor the appropriate material to a specific need.[22]

The purpose of the present study was to investigate the effectiveness of the performance of TiO_2 anatase and rutile, in their pure form or as a mixture, as alternative inorganic MALDI matrix for the analysis of some small molecules (<500 Da) and compare their performance with the more commonly used organic matrices. For the present study, we selected as analytes caffeine, PEG200, chloroaniline and quercetin, which belong to different classes of compounds we have investigated before.[23]

3.1.2. Results and discussion

Inorganic matrices

Caffeine, PEG200, chloroaniline and quercetin, four compounds from different classes, were analysed by matrix assisted desorption ionization, using TiO_2 anatase, TiO_2 rutile and TiO_2 Degussa P25 (70% anatase and 30% rutile) as matrices. Our objectives were to evaluate whether the different physical properties of TiO_2 polymorphs could

influence their performance as MALDI matrices and be used with advantage to obtain optimized mass spectra.

Figure 3.1 shows the MALDI mass spectra of caffeine (a), PEG200 (b), quercetin (c) and 2-chloroaniline (d) using TiO_2 anatase as matrix. In the MALDI spectra, caffeine, PEG200 and quercetin appear mainly as alkali cation (sodium or potassium) adducts whereas, interestingly, 2-chloroaniline ionizes preferentially as radical cation $M^{+\bullet}$.

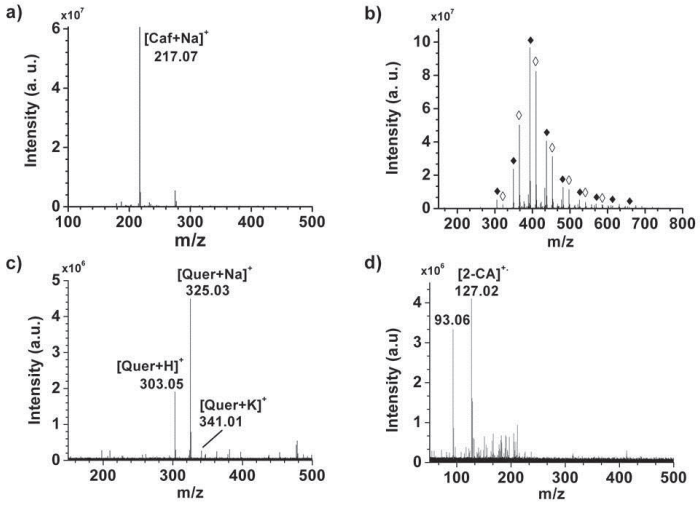

Figure 3.1. MALDI mass spectra using TiO_2 anatase as matrix of: a) caffeine; b) PEG200 (♦- sodium adducts, ◊-potassium adducts); c) quercetin; d) 2-chloroaniline.

The caffeine mass spectrum, Figure 3.1a, presents characteristic peaks at m/z 195 $[Caf+H]^+$, m/z 217 $[Caf+Na]^+$ and m/z 233 $[Caf+K]^+$. The signal intensities of protonated and potassiated caffeine are rather low when compared with the signal of sodiated caffeine.

PEG200 mass spectrum is depicted in Figure 3.1b. This mass spectrum exhibits abundant sodiated and potassiated ions. Protonated molecules are absent in the spectrum. Moreover, PEG200 exhibits a spectrum typical of a polymer. It shows, as expected, oligomeric

distributions with a difference of 44 mass units corresponding to C_2H_4O, with no fragmentation within the repeating unit.

The quercetin mass spectrum (Figure 3.1c), shows that the sodium adduct ion $[Quer+Na]^+$ and the protonated molecule $[Quer+H]^+$ are preferentially formed (m/z 325 and m/z 303 respectively). Nevertheless, the potassium adduct $[Quer+K]^+$ at m/z 341 is present, even though with lower abundance.

2-Chloroaniline ionizes preferably to a radical cation at m/z 127 (Figure 3.1d), although a protonated molecule at m/z 128 can also be observed. A closer inspection of this spectrum reveals the presence of sodium and potassium adducts (m/z 150 and m/z 166 respectively) that are less abundant, however, than the radical cation and the protonated molecule. The formation of radical ions under MALDI conditions is not uncommon, as previously reported by Lou *et al.*[24] These authors attributed the formation of radical cations during MALDI ionization of trialkoxy anilines and oligo-peptide anilides to the low ionization energy (IE) of anilines. Taking into account the reported ionization energy for 2-chloroaniline (8.50 eV [25]), the behaviour of this compound might be expected. Nevertheless, since the reported ionization energy for caffeine and quercetin are also rather low, 7.95 eV [25] and 7.22 eV [26], we anticipated a similar behaviour for these analytes, *i.e.* ionization to radical cations. Such behaviour, however, was not observed, which suggests that the formation of radical cations under MALDI conditions does not depend solely on the ionization energy of the analyte. There are reports in the literature correlating the oxidation potential and the formation of radical ions.[27] Our observations on 2-chloroaniline led us to further study the formation of radical cations when TiO_2 is used as

matrix. This is an ongoing work and the preliminary results are presented next. The investigation on the formation of radical ions using TiO_2 anatase as matrix was extended by acquiring the MALDI mass spectra of benzidine, 4-bromoaniline, 4-aminobiphenyl, 2-chloroaniline, 3-nitroaniline, 4-nitroaniline and caffeine. All these analytes were ionized as radical cations and the results are summarized in Table 3.1. The graphical representation is depicted in Figure 3.2.

Table 3.1. Ionization energy (eV), Redox potential (V vs. SCE) and radical ion abundance for the analytes under study.

Analyte	IE (eV)	E^0 (V vs SCE)	Radical Ion Abundance
Benzidine	6.9	0.50	3.33E+07
4-aminobiphenyl	7.5	0.85	4.88E+06
4-bromoaniline	7.78	1.02	8.10E+05
2-chloroaniline	8.5	1.20	1.06E+06
3-nitroaniline	8.31	1.33	1.53E+06
4-nitroaniline	8.43	1.43	4.55E+05
Caffeine	7.95	1.45	3.23E+05

As can be seen in Figure 3.2, there is a correlation between the redox potential and the formation of radical ions when TiO_2 anatase is used. As such, it seems reasonable to assume that the formation of radical ions mainly results from the abstraction of electrons from the analytes by the photogenerated holes in the valence band. Adsorption of the analyte at the surface is then mandatory for an efficient ionization.

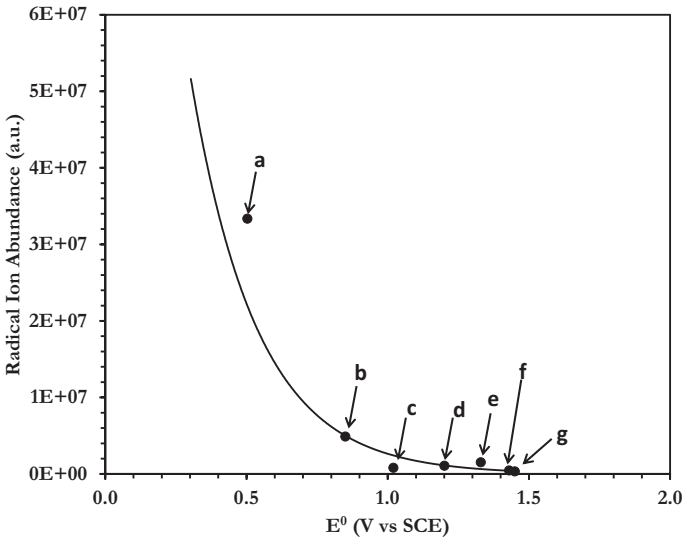

Figure 3.2. Redox Potential (E^0) vs. Radical ion abundance (the data follows an exponential trend, $y=(2\times10^8)\times e^{-4.3x}$; $R^2=0.9$; **a** - benzidine, **b** - 4-aminobiphenyl, **c** - 4-bromoaniline, **d** - 2-chloroaniline, **e** - 3-nitroaniline, **f** - 4-nitroaniline, **g** - caffeine).

We should like to emphasize that, in the analyte mass spectra, background resulting from matrix interference peaks was absent within the measured mass range. This may be due to the fact that inorganic matrices are stable during the laser desorption process.[17] These results can be attributed to special morphological properties of the matrix [28] that provide uniform dispersion of analytes, as well as an efficient energy transfer of the laser irradiation to the analyte. Indeed, it is not the first time that the efficiency of inorganic matrices is attributed to morphological characteristics (highly ordered mesostructure, high surface area and large pore volume).[17] Thus, the large surface area of the synthesized TiO_2 anatase phase (102 m^2/g [28]), together with its mesostructure, favour the dispersion of the analyte in the matrix, leading to an efficient formation of metal adduct ions.

Using TiO_2 rutile phase as matrix (results not shown), 2-chloroaniline was not ionized and caffeine was detected only as sodium adduct, with a low signal. PEG200 and quercetin showed an ionization behaviour similar to that obtained with the anatase phase as matrix, although with a clear decrease in sensitivity in the case of PEG200. Besides, the quercetin mass spectrum is hampered by background impurities suppressing the analyte signal. We therefore concluded that the use of TiO_2 rutile phase as matrix did not improve the analyte spectra. This result might be expected, since the rutile phase is a high temperature form with a reduced surface area.

With respect to the use of the mixture of anatase and rutile (70% anatase and 30% rutile), commercial TiO_2 P25, the results obtained are presented in Figure 3.3.

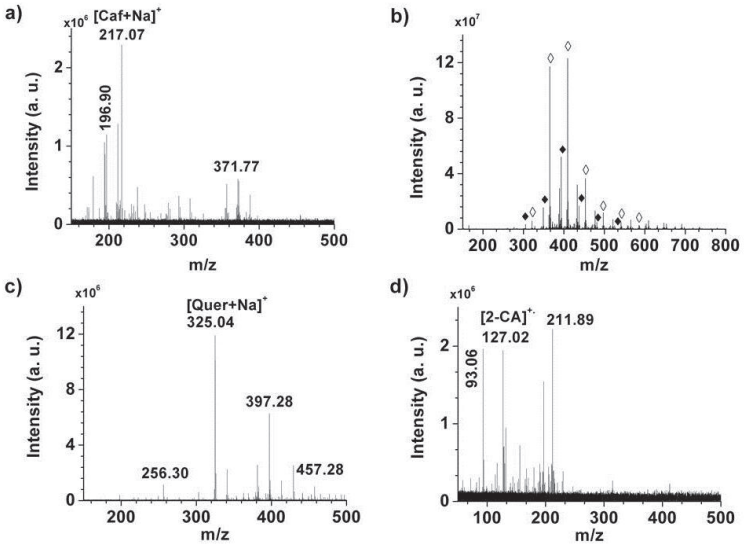

Figure 3.3. MALDI mass spectra using TiO_2 P25 as matrix of: a) caffeine; b) PEG200 (♦- sodium adducts, ◊-potassium adducts); c) quercetin; d) 2-chloroaniline.

The TiO_2 mixture shows a good ionization performance, although with quite high background. A closer analysis of the background

showed the presence of various titanium oxide clusters. Titanium species could be easily assigned due to combination of the unique isotopic characteristics of titanium and the high resolution of the instrument. TiO_2 P25 is a mixture of two phases (anatase and rutile) hence; the stability of the material upon laser irradiation may be affected. The UV laser used generates vacant oxygen sites that weaken the crystalline structure. It seems reasonable to assume that these sites are not randomly distributed but, instead, located on certain planes according to the crystal structure. Therefore, some of the high background peaks we observe in the spectra (as Figure 3.4 illustrates) can be attributed to non-stoichiometric Magneli type phases ($TinO_{2n-1}$),[29] such as Ti_4O_7 or Ti_2O_3 with H/OH species attached. It is noted that a previous literature report [29] suggested the formation of Ti_xO_{2x} clusters with a slight stoichiometric deviation.

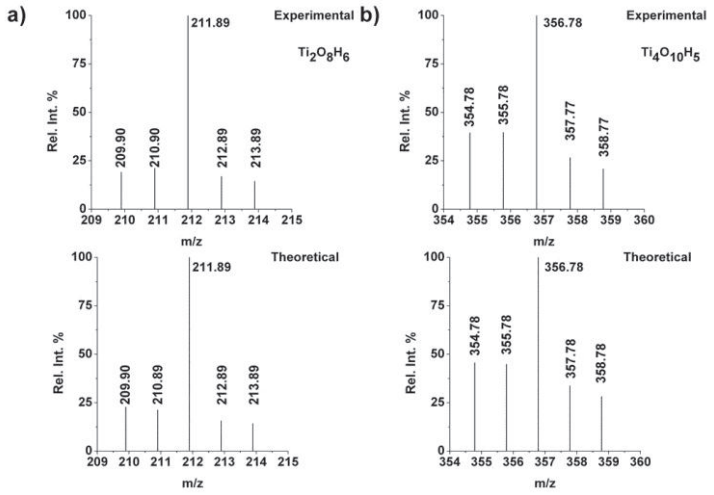

Figure 3.4. Examples of theoretical and experimental isotopic patterns: a) $Ti_2O_8H_6$ (m/z 211.89); b) $Ti_4O_{10}H_5$ (m/z 356.78).

With TiO_2 P25 as matrix, the analytes were ionized by cationization, with the exception of 2-chloroaniline, similarly to what

was observed with anatase and rutile as matrices. 2-chloroaniline ionizes preferentially to a radical cation similarly to what occurred when the anatase phase was used as matrix.

In summary, the efficiency as MALDI matrix of the TiO_2 anatase we synthesized [28] can be attributed to the mesoporosity and surface area of this material and also to the TiO_2 band gap value obtained (3.2eV). The latter value is in the same order of magnitude of the used laser, which can favour electron charge transfer and thus contribute to the formation of 2-chloroaniline radical cations. For the other analytes, gas-phase processes, or even desorption of pre-formed ions, may be responsible for their ionization (mainly as alkali adducts).

Organic matrices

For comparison purposes, we observed the MALDI spectra of the compounds under study using cinnamic acid and 2,5-dihydroxybenzoic acid, commonly used organic matrices. With cinnamic acid as matrix, caffeine was not ionized. When 2,5-DHB was used, caffeine was ionized preferably as sodiated molecule (Figure 3.5), although with significant suppression of the analyte signal, which is clear from the high background noise.

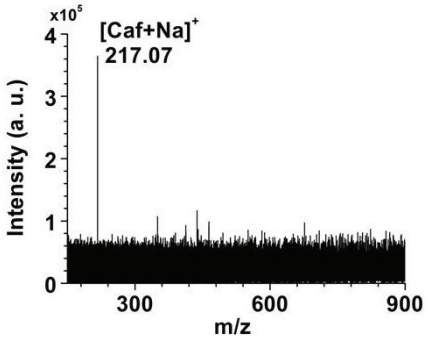

Figure 3.5. MALDI mass spectrum of caffeine using 2,5-DHB as matrix.

2-chloroaniline could not be ionized by either of the organic matrices studied.

PEG mass spectra using cinnamic acid and 2,5-DHB as matrices, Figure 3.6a and Figure 3.6b respectively, show many sodium and potassium adducts, besides matrix interfering peaks, with more intense analyte signals in the latter case. Moreover, with cinnamic acid, the MALDI mass spectrum exhibits only a few analyte ions.

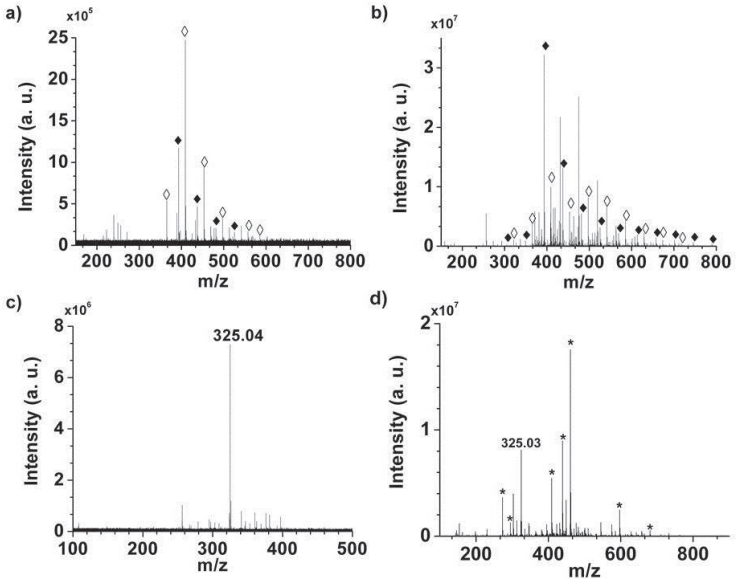

Figure 3.6. MALDI mass spectra of: a) PEG200 using cinnamic acid as matrix; b) PEG200 using 2,5-DHB as matrix; c) quercetin using cinnamic acid as matrix; d) quercetin using 2,5-DHB as matrix. (♦- sodium adducts, ◊-potassium adducts, *-matrix interference peaks)

With cinnamic acid and 2,5-DHB as matrices (Figure 3.6c and Figure 3.6d), quercetin ionizes preferentially in the form of a sodium adduct at m/z 325. Moreover, with 2,5-DHB, a large number of intense matrix interfering peaks are observed.

When comparing the mass spectra of PEG200 (Figure 3.6a and Figure 3.6b) using organic matrices, with the corresponding mass

spectrum using the nanosized TiO_2 anatase (Figure 3.1b), it is clear that with the latter matrix a much better performance can be obtained.

With respect to quercetin with cinnamic acid (Figure 3.6c), only the sodiated molecule is detected and the protonated molecule is absent. With TiO_2 anatase (Figure 3.1c), besides the sodiated molecule (m/z 325), a reasonably abundant signal for the protonated molecule (m/z 303) can be observed. These two signals, together with a lower signal for the potassiated molecule (m/z 341), might be useful as quercetin diagnostic ions when the matrix TiO_2 anatase is used.

Nanosized TiO_2 anatase appeared therefore to be more efficient as MALDI matrix than the commonly used organic matrices cinnamic acid and 2,5 dihydroxybenzoic acid.

We believe that with this work we may reinforce the use of inorganic matrices in MALDI analysis and, as such, promote the use of this technique for the analysis of small molecules.

3.1.3. Conclusions

The results here reported for four analytes, caffeine, PEG200, 2-chloroaniline and quercetin, compounds from different classes, demonstrate the potential of nanosized TiO_2 anatase phase for direct MALDI analysis of low molecular weight compounds.

Neither of the used organic matrices, cinnamic acid and 2,5-DHB, were able to ionize 2-chloroaniline and caffeine was only ionized by the latter. PEG200 mass spectra using both organic matrices showed many matrix interfering peaks and, moreover, only a few analyte ions with

cinnamic acid. Quercetin spectra showed a large number of intense matrix interfering peaks with 2,5-DHB in particular.

With respect to TiO_2 anatase, all the analytes under study were ionized. Besides strong analyte signals, background from TiO_2 matrix peaks was absent in the mass spectra. Moreover, TiO_2 pure forms, anatase and rutile, the former in particular, revealed a better performance as matrices than the TiO_2 mixture. Furthermore, the absence of matrix peaks when TiO_2 pure forms are used, has been attributed to enhanced stability of these materials upon the laser irradiation. It is also shown that the TiO_2 phase type plays an important role in the analyte ionization process. The nanosized TiO_2 anatase showed to be a better matrix for the MALDI analysis of small molecules.

3.2. Flavonoid-Matrix cluster ions in MALDI Mass Spectrometry

3.2.1. Introduction

Matrix-Assisted Laser Desorption/Ionization (MALDI) has been used extensively for the mass spectrometric analysis of large, non-volatile biomolecules (e.g. peptides,[30] proteins,[31] oligonucleotides and oligosaccharides), synthetic polymers of high molecular weight, fullerenes and fullerene derivatives, high molecular weight environmental materials (e.g. humic and fulvic acids), as well as, under certain conditions, noncovalent complexes.[32] The application of MALDI to the analysis of small molecules is rendered difficult because of usually high matrix background signals in the low mass region.[3, 33]

The MALDI ionization process can be roughly divided into two steps: firstly the analyte molecules must be desorbed from a solid crystalline matrix into the vacuum and secondly the desorption plume must be ionized.[34] The desorption process has been the subject of a number of studies that led to several theoretical models to accurately describe the desorption process.[32, 34] It is now believed that this desorption process has mechanical elements and that it is independent of the ionization processes.[35] It has become generally accepted that after photon absorption from the laser beam, the matrix molecules go through a rapid phase change, from the solid to the gas phase. The sublimed matrix molecules form a dense gas plume embedding the analyte molecules, which undergoes a supersonic expansion into the vacuum, carrying the analyte into the gas phase either as neutrals, or

already as ionized species.[34] Despite the large number of MALDI applications, the nature of the ionization process that leads to the ionization of the analyte is still not fully understood.

The matrix plays an important role in MALDI. It absorbs the laser light energy (UV or IR pulsed laser) causing substrate vaporization (converting the photon energy into mechanical energy) and allowing an easier analyte ionization. For such purpose, high UV absorbance (typically for a 337 nm nitrogen laser), solubility in solvents and long lifetime under vacuum conditions, are some of the properties required for a good MALDI matrix.[2]

Matrix-analyte cluster formation is not uncommon in MALDI mass spectrometry. Many of the common matrices show complex ionization behaviour, yielding protonated and deprotonated molecules and even-electron cluster ions.[35-37] These cluster ions may play an important role in the MALDI ionization process and it is believed that they form the prerequisite for an efficient photoionization.[38] Cluster proton transfer, for example, may contribute to the MALDI ionization process since it is expected that small matrix/analyte cluster ions will be formed during the laser induced phase transition[39] resulting in protonated analyte species.[36, 40]

2,5-dihydroxybenzoic acid (2,5-DHB) is probably, of all MALDI matrices, the most thoroughly studied.[41] It is therefore an excellent matrix for investigating cluster ion formation and thus contributing to further elucidate the nature of the ionization process. Flavonoids, on the other hand, are compounds of recognized biological interest, also thoroughly studied, which makes them excellent analyte model molecules for cluster ion investigation. The behaviour of some

flavonoids under MALDI conditions have been already reported in the literature,[42, 43] but to our knowledge no evidence for the formation of flavonoids-matrix ion clusters has been presented. We decided therefore to investigate, under MALDI conditions, the formation of analyte/matrix cluster ions using as analytes some flavonoids we have been studying for a few years already[33, 44-49] and, as matrix, 2,5-DHB. Our interest in the present report is mainly focused on whether cluster ion formation and/or reactions in the ionized clusters could be detected, as well as on the nature of the detected species. These cluster ion species, however, might also be helpful for the analysis of this type of analytes when present in trace amounts in complex mixtures.

3.2.2. Results and Discussion

2,5-DHB behaviour

Figure 3.7a depicts the 2,5-DHB mass spectrum. Interestingly, abundant protonated multimer species based on 2,5-DHB dehydrated moieties could be detected. The protonated dimer and trimer dehydrated 2,5-DHB species were found at m/z 273 and m/z 409, the structure of which was proposed by Wallace *et al.*[41] The sodiated dimer (m/z 295) and trimer (m/z 431) were also found, but with a lower abundance. This observation is consistent with the fact that formic acid was added to the 2,5-DHB suspension, thus promoting protonation. The formation of the protonated dimeric species was already reported by Wallace *et al.*[41] The condensation of more than three 2,5-DHB molecules had not been predicted by these authors since they assumed that the resulting structures would have unfavourable geometries,

resulting in ring strain.[41] Nevertheless, we also found, and with significant abundance, protonated tetramers at m/z 545, pentamers at m/z 681, hexamers at m/z 817 and heptamers at m/z 953 (Figure 3.7). Our attributions for the ions at m/z 273, m/z 409 and m/z 545 were confirmed by MS^2 experiments (Figure 3.7b-d) and by accurate mass data presented in Table 3.2. The remaining attributions were confirmed only by accurate mass data (Table 3.2).

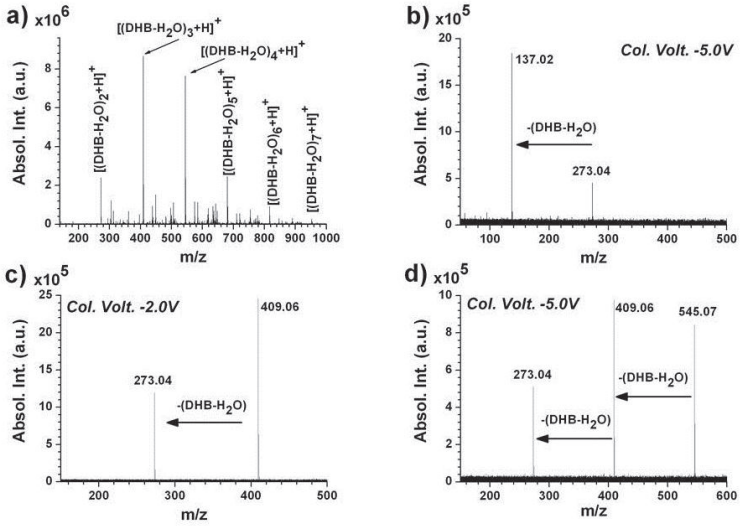

Figure 3.7. Laser Desorption Ionization Mass Spectra of 2,5-DHB, at a laser power of 80%: a) full scan spectrum; b) MS^2 spectrum of m/z 273.04 at a collision voltage of -5.0 V; c) MS^2 spectrum of m/z 409.06 at a collision voltage of -2.0 V; d) MS^2 spectrum of m/z 545.07 at a collision voltage of -5.0 V.

Besides the multimeric matrix species resulting from DHB dehydration, we also found evidence for the formation of other DHB cluster ions, even though with a much lower abundance. For example, in the spectrum of 2,5-DHB (Figure 3.7), high accuracy mass measurements allowed us to attribute the ion at m/z 313.03178 to $[DHB+(DHB-H_2O)+Na]^+$ (with an error of 0.29 ppm) and the ion at

m/z 335.01372 to $[(DHB\text{-}H+Na)+(DHB\text{-}H_2O)+Na]^+$ (with an error of 0.00 ppm).

Table 3.2. 2,5-DHB cluster ion attributions (dehydrated entities only).

Ion	*m/z*		Error (ppm)
	Theoretical	Measured	
$[(DHB\text{-}H_2O)_2+H]^+$	273.03936	273.03935	0.05
$[(DHB\text{-}H_2O)_2+Na]^+$	295.02131	295.02142	-0.38
$[(DHB\text{-}H_2O)_3+H]^+$	409.05541	409.05540	0.02
$[(DHB\text{-}H_2O)_3+Na]^+$	431.03735	431.03738	-0.06
$[(DHB\text{-}H_2O)_4+H]^+$	545.07145	545.07124	0.39
$[(DHB\text{-}H_2O)_4+Na]^+$	567.05340	567.05292	0.84
$[(DHB\text{-}H_2O)_5+H]^+$	681.08750	681.08745	0.07
$[(DHB\text{-}H_2O)_6+H]^+$	817.10354	817.10375	-0.26
$[(DHB\text{-}H_2O)_7+H]^+$	953.11958	953.11975	-0.17

$DHB\text{-}H_2O=C_7H_4O_3$

Quercetin behaviour

The analysis of the MALDI mass spectrum of quercetin (Figure 3.8a) reveals that quercetin ionizes preferentially as a sodium adduct (*m/z* 325), although the protonated molecule is also abundant (*m/z* 303). We also found experimental evidence for the formation of quercetin and matrix cluster ions. From the MS^2 spectra presented in Figure 3.8b-d and taking into account the accurate mass data presented in Table 3.3 the ions at *m/z* 461 and *m/z* 575 were attributed to $[Quer+(DHB\text{-}H_2O)+Na]^+$ and $[Quer+(DHB\text{-}H_2O)_2+H]^+$, respectively. An interesting observation concerns the spectrum shown in Figure 3.8c, in which the ion at *m/z* 575 loses 136Da (dehydrated DHB) in order to form the ion at *m/z* 439, that corresponds to $[Quer+(DHB\text{-}H_2O)+H]^+$,

and loses 302 Da (quercetin) as well, in order to form the ion at m/z 273 that corresponds, as observed for DHB, to $[(DHB\text{-}H_2O)_2+H]^+$.

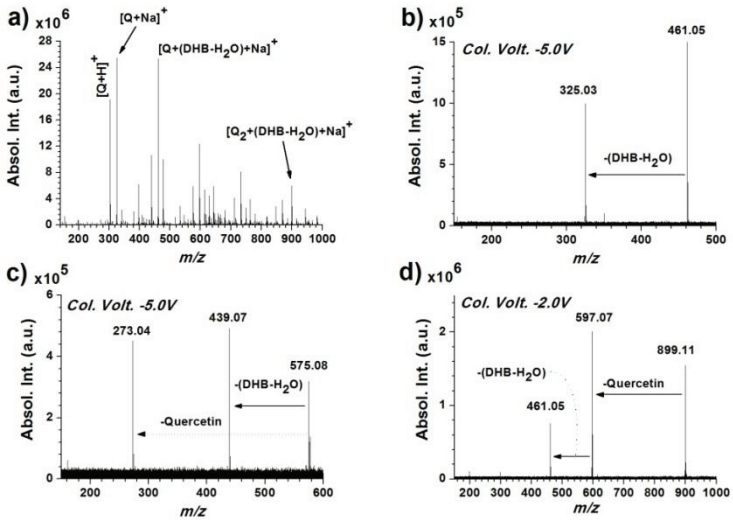

Figure 3.8. MALDI Mass Spectra of quercetin at a laser power of 80%: a) full scan spectrum; b) MS^2 spectrum of m/z 461.05 at a collision voltage of -5.0 V; c) MS^2 spectrum of m/z 575.08 at a collision voltage of -5.0 V; d) MS^2 spectrum of m/z 899.11 at a collision voltage of -2.0 V. (Q stands for Quercetin)

The ion at m/z 439 loses 136 Da (Figure 3.9), that corresponds to DHB-H_2O, to form the protonated quercetin molecule at m/z 303. The ion corresponding to $[DHB\text{-}H_2O+H]^+$, observed in the 2,5-DHB MALDI mass spectrum, was not detected. This fact may be indicative of the occurrence of a proton transfer reaction between the protonated DHB-H_2O and the quercetin molecule within the cluster structure.

Furthermore, the fact that protonated quercetin is not present in the m/z 575 product ion spectrum (Figure 3.8c) allowed us to speculate that the proton transfer between $[(DHB\text{-}H_2O)_2+H]^+$ and quercetin is not energetically favoured, i.e. the proton affinity of quercetin may be lower than the proton affinity of the dehydrated DHB cluster ion. A

possible structure for the ion at *m/z* 575, consistent with its product ion spectrum (Figure 3.8c) is depicted in Scheme 3.1. Moreover, this proposal, where hydrogen bonds are formed, seems reasonable, taking into account literature reports on the formation of hydrogen bonded clusters using mass spectrometry desorption ionization techniques.[40, 50, 51]

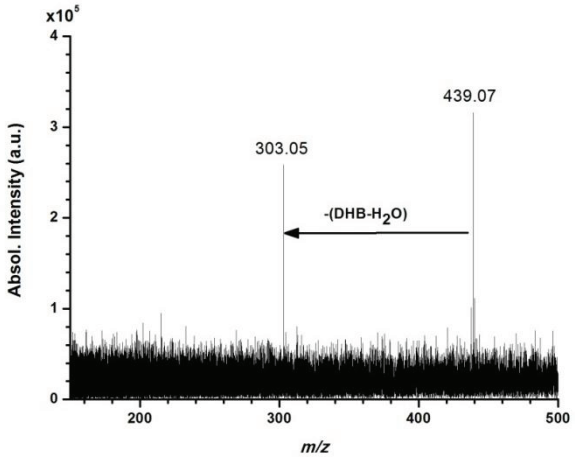

Figure 3.9. MS^2 spectrum of the ion at *m/z* 439 at a collision voltage of -3 V.

The ion at *m/z* 899, also present in quercetin MALDI mass spectrum, loses 302 Da (quercetin) to form the ion at *m/z* 597 (Figure 3.8d) which may, in turn, lose 136 Da (DHB-H_2O) to form the ion at *m/z* 461. Taking into account these losses and the accurate mass data (Table 3.3), we can attribute the peak at *m/z* 899 to $[Quer_2+(DHB-H_2O)_2+Na]^+$.

In addition, we also found evidence for quercetin clusters with metal cations. Indeed, based on MS^2 experiments (see Figure 3.10), the ions at *m/z* 627, *m/z* 945 and *m/z* 1247 (low intensity signals) were attributed to sodiated quercetin dimer, potassiated quercetin trimer and

potassiated quercetin tetramer, respectively. Similar sodiated quercetin multimers (n>2) could not be detected.

Table 3.3. Quercetin-DHB cluster ion attributions. (Quer stands for quercetin)

Ion	*m/z*		Error (ppm)
	Theoretical	Measured	
$[Quer+H]^+$	303.04993	303.04982	0.36
$[Quer+Na]^+$	325.03187	325.03175	0.37
$[Quer+K]^+$	341.00581	341.00584	-0.09
$[Quer+(DHB-H_2O)+H]^+$	439.06597	439.06579	0.41
$[Quer+(DHB-H_2O)+Na]^+$	461.04792	461.04778	0.30
$[Quer+(DHB-H_2O)+K]^+$	477.02185	477.02178	0.15
$[Quer+(DHB-H_2O)_2+H]^+$	575.08202	575.08175	0.47
$[Quer+(DHB-H_2O)_2+Na]^+$	597.06396	597.06383	0.22
$[Quer+(DHB-H_2O)_2+K]^+$	613.03790	613.03793	-0.05
$[Quer+(DHB-H_2O)_3+H]^+$	711.09806	711.09745	0.86
$[Quer+(DHB-H_2O)_3+Na]^+$	733.08001	733.0796	0.56
$[Quer+(DHB-H_2O)_3+K]^+$	749.05394	749.05326	0.91
$[Quer+(DHB-H_2O)_4+H]^+$	847.11411	847.11359	0.61
$[Quer+(DHB-H_2O)_4+Na]^+$	869.09605	869.09641	-0.41
$[Quer+(DHB-H_2O)_4+K]^+$	885.06999	885.06775	2.53
$[Quer_2+(DHB-H_2O)_2+Na]^+$	899.10661	899.10636	0.28

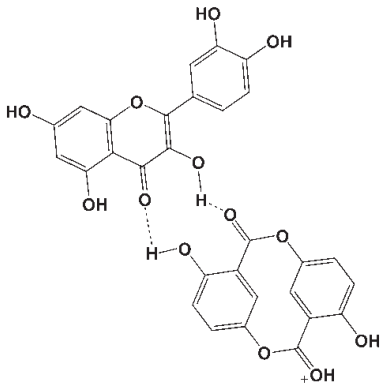

Scheme 3.1: Proposed structure for the ion at *m/z* 575 $[Quer+(DHB-H_2O)_2+H]^+$.

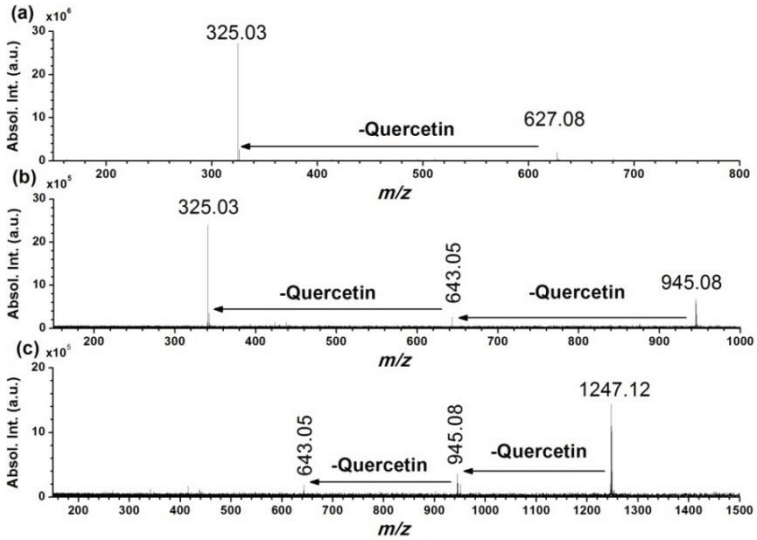

Figure 3.10. MS^2 spectrum of: a) m/z 627.08 at a collision voltage of -0.5 V; b) MS^2 spectrum of m/z 945.08 at a collision voltage of -1.5 V; c) MS^2 spectrum of m/z 1247.12 at a collision voltage of -0.5 V.

It appears therefore to be clear from our experimental results, that the potassiated high mass cluster ions are much more stable than the sodiated and protonated counterparts. The formation of high mass Na^+-bound quercetin clusters has been previously reported in the literature using electrospray ionization[52], but not, to the best of our knowledge, under MALDI conditions. Moreover, the high abundance of potassiated cluster ions is an interesting observation that, to best of our knowledge, has not yet been reported. The high abundance of potassiated clusters can be attributed to a stabilization phenomenon perpetrated by the metal cation, potassium in this case. This does not seem unreasonable, since it is known that the cation size plays an important role in cluster formation processes for nucleobases.[53-55] Moreover, it has been reported for sugars that the smaller the alkali metal ion, the greatest the fragmentation of the analyte, and hence the lower the stabilization by the metal.[56]

Myricetin behaviour

The MALDI mass spectrum of myricetin is depicted in Figure 3.11a. The analysis of this spectrum reveals that myricetin ionizes in the form of a protonated molecule (*m/z* 319), as well as in the form of a sodium adduct (*m/z* 341). We have also found experimental evidence for the formation of myricetin and DHB cluster ions, similarly to what was found for quercetin. The MS^2 spectra of the ions at *m/z* 591, *m/z* 863 and *m/z* 931 are presented in Figure 3.11b-d, respectively. The ion at *m/z* 591 (Figure 3.11b) loses 136 Da, corresponding to the loss of one DHB-H_2O moiety, in order to form the ion at *m/z* 455. The ion at *m/z* 591 can also lose 318 Da, that corresponds to neutral myricetin, thus forming the ion at *m/z* 273, attributed to $[(DHB\text{-}H_2O)_2+H]^+$. This information, along with the accurate mass data presented in Table 3.4, allowed us to attribute the ion at *m/z* 591 to $[Myr+(DHB\text{-}H_2O)_2+H]^+$.

The ion at *m/z* 863 (Figure 3.11c) loses 318 Da, that corresponds to neutral myricetin, forming the ion at *m/z* 545. This ion can, in turn, lose 136Da, (DHB-H_2O), to form the ion at *m/z* 409. The latter ion can lose another 136 Da to form the ion at *m/z* 273. Taking into account these observations, as well as the accurate mass data presented in Table 3.4, we can attribute the ion at *m/z* 863 to $[Myr+(DHB\text{-}H_2O)_4+H]^+$.

The ion at *m/z* 931 (Figure 3.11d) loses 318 Da (neutral myricetin), forming the ion at *m/z* 613 that, in turn, can lose 136 Da (DHB-H_2O), giving rise to the ion at *m/z* 477. Taking into account this information and the accurate mass data presented in Table 3.4, we can attribute the ion at *m/z* 931 to $[Myr_2+(DHB\text{-}H_2O)_2+Na]^+$.

The protonated dimer, unlike quercetin, was not found. Nevertheless, the sodiated dimer was found at m/z 659, with a low abundance (see Table 3.4). Myricetin trimer (protonated or sodiated) was also not found.

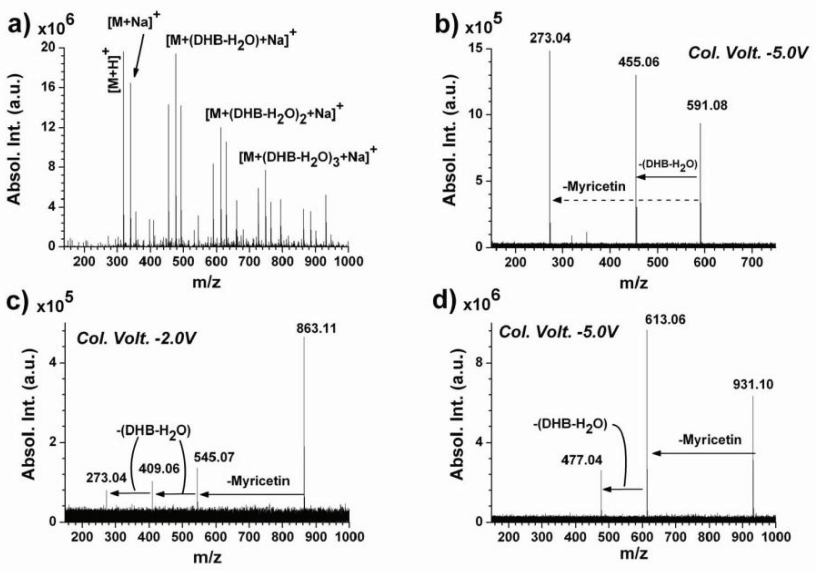

Figure 3.11. MALDI Mass Spectra of myricetin at a laser power of 80%: a) full scan spectrum; b) MS^2 spectrum of m/z 591.08 at a collision voltage of -5.0 V; c) MS^2 spectrum of m/z 863.11 at a collision voltage of -2.0 V; d) MS^2 spectrum of m/z 931.10 at a collision voltage of -5.0 V. (M stands for Myricetin)

Table 3.4. Myricetin-DHB cluster ion attributions. (Myr stands for myricetin)

Ion	*m/z*		Error (ppm)
	Theoretical	Measured	
$[Myr+H]^+$	319.04484	319.04478	0.19
$[Myr+Na]^+$	341.02679	341.02674	0.15
$[Myr+K]^+$	357.00073	357.00073	0.00
$[Myr+(DHB-H_2O)+H]^+$	455.06089	455.06078	0.24
$[Myr+(DHB-H_2O)+Na]^+$	477.04283	477.04289	-0.13
$[Myr+(DHB-H_2O)+K]^+$	493.01675	493.01675	0.00
$[Myr+(DHB-H_2O)_2+H]^+$	591.07693	591.07694	-0.02
$[Myr+(DHB-H_2O)_2+Na]^+$	613.05888	613.05901	-0.21
$[Myr+(DHB-H_2O)_2+K]^+$	629.03281	629.03282	-0.02
$[Myr+(DHB-H_2O)_3+H]^+$	727.09298	727.09284	0.19
$[Myr+(DHB-H_2O)_3+Na]^+$	749.07492	749.07494	-0.03
$[Myr+(DHB-H_2O)_3+K]^+$	765.04886	765.04792	1.23
$[Myr+(DHB-H_2O)_4+H]^+$	863.10902	863.10849	0.61
$[Myr+(DHB-H_2O)_4+Na]^+$	885.09096	885.09124	-0.32
$[Myr_2+Na]^+$	659.06436	659.06449	-0.20
$[Myr_2+(DHB-H_2O)_2+Na]^+$	931.09644	931.09621	0.25

Luteolin behaviour

Figure 3.12a depicts the MALDI mass spectrum of luteolin. The analysis of this spectrum reveals that luteolin ionizes in the form of a protonated molecule (*m/z* 287), but mainly in the form of a sodium adduct (*m/z* 309). The potassium adduct was also found (*m/z* 325), although with significantly less abundance than the latter. Similarly to quercetin and myricetin, luteolin also forms ion clusters with the matrix. However, the number of clusters formed is lower than the ones formed with quercetin and myricetin. The MS^2 spectra of the ions at *m/z* 423, *m/z* 559 and *m/z* 581 are presented in Figure 3.12b-d, respectively. The ion at *m/z* 423 (Figure 3.12b) loses 136 Da (DHB-H_2O) to form the ion

at m/z 287 (protonated luteolin). This fragmentation, along with the accurate mass data presented in Table 3.5, allowed us to attribute the m/z 423 ion to $[Lut+(DHB-H_2O)+H]^+$.

The ion at m/z 559 (Figure 3.12c) loses 136 Da (DHB-H_2O), thus forming the ion m/z 423, i.e. $[Lut+(DHB-H_2O)+H]^+$, meaning that the ion isolated can be attributed to $[Lut+(DHB-H_2O)_2+H]^+$ in agreement with the accurate mass data (Table 3.5). This ion (m/z 559) can also lose neutral luteolin (286 Da), giving rise to the ion at m/z 273 and also two DHB-H_2O (272 Da) affording the ion at m/z 287. Taking into account the abundances of the ions at m/z 273 and m/z 287, it seems clear that the ion at m/z 273 is more stable than the ion at m/z 287, i.e. the loss of neutral luteolin is energetically more favourable than the loss of two dehydrated 2,5-DHB molecules.

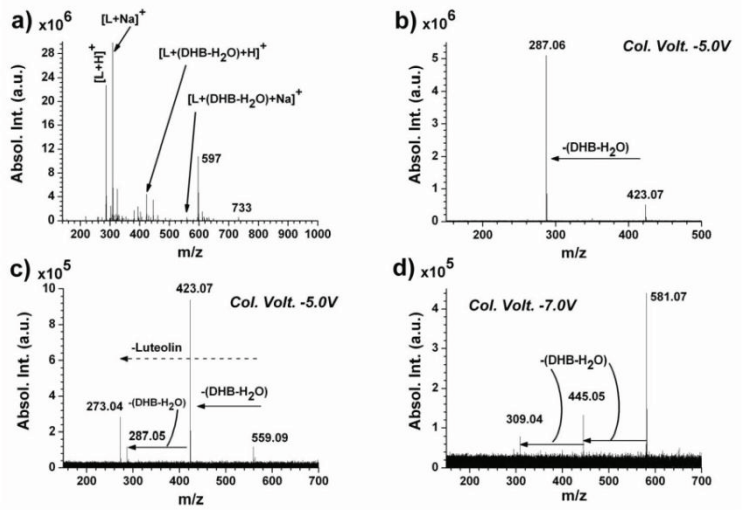

Figure 3.12. MALDI Mass Spectra of luteolin at a laser power of 80%: a) full scan spectrum; b) MS^2 spectrum of m/z 423.07 at a collision voltage of -5.0 V; c) MS^2 spectrum of m/z 559.09 at a collision voltage of -5.0 V; d) MS^2 spectrum of m/z 581.07 at a collision voltage of -7.0 V. (L stands for Luteolin)

Table 3.5. Luteolin-DHB cluster ion attributions. (Lut stands for luteolin)

Ion	*m/z*		Error (ppm)
	Theoretical	Measured	
$[Lut+H]^+$	287.05502	287.05495	0.23
$[Lut+Na]^+$	309.03696	309.03684	0.39
$[Lut+K]^+$	325.01090	325.01093	-0.10
$[Lut+(DHB-H_2O)+H]^+$	423.07106	423.07183	-1.82
$[Lut+(DHB-H_2O)+Na]^+$	445.05300	445.05359	-1.32
$[Lut+(DHB-H_2O)+K]^+$	461.02694	461.02740	-1.00
$[Lut+(DHB-H_2O)_2+H]^+$	559.08710	559.08815	-1.87
$[Lut+(DHB-H_2O)_2+Na]^+$	581.06905	581.06927	-0.38

The ion at *m/z* 581 (Figure 3.12d) loses one dehydrated 2,5-DHB molecule (136 Da), forming the ion at *m/z* 445. This ion (*m/z* 445) can lose another 136 Da, affording the ion at *m/z* 309 that is attributed to the sodiated luteolin. Taking into account this fragmentation pattern and the accurate mass data (Table 3.5), we can attribute the *m/z* 581 ion to $[Lut+(DHB-H_2O)_2+Na$.

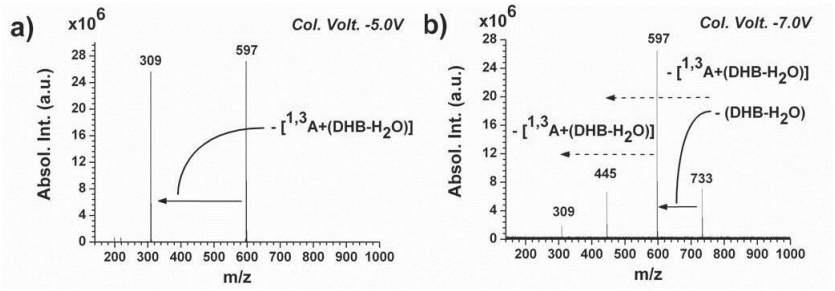

Figure 3.13. MS^2 spectra of the luteolin ions at: a) *m/z* 597 (collision voltage -5.0 V); b) *m/z* 733 (collision voltage -7.0 V).

Furthermore, in the MALDI mass spectrum of luteolin (Figure 3.12a) there is a relatively large peak at *m/z* 597 and a less intense peak at *m/z* 733. The MS^2 spectra of these ions are presented in Figure 3.13. The ion at *m/z* 597 (Figure 3.13a) loses 288 Da, affording the sodiated

luteolin at m/z 309. The ion at m/z 733 (Figure 3.13b) loses 136 Da, corresponding to one dehydrated DHB molecule, thus forming the ion at m/z 597. It can also lose 288 Da, originating the ion at m/z 445, that was earlier attributed to $[Lut+(DHB-H_2O)+Na]^+$. The loss of 288 Da is consistent with the loss of a luteolin neutral fragment ($^{1,3}A$) attached to a dehydrated DHB molecule. To support these attributions, we found evidence for the formation of $[^{1,3}B+(DHB-H_2O)+H]^+$ ion at m/z 271.06027 and $[^{1,3}B+(DHB-H_2O)+Na]^+$ at m/z 293.04184 with -0.63 ppm and 0.68 ppm of error, respectively. The ion nomenclature, well documented in the literature,[57] is presented in Scheme 3.2 for the particular case of luteolin. Taking into account these findings, the ion at m/z 733 is attributed to $[Lut+(DHB-H_2O)_2+(^{1,3}A)+Na]^+$ and the ion at m/z 597 to $[Lut+(DHB-H_2O)+(^{1,3}A)+Na]^+$, with 5.23 and 1.99 ppm of error, respectively.

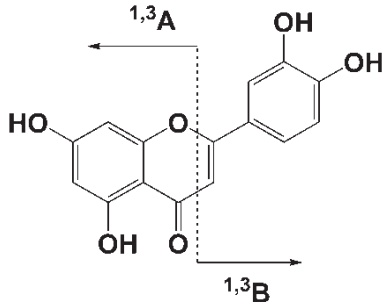

Scheme 3.2: $^{1,3}A$ and $^{1,3}B$ ions for luteolin, according to systematic ion nomenclature.[57]

Kaempferol behaviour

Figure 3.14a depicts the MALDI mass spectrum of kaempferol, a flavonol with the same molecular formula as luteolin, a flavone (Scheme 3.3).

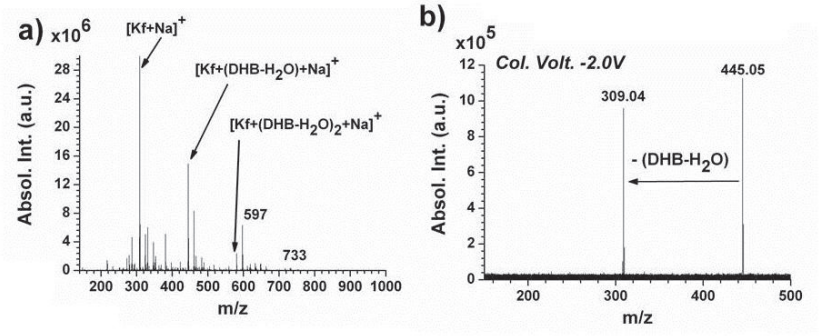

Figure 3.14. MALDI Mass Spectra of kaempferol at a laser power of 80%: a) full scan spectrum; b) MS^2 spectrum of m/z 445.05 at a collision voltage of -2.0 V. (Kf stands for Kaempferol)

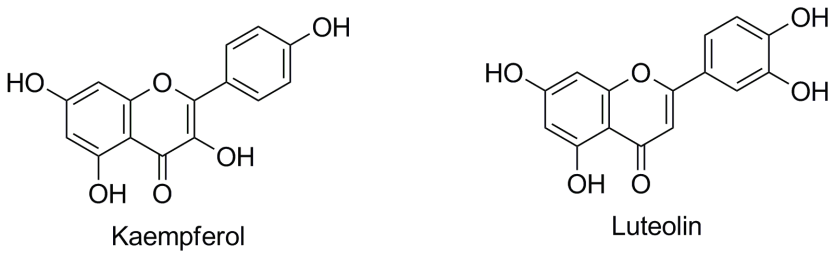

Scheme 3.3. Kaempferol and Luteolin structure

The analysis of this spectrum shows that kaempferol forms ion clusters with the matrix in greater number than luteolin. In fact, quercetin, myricetin and kaempferol form a far greater number of clusters with the matrix than luteolin, i.e. the structural features of the analyte influence their ability to form clusters. The presence of the OH

group in the C-ring of kaempferol allows for an easier cluster ion formation. Comparing the kaempferol spectrum (Figure 3.14a) with the luteolin spectrum (Figure 3.12a), it appears that the main differences between these two isobaric flavonoid aglycons are mainly related to the actual number of clusters (higher for kaempferol).

The MS^2 spectrum of the ion at m/z 445 is depicted in Figure 3.14b. This ion loses 136 Da, i.e. DHB-H_2O, originating the ion at m/z 309, attributed to the sodiated kaempferol, with an error of about 1.2 ppm (see Table 3.6), similarly to what was observed for luteolin. The MS^2 spectrum of the ion at m/z 581 is depicted in Figure 3.15. This ion loses 136 Da, i.e. DHB-H_2O, affording the ion at m/z 445 (already addressed above) and was attributed to a sodiated cluster composed of kaempferol and two dehydrated DHB moieties, with an error well below 0.5 ppm (see Table 3.6). The remaining attributions, presented in Table 3.6, were made taking into account the accurate mass data.

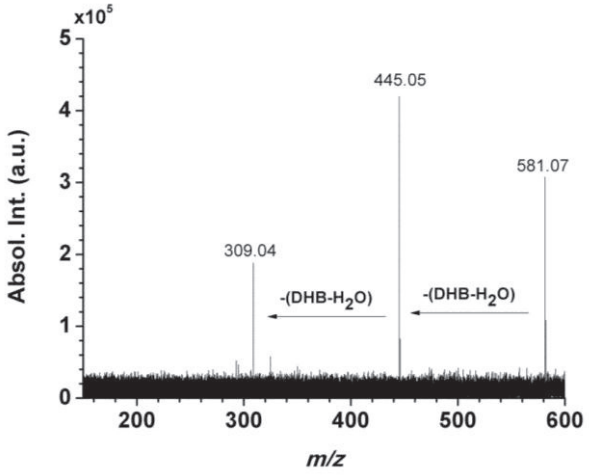

Figure 3.15. MS^2 spectrum of the m/z 581 ion of Kaempferol, at a collision voltage of -5 V.

Kaempferol also exhibits the neutral fragment/dehydrated DHB that were found for luteolin. Moreover, with kaempferol we found the $[Kaem+(DHB-H_2O)+^{1,3}A+Na]^+$ ion at m/z 597.06065 and the $[Kaem+(DHB-H_2O)_2+^{1,3}A+Na]^+$, at m/z 733.07619, with 5.54 and 5.21 ppm of error, respectively. These attributions were made taking into account the accurate mass data presented and MS^2 spectra depicted in Figure 3.16.

Also similarly to luteolin, we found the corresponding $[^{1,3}B+(DHB-H_2O)+H]^+$ at m/z 271.06018 and the $[^{1,3}B+(DHB-H_2O)+Na]^+$ at 293.04213, with -0.30 and -0.31 ppm of error, respectively. The $^{1,3}B^+$ ion, typical in flavonoid fragmentation, was already reported in the literature for kaempferol, but under ESI conditions.[58] It is worth mentioning that these cluster ions with retro Diels Alder fragments, intact flavonoids and dehydrated DHB, here reported, were detected only for kaempferol and luteolin. For quercetin and myricetin, only the protonated retro Diels Alder fragment and dehydrated DHB ions, $[^{1,3}B+(DHB-H_2O)]^+$, were detected, but with a very low abundance.

Table 3.6. Kaempferol-DHB cluster ion attributions. (Kaem stands for kaempferol)

Ion	*m/z*		Error (ppm)
	Theoretical	Measured	
$[Kaem+H]^+$	287.05502	287.05489	0.44
$[Kaem+Na]^+$	309.03696	309.03660	1.16
$[Kaem+K]^+$	325.01090	325.01096	-0.20
$[Kaem+(DHB-H_2O)+H]^+$	423.07106	423.07114	-0.19
$[Kaem+(DHB-H_2O)+Na]^+$	445.05300	445.05276	0.55
$[Kaem+(DHB-H_2O)+K]^+$	461.02694	461.02716	-0.48
$[Kaem+(DHB-H_2O)_2+H]^+$	559.08710	559.08690	0.36
$[Kaem+(DHB-H_2O)_2+Na]^+$	581.06905	581.06904	0.01
$[Kaem+(DHB-H_2O)_3+Na]^+$	717.08509	717.08300	2.91
$[Kaem_2+(DHB-H_2O)_2+Na]^+$	731.10074	731.09923	2.07

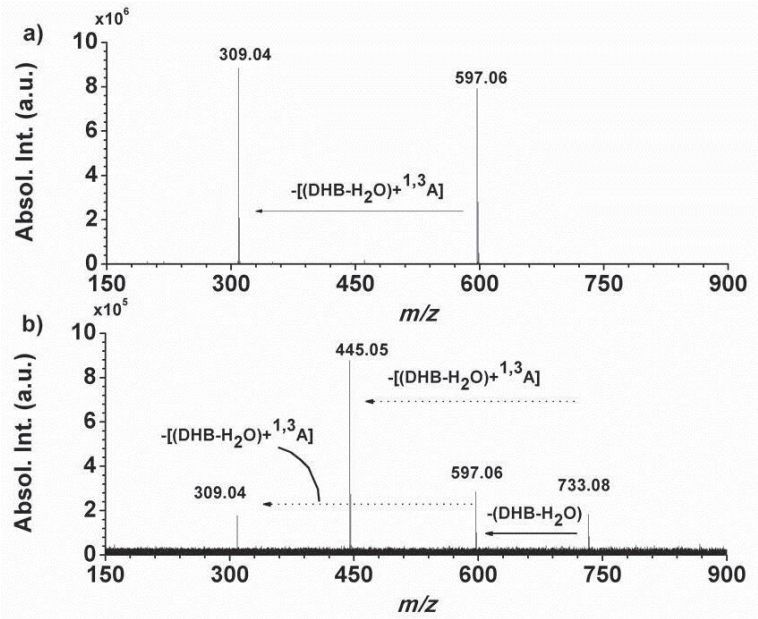

Figure 3.16. MS^2 spectrum of kaempferol ions at: a) *m/z* 597 (collision voltage -5.0 V); b) *m/z* 733 (collision voltage -5.0 V).

3.2.3. Conclusions

For 2,5-DHB we found evidence for the formation of multimeric species based on the dehydrated DHB moiety. Besides dehydrated DHB dimers and trimers species, already documented, we also found tetramers (confirmed by means of MS^2 experiments), pentamers, hexamers and heptamers, confirmed by high accuracy mass measurements.

All the flavonoids under study formed cluster ions (protonated, sodiated and potassiated) with the dehydrated DHB moiety. We also found evidence for the formation of a sodiated quercetin dimer attached to two dehydrated DHB molecules. Myricetin behaved quite similarly to quercetin. Unlike quercetin and myricetin, which readily form cluster ions with various dehydrated DHB molecules, luteolin and kaempferol only form clusters with up to one dehydrated DHB (luteolin) or up to two dehydrated DHB molecules (kaempferol). For these two flavonoids, we found evidence for the formation of cluster ions involving retro Diels Alder fragments and intact flavonoids molecules, as well as the corresponding protonated retro Diels Alder fragment with dehydrated DHB molecules.

3.3. References

1. Ashcroft, A.E., *Ionization Methods in Organic Mass Spectrometry*. 1997, Cambridge: The Royal Society of Chemistry.
2. Vestal, M.L., *Methods of Ion Generation.* Chemical Reviews, 2001. **101**(2): p. 361-376.
3. Guo, Z. and L. He, *A binary matrix for background suppression in MALDI-MS of small molecules.* Analytical and Bioanalytical Chemistry, 2007. **387**(5): p. 1939-1944.
4. Tanaka, K., et al., *Protein and polymer analyses up to m/z 100 000 by laser ionization time-of-flight mass spectrometry.* Rapid Communications in Mass Spectrometry, 1988. **2**(8): p. 151-153.
5. Sunner, J., E. Dratz, and Y.-C. Chen, *Graphite surface-assisted laser desorption/ionization time-of-flight mass spectrometry of peptides and proteins from liquid solutions.* Analytical Chemistry, 1995. **67**(23): p. 4335-4342.
6. Dale, M.J., R. Knochenmuss, and R. Zenobi, *Graphite/Liquid Mixed Matrices for Laser Desorption/Ionization Mass Spectrometry.* Analytical Chemistry, 1996. **68**(19): p. 3321-3329.
7. Kinumi, T., et al., *Matrix-assisted laser desorption/ionization time-of-flight mass spectrometry using an inorganic particle matrix for small molecule analysis.* Journal of Mass Spectrometry, 2000. **35**(3): p. 417-422.
8. Cuiffi, J.D., et al., *Desorption-Ionization Mass Spectrometry Using Deposited Nanostructured Silicon Films.* Analytical Chemistry, 2001. **73**(6): p. 1292-1295.

9. Shen, Z., et al., *Porous Silicon as a Versatile Platform for Laser Desorption/Ionization Mass Spectrometry.* Analytical Chemistry, 2000. **73**(3): p. 612-619.

10. Finkel, N.H., et al., *Ordered Silicon Nanocavity Arrays in Surface-Assisted Desorption/Ionization Mass Spectrometry.* Analytical Chemistry, 2005. **77**(4): p. 1088-1095.

11. Go, E.P., et al., *Desorption/Ionization on Silicon Nanowires.* Analytical Chemistry, 2005. **77**(6): p. 1641-1646.

12. Xu, S., et al., *Carbon Nanotubes as Assisted Matrix for Laser Desorption/Ionization Time-of-Flight Mass Spectrometry.* Analytical Chemistry, 2003. **75**(22): p. 6191-6195.

13. Chen, W.-Y., et al., *Carbon nanotubes as affinity probes for peptides and proteins in MALDI MS analysis.* Journal of the American Society for Mass Spectrometry, 2004. **15**(11): p. 1629-1635.

14. Ren, S.-f., et al., *Immobilized carbon nanotubes as matrix for MALDI-TOF-MS analysis: Applications to neutral small carbohydrates.* Journal of the American Society for Mass Spectrometry, 2005. **16**(3): p. 333-339.

15. Wang, C.-h., et al., *High-sensitivity matrix-assisted laser desorption/ionization Fourier transform mass spectrometry analyses of small carbohydrates and amino acids using oxidized carbon nanotubes prepared by chemical vapor deposition as matrix.* Analytica Chimica Acta, 2007. **604**(2): p. 158-164.

16. Shan, Z., et al., *Mesoporous tungsten titanate as matrix for matrix-assisted laser desorption/ionization time-of-flight mass spectrometry*

analysis of biomolecules. Analytica Chimica Acta, 2007. **593**(1): p. 13-19.

17. Yuan, M., et al., *Preparation of highly ordered mesoporous WO3-TiO2 as matrix in matrix-assisted laser desorption/ionization mass spectrometry*. Microporous and Mesoporous Materials, 2005. **78**(1): p. 37-41.

18. Lee, C.-S., et al., *Analysis of small molecules by desorption/ionization on mesoporous silicate (DIOM)-mass spectrometry (MS)*. Microporous and Mesoporous Materials, 2007. **98**(1-3): p. 200-207.

19. Chen, C.-T. and Y.-C. Chen, *Desorption/ionization mass spectrometry on nanocrystalline titania sol-gel-deposited films*. Rapid Communications in Mass Spectrometry, 2004. **18**(17): p. 1956-1964.

20. Chen, C.-T. and Y.-C. Chen, *Molecularly Imprinted TiO_2-Matrix-Assisted Laser Desorption/Ionization Mass Spectrometry for Selectively Detecting α-Cyclodextrin*. Analytical Chemistry, 2004. **76**(5): p. 1453-1457.

21. Guan, B., et al., *Characterization of Synthesized Titanium Oxide Nanoclusters by MALDI-TOF Mass Spectrometry*. Journal of the American Society for Mass Spectrometry, 2007. **18**(3): p. 517-524.

22. Nag, M., P. Basak, and S.V. Manorama, *Low-temperature hydrothermal synthesis of phase-pure rutile titania nanocrystals: Time temperature tuning of morphology and photocatalytic activity*. Materials Research Bulletin, 2007. **42**(9): p. 1691-1704.

23. *Unpublished results*.

24. Lou, X., et al., *Radical cation formation in characterization of novel C_3-symmetric disks and their precursors by matrix-assisted laser desorption/ionization time-of-flight mass spectrometry*. Journal of Mass Spectrometry, 2006. **41**(5): p. 659-669.

25. Lias, S.G., R.D. Levin, and S.A. Kafafi, *Ion Energetics Data*, in *NIST ChemistryWebBook, NIST Standard Reference Database Number 69*, P.J. Linstrom and W.G. Mallard, Editors. June 2005, National Institute of Standards and Technology: Gaithersburg MD, 20899

26. Mendoza-Wilson, A.M. and D. Glossman-Mitnik, *CHIH-DFT study of the electronic properties and chemical reactivity of quercetin*. Journal of Molecular Structure: THEOCHEM, 2005. **716**(1-3): p. 67-72.

27. Guaratini, T., et al., *New chemical evidence for the ability to generate radical molecular ions of polyenes from ESI and HR-MALDI mass spectrometry*. The Analyst, 2004. **129**(12): p. 1223-1226.

28. Castro, A.L., et al., *Synthesis of anatase TiO_2 nanoparticles with high temperature stability and photocatalytic activity*. Solid State Sciences, 2008. **10**(5): p. 602-606.

29. Radecka, M., et al., *Effect of oxygen nonstoichiometry on photo-electrochemical properties of TiO2-x*. Journal of Power Sources, 2007. **173**(2): p. 816-821.

30. Karas, M., D. Bachmann, and F. Hillenkamp, *Influence of the wavelength in high-irradiance ultraviolet laser desorption mass spectrometry of organic molecules*. Anal. Chem., 1985. **57**.

31. Karas, M. and F. Hillenkamp, *Laser desorption ionization of proteins with molecular masses exceeding 10,000 daltons.* Analytical Chemistry, 1988. **60**(20): p. 2299-2301.

32. Zenobi, R. and R. Knochenmuss, *Ion formation in MALDI mass spectrometry.* Mass Spectrometry Reviews, 1998. **17**(5): p. 337-366.

33. Castro, A., et al., *Titanium dioxide anatase as matrix for matrix-assisted laser desorption/ionization analysis of small molecules.* Rapid Communications in Mass Spectrometry, 2008. **22**(23): p. 3761-3766.

34. Meffert, A. and J. Grotenmeyer, *Dissociative proton transfer in cluster ions: clusters of aromatic carboxylic acids with amino acids.* International Journal of Mass Spectrometry, 2001. **210-211**: p. 521-530.

35. Wong, C. and T. Chan, *Cationization Processes in Matrix-assisted Laser Desorption/Ionization Mass Spectrometry: Attachment of Divalent and Trivalent Metal Ions.* Rapid Communications in Mass Spectrometry, 1997. **11**(5): p. 513-519.

36. Karas, M. and R. Kruger, *Ion Formation in MALDI: The Cluster Ionization Mechanism.* Chemical Reviews, 2003. **103**(2): p. 427-440.

37. Mele, A. and L. Malpezzi, *Noncovalent association phenomena of 2,5-dihydroxybenzoic acid with cyclic and linear oligosaccharides. A matrix-assisted laser desorption/ionization time-of-flight mass spectrometric and X-ray crystallographic study.* Journal of the American Society for Mass Spectrometry, 2000. **11**: p. 228.

38. Karas, M., M. Glückman, and J. Schäfer, *Ionization in matrix-assisted laser desorption/ionization: singly charged molecular ions are the lucky survivors*. Journal of Mass Spectrometry, 2000. **35**: p. 1.

39. Land, C. and G. Kinsel, *Investigation of the mechanism of intracluster proton transfer from sinapinic acid to biomolecular analytes*. Journal of the American Society for Mass Spectrometry, 1998. **9**(10): p. 1060-1067.

40. Land, C. and G. Kinsel, *The mechanism of matrix to analyte proton transfer in clusters of 2,5-dihydroxybenzoic acid and the tripeptide VPL*. Journal of the American Society for Mass Spectrometry, 2001. **12**(6): p. 726-731.

41. Wallace, W., M. Arnould, and R. Knochenmuss, *2,5-Dihydroxybenzoic acid: laser desorption/ionisation as a function of elevated temperature*. International Journal of Mass Spectrometry, 2005. **242**(1): p. 13-22.

42. March, R., et al., *High-energy and low-energy collision-induced dissociation of protonated flavonoids generated by MALDI and by electrospray ionization*. International Journal of Mass Spectrometry, 2007. **262**(1-2): p. 51-66.

43. Grant, D. and R. Helleur, *Rapid screening of anthocyanins in berry samples by surfactant-mediated matrix-assisted laser desorption/ionization time-of-flight mass spectrometry*. Rapid Communications in Mass Spectrometry, 2008. **22**(2): p. 156-164.

44. Santos, M., et al., *Influence of the metabolic profile on the in vivo antioxidant activity of quercetin under a low dosage oral regimen in rats*. British Journal of Pharmacology, 2009. **153**(8): p. 1750-1761.

45. Amaral, S., et al., *Plant extracts with anti-inflammatory properties-A new approach for characterization of their bioactive compounds and establishment of structure-antioxidant activity relationships.* Bioorganic & Medicinal Chemistry, 2009. **17**(5): p. 1876-1883.

46. Justino, G., et al., *Plasma quercetin metabolites: structure-antioxidant activity relationships.* Archives of Biochemistry and Biophysics 2004. **432**(1): p. 109-121.

47. Fernandez, M., et al., *Iron and copper chelation by flavonoids: an electrospray mass spectrometry study.* Journal of Inorganic Biochemistry, 2002. **92**(2): p. 105-111.

48. Justino, G., C. Borges, and M. Florêncio, *Electrospray ionization tandem mass spectrometry fragmentation of protonated flavone and flavonolaglycones: a re-examination.* Rapid Communications in Mass Spectrometry, 2009. **23**(2): p. 237-248.

49. Mira, M., et al., *Interations of Flavonoids with Iron and Copper Ions: A Mechanism for their Antioxidant Activity.* Free Radical Research, 2002. **36**(11): p. 1199-1208.

50. Mele, A., W. Panzeri, and A. Selva, *Fast Atom Bombardment Mass Spectrometric and Tandem Mass Spectrometric Investigation in Thioglycerol on Protonated Non-covalent Associations of β-Cyclodextrin with 2-Acetyl, 2-Propionyl-1-pyrroline and 5-Acetyl-2,3-dihydro-1,4-thiazine, Roast Smelling Odorants in Food. Role of the Matrix.* Journal of Mass Spectrometry, 1997. **32**(8): p. 807-812.

51. Kinsel, G., et al., *Ionization energy reductions in small 2,5-dihydroxybenzoic acid–proline clusters.* Journal of Mass Spectrometry, 2002. **37**(11): p. 1131-1140.

52. Croley, T., et al., *Observation of Na^+-bound oligomers of quercetin in the gas phase.* Rapid Communications in Mass Spectrometry, 2000. **14**(23): p. 2154-2157.

53. Koch, K., et al., *Clustering of nucleobases with alkali metals studied by electrospray ionization tandem mass spectrometry: implications for mechanisms of multistrand DNA stabilization.* Journal of Mass Spectrometry, 2002. **37**(7): p. 676-686.

54. Desfrançois, C., S. Carles, and J. Schermann, *Weakly Bound Clusters of Biological Interest.* Chemical Reviews, 2000. **100**(11): p. 3943–3962.

55. Aggerholm, T., et al., *Clustering of nucleosides in the presence of alkali metals: Biologically relevant quartets of guanosine, deoxyguanosine and uridine observed by ESI-MS/MS*. Journal of Mass Spectrometry, 2003. **38**: p. 87-97.

56. Fujii, T., *Alkali-metal ion/molecule association reactions and their applications to mass spectrometry*. Mass Spectrometry Reviews, 2000. **19**(3): p. 111-138.

57. Ma, Y., et al., *Characterization of flavone and flavonol aglycones by collision-induced dissociation tandem mass spectrometry*. Rapid Communications in Mass Spectrometry, 1997. **11**(12): p. 1357-1364.

58. March, R. and X.-S. Miao, *A fragmentation study of kaempferol using electrospray quadrupole time-of-flight mass spectrometry at high mass resolution.* International Journal of Mass Spectrometry, 2004. **231**(2-3): p. 157-167.

Chapter 4
Aromatic Amines

In this chapter, the gas-phase behaviour of aniline derivatives (haloanilines and nitroanilines) under electrospray ionization mass spectrometry conditions is addressed, using both low resolution and high resolution mass measurements. Fragmentation mechanisms for all aniline derivatives are proposed taking into account MS^2 experiments performed in a low resolution system, as well as MS^3 experiments and accurate mass measurements performed in a FTICR system. The probable protonation site is addressed taking into account semi-empirical calculations, as well as more sophisticated DFT calculations. The isomer identification was performed in a low resolution system using for that purpose competitive fragmentation of proton-bound heterodimers. The feasibility of the use of such method was first accessed by determining the gas-phase proton affinity and basicity values for the reference compound used throughout this section, 4-nitroaniline, the one for which there are gas-phase thermochemical data in the literature. The values determined are in close agreement with the literature values. It was found that the isomers can indeed be identified using this method through the branching ratio values. We also present the preliminary results on the behaviour of the protonated aniline derivatives when subjected to electron capture dissociation (ECD) conditions. No fragmentation products were detected; nevertheless, evidence was found for the formation of multi-charged species for these small analytes.

4 Aromatic Amines: Distinguishing isomers through mass spectrometry

4.1 Introduction

From an industrial point of view, primary aromatic amines are very useful chemicals, since they can be transformed into a great variety of products, such as pesticides, pharmaceuticals, explosives, rubber, epoxy polymers, azo-dyes and aromatic polyurethane products.[1] Of these, the halogenated derivatives of aniline are important intermediates in the manufacture of dyes and agricultural products.[2] As such, they are often discharged as industrial waste into the environment, constituting a significant group of pollutants,[3] thus making the isomer identification an important analytical issue.

There are a few studies in the literature on the determination of aromatic amines in environmental and food matrixes using LC-MS (High-Performance Liquid Chromatography-Mass Spectrometry), LC-MS/MS (High-Performance Liquid Chromatography-Tandem Mass Spectrometry) and GC-MS (Gas Chromatography-Mass Spectrometry), with or without the use of preparation techniques such as SPME (Solid Phase Microextraction).[1, 4-8] Nevertheless, to our knowledge, studies on the fragmentation mechanisms and gas-phase behaviour of chloroanilines are lacking. Indeed, the studies found in the literature concern non-chlorinated aromatic amines, e.g. Maziarz and Wood studied the gas-phase dimerization of dimethylaniline using a FTMS (Fourier Transform Mass Spectrometer),[9] or derivatized systems, e.g.

Trainor and Vouros studied derivatized chloroanilines using EC-NCIMS (Electron Capture Negative ion Chemical Ionization Mass Spectrometry).[10] Moreover, a study conducted by Kotiaho, *et al.* is reported in the literature on the formation of chloroanilines during the chlorination of water samples with organic amines.[11] Haloanilines were studied from a mass spectrometric viewpoint by Jariwala and co-workers,[3] with the purpose of isomer identification using derivatization procedures and taking into account the underutilized *ortho* effect.

Regarding isomer identification using mass spectrometry techniques, there are reports in the literature on the differentiation of enantiomers,[12, 13] differentiation and quantification of isomeric tripeptide mixtures,[14] discrimination of isomers of di-substituted benzene derivatives,[15] identification of stereoisomers of hexoses,[16] epimers of alcohols,[17] among others. Some of these works reported the use of the kinetic method for identification and quantification of isomers.[12-14, 17]

The kinetic method was developed in order to determine thermochemical properties whenever the equilibrium method was either not applicable or the instrumentation was not available and was based on the rates of competitive dissociation of mass-selected cluster ions.[18] Over the years, the kinetic method has been subjected to a great deal of discussion, for example see the Special Feature issue of volume 34 of Journal of Mass Spectrometry.[19-22]

As mentioned above, the method is based on the rates of competitive dissociation of mass-selected cluster ions. For example, the proton-bound dimer $A\text{-}H^{+}\text{-}B$ dissociates as shown in Equation 4.1,

where k_1 and k_2 are the rate constants for the competitive dissociations of the cluster ion to yield AH^+ and BH^+, respectively.

$$AH^+ + B \overset{k_1}{\leftarrow} AHB^+ \overset{k_2}{\rightarrow} BH^+ + A \qquad \text{(Equation 4.1)}$$

The restricted kinetic method, *i.e.* the kinetic method in its simplest form, is based on the assumptions of negligible differences in the entropy requirements for the competitive channels, negligible reverse activation energies and the absence of isomeric forms of the activated cluster ion.[18, 23] When these conditions are satisfied, the ratio of the fragment ion abundances is related, for example, to the differences of proton affinities, $\Delta(\Delta H)$ of the two bases by Equation 4.2, where T_{eff} is the effective temperature of the activated dimer (for more information on the effective temperature see reference [21]).

$$ln\left(\frac{k_1}{k_2}\right) = ln\frac{[AH^+]}{[BH^+]} \approx \frac{\Delta(\Delta H)}{RT_{eff}} \qquad \text{(Equation 4.2)}$$

Considering proton affinity (PA), Equation 4.2 can be rearranged in order to obtain Equation 4.3, where PA(A) and PA(B) are the proton affinities of a reference compound and the unknown, respectively.

$$ln\frac{[AH^+]}{[BH^+]} = \frac{PA(A)}{RT_{eff}} - \frac{PA(B)}{RT_{eff}} = mPA(A) - b \qquad \text{(Equation 4.3)}$$

Combining each unknown species, B, with a series of compounds A of known proton affinity, it is possible to determine the proton

affinity of B, through a plot of ln $[AH^+]/[BH^+]$ vs PA where the slope is $1/R_{Teff}$ and the y-intercept is $-(PA(B)/RT_{eff})$.

Since the kinetic method employs tandem mass spectrometry, the compounds of interest need not be available in pure form (unlike equilibrium methods) and can be performed in any mass spectrometer able to perform MS^2 experiments (for example, the equilibrium method needs dedicated systems). The method is sensible to small differences in thermochemical values and applicable to non-volatile compounds where insufficient vapour pressure limits the application of other methods.[18]

The use of the interaction between ions and electrons resulted in the development of new fragmentation methods.[24] Electron capture dissociation (ECD)[25-27] involves the irradiation of multiply-charged cations with very low-energy electrons (< 0.2 eV), capture of these electrons by the precursor ion and subsequent decomposition of the charge reduced species. Using higher energy electrons, which was termed as '*hot*' ECD,[28] electronic excitation accompanies electron capture. For anions, the electron detachment dissociation (EDD) may be applied.[29]

As shown by the name, ECD cannot be applied to singly-charged precursor ions as the product is neutral and cannot be detected in the mass spectrometer. Nevertheless, if high-energy electrons are used, further ionization and/or excitation may occur, and the dissociation of the singly-charged ion is possible. Over the years these methods have had a great deal of names, electron induced excitation of ions from organics (EIEIO),[30] electronic excitation dissociation (EED)[31] and electron ionization dissociation (EID).[32] O'Hair and co-workers suggested electron-induced dissociation (also EID) as a generic

description of these methods.[33] EID has been successfully applied to singly-charged peptide ions,[32, 33] metabolites,[34] gold hydride dimers,[35] sodium chloride cluster cations,[36] and recently to the structural analysis of oxo-centred trinuclear carboxylate-bridged iron complexes.[37]

In this chapter, we present the fragmentation mechanisms of aniline derivatives (nitro and haloanilines), the use of competitive fragmentations of proton-bound dimers has a tool to differentiate isomers and the preliminary results of the interaction between singly-charged protonated molecules of aniline derivatives with low and high-energy electrons.

4.2 Results and discussion

4.2.1 Fragmentation mechanisms of Haloanilines

All the haloanilines studied showed abundant protonated molecules in the full scan mass spectra (see Appendix A).

Before examining the fragmentation pathways for these analytes, we should carefully examine the probable protonation site for anilines. At first glance, the most obvious protonation site for anilines is the nitrogen of the amino group. Nevertheless, the amino group donates electrons by resonance and it is considered an activator, thus directing the attack to the *ortho* and *para* positions (Scheme 4.1); it is then reasonable to consider ring protonation sites.

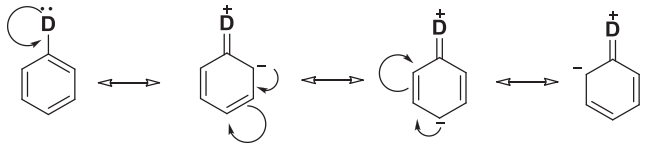

Scheme 4.1: Resonance donation to benzene.

The semi-empirical (PM6) and DFT estimates of $\Delta_r H$ of the protonation reaction of 2-fluoroaniline are presented in Table 4.1.

Table 4.1. PM6 (semi-empirical) and mPW1PW91 (DFT) $\Delta_r H$ estimates for the protonation reaction of 2-fluoroaniline.

	$\Delta_r H$ (kJ mol^{-1})				
Structure	**PM6**	**DFT**	**Structure**	**PM6**	**DFT**
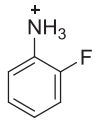	638.1	<u>-876.6</u>	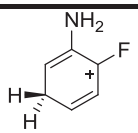	772.1	-801.1
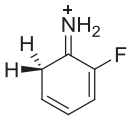	689.2	-851.4	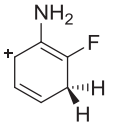	776.9	-788.9
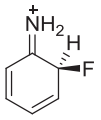	702.1	-823.3	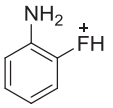	939.9	<u>-876.6</u>
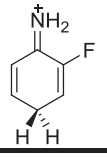	675.2	-873.3	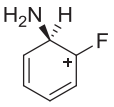	825.0	-724.9

Note: the lowest energies are <u>underlined</u>.

For the protonation at the fluorine atom it was found that, after the DFT geometry optimization, the hydrogen migrated to the nitrogen, resulting in a structure similar to the one obtained when the protonation was considered to occur at the nitrogen. It is also clear that the protonation at *ortho* and *para* positions results in structures with the lowest $\Delta_r H$ values, which is in close agreement to what was predicted by

the directing properties of the amino group (Scheme 4.1). Bearing this in mind, it is reasonable to assume that protonation in the remaining haloanilines can also occur at the amino group or at the *ortho* and *para* positions; thus, to save computing time, only these will be considered. The structures considered for the theoretical calculations are depicted in Scheme 4.2.

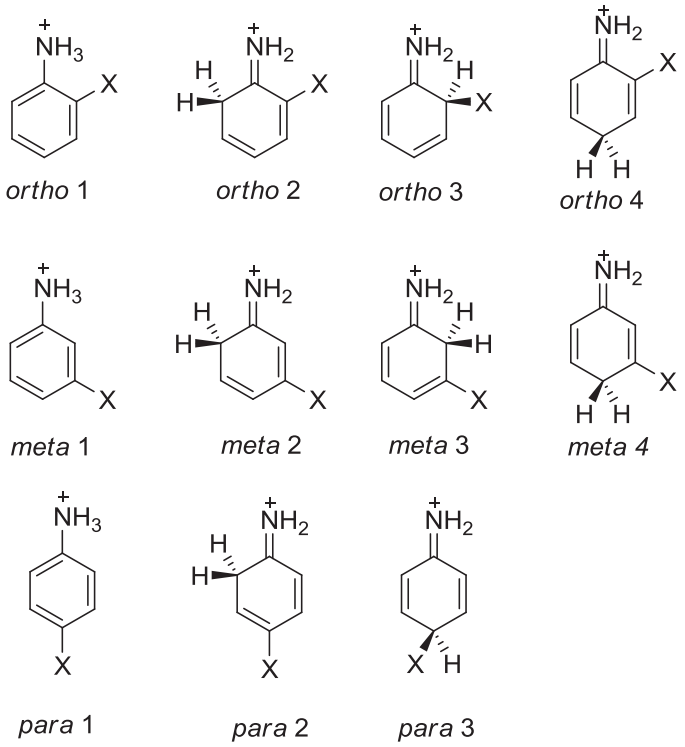

Scheme 4.2. Possible structures for the protonated molecules of the haloanilines under study.

The $\Delta_r H$ of the protonation for the haloanilines under study are presented in Table 4.2. Generally, there is a good agreement between the trend of the PM6 data and that of DFT data. Nevertheless, there are four exceptions, 3-chloroaniline, 3-bromoaniline, 3-iodoaniline and 4-

iodoaniline, for which the protonation at the *para* position of the aromatic ring seems to be favoured. The difference between the DFT $\Delta_r H$ at the amino group and at the *para* position of the aromatic ring is, however, less than 20 kJ mol^{-1} for all these exceptions. As such, it seems reasonable to assume that protonation for the haloanilines occurs at the amino group.

Table 4.2. PM6 and mPW1PW91 estimates of the protonation enthalpies ($\Delta_r H$ in kJ mol^{-1}) for the possible structures of the protonated molecules of the haloanilines under study.

	$\Delta_r H$ (kJ mol^{-1})							
	F		Cl		Br		I	
Structure	**PM6**	**DFT**	**PM6**	**DFT**	**PM6**	**DFT**	**PM6**	**DFT**
ortho 1	<u>638.1</u>	<u>-876.6</u>	<u>641.9</u>	<u>-876.2</u>	<u>638.2</u>	<u>-880.4</u>	<u>641.6</u>	<u>-882.7</u>
ortho 2	689.2	-851.4	685.7	-850.6	680.9	-853.4	676.7	-856.5
ortho 3	702.1	-823.3	705.6	-823.3	698.3	-831.8	682.4	-852.4
ortho 4	675.2	-873.3	673.0	-869.7	669.1	-872.3	665.3	-874.9
meta 1	<u>661.4</u>	-869.9	<u>656.6</u>	-867.4	<u>655.4</u>	-868.5	<u>651.6</u>	-870.3
meta 2	677.9	-874.6	675.2	-867.3	681.1	-868.2	680.8	-869.8
meta 3	684.5	-864.4	679.6	-861.8	680.9	-862.9	678.9	-864.9
meta 4	667.4	<u>-887.2</u>	664.9	<u>-881.4</u>	668.5	<u>-882.0</u>	668.2	<u>-883.6</u>
para 1	<u>645.6</u>	<u>-882.1</u>	<u>649.7</u>	<u>-871.0</u>	<u>654.1</u>	<u>-871.2</u>	<u>654.7</u>	-871.8
para 2	688.0	-854.3	686.0	-849.4	685.9	-850.9	681.9	-853.4
para 3	700.7	-832.7	698.2	-842.4	686.2	-857.0	667.9	<u>-878.2</u>

Note: the lowest energies are <u>underlined</u>

The ESI-MS^2 spectra of the protonated molecules of the haloanilines are presented in Table 4.3 (the spectra are presented in Appendix A).

Table 4.3: ESI-MS^2 data at CEL=30% for the haloanilines under study (the relative abundance, %, of each product ion is presented between brackets).

		$[M+H]^+$	$[M+H-X^{\bullet}]^{+\bullet}$	$[M+H-HX]^+$
Fluoroaniline	**2**	*m/z* 112 (25)	-	*m/z* 92 (100)
	3	*m/z* 112 (100)	-	*m/z* 92 (15)
	4	*m/z* 112 (100)	-	*m/z* 92 (36)
Chloroaniline	**2**	*m/z* 128 (25)	*m/z* 93 (100)	*m/z* 92 (59)
	3	*m/z* 128 (100)	*m/z* 93 (92)	-
	4	*m/z* 128 (100)	*m/z* 93 (57)	-
Bromoaniline	**2**	*m/z* 172 (31)	*m/z* 93 (100)	*m/z* 92 (18)
	3	*m/z* 172 (90)	*m/z* 93 (100)	-
	4	*m/z* 172 (70)	*m/z* 93 (100)	-
Iodoaniline	**2**	*m/z* 220 (28)	*m/z* 93 (100)	-
	3	*m/z* 220 (100)	*m/z* 93 (82)	-
	4	*m/z* 220 (100)	*m/z* 93 (88)	-

From the data presented in Table 4.3, it is clear that there are two main fragmentation pathways for the protonated molecules of the haloanilines. These are the loss of HX (X=halogen) to afford the ion at *m/z* 92 and the loss of the halogen radical ($X^{\bullet}$) to afford the ion at *m/z* 93. The loss of neutral HX was only observed for the fluoroanilines and for 2-chloroaniline and 2-bromoaniline, while the loss of the halogen radical was observed for all haloanilines with the exception of the fluoroanilines. The fragmentation mechanisms are depicted in Scheme 4.3.

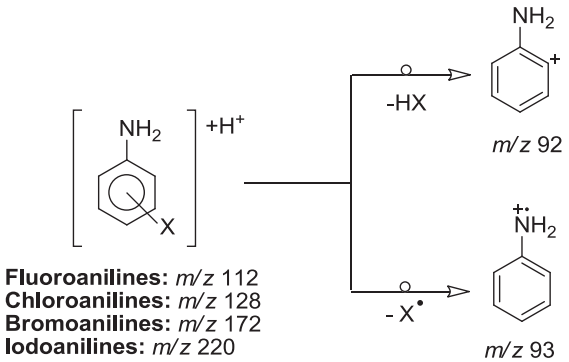

Scheme 4.3: Fragmentation mechanism proposal for the protonated molecules of the haloanilines.

The loss of HF was already reported for fluoroanilines under electron ionization (EI) conditions.[38] Tajima and co-workers[38] discovered that the eliminated HF molecule contained the amino hydrogen atom and proposed a "ring-walk" mechanism in which the fluorine atom migrates to the ortho position. A similar behaviour was reported for 4-fluorotoluene and 4-chlorotoluene.[39] Taking into account that the typical ion residence time within the ion trap is a few hundred milliseconds (the maximum ejection time for these MS^2 experiments was set to 200 ms) and that this phenomenon was detected in a sector mass spectrometer,[38] for which the typical ion residence time within the ion source is *ca.* 10^{-6} s, it is reasonable to assume that this ring walk is possible in ion trap mass spectrometry conditions. With this in mind, it is understandable that the m/z 92 for the *ortho* isomer has the highest relative abundance of the three.

4.2.2 Fragmentation mechanisms of Nitroanilines

Scheme 4.4 shows the possible structures for the protonated molecules of the nitroanilines under study. The semi-empirical calculations (Table 4.4) show that the most probable protonation site for 2- and 4-nitroaniline is the oxygen of the nitro group and for 3-nitroaniline the nitrogen of the amino group, which is in close agreement with the results obtained by DFT calculations.

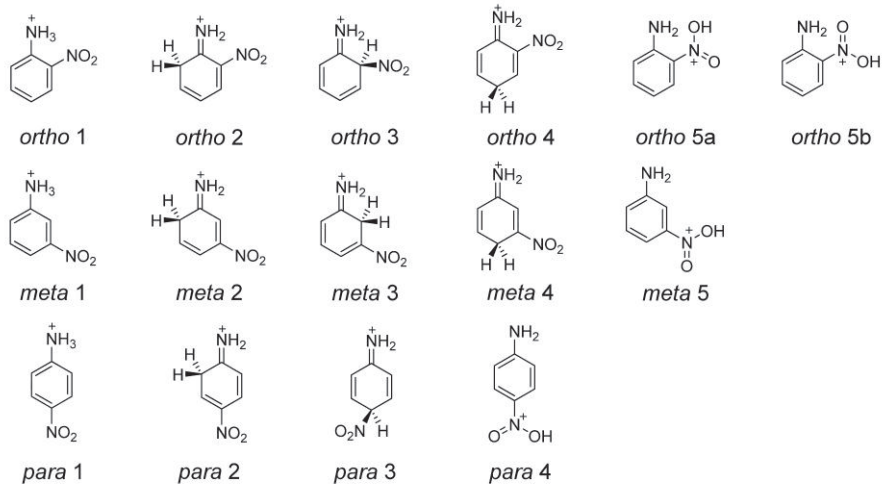

Scheme 4.4: Possible structures for the protonated molecules of the nitroanilines under study.

Table 4.4. PM6 and mPW1PW91 estimates of the protonation reaction enthalpy ($\Delta_r H$ in kJ mol^{-1}) for the nitroanilines under study.

2-Nitro Structure	$\Delta_r H$ (kJ mol^{-1}) PM6	DFT	3-Nitro Structure	$\Delta_r H$ (kJ mol^{-1}) PM6	DFT	4-Nitro Structure	$\Delta_r H$ (kJ mol^{-1}) PM6	DFT
ortho 1	687.7	-864.2	*meta* 1	685.3	-842.2	*para* 1	707.3	-830.2
ortho 2	728.5	-817.7	*meta* 2	734.5	-810.8	*para* 2	734.8	-811.2
ortho 3	762.2	-789.3	*meta* 3	723.7	-820.2	*para* 3	748.1	-805.1
ortho 4	721.0	-831.9	*meta* 4	720.2	-833.6	*para* 4	637.5	-896.4
ortho 5a	677.7	-857.6	*meta* 5	708.4	-845.4			
ortho 5b		-873.8						

The ESI-MS^2 spectra for the protonated nitroanilines are depicted in Figure 4.1 and it is clear that all can be distinguished by their CID spectra.

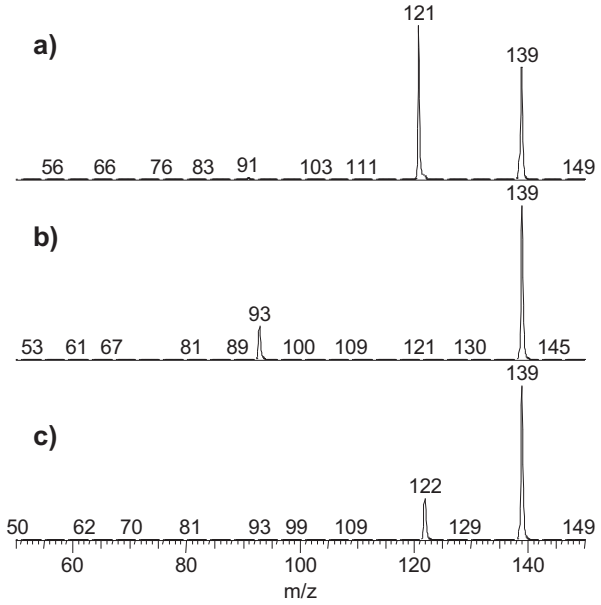

Figure 4.1. ESI-MS^2 spectra at CEL=15% of the protonated molecules of: a) 2-nitroaniline; b) 3-nitroaniline; c) 4-nitroaniline.

The protonated molecule of 2-nitroaniline (Figure 4.1a), *m/z* 139, loses 18 Da, attributed to H_2O, affording the *m/z* 121 ion. Since this loss is not detected for the other two nitroanilines, it can be attributed to an *ortho* effect. This effect is well documented in the literature for electron ionization,[3, 40-42] nevertheless, this effect was also observed when using electrospray ionization.[43] The MS^3 spectrum of the ion at *m/z* 121 is depicted in Figure 4.2, and it is clear that the *m/z* 121 ion loses $NO^{\bullet}$ to afford the ion at *m/z* 91.

The fragmentation mechanism proposal for the protonated molecule of 2-nitroaniline is depicted in Scheme 4.5.

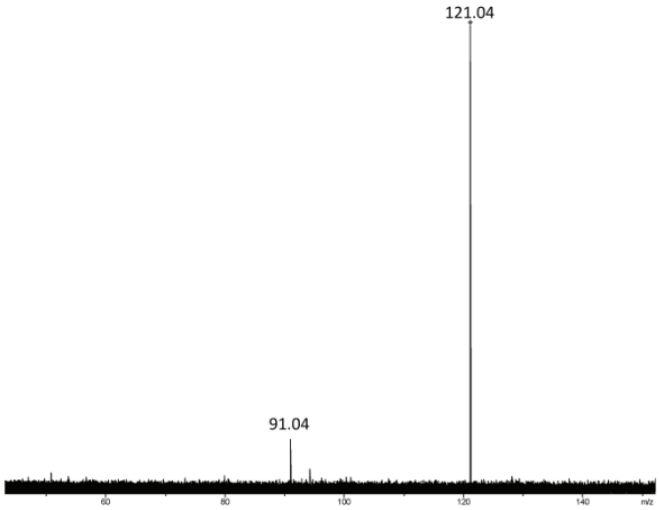

Figure 4.2. SORI-CAD MS^3 spectrum of the m/z 121.04 ion of 2-nitroaniline (SORI power: 0.35%).

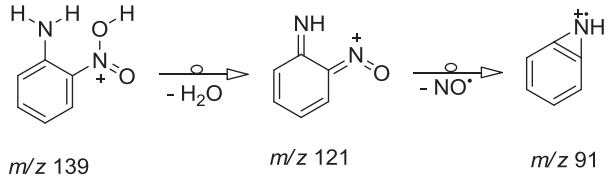

Scheme 4.5: Fragmentation mechanism proposal for the protonated molecule of 2-nitroaniline.

The protonated molecule of 3-nitroaniline (Figure 4.1b) loses 46 Da, attributed to NO_2 radical, affording the ion at m/z 93. Even-electron ions, such as protonated molecules, do not usually lose a radical to form an odd-electron ion, since it is a violation of the 'even-electron rule'.[44] Nevertheless, there are reports in the literature on the fragmentation of many small even-electron ions that do not obey the rule.[45-47] These exceptions to the 'even-electron rule' were proposed to involve radical eliminations leading to odd-electron fragment ions of exceptional stability.[46] The fragmentation mechanism for the protonated molecule of 3-nitroaniline is depicted in Scheme 4.6.

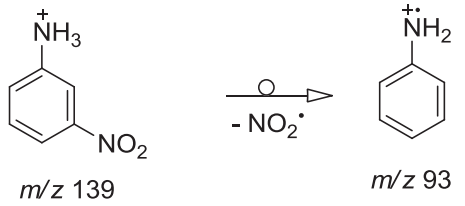

Scheme 4.6: Fragmentation mechanism proposal for the protonated molecule of 3-nitroaniline.

The protonated 4-nitroaniline (Figure 4.1c) loses 17 Da, which may be attributed to hydroxyl radical ($HO^{\bullet}$) or NH_3. Taking into account the most probable protonation site for 4-nitroaniline, the oxygen of the nitro group, it is reasonable to assume the loss of hydroxyl radical ($HO^{\bullet}$) to be most probable. In fact, the chemical ionization mass spectra of nitroanilines, using H_2 as reagent gas, are available in the literature[48] and the ion at m/z 122 was assigned to the loss of hydroxyl radical from the protonated molecule. The ESI-FTICR-MS experiments allowed us to attribute this loss to $HO^{\bullet}$ and to assign the ion composition $C_6H_6N_2O^{+\bullet}$ with an error of 0.4 ppm. The loss of hydroxyl radical has been reported in the literature for a wide variety of nitroaromatic compounds under electron ionization (EI),[49-52] chemical ionization,[48] and electrospray (ESI).[47] The ion at m/z 122 was isolated and fragmented by means of SORI-CAD and the MS^3 spectrum is depicted in Figure 4.3.

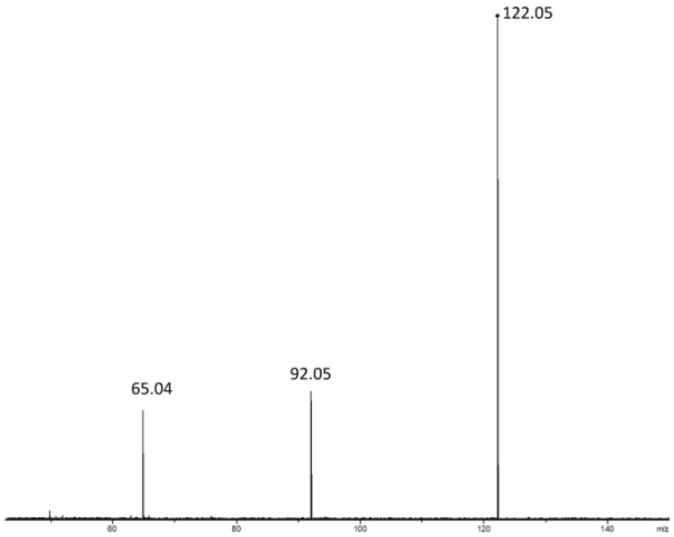

Figure 4.3. SORI-CAD MS^3 spectrum of the *m/z* 122.05 ion of 4-nitroaniline (SORI power: 0.35%).

From this MS^3 spectrum, it is clear that the ion at *m/z* 122 can afford the ion at *m/z* 92 by loss of nitrosyl radical ($NO^{\bullet}$), with an attribution error of -0.5 ppm, and the ion at *m/z* 65 can be attributed to the concerted loss of $HCN+NO^{\bullet}$ with an attribution error of -1.4 ppm. These ions, however, have very low abundances on the MS^2 spectrum of the protonated molecule (Figure 4.1c). The fragmentation mechanism for the protonated molecule of 4-nitroaniline is depicted in Scheme 4.7.

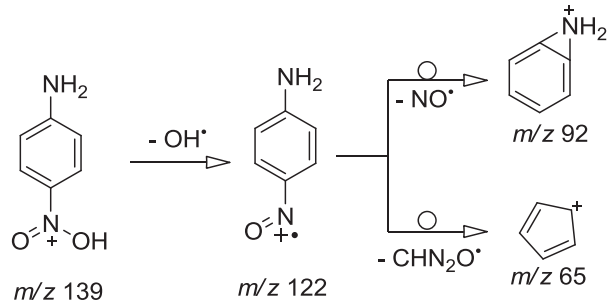

Scheme 4.7: Fragmentation mechanism proposal for the protonated molecule of 4-nitroaniline.

The H_2 CI mass spectra of nitroanilines (Figure 4.4) are available in the literature,[48] as such, it is interesting to compare the results from both ionization techniques. Comparing the spectra obtained using both techniques, it is obvious that there is a striking difference in the fragmentations that are larger for H_2 CI mass spectrometry conditions (Figure 4.4) than for ESI CID (Figure 4.1).

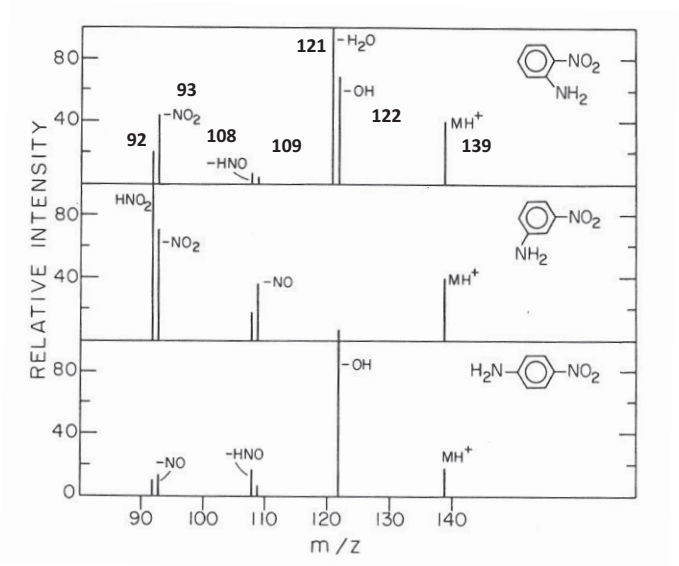

Figure 4.4. H_2 CI mass spectra of nitroanilines (taken from reference [48]).

In our experiments, the collision induced dissociation of the protonated nitroanilines afforded only the $[M+H-H_2O]^+$ ion for the *ortho* isomer, the $[M+H-NO_2]^{+\bullet}$ ion for the *meta* isomer and the $[M+H-HO]^{+\bullet}$ ion for the *para* isomer. Under CI mass spectrometry conditions, the losses of hydroxyl radical ($HO^\bullet$), nitrosyl radical ($NO^\bullet$), HNO, $NO_2^\bullet$ and HNO_2 were detected for all nitroanilines (the loss of H_2O was only detected for 2-nitroaniline). The difference observed can be

attributed to the energy of the ionization/fragmentation process, which is larger for H_2 CI than for ESI-MS/MS-CID.[48]

4.2.3 Distinguishing isomers through mass spectrometry: Competitive fragmentation of proton-bound heterodimers

For chloro and bromoanilines, the fragmentation alone is sufficient to distinguish 2-chloro and 2-bromoaniline from the 3- and 4-isomers, due to the loss of HCl and HBr, respectively. These two isomers could not be distinguished from the fragmentation alone. With respect to fluoro and iodoanilines, they exhibited only one product ion that results from the loss of HF and $I^{\bullet}$ respectively and does not allow for the differentiation of these compounds.

Nevertheless, and as mentioned in the introduction, the use of competitive fragmentation of proton-bound dimers (i.e. the kinetic method) can be used to distinguish isomers.

Gas-phase proton affinities and basicities are available in the literature for 3- and 4-fluoroanilines, 3- and 4-chloroanilines, 3-bromoaniline and 4-nitroaniline (Table 4.5).

Table 4.5: Proton affinities (PA) and gas-phase basicities (GB) of haloanilines and 4-nitroaniline (taken from reference [53]). These values were assumed to have an error of 8.4 kJ mol^{-1}.

	PA (kJ mol^{-1})	GB (kJ mol^{-1})
4-Nitroaniline	866.0	834.2
3-Fluoroaniline	867.3	835.5
3-Chloroaniline	868.1	836.3
4-Fluoroaniline	871.5	839.7
3-Bromoaniline	873.2	841.4
4-Chloroaniline	873.8	842.0

To access if the kinetic method is applicable to these compounds, we decided to estimate the proton affinity and gas-phase basicity of 4-nitroaniline in order to compare it with the literature data (PA = 866.0 kJ mol^{-1}; GB = 834.2 kJ mol^{-1}).

As an example, Figure 4.5 shows a full scan mass spectrum of a mixture of 4-nitroaniline and 4-fluoroaniline (Figure 4.5a) and an MS^2 spectrum of the heterodimer (*m/z* 250) at a collision energy level of 5% (Figure 4.5b). From the MS^2 spectrum of the heterodimer, it is possible to determine the branching ratio and apply the kinetic method formalism. Repeating the same procedure to the other references present in Table 4.5 it is possible to construct Table 4.6.

3-Bromo and 4-chloroanilines were removed from the data, since their behaviour was somewhat unexpected (Figure 4.6a and b). Indeed, according to the gas-phase thermochemical data presented in Table 4.5, after fragmentation of the heterodimer the abundance of the protonated molecule of 4-nitroaniline should have been lower than that of 4-chloroaniline and 3-bromoaniline. The MS^2 presented in Figure 4.6 show the opposite, thus these two systems were not considered when calculating the proton affinity and gas-phase basicity of 4-nitroaniline.

For these two systems, isomerization reactions could be responsible for this behaviour. For the particular case of 4-chloroaniline, the migration from the *para* to the *meta* position should be energetically favourable. This type of migration has already been reported by Parry *et al.* [39] for *para*-halotoluenes and it seems to be a reasonable explanation for this observation. In fact, the branching ratio found for 4-chloroaniline is comparable to the one found for 3-chloroaniline, which supports the assumption of isomerization.

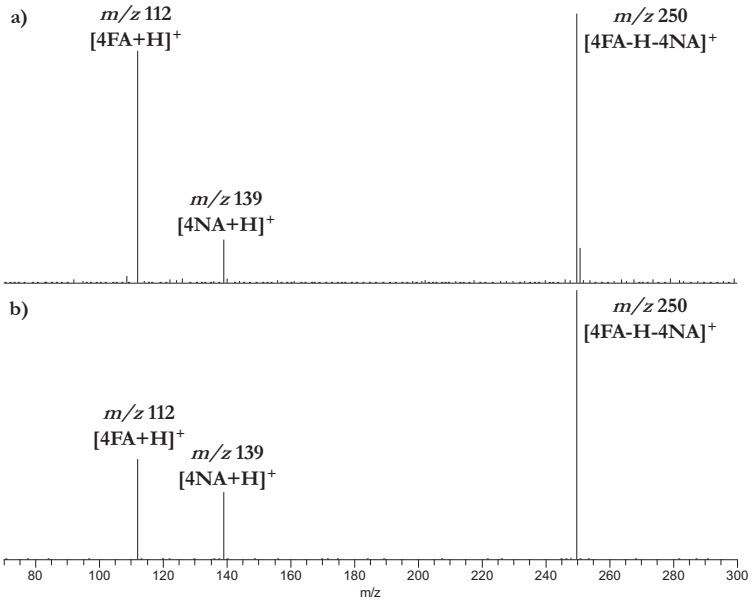

Figure 4.5: a) Full scan mass spectrum of a mixture of 4-nitroaniline and 4-fluoroaniline; b) MS^2 spectrum of the heterodimer [4-fluoroaniline+H+4-nitroaniline]$^+$ (*m/z* 250) at a collision energy level (CEL) of 5%.

Table 4.6. Values of $Ab(AH^+)/Ab(BH^+)$ and $Ln[Ab(AH^+)/Ab(BH^+)]$. (AH^+ reference ion, BH^+ unknown ion)

	PA (kJ mol^{-1})	GB (kJ mol^{-1})	$Ab(AH^+)/Ab(BH^+)$	$Ln[Ab(AH^+)/Ab(BH^+)]$
3-F	867.3	835.5	2.3	0.8
3-Cl	868.1	836.3	2.7	1.0
4-F	871.5	839.7	0.7	-0.4
3-Br	*873.2*	*841.4*	*2.6*	*1.0*
4-Cl	*873.8*	*842.0*	*2.3*	*0.8*

Note: 3-bromoaniline and 4-chloroaniline are presented in italic because they were not considered when constructing the ln(abundance ratio) vs GB or PA graphical representation. See explanation in the text.

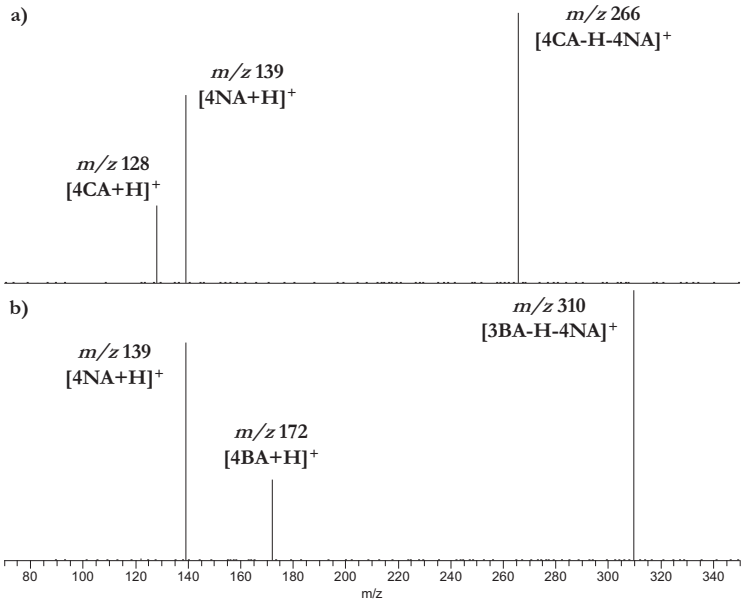

Figure 4.6. ESI-MS^2 spectra at collision energy level 5% of a) 4-chloroaniline + 4-nitroaniline proton-bound heterodimer (m/z 266); b) 3-bromoaniline + 4-nitroaniline proton-bound heterodimer (m/z 310).

With the data collected so far, it is possible to construct a plot of Ln[Ab(AH$^+$)/Ab(BH$^+$)] as function of the gas-phase basicity and proton affinity (Figure 4.7).

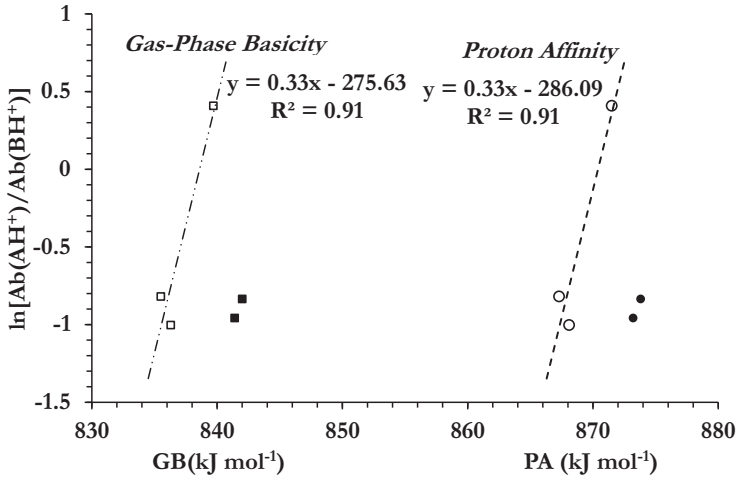

Figure 4.7. Ln[Ab(AH$^+$)/Ab(BH$^+$)] vs gas-phase basicity (kJ mol^{-1}) and proton affinity (kJ mol^{-1}). (AH$^+$ – reference ion, BH$^+$ – unknown ion)

The proton affinity/gas-phase basicity is the intercept of the least mean squares trendline with the *x*-axis. For 4-nitroaniline, the proton affinity was estimated to be 866.3±0.8 kJ mol^{-1} and the gas-phase acidity 834.5±0.8 kJ mol^{-1}. These values are in close agreement with the literature values (Table 4.5), which are 866.0 kJ mol^{-1} and 834.2 kJ mol^{-1} for the proton affinity and gas-phase basicity, respectively. As such, it seems reasonable to apply this methodology in an attempt to identify isomers.

The branching ratios for the product ions of the proton-bound dimers are presented in Figure 4.8 and proved to be an important tool to distinguish isomers.

As such, for fluoroanilines the ion abundance ratio is clearly different for all isomers. For 2-fluoroaniline the average ion abundance ratio is 0.6, for 3-fluoroaniline 0.4 and for 4-fluoroaniline 1.5.

For the chloroanilines, the *ortho* isomer could be easily distinguished from the *meta* and *para* isomers by the fragmentation pattern alone. As such, the ion abundance ratio will only be used to distinguish the *meta* from the *para* isomer. Similarly to what was observed for the fluoroanilines, the *meta* and *para* isomers of chloroanilines can easily be distinguished using the ion abundance ratios. For 3-chloroaniline the average ion abundance ratio is 0.37, while for 4-chloroaniline is 0.43.

The situation described for the chloroanilines was also found for bromoanilines, *i.e.* the *ortho* isomer is easily distinguished from the *meta* and *para*. As such, in this situation, the ion abundance ratios will be used to distinguish the *meta* from the *para* isomer. Again, the ion abundance ratios proved to be useful in distinguishing the *meta* from the *para*

isomers, 3-bromoaniline has an average ion abundance ratio of 0.38, while for 4-bromoaniline the average ion abundance ratio is *ca.* 0.34.

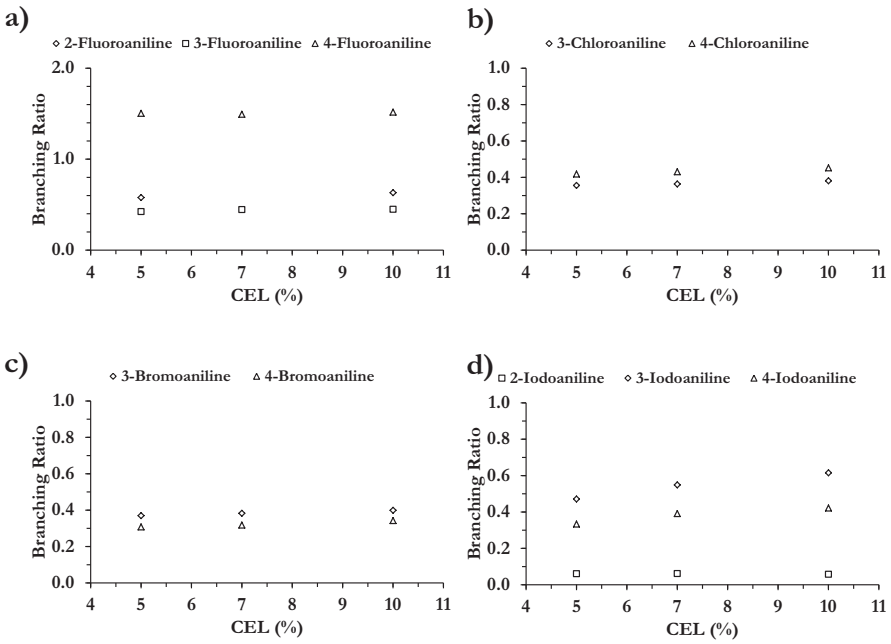

Figure 4.8. Branching ratios at collision energy levels of 5% to 10% for the haloanilines under study: a) fluoroanilines; b) chloroanilines; c) bromoanilines; d) iodoanilines.

For iodoanilines, and similarly to what was observed for fluoroanilines, the fragmentation pattern was not helpful in distinguishing the isomers. Nevertheless, from the ion abundance ratios we were able to make such distinction. The 2-iodoaniline has an average ion abundance ratio of 0.06, 3-iodoaniline 0.55 and 4-iodoaniline 0.41.

4.2.4 Electron Capture Dissociation/Electron Induced Dissociation of protonated aromatic amines

When an electron interacts with a polyatomic cation, the outcome is dependent upon the electron's energy.[54] At very low energies (< 0.1 eV), the major outcome is dissociative electron capture. At higher energies (a few electronvolts), vibration induced dissociation can occur, and above the ionization limit (> 9 eV), ejection of an electron can occur resulting in further ionization (see Equation 4.4).

$$[M + nH]^{n+} + e^{-} \rightarrow [M + nH]^{(n+1)+\cdot} + 2e^{-} \qquad \text{(Equation 4.4)}$$

These processes are well established for large multi-charged analytes. For singly-charged analytes the interaction with low energy electrons will only result in the diminishing of the ion signal rather than fragmentation.[27] Nevertheless, there are reports in the literature where higher energy electrons were used to fragment singly-charged analytes.[33]

Interestingly, during the ECD experiments we found ion signals that could be attributed to multiply charged species for all the aromatic aniline derivatives studied. The high accuracy mass measurements that allowed these attributions are presented in Table 4.7.

It is clear from the data presented in Table 4.7 that the attribution errors are quite large when compared with the normal errors obtained in our FT-ICR system (< 5 ppm). Nevertheless, we should take into account that all measurements were performed with an electron beam shooting at the centre of the ICR cell, which invalidates any calibration performed earlier.

Table 4.7. ECD MS^2 spectra ion attributions for the aniline derivatives under study.

		***m/z* meas.**	***m/z* calc.**	**Error (ppm)**
2-Fluoro	$[M+H]^+$	112.05479	112.05570	8.1
	$[M+H]^{2+\bullet}$	56.02781	56.02758	-4.1
	$[M+H]^{3+}$	n. d.	-	-
3-Fluoro	$[M+H]^+$	112.05470	112.05570	9.0
	$[M+H]^{2+\bullet}$	56.02783	56.02758	-4.5
	$[M+H]^{3+}$	n. d.	-	-
4-Fluoro	$[M+H]^+$	112.05475	112.05570	8.5
	$[M+H]^{2+\bullet}$	56.02782	56.02758	-4.3
	$[M+H]^{3+}$	n. d.	-	-
2-Chloro	$[M+H]^+$	128.02517	128.02615	7.7
	$[M+H]^{2+\bullet}$	64.01305	64.01280	-3.8
	$[M+H]^{3+}$	n. d.	-	-
3-Chloro	$[M+H]^+$	128.02518	128.02615	7.6
	$[M+H]^{2+\bullet}$	64.01305	64.01280	-3.8
	$[M+H]^{3+}$	n. d.		
4-Chloro	$[M+H]^+$	128.02468	128.02615	11.5
	$[M+H]^{2+\bullet}$	64.01292	64.01280	-1.8
	$[M+H]^{3+}$	n. d.	-	-
2-Bromo	$[M+H]^+$	171.97458	171.97564	6.2
	$[M+H]^{2+\bullet}$	85.98781	85.98755	-3.1
	$[M+H]^{3+}$	57.32563	57.32485	-13.7
3-Bromo	$[M+H]^+$	171.97446	171.97564	6.9
	$[M+H]^{2+\bullet}$	85.98784	85.98755	-3.4
	$[M+H]^{3+}$	57.32563	57.32485	-13.7
4-Bromo	$[M+H]^+$	171.97458	171.97564	6.1
	$[M+H]^{2+\bullet}$	85.98781	85.98755	-3.1
	$[M+H]^{3+}$	57.32565	57.32485	-14.0
2-Iodo	$[M+H]^+$	219.96027	219.96177	6.8
	$[M+H]^{2+\bullet}$	109.98098	109.98061	-3.4
	$[M+H]^{3+}$	73.32126	73.32022	-14.2
3-Iodo	$[M+H]^+$	219.96034	219.96177	6.5
	$[M+H]^{2+\bullet}$	109.98097	109.98061	-3.2
	$[M+H]^{3+}$	73.32126	73.32022	-14.1
4-Iodo	$[M+H]^+$	219.96041	219.96177	6.2
	$[M+H]^{2+\bullet}$	109.98095	109.98061	-3.1
	$[M+H]^{3+}$	73.32126	73.32022	-14.2
2-Nitro	$[M+H]^+$	139.04910	139.05020	8.0
	$[M+H]^{2+\bullet}$	69.52510	69.52483	-4.0
	$[M+H]^{3+}$	46.35046	46.34970	-16.4
3-Nitro	$[M+H]^+$	139.04864	139.05020	11.2
	$[M+H]^{2+\bullet}$	69.52522	69.52483	-5.6
	$[M+H]^{3+}$	n. d.	-	-
4-Nitro	$[M+H]^+$	139.04910	139.05020	7.9
	$[M+H]^{2+\bullet}$	69.52510	69.52483	-4.0
	$[M+H]^{3+}$	46.35048	46.34970	-16.7

In spite of this situation, the isotopic pattern analysis confirms our attributions. As an example, the ECD spectrum of the protonated molecule of 2-bromoaniline is presented in Figure 4.9; the inset depicts an expansion of the m/z 50 – 90 range and the theoretical isotopic patterns of the $[M+H]^{2+\bullet}$ and $[M+H]^{3+}$ ions.

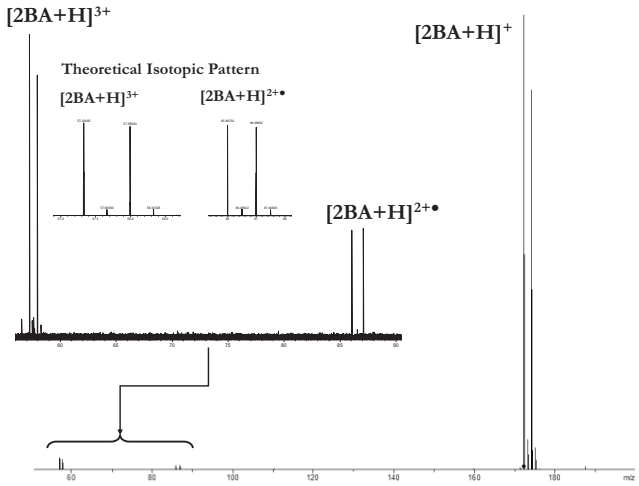

Figure 4.9. ECD mass spectrum of the protonated molecule of 2-bromoaniline (electron energy = 0.2 eV, electron pulse length 0.05s).

The process depicted by Equation 4.4 is valid for large multi-charged analytes, for which the energy threshold is about 9 eV. Nevertheless, for the aniline derivatives studied, this phenomenon was observed for relatively low electron energies (< 3 eV). There are reports in the literature that state the ECD cathode can reach temperatures of 900ºC; [55, 56] one may question if that may not have some influence and allow the formation of these ions at the relatively low electron energies observed. Some further experiments may help to clarify this phenomenon.

Varying the electron energy and acquiring the spectra at the same instrumental conditions showed that there is an overall decrease in the

ion signal with no fragmentation being detected (Figure 4.10). It should be mentioned however that all experiments were performed at an ECD pulse length of 50 ms, which can influence the fragmentation in the sense that lower energies will need longer pulse lengths, while higher energies will need lower pulse lengths. Furthermore, it was found that for 4-fluoroaniline, chloroanilines and bromoanilines a signal enhancement was detected at an energy range of 0-2 eV, whereas for the other aniline derivatives the ion signal simply decreased with the increasing electron energy (Figure 4.10).

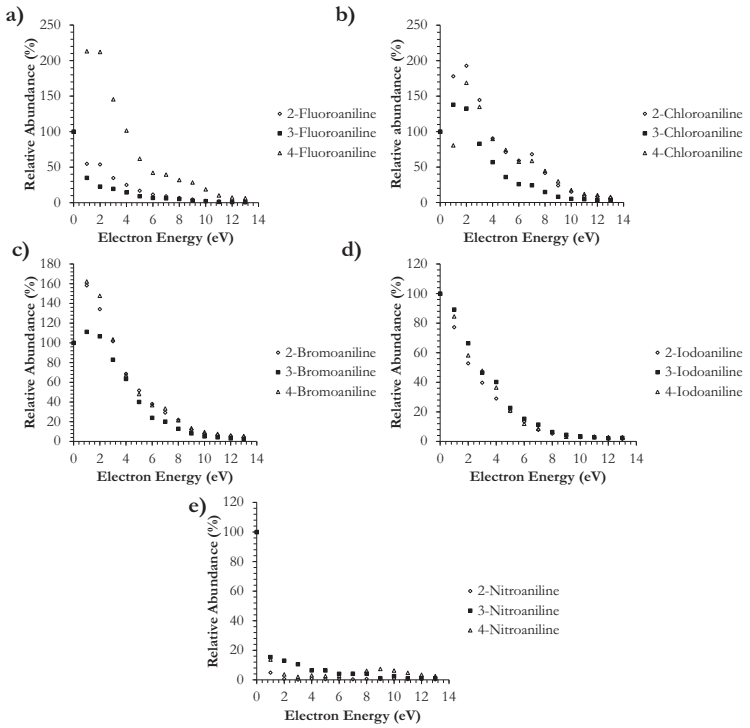

Figure 4.10. Relative abundance variation with the electron energy: a) fluoroanilines; b) chloroanilines; c) bromoanilines; d) iodoanilines; e) nitroanilines. (The abundance was calculated relative to the protonated molecule at electron energy=0 eV)

4.3 Conclusions

In this chapter we presented the fragmentation patterns of different substituted anilines. All aniline derivatives showed little fragmentation and in most cases the fragmentation was not helpful in distinguishing the various isomers. The exceptions were 2-chloro and 2-bromoaniline, for which the loss of HCl and HBr allowed the differentiation of the respective isomers, and the nitroanilines which exhibited different fragmentation pathways for all three isomers.

Regarding the isomer identification of haloanilines, using competitive fragmentation of proton bound dimers, it was possible to distinguish all isomers through the branching ratio values by pairing each of them with 4-nitroaniline.

The ECD results are still preliminary; nevertheless, the multiply charged species $[M+H]^{2+\bullet}$ and $[M+H]^{3+}$ were detected (to note that the $[M+H]^{3+}$ ion was detected only for bromo, iodo and nitroanilines due to mass range restrictions). To access the origin of these multiply-charged species, more experiments are needed, for example, it is planned to vary the ECD pulse length to determine its influence in the MS^2 spectrum of singly-charged protonated aniline derivatives.

4.4 References

1. Mortensen, S.K., et al., *Specific determination of 20 primary aromatic amines in aqueous food simulants by liquid chromatography-electrospray ionization-tandem mass spectrometry*. Journal of Chromatography A, 2005. **1091**(1-2): p. 40-50.
2. Padmanabhan, J., et al., *Theoretical Study on the Complete Series of Chloroanilines*. Journal of Physical Chemistry A, 2006. **110**(32): p. 9900-9907.
3. Jariwala, F.B., M. Figus, and A.B. Attygalle, *Ortho Effect in Electron Ionization Mass Spectrometry of N-Acylanilines Bearing a Proximal Halo Substituent*. Journal of the American Society for Mass Spectrometry, 2008. **19**(8): p. 1114-1118.
4. Fromberg, A., et al., *Analysis of chloro- and nitroanilines and -benzenes in soils by headspace solid-phase microextraction*. Journal of Chromatography A, 1996. **746**(1): p. 71-81.
5. Müller, L., E. Fattore, and E. Benfenati, *Determination of aromatic amines by solid-phase microextraction and gas chromatography-mass spectrometry in water samples*. Journal of Chromatography A, 1997. **791**(1-2): p. 221-230.
6. Lacorte, S., et al., *Determination of chlorobenzidines in industrial effluent by solid-phase extraction and liquid chromatography with electrochemical and mass spectrometric detection*. Journal of Chromatography A, 1999. **833**(2): p. 181-194.
7. Sutthivaiyakit, P., et al., *LC-MS/MS method for the confirmatory determination of aromatic amines and its application in textile analysis*. Analytical and Bioanalytical Chemistry, 2005. **381**(1): p. 268-276.

8. Wang, W., et al., *Solid-Phase Microextraction of Aromatic Amines with an Amide Bridged Calix[4]arene Coated Fiber*. Chromatographia, 2005. **61**(1): p. 75-80.
9. Maziarz, E.P. and T.D. Wood, *Gas-phase dimerization of dimethylaniline in an external electrospray Fourier transform mass spectrometer*. Journal of Mass Spectrometry, 1998. **33**(1): p. 45-54.
10. Trainor, T.M. and P. Vouros, *Electron capture negative ion chemical ionization mass spectrometry of derivatized chlorophenols and chloroanilines*. Analytical Chemistry, 1987. **59**(4): p. 601-610.
11. Kotiaho, T., M.J. Hayward, and R.G. Cooks, *Direct determination of chlorination products of organic amines using membrane introduction mass spectrometry*. Analytical Chemistry, 1991. **63**(17): p. 1794-1801.
12. Tao, W.A., L. Wu, and R.G. Cooks, *Differentiation and quantitation of isomeric dipeptides by low-energy dissociation of copper(II)-bound complexes*. Journal of the American Society for Mass Spectrometry, 2001. **12**(5): p. 490-496.
13. Tao, W.A., et al., *Copper(II)-Assisted Enantiomeric Analysis of d,l-Amino Acids Using the Kinetic Method: Chiral Recognition and Quantification in the Gas Phase*. Journal of the American Chemical Society, 2000. **122**(43): p. 10598-10609.
14. Wu, L., et al., *Recognition and quantification of binary and ternary mixtures of isomeric peptides by the kinetic method: metal ion and ligand effects on the dissociation of metal-bound complexes*. Journal of the American Society for Mass Spectrometry, 2003. **14**(2): p. 152-160.

15. Bjarnason, A., et al., *Isomer discrimination of disubstituted benzene derivatives through gas-phase iron(I) ion reactions in a Fourier-transform mass spectrometer.* Analytical Chemistry, 1989. **61**(17): p. 1889-1894.

16. Puzo, G., J.J. Fournie, and J.C. Prome, *Identification of stereoisomers of some hexoses by mass spectrometry using fast atom bombardment and mass ion kinetic energy.* Analytical Chemistry, 1985. **57**(4): p. 892-894.

17. Majumdar, T.K., et al., *Epimer distinction and structural effects on gas-phase acidities of alcohols measured using the kinetic method.* Journal of the American Chemical Society, 1992. **114**(8): p. 2897-2903.

18. Cooks, R.G. and P.S.H. Wong, *Kinetic Method of Making Thermochemical Determinations: Advances and Applications.* Accounts of Chemical Research, 1998. **31**(7): p. 379-386.

19. Capriolli, R., *The kinetic method.* Journal of Mass Spectrometry, 1999. **34**(2): p. 73.

20. Armentrout, P.B., *Is the kinetic method a thermodynamic method?* Journal of Mass Spectrometry, 1999. **34**(2): p. 74-78.

21. Drahos, L. and K. Vékey, *How closely related are the effective and the real temperature.* Journal of Mass Spectrometry, 1999. **34**(2): p. 79-84.

22. Cooks, R.G., J.T. Koskinen, and P.D. Thomas, *The kinetic method of making thermochemical determinations.* Journal of Mass Spectrometry, 1999. **34**(2): p. 85-92.

23. McLuckey, S.A., D. Cameron, and R.G. Cooks, *Proton affinities from dissociations of proton-bound dimers.* Journal of the American Chemical Society, 1981. **103**(6): p. 1313-1317.

24. Cooper, H.J., K. Håkansson, and A.G. Marshall, *The role of electron capture dissociation in biomolecular analysis.* Mass Spectrometry Reviews, 2005. **24**(2): p. 201-222.

25. Zubarev, R.A., N.L. Kelleher, and F.W. McLafferty, *Electron Capture Dissociation of Multiply Charged Protein Cations. A Nonergodic Process.* Journal of the American Chemical Society, 1998. **120**(13): p. 3265-3266.

26. Zubarev, R.A., et al., *Towards an understanding of the mechanism of electron- capture dissociation: a historical perspective and modern ideas.* European Journal of Mass Spectrometry, 2002. **8**(5): p. 337-349.

27. Zubarev, R.A., *Electron-capture dissociation tandem mass spectrometry.* Current Opinion in Biotechnology, 2004. **15**(1): p. 12-16.

28. Kjeldsen, F., et al., *Dissociative capture of hot (3-13 eV) electrons by polypeptide polycations: an efficient process accompanied by secondary fragmentation.* Chemical Physics Letters, 2002. **356**(3-4): p. 201-206.

29. Budnik, B.A., K.F. Haselmann, and R.A. Zubarev, *Electron detachment dissociation of peptide di-anions: an electron-hole recombination phenomenon.* Chemical Physics Letters, 2001. **342**(3-4): p. 299-302.

30. Cody, R.B. and B.S. Freiser, *Electron impact excitation of ions from organics: an alternative to collision induced dissociation.* Analytical Chemistry, 1979. **51**(4): p. 547-551.

31. Nielsen, M.L., et al., *Intramolecular hydrogen atom transfer in hydrogen-deficient polypeptide radical cations.* Chemical Physics Letters, 2000. **330**(5-6): p. 558-562.

32. Fung, Y.M.E., C.M. Adams, and R.A. Zubarev, *Electron Ionization Dissociation of Singly and Multiply Charged Peptides*. Journal of the American Chemical Society, 2009. **131**(29): p. 9977-9985.

33. Lioe, H. and R. O'Hair, *Comparison of collision-induced dissociation and electron-induced dissociation of singly protonated aromatic amino acids, cystine and related simple peptides using a hybrid linear ion trap–FT-ICR mass spectrometer*. Analytical and Bioanalytical Chemistry, 2007. **389**(5): p. 1429-1437.

34. Yoo, H.J., H. Liu, and K. Håkansson, *Infrared Multiphoton Dissociation and Electron-Induced Dissociation as Alternative MS/MS Strategies for Metabolite Identification*. Analytical Chemistry, 2007. **79**(20): p. 7858-7866.

35. Khairallah, G.N., R.A.J. O'Hair, and M.I. Bruce, *Gas-phase synthesis and reactivity of binuclear gold hydride cations, $(R_3PAu)_2H^+$ (R = Me and Ph)*. Dalton Transactions, 2006(30): p. 3699-3707.

36. Feketeová, L. and R.A.J. O'Hair, *Comparison of collision- versus electron-induced dissociation of sodium chloride cluster cations*. Rapid Communications in Mass Spectrometry, 2009. **23**(1): p. 60-64.

37. Kaczorowska, M.A. and H.J. Cooper, *Electron Induced Dissociation: A Mass Spectrometry Technique for the Structural Analysis of Trinuclear Oxo-Centred Carboxylate-Bridged Iron Complexes*. Journal of the American Society for Mass Spectrometry, 2010. **In Press**.

38. Tajima, S., et al., *Unimolecular HF Loss from the Molecular Ions of Fluorophenols and Fluoroanilines. A 'Ring-walk' Mechanism of a Fluorine Atom*. Rapid Communications in Mass Spectrometry, 1996. **10**(9): p. 1076-1078.

39. Parry, A., et al., *Thermodynamic studies of gas-phase proton transfer equilibria involving benzene: a reassessment of earlier data.* Journal of the Chemical Society, Faraday Transactions, 1992. **88**(22): p. 3331-3337.

40. Schwarz, H., *Some newer aspects of mass spectrometric ortho effects*, in *Topics in Current Chemistry: Organic Chemistry*. 1978, Springer-Verlag: Berlin. p. 231-263.

41. Attygalle, A., et al., *An unprecedented ortho effect in mass spectrometric fragmentation of even-electron negative ions from hydroxyphenyl carbaldehydes and ketones.* Tetrahedron Letters, 2006. **47**(27): p. 4601-4603.

42. Bobyleva, M.S., N.S. Kulikov, and S.I. Bobrovskii, *Mass spectrometry and structure of heterocyclic ions by collisional activation.* Chemistry of Heterocyclic Compounds, 1989. **25**(3): p. 274-279.

43. Holman, S.W., P. Wright, and G.J. Langley, *High-throughput approaches towards the definitive identification of pharmaceutical drug metabolites. 1. Evidence for an ortho effect on the fragmentation of 4-benzenesulfinyl-3-methylphenylamine using electrospray ionisation mass spectrometry.* Rapid Communications in Mass Spectrometry, 2008. **22**(15): p. 2355-2365.

44. McLafferty, F.W. and F. Turecek, *Interpretation of Mass Spectra.* 4th ed. 1993, Sausalito, California: University Science Books.

45. Karni, M. and A. Mandelbaum, *The 'even-electron rule'*. Organic Mass Spectrometry, 1980. **15**(2): p. 53-64.

46. Williams, J.P., et al., *Collision-induced fragmentation pathways including odd-electron ion formation from desorption electrospray ionisation generated protonated and deprotonated drugs derived from tandem accurate mass*

spectrometry. Journal of Mass Spectrometry, 2006. **41**(10): p. 1277-1286.

47. Levsen, K., et al., *Even-electron ions: a systematic study of the neutral species lost in the dissociation of quasi-molecular ions*. Journal of Mass Spectrometry, 2007. **42**(8): p. 1024-1044.
48. Harrison, A.G., *Chemical Ionization Mass Spectrometry*. 1983, Boca Raton, Florida: CRC Press, Inc.
49. Shukla, A., G. Nicol, and J. Futrell, *Tandem mass spectrometric study of 1,3,5-trinitrobenzene molecular ion: an unusual ortho effect involving a hydrogen atom from the aromatic ring*. Journal of Mass Spectrometry, 2000. **35**(7): p. 885-890.
50. Harley-Mason, J., T.P. Toube, and D.H. Williams, *Studies in mass spectrometry. Part VIII. peri- and ortho-Effects in the mass spectra of some aromatic nitro-compounds*. Journal of the Chemical Society B: Physical Organic, 1966: p. 396-400.
51. Herbert, R. and D.G. Wibberley, *1H-pyrrolo[2,3-b]pyridines. Part II. Fragmentation of some 1H-pyrrolo[2,3-b]pyridines induced by electron impact*. Journal of the Chemical Society B: Physical Organic, 1970: p. 459-463.
52. Robinson, G.E., C.B. Thomas, and J.M. Vernon, *The mass spectra of nitrophenyl(phenyl)methanes: the formation of an M-17 ion from the meta- and para-isomers*. Journal of the Chemical Society B: Physical Organic, 1971: p. 1273-1282.
53. Hunter, E.P. and S.G. Lias, *Proton Affinity Evaluation*, in *NIST Chemistry WebBook, NIST Standard Reference Database Number 69*, P.J. Linstrom and W.G. Mallard, Editors, National Institute of Standards and Technology: Gaithersburg, MD.

54. Zubarev, R.A., *Reactions of polypeptide ions with electrons in the gas phase*. Mass Spectrometry Reviews, 2003. **22**(1): p. 57-77.

55. Tsybin, Y.O., et al., *Combined infrared multiphoton dissociation and electron capture dissociation with a hollow electron beam in Fourier transform ion cyclotron resonance mass spectrometry*. Rapid Communications in Mass Spectrometry, 2003. **17**(15): p. 1759-1768.

56. Tsybin, Y.O., et al., *Electron capture dissociation Fourier transform ion cyclotron resonance mass spectrometry in the electron energy range 0–50 eV*. Rapid Communications in Mass Spectrometry, 2004. **18**(14): p. 1607-1613.

Chapter 5
Isoflavones

Five isoflavones (daidzein, genistein, formononetin, prunetin and biochanin A), known for their biological properties, are investigated by electrospray ionization mass spectrometry in the positive ion mode. The most probable protonation sites are determined taking into account semi-empirical calculations using the PM6 Hamiltonian. Fragmentation mechanisms are proposed based on accurate mass measurements, MS^3 experiments and supported by the semi-empirical calculations. Some of the fragmentations were found to be dependent on the substitution pattern of the B-ring and the ions afforded by these fragmentations can be considered as diagnostic ions. It was indeed possible to distinguish between prunetin and biochanin A, two isobaric isoflavone aglycones included in this study. Furthermore, a comparison of the fragmentation patterns of genistein and biochanin A, two isoflavones, with the fragmentation of their flavone counterparts, apigenin and acacetin, enabled to identify some key ions mainly due to structural features, allowing for the distinction between these two classes of compounds.

This chapter was based on a paper entitled "Electrospray FTICR mass spectrometry of five isoflavone aglycones: Some new insights" by Paulo J. Amorim Madeira, Carlos Borges and M. Helena Florêncio, submitted to *Rapid Communications in Mass Spectrometry*.

5 Electrospray FT-ICR Mass Spectrometry of five isoflavone aglycones: Some new insights

5.1 Introduction

Flavonoids make up a large group of naturally occurring compounds in plants [1, 2] and have many diverse applications and properties.[3] They appear quite often as O-glycosides, but free aglycones are also frequently isolated.[4] Flavonoids are responsible for many phenomena such as the shades of yellow, orange, and red in flowering plants, and important factors for plant growth, development and defense.[5] Many flavonoids (free aglycones and their glycosides) are endowed with biological activities, namely anti-inflammatory, anti-allergic and anti-tumoral, among others.[5-8] Furthermore, they have been shown to inhibit several enzymes, including lipoxygenase and cyclooxygenase, xanthine oxidase, NADH (reduced form of nicotinamide adenine dinucleotide) oxidase, among others.[5, 9-11] These biological properties are thought to be due to their antioxidant properties, which are displayed by limiting the production and/or scavenging of reactive oxygen species (ROS), [12-15] or even chelating metal ions preventing their participation in free radical generation reactions.[16, 17] Several studies have shown that they are present in high concentrations in fruits and vegetables.[4, 18] Flavones are one of the largest groups of flavonoids present in plants; however, in certain plant families other types of flavonoids can be found, *e.g.* isoflavones in *Leguminous* species.[4] Compounds of this class are considered a

potential therapeutic agent, particularly in the area of women's health.[3] They have estrogenic activity and are associated with prevention of breast and prostate cancer, in addition to cardiovascular disease.[3] The four most common isoflavones associated with phytoestrogenic herbs or extracts are daidzein, genistein, formononetin and biochanin A, found to occur as glucosides, glucoside manolate esters or as free aglycones.[3]

We decided to undergo a detailed Fourier Transform Ion Cyclotron Resonance (FTICR) mass spectrometry study, in the positive ion mode, of the gas-phase behaviour of five isoflavones (daidzein, genistein, prunetin, formononetin and biochanin A), following a previous study by some of us[4] and taking into account a reference study by Magda Claeys.[19] The fragmentation pattern of genistein, daidzein, formononetin and biochanin A in the negative ion mode has already been reported in the literature;[20, 21] nevertheless, and to the best of our knowledge, there is a lack of detailed studies on the gas-phase behaviour of these isoflavones in the positive ion mode. The behaviour under positive ion mode of daidzein[22-24] and genistein[22, 24] has already been reported. Nevertheless, of the available reports only one addressed specifically the fragmentation of daidzein,[23] while the others addressed quantification and identification through liquid chromatography-mass spectrometry (LC-MS) and liquid chromatography-tandem mass spectrometry (LC-MS/MS) experiments, without detailing the fragmentation pathways.[22, 24] Moreover, none of these reports indicated probable protonation sites. For the other three isoflavones, to the best of our knowledge, there are no studies addressing their gas-phase behaviour. Semi-empirical calculations were

performed to support the proposed fragmentation mechanisms. These inexpensive computational methodologies have been used successfully in a wide variety of mass spectrometry studies, including the fragmentation under ESI conditions of flavonoids[25-28] and α,β-unsaturated γ-lactones fused to furanose rings,[29] the fragmentation under EI conditions of buspirone,[30] complexation studies,[31, 32] evaluation of the strength of non-covalent interactions[33] and the study of fullerene derivatives,[34] to cite just a few.

The nomenclature used throughout this chapter to define the various product ions has been proposed by Claeys and co-workers,[19] adapted from those developed by Mabry and Markham[35] and Domon and Costello.[36]

5.2 Results and Discussion

The ESI-MS spectra of the five isoflavones under study (Figure 5.1) exhibited highly abundant protonated molecules and the corresponding sodiated and potassiated signals (the attribution errors are presented in Table 5.1).

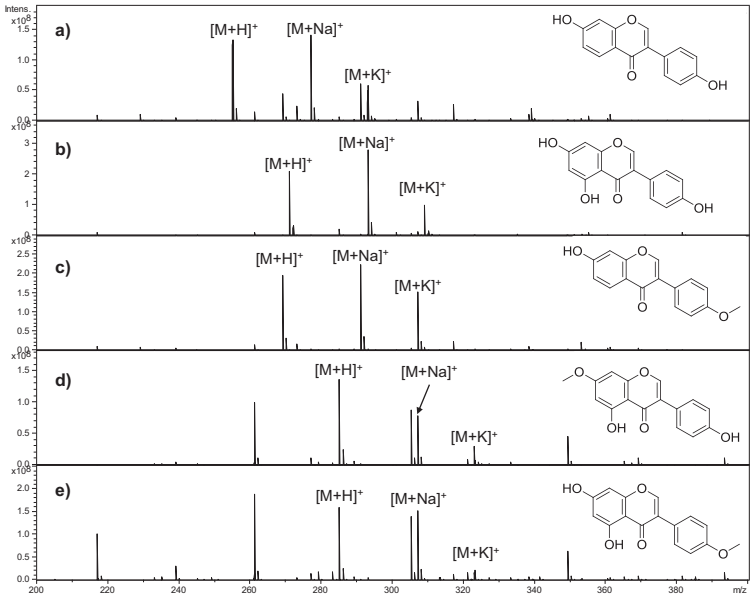

Figure 5.1. ESI FTICR-MS full scan mass spectra of: a) daidzein; b) genistein; c) formononetin; d) prunetin and e) biochanin A.

Table 5.1. Accurate mass data and attribution errors for the isoflavones under study.

		***m/z* found**	***m/z* calcd**	**Error (ppm)**
Daidzein	$[M+H]^+$	255.06532	255.06518	-0.5
	$[M+Na]^+$	277.04738	277.04713	-0.9
	$[M+K]^+$	293.02116	293.02107	-0.3
Genistein	$[M+H]^+$	271.06054	271.06010	-1.6
	$[M+Na]^+$	293.04169	293.04205	1.2
	$[M+K]^+$	309.01580	309.01598	0.6
Formononetin	$[M+H]^+$	269.08097	269.08084	-0.5
	$[M+Na]^+$	291.06313	291.06278	-1.2
	$[M+K]^+$	307.03712	307.03672	-1.3
Prunetin	$[M+H]^+$	285.07581	285.07575	-0.2
	$[M+Na]^+$	307.05784	307.05770	-0.5
	$[M+K]^+$	323.03162	323.03163	0.0
Biochanin A	$[M+H]^+$	285.07556	285.07575	0.7
	$[M+Na]^+$	307.05780	307.05770	-0.3
	$[M+K]^+$	323.03093	323.03163	2.2

5.2.1 Protonation site by semi-empirical calculations

The Molecular Electrostatic Potential (MEP) surface minima and the protonation reaction enthalpy, $\Delta_r H$, are presented in Table 5.2 and Table 5.3, respectively.

From the data presented in Table 5.2, it is clear that the electrostatic potential at the C^4 carbonyl group always has the lowest value. This means that when a proton approaches the compound it will be likely trapped by the C^4 carbonyl function. Furthermore, the heat of formation data presented in Table 5.3 reinforces the assumption that protonation is more likely to occur at the C^4 carbonyl function, since it is always the lowest energy form of all the possible protonation sites. In fact, these results are in agreement with what is described in the literature for flavones and flavonols.[19, 25, 26] An interesting observation concerns the fact that for genistein, prunetin and biochanin A the O^5 atom is not an electrostatic potential minimum. Nevertheless, the semi-empirical estimate of the protonation enthalpy lies well within the average unassigned error for the PM6 method (about 34 kJ mol^{-1}, for more information see MOPAC manual[37]). Hence, it is reasonable to assume that for these compounds protonation will occur at the C^4 keto group.

Table 5.2. Molecular Electrostatic Potential (MEP) surface minima (kJ mol^{-1}) calculated using the AM1[38] Hamiltonian implemented in MOPAC2009[37] (the minima are underlined).

	MEP minima (kJ mol^{-1})				
Atom	**Daidzein**	**Formononetin**	**Genistein**	**Prunetin**	**Biochanin A**
O^1	-120.9	-124.3	-125.5	-130.1	-128.9
$O^{4'}$	-223.8	-222.6	-227.6	-229.7	-226.4
O^4	-274.1	-277.0	-421.7	-428.0	-424.7
O^7	-186.2	-187.9	-179.1	-179.9	-180.7

Table 5.3. Protonation reaction enthalpy, $\Delta_r H$ (kJ mol^{-1}), for the isoflavones under study (the lowest Δ_rH for each possible site is underlined) calculated using the PM6[39] method as implemented in MOPAC2009.[37]

	$\Delta_r H$ (kJ mol^{-1})				
Atom	**Daidzein**	**Formononetin**	**Genistein**	**Prunetin**	**Biochanin A**
O^1	820.2	817.6	787.4	775.7	784.7
O$^{4'}$	756.3	738.6	755.1	745.8	733.5
O^4	656.3	544.2	622.0	609.8	609.4
O^5	-	-	609.8	597.6	609.4
O^7	807.4	808.4	809.1	786.9	810.5

5.2.2 Fragmentation of hydroxyisoflavones (daidzein and genistein)

The ESI-MS^2 of the protonated molecules of daidzein and genistein at collision energy of 17 eV are presented in Figure 5.2a and b, respectively.

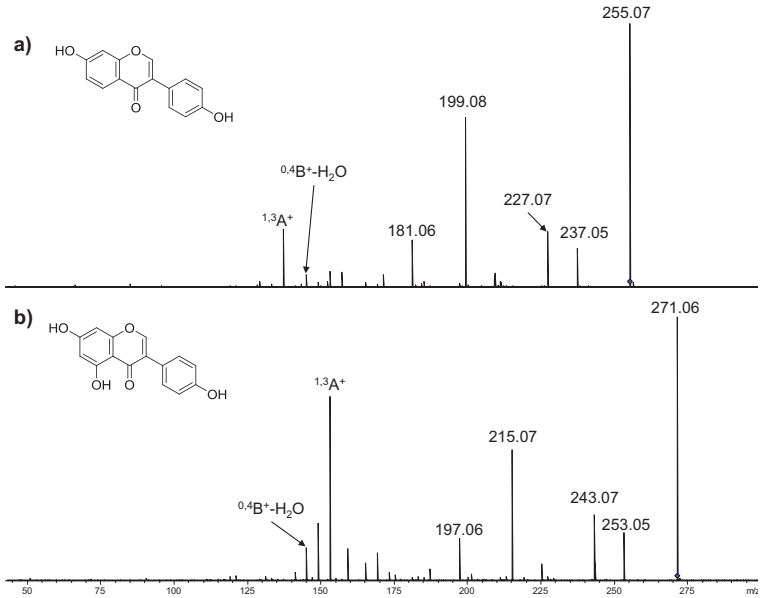

Figure 5.2. ESI-MS^2 spectra at collision energy of 17 eV of the protonated molecules of: a) daidzein; b) genistein.

Both protonated compounds can lose H_2O, affording the ions at m/z 237.05 and m/z 253.05, for daidzein and genistein respectively. Taking into account the structure of these compounds, for daidzein the loss of H_2O can occur from the hydroxyl groups at $C^{4'}$ or C^7, whereas for genistein this loss can occur from the hydroxyl groups at $C^{4'}$, C^5 and C^7. To determine the most probable fragmentation pathway, semi-empirical calculations were performed. For daidzein, the loss of H_2O from $C^{4'}$ afforded an ion with a ΔH_f = 784.1 kJ mol^{-1}, while for the loss of H_2O from the C^7 the value obtained was ΔH_f = 866.8 kJ mol^{-1}. The difference between the ΔH_f of both species is *ca.* 80 kJ mol^{-1}, which, taking into account the average unassigned error for PM6 calculations (see the previous section), makes reasonable to assume that the loss of H_2O for daidzein will occur from $C^{4'}$. For genistein, the loss of H_2O from $C^{4'}$ afforded an ion with ΔH_f = 571.0 kJ mol^{-1}, from C^5 yielded an ion with ΔH_f = 641.1 kJ mol^{-1} and from C^7 afforded an ion with ΔH_f = 601.9 kJ mol^{-1}. The loss from $C^{4'}$ yielded the ion with the lowest ΔH_f, thus making it reasonable to assume that this loss will also occur from the B-ring (even though the ΔH_f between the $C^{4'}$ and C^7 losses lie within the considered average unassigned error).

Both protonated compounds can also lose CO proposed to occur from the C-ring, affording the ions at m/z 227.07 for daidzein and m/z 243.07 for genistein. These ions, m/z 227.07 for daidzein and m/z 243.07 for genistein, can lose another CO to afford the ions at m/z 199.08 (daidzein) and m/z 215.07 (genistein). These fragmentations were confirmed by MS^3 experiments (Figure 5.3).

For genistein, the ion at m/z 243.07 can also lose H_2O, affording the ion at m/z 225.05 and this fragmentation was confirmed by means

of MS^3 experiments (Figure 5.3b). The ions at m/z 199.08 and m/z 215.07, for daidzein and genistein respectively, can lose H_2O, affording the ions at m/z 181.06 for daidzein and m/z 197.06 for genistein (Figure 5.4).

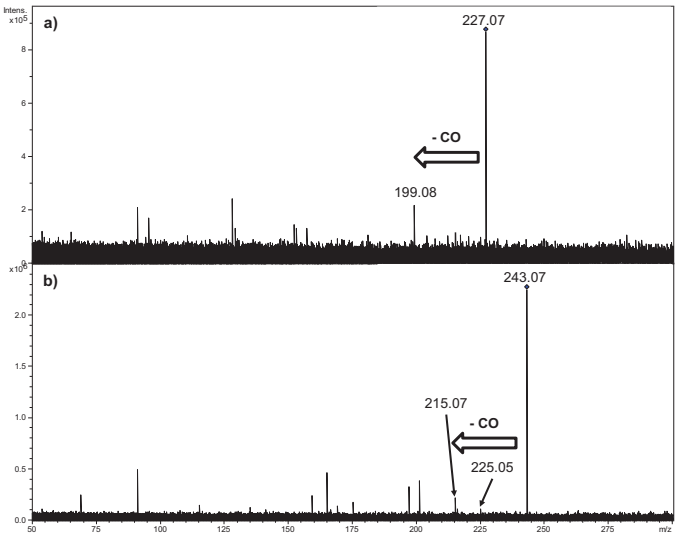

Figure 5.3. MS^3 spectra of the $[M+H-CO]^+$ ions of: a) daidzein, SORI power 0.40%; b) genistein, SORI power 0.45%.

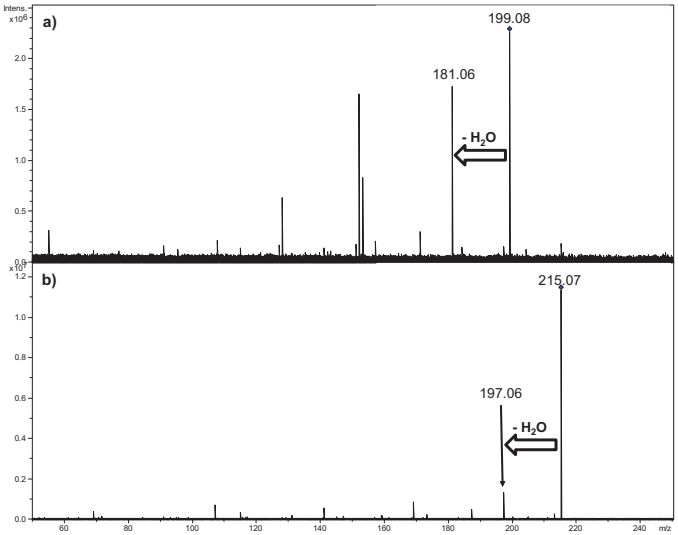

Figure 5.4. MS^3 spectra of the $[M+H-2CO]^+$ ions of: a) daidzein, SORI power 0.40%; b) genistein, SORI power 0.35%.

The ions at m/z 133.03 for daidzein (relative abundance of 1.4%, Figure 5.2a) and m/z 149.02 for genistein (Figure 5.2b) were attributed to $[M+H-B-CO]^+$, with errors of 0.4 ppm and 0.1 ppm, respectively.

The $^{1,3}A^+$ and $^{1,3}B^+$ ions resulting from retro Diels-Alder fragmentation were found for these two isoflavones. The $^{1,3}A^+$ ions were found at m/z 137.02 for daidzein (relative abundance of 22%) and m/z 153.02 for genistein (relative abundance of 68%), with errors of 0.0 and 0.1 ppm, respectively. The m/z 153 ion was already reported in the literature for genistein;[22] nevertheless, an ion structure was not proposed in that study. The $^{0,4}B^+$-H_2O ions were found at m/z 145.03 (relative abundances of 5% for daidzein and 12% for genistein) for both compounds and were attributed with errors of 0.0 and -0.1 ppm for daidzein and genistein, respectively. The presence of the m/z 145 product ion has already been reported in the literature,[22] nevertheless no structure was proposed for this ion. The $^{1,3}B^+$ ions were found at m/z 119.05, but with relative abundances lower than 2%.

The observations described so far are summarized in Scheme 5.1, which depicts the fragmentation mechanism proposed for the protonated molecules of daidzein and genistein. The attributions for daidzein are in agreement to the ones proposed by March *et al.*[23] The accurate mass measurement data, ion formula, attribution and mass errors are presented in Table 5.4 and Table 5.5, for daidzein and genistein, respectively.

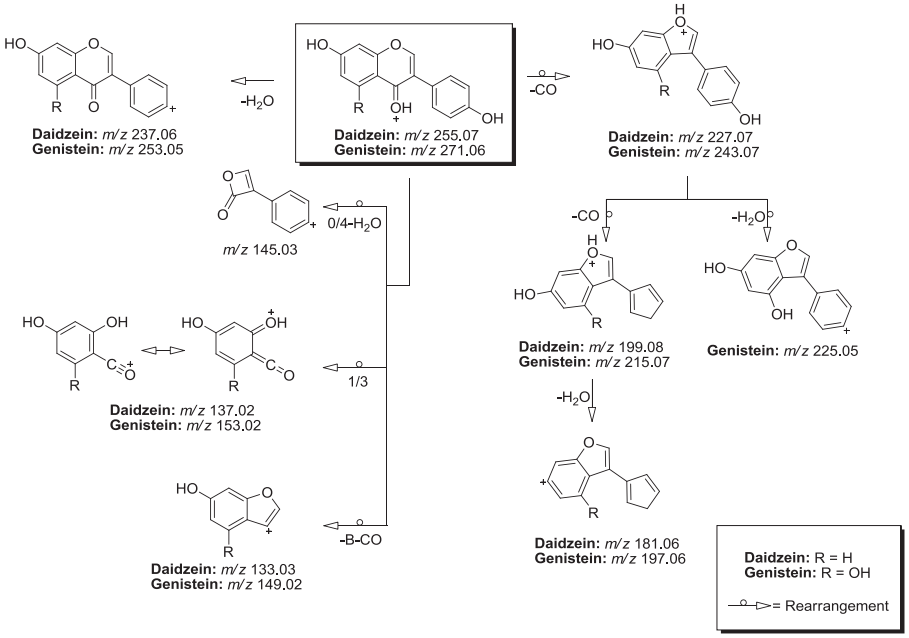

Scheme 5.1. Fragmentation mechanism proposed for the protonated molecules of daidzein and genistein.

Table 5.4. Accurate mass measurements, ion formula, attributions and mass errors for the MS^2 spectrum of the protonated daidzein.

Meas. *m/z*	Calcd. *m/z*	Ion Formula	Attribution	Error (ppm)
255.06516	255.06519	$C_{15}H_{11}O_4^+$	$[M+H]^+$	0.1
237.05462	237.05462	$C_{15}H_9O_3^+$	$[M+H-H_2O]^+$	0.0
227.07029	227.07027	$C_{14}H_{11}O_3^+$	$[M+H-CO]^+$	-0.1
199.07535	199.07536	$C_{13}H_{11}O_2^+$	$[M+H-2CO]^+$	0.0
181.06482	181.06479	$C_{13}H_9O^+$	$[M+H-2CO-H_2O]^+$	-0.2
145.02840	145.02841	$C_9H_5O_2^+$	$^{0,4}B^+-H_2O$	0.0
137.02332	137.02332	$C_7H_5O_3^+$	$^{1,3}A^+$	0.0
133.02836	133.02841	$C_8H_5O_2^+$	$[M+H-B-CO]^+$	0.4
119.04910	119.04914	$C_8H_7O^+$	$^{1,3}B^+$	0.4

Table 5.5: Accurate mass measurements, ion formula, attributions and mass errors for the MS^2 spectrum of the protonated genistein.

Meas. *m/z*	Calcd. *m/z*	Ion Formula	Attribution	Error (ppm)
271.06014	271.06010	$C_{15}H_{11}O_5^+$	$[M+H]^+$	-0.2
253.04951	253.04954	$C_{15}H_9O_4^+$	$[M+H-H_2O]^+$	0.1
243.06515	243.06519	$C_{14}H_{11}O_4^+$	$[M+H-CO]^+$	0.1
225.05461	225.05462	$C_{14}H_9O_3^+$	$[M+H-CO-H_2O]^+$	0.1
215.07027	215.07027	$C_{13}H_{11}O_3^+$	$[M+H-2CO]^+$	0.0
197.05972	197.05971	$C_{13}H_9O_2^+$	$[M+H-2CO-H_2O]^+$	-0.1
153.01823	153.01824	$C_7H_5O_4^+$	$^{1,3}A^+$	0.1
149.02330	149.02332	$C_8H_5O_3^+$	$[M+H-B-CO]^+$	0.1
145.02842	145.02841	$C_9H_5O_2^+$	$^{0,4}B^+-H_2O$	-0.1
119.04911	119.04914	$C_8H_7O^+$	$^{1,3}B^+$	0.3

5.2.3 Fragmentation of methoxyisoflavones (formononetin, prunetin and biochanin A)

The ESI-MS^2 of the protonated molecules of formononetin, prunetin and biochanin A at collision energy of 17 eV are presented in Figure 5.5a-c, respectively.

It is clear from the MS^2 spectra depicted in Figure 5.5a and c that formononetin and biochanin A lose 15 Da to afford the ions at *m/z* 254.06 and *m/z* 270.05. The accurate mass measurements allowed us to attribute this loss to $^{\bullet}CH_3$, with errors of -0.1 ppm for formononetin and 0.0 ppm for biochanin A. Although even-electron ions, such as protonated molecules, do not usually lose radicals, a violation of the 'even-electron rule',[40, 41] exceptions to this rule have been reported in the literature.[41-43] By means of MS^3 experiments (Figure 5.6), it was possible to observe that these $[M+H-CH_3]^{+\bullet}$ ions can in turn lose $H^{\bullet}$, affording the ions at *m/z* 253.05 for formononetin and *m/z* 269.04 for biochanin A.

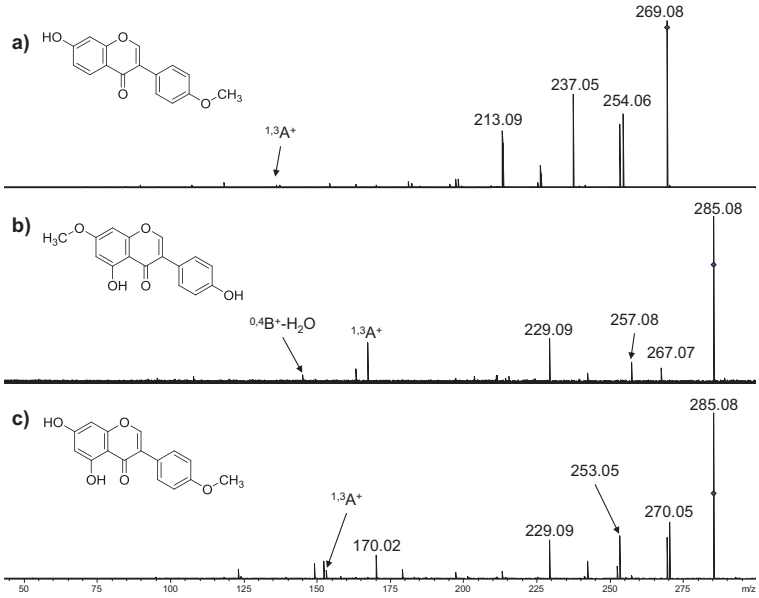

Figure 5.5. ESI-MS^2 spectra at collision energy of 17 eV of the protonated molecules of: a) formononetin; b) prunetin; c) biochanin A.

Interestingly, the loss of $^{\bullet}CH_3$ was not detected for prunetin, in which the methoxy group is attached to the A-ring. The same behaviour was found for the loss of CH_3OH, which was detected for formononetin (m/z 237.05 attributed with an error of 0.2 ppm) and for biochanin A (m/z 253.05 attributed with an error of 0.2 ppm) and not detected for prunetin. Taking into account this behaviour and the semi-empirical data presented in Table 5.6 (for the particular case of the isobaric prunetin and biochanin A), it is reasonable to assume that the loss from the A-ring is not favoured whereas the loss from the B-ring is favoured.

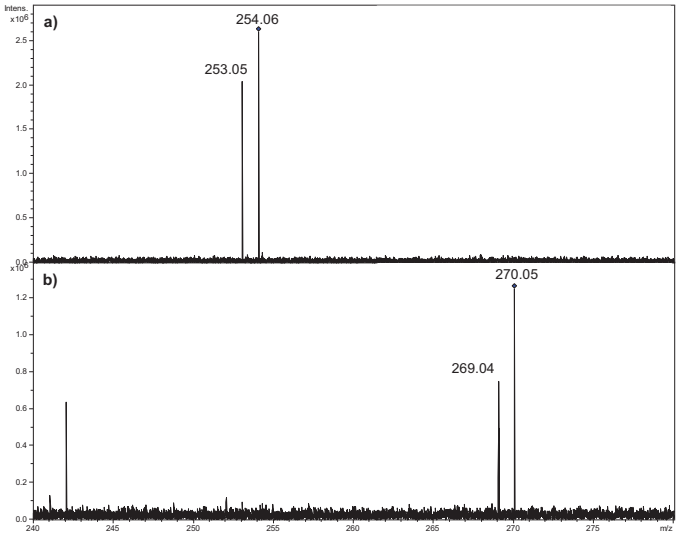

Figure 5.6. MS^3 spectra of the $[M+H-CH_3]^{+\bullet}$ ions of: a) formononetin, SORI power 0.40%; b) biochanin A, SORI power 0.50%.

Table 5.6. $\Delta_f H$ (kJ mol^{-1}) of the ions resulting from the loss of CH_3OH and $^{\bullet}CH_3$ from the protonated molecules of prunetin and biochanin A (the lowest $\Delta_f H$ is underlined) calculated using the PM6[39] method as implemented in MOPAC2009.[37]

	Isoflavone	Ion Structure	$\Delta_f H$ (kJ mol^{-1})
Loss of CH_3OH	**Prunetin**	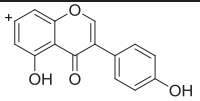	601.9
	Biochanin A	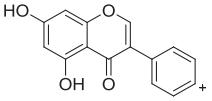	<u>571.0</u>
Loss of $^{\bullet}CH_3$	**Prunetin**	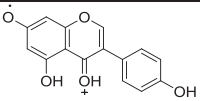	223.2
	Biochanin A	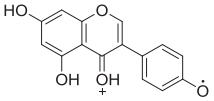	<u>163.0</u>

As mentioned above, the losses of $^{\bullet}CH_3$ and CH_3OH were not detected for prunetin. For this compound, however, the loss of H_2O to afford the ion at m/z 267.07 was detected and this ion was attributed to

$[M+H-H_2O]^+$ with an error of 0.6 ppm. This behaviour led us to examine more closely the structure of the $[M+H-H_2O]^+$ ion for daidzein and genistein (these isoflavones were discussed above). Daidzein, genistein and prunetin have a hydroxyl group at the B-ring; nevertheless, they also have other hydroxyl groups from which the loss of H_2O might be feasible. To access which of them is responsible for the loss of H_2O, semi-empirical calculations were performed and the data are presented in Table 5.7.

Table 5.7. $\Delta_f H$ (kJ mol^{-1}) for the $[M+H-H_2O]^+$ ions for daidzein, genistein and prunetin (the lowest $\Delta_f H$ is underlined) calculated using the PM6[39] method as implemented in MOPAC2009.[37]

Isoflavone	$[M+H-H_2O]^+$ Structure	$\Delta_f H$ (kJ mol^{-1})
Daidzein	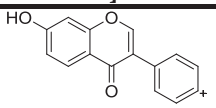	<u>784.1</u>
	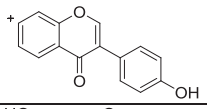	866.8
Genistein	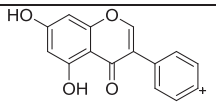	<u>571.0</u>
	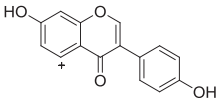	641.1
	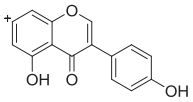	601.9
Prunetin	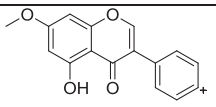	<u>580.1</u>
	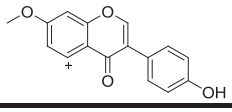	636.0

From the semi-empirical data presented, it is clear that the loss of H_2O from the B-ring results in a structure with the lowest ΔH_f, thus

making it more favourable. This finding is consistent with the loss of H_2O from the protonated prunetin.

For prunetin and biochanin A, the loss of CO from the protonated molecules to afford the ion at m/z 257.08 was detected (to note that the relative abundance of the m/z 257.08 for biochanin A is lower than 2%). The loss of two CO molecules was detected for the three methoxyisoflavones. This loss afforded the ion at m/z 213.09 for formononetin and the ions at m/z 229.09 for prunetin and biochanin A. It should be mentioned that the m/z 229.09 ion for prunetin can also be formed from the loss of CO by the m/z 257.08 ion (MS^3 shown in Figure 5.7).

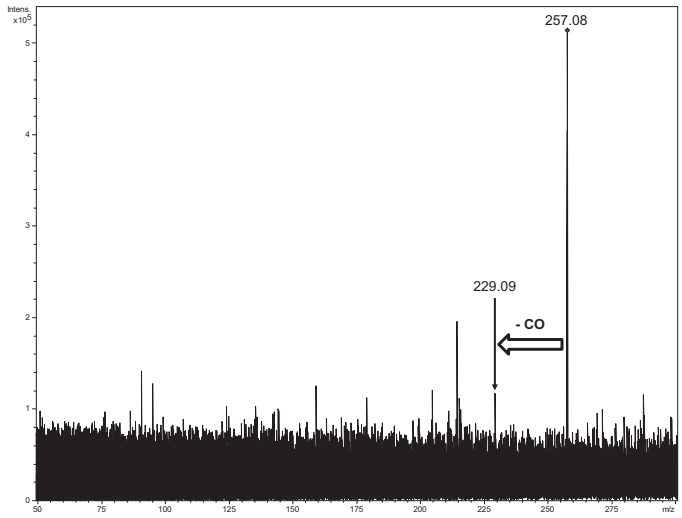

Figure 5.7. MS^3 spectrum of the $[M+H-CO]^{+\bullet}$ ion of prunetin, SORI power 0.45%.

Retro Diels-Alder fragmentation was also observed, that is, the $^{1,3}A^+$ ions were detected for the three methoxyisoflavones, at m/z 137.02 for formononetin with an error of 0.5 ppm, at m/z 167.03 for prunetin with an error of 0.6 ppm and at m/z 153.02 for biochanin A with an

error of 0.1 ppm. The $^{0,4}B^{+}$-H_2O ion detected at *m/z* 145.03, albeit with a low relative abundance (< 5%) for prunetin only, was attributed with an error of -0.7 ppm.

For prunetin and biochanin A, ions at *m/z* 163.04 and *m/z* 149.02, respectively, were found. With the accurate mass data, it was possible to attribute these signals to $[M+H-B-CO]^{+}$ ions, with errors of -0.1 ppm for prunetin and 0.0 ppm for biochanin A.

The ion at *m/z* 170.02, found for biochanin A, was attributed to a radical ion, $C_7H_6O_5^{+\bullet}$ with an error of -0.1 ppm. As mentioned before (*vide supra*), radical elimination from even-electron ions can occur if the generated product ions have high stability.[42] This appears to be the case, since the relative abundance of the *m/z* 170.02 is *ca.* 15%. For this particular loss, $C_9H_7^{\bullet}$, extensive rearrangements are expected to occur and a structure could not be proposed at this point.

The observations described so far are summarized in Scheme 5.2, which depicts the fragmentation mechanism proposal for the protonated molecules of formononetin, prunetin and biochanin A. The accurate mass measurement data, ion formula, attribution and mass errors for formononetin, prunetin and biochanin A are presented in Table 5.8, Table 5.9 and Table 5.10, respectively.

Table 5.8: Accurate mass measurements, ion formula, attributions and mass errors for the MS^2 spectrum of the protonated formononetin.

Meas. *m/z*	Calcd. *m/z*	Ion Formula	Attribution	Error (ppm)
269.08069	269.08084	$C_{16}H_{13}O_4^{+}$	$[M+H]^{+}$	0.5
254.05742	254.05736	$C_{15}H_{10}O_4^{+\bullet}$	$[M+H-CH_3]^{+\bullet}$	-0.2
253.04954	253.04954	$C_{15}H_9O_4^{+}$	$[M+H-CH_3-H]^{+}$	0.0
237.05458	237.05462	$C_{15}H_9O_3^{+}$	$[M+H-CH_3OH]^{+}$	0.2
213.09103	213.09101	$C_{14}H_{13}O_2^{+}$	$[M+H-2CO]^{+}$	-0.1
137.02325	137.02332	$C_7H_5O_3^{+}$	$^{1,3}A^{+}$	0.5

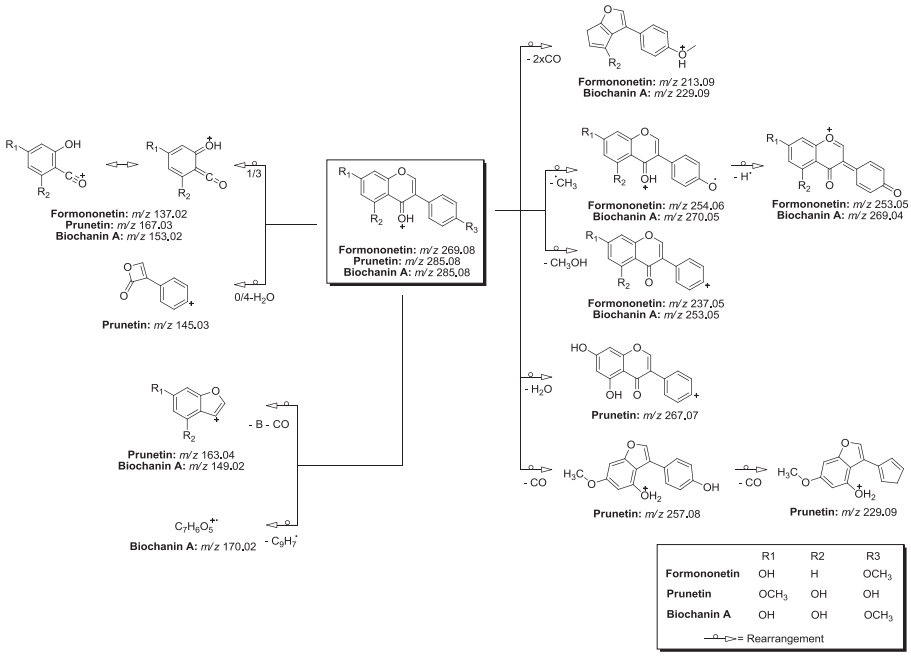

Scheme 5.2: Fragmentation mechanism proposed for the protonated molecules of formononetin, prunetin and biochanin A.

Table 5.9: Accurate mass measurements, ion formula, attributions and mass errors for the MS^2 spectrum of the protonated prunetin.

Meas. *m/z*	Calcd. *m/z*	Ion Formula	Attribution	Error (ppm)
285.07577	285.07575	$C_{16}H_{13}O_5^+$	$[M+H]^+$	-0.1
267.06502	267.06519	$C_{16}H_{11}O_4^+$	$[M+H-H_2O]^+$	0.6
257.08098	257.08084	$C_{15}H_{13}O_4^+$	$[M+H-CO]^+$	-0.6
229.08584	229.08592	$C_{14}H_{13}O_3^+$	$[M+H-2CO]^+$	0.3
167.03378	167.03389	$C_8H_7O_4^+$	$^{1,3}A^+$	0.6
163.03890	163.03897	$C_9H_7O_3^+$	$[M+H-B-CO]^+$	0.4
145.02850	145.02841	$C_9H_5O_2^+$	$^{0,4}B^+-H_2O$	-0.7

Table 5.10: Accurate mass measurements, ion formula, attributions and mass errors for the MS^2 spectrum of the protonated biochanin A.

Meas. *m/z*	Calcd. *m/z*	Ion Formula	Attribution	Error (ppm)
285.07579	285.07575	$C_{16}H_{13}O_5^+$	$[M+H]^+$	-0.1
270.05228	270.05227	$C_{15}H_{10}O_5^{+\bullet}$	$[M+H-CH_3]^{+\bullet}$	0.0
269.04449	269.04445	$C_{15}H_9O_5^+$	$[M+H-CH_3-H]^+$	-0.2
253.04948	253.04954	$C_{15}H_9O_4^+$	$[M+H-CH_3OH]^+$	0.2
170.02098	170.02097	$C_7H_6O_5^{+\bullet}$	$[M+H-C_9H_7]^{+\bullet}$	-0.1
153.01822	153.01824	$C_7H_5O_4^+$	$^{1,3}A^+$	0.1
149.02332	149.02332	$C_8H_5O_3^+$	$[M+H-B-CO]^+$	0.0

For flavones and flavonols, it is reported in the literature that the $^{0,4}B^+$ ion loses H_2O to afford the $^{0,4}B^+$-H_2O ion.[19, 26] For the isoflavones under study, the $^{0,4}B^+$ ion was not detected in any of the MS^2 spectra; nevertheless, the $^{0,4}B^+$-H_2O is present in all, even though in some cases with rather low abundance, namely for formononetin and biochanin A. This could mean that, unlike flavones and flavonones[19], isoflavones suffer a concerted loss of H_2O with the 0/4 fragmentation, hence the location of the B-ring may greatly influence the retro Diels-Alder fragmentations. These fragmentations proved indeed to be very valuable in the distinction of isomers from different classes of flavonoids.

To shed some light on this particular subject, we decided to compare the fragmentation of genistein and biochanin A with the fragmentation of the corresponding flavone isomers, *i.e.* apigenin and acacetin,[19] respectively (Scheme 5.3).

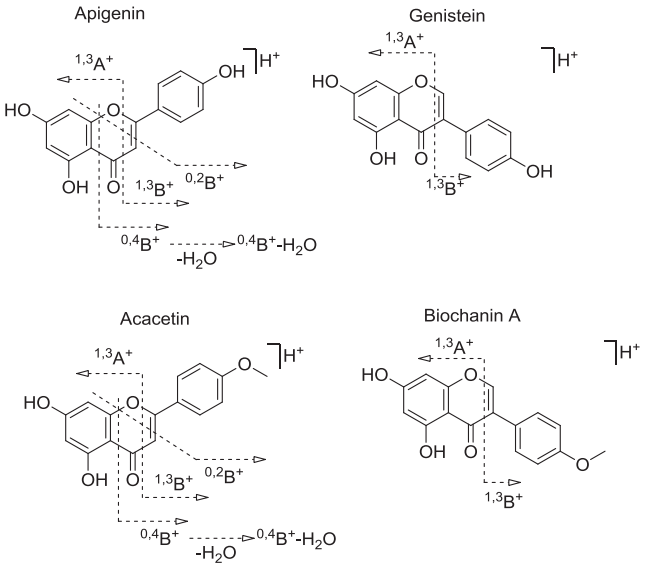

Scheme 5.3. C-ring fragmentation comparison between flavones and isoflavones (for flavones the data was collected from reference [19]).

For flavones, the low-energy CID of the $[M+H]^+$ ions afforded the $^{1,3}A^+$, $^{1,3}B^+$ and $^{0,4}B^+$ ions (resulting from retro Diels-Alder fragmentations) and $^{0,2}B^+$ ions. For isoflavones, the only C-ring fragmentations detected were those that afforded the $^{1,3}A^+$ and $^{1,3}B^+$ ions (retro Diels-Alder fragmentations) and the $^{0,4}B^+$-H_2O ion. The MS^2 spectra used in this comparison were acquired under different activating conditions; nevertheless, it seems reasonable to assume that these differences in fragmentation behaviour are mainly due to structural features. In fact, semi-empirical calculations were performed to estimate the Δ_fH of the $^{0,4}B^+$ ions for apigenin, genistein, acacetin and biochanin A and the results are presented in Table 5.11.

It is clear that the $^{0,4}B^+$ ion always has the lowest heat of formation for flavones, *i.e.* the formation of the $^{0,4}B^+$ ion is energetically more favoured for flavones than for isoflavones.

Table 5.11: $\Delta_f H$ (kJ mol^{-1}) for the $^{0,4}B^+$ for apigenin, genistein, acacetin and biochanin A calculated using the PM6[39] method as implemented in MOPAC2009.[37] (the lowest $\Delta_f H$ is underlined)

$^{0,4}B^+$ ion	$\Delta_f H$ (kJ mol^{-1})
Apigenin	278.3
Genistein	392.0
Acacetin	375.5
Biochanin A	402.1

5.3 Conclusions

The most probable protonation site was found to be the C^4 keto group, taking into account semi-empirical calculations. Accurate mass measurements and MS^3 experiments on some key ions, together with semi-empirical calculations, enabled to identify some characteristic behaviour. Losses of $^{\bullet}CH_3$ and CH_3OH were detected only when the methoxy group is attached to the B-ring. The resulting ions can then be used as diagnostic ions for the identification of isomers (as was the case of prunetin and biochanin A).

The C-ring fragmentations detected afforded retro Diels-Alder ions ($^{1,3}A^+$ and $^{1,3}B^+$). The $^{0,4}B^+$ ions were not detected for any of the isoflavones under study. Semi-empirical calculations showed that energetic factors might be responsible for the absence of the $^{0,4}B^+$ ion in these isoflavones. Comparison of the fragmentation of isoflavones (genistein and biochanin A) with their flavone counterparts (apigenin and acacetin) clearly shows that the position of the B-ring greatly influences fragmentation.

5.4 References

1. Harborne, J.B., *The Flavonoids: Advances in Research Since 1986*. 1994, London: Chapman and Hall.
2. Harborne, J.B., *Methods in Plant Biochemistry, vol. 1, Plant Phenolics*. 1989, London: Academic Press.
3. Swinny, E.E. and K.R. Markham, *Applications of flavonoid analysis and identification: Isoflavones (phytoestrogens) and 3-deoxyanthocyanins*, in *Flavonoids in health and disease*, C.A. Rice-Evans and L. Parker, Editors. 2003, Marcel Dekker, Inc.: New York. p. 97-122.
4. Borges, C., et al., *Structural characterisation of flavonoids and flavonoid-O-glycosides extracted from Genista tenera by fast-atom bombardment tandem mass spectrometry*. Rapid Communications in Mass Spectrometry, 2001. **15**(18): p. 1760-1767.
5. Pietta, P.-G., C. Gardana, and A. Pietta, *Flavonoids in herbs*, in *Flavonoids in health and disease*, C.A. Rice-Evans and L. Parker, Editors. 2003, Marcel Dekker, Inc.: New York. p. 43-69.
6. Prior, R.L. and G. Cao, *Flavonoids: Diet and Health Relationships*. Nutrition in Clinical Care, 2000. **3**(5): p. 279-288.
7. Ielpo, M.T.L., et al., *Immunopharmacological properties of flavonoids*. Fitoterapia, 2000. **71**(Supplement 1): p. S101-S109.
8. Craig, W.J., *Health-promoting properties of common herbs*. American Journal of Clinical Nutrition, 1999. **70**(3): p. 491S-499.
9. Valerio, L.G., et al., *Induction of human NAD(P)H:quinone oxidoreductase (NQO1) gene expression by the flavonol quercetin*. Toxicology Letters, 2001. **119**(1): p. 49-57.

10. Dugas, A.J., et al., *Evaluation of the Total Peroxyl Radical-Scavenging Capacity of Flavonoids: Structure/Activity Relationships.* Journal of Natural Products, 2000. **63**(3): p. 327-331.
11. Samman, S., P.M.L. Wall, and E. Farmakalidis, *Flavonoids and other phytochemicals in relation to coronary heart disease*, in *Antioxidants in human health and disease*, T.K. Basu, N.J. Temple, and M.L. Carg, Editors. 1999, CABI: Wallingford, UK. p. 175-187.
12. Zandi, P. and M.H. Gordon, *Antioxidant activity of extracts from old tea leaves.* Food Chemistry, 1999. **64**(3): p. 285-288.
13. Pietta, P.-G., *Flavonoids as Antioxidants.* Journal of Natural Products, 2000. **63**(7): p. 1035-1042.
14. Amaral, S., et al., *Plant extracts with anti-inflammatory properties--A new approach for characterization of their bioactive compounds and establishment of structure-antioxidant activity relationships.* Bioorganic & Medicinal Chemistry, 2009. **17**(5): p. 1876-1883.
15. Silva, M.M., et al., *Structure-antioxidant Activity Relationships of Flavonoids: A Re-examination.* Free Radical Research, 2002. **36**(11): p. 1219 - 1227.
16. Mira, L., et al., *Interactions of Flavonoids with Iron and Copper Ions: A Mechanism for their Antioxidant Activity.* Free Radical Research, 2002. **36**(11): p. 1199 - 1208.
17. Fernandez, M.T., et al., *Iron and copper chelation by flavonoids: an electrospray mass spectrometry study.* Journal of Inorganic Biochemistry, 2002. **92**(2): p. 105-111.
18. Robards, K. and M. Antolovich, *Analytical chemistry of fruit bioflavonoids: A review.* Analyst, 1997. **122**: p. 11R-34R.

19. Ma, Y.L., et al., *Characterization of flavone and flavonol aglycones by collision-induced dissociation tandem mass spectrometry.* Rapid Communications in Mass Spectrometry, 1997. **11**(12): p. 1357-1364.

20. Kang, J., L.A. Hick, and W.E. Price, *A fragmentation study of isoflavones in negative electrospray ionization by MS^n ion trap mass spectrometry and triple quadrupole mass spectrometry.* Rapid Communications in Mass Spectrometry, 2007. **21**(6): p. 857-868.

21. Kang, J., W.E. Price, and L.A. Hick, *Simultaneous determination of isoflavones and lignans at trace levels in natural waters and wastewater samples using liquid chromatography/electrospray ionization ion trap mass spectrometry.* Rapid Communications in Mass Spectrometry, 2006. **20**(16): p. 2411-2418.

22. Otieno, D.O., H. Rose, and N.P. Shah, *Profiling and quantification of isoflavones in soymilk from soy protein isolate using extracted ion chromatography and positive ion fragmentation techniques.* Food Chemistry, 2007. **105**(4): p. 1642-1651.

23. March, R.E., et al., *High-energy and low-energy collision-induced dissociation of protonated flavonoids generated by MALDI and by electrospray ionization.* International Journal of Mass Spectrometry, 2007. **262**(1-2): p. 51-66.

24. Satterfield, M., D.M. Black, and J.S. Brodbelt, *Detection of the isoflavone aglycones genistein and daidzein in urine using solid-phase microextraction-high-performance liquid chromatography-electrospray ionization mass spectrometry.* Journal of Chromatography B: Biomedical Sciences and Applications, 2001. **759**(1): p. 33-41.

25. Ma, Y.-L., et al., *Internal glucose residue loss in protonated O-diglycosyl flavonoids upon low-energy collision-induced dissociation.* Journal of the American Society for Mass Spectrometry, 2000. **11**(2): p. 136-144.
26. Justino, G.C., C.M. Borges, and M.H. Florêncio, *Electrospray ionization tandem mass spectrometry fragmentation of protonated flavone and flavonol aglycones: a re-examination.* Rapid Communications in Mass Spectrometry, 2009. **23**(2): p. 237-248.
27. Franski, R., et al., *Electrospray mass spectrometric decomposition of some glucuronic acid-containing flavonoid diglycosides.* Phytochemical Analysis, 2003. **14**(3): p. 170-175.
28. Franski, R., et al., *Differentiation of Interglycosidic Linkages in Permethylated Flavonoid Glycosides from Linked-Scan Mass Spectra (B/E).* Journal of Agricultural and Food Chemistry, 2002. **50**(5): p. 976-982.
29. Madeira, P.J.A., et al., *Electrospray Ionization Mass Spectrometry analysis of newly synthesised a,β-unsaturated γ-lactones fused to sugars.* Rapid Communications in Mass Spectrometry, 2010. **24**: p. 1049-1058.
30. Zayed, M.A., et al., *Mass spectrometric investigation of buspirone drug in comparison with thermal analyses and MO-calculations.* Spectrochimica Acta, Part A: Molecular and Biomolecular Spectroscopy, 2007. **67**(2): p. 522-530.
31. Przybylski, P., et al., *ESI MS and PM5 semiempirical studies of gossypol schiff base with (R)-tetrahydrofurfurylamine complexes and monovalent cations.* Journal of Molecular Structure, 2004. **693**(1-3): p. 95-102.
32. Huczynski, A., B. Brzezinski, and F. Bartl, *Structures of complexes of benzyl and allyl esters of monensin A with Mg^{2+}, Ca^{2+}, Sr^{2+}, Ba^{2+} cations*

studied by ESI-MS and PM5 methods. Journal of Molecular Structure, 2008. **886**(1-3): p. 9-16.

33. Ishikawa, K., T. Nakamura, and Y. Koga, *Cross-checking of nanoelectrospray ionization mass spectrometry and computer simulation for the evaluation of the interaction strength of non-covalently bound enkephalins in solution*. Journal of Mass Spectrometry, 2001. **36**(8): p. 937-942.
34. Khairallah, G. and J.B. Peel, *Cyano Adduct Anions of C70: Electrospray Mass Spectrometric Studies*. Journal of Physical Chemistry A, 1997. **101**(36): p. 6770-6774.
35. Mabry, T.J. and K.R. Markahm, in *The Flavonoids*, J.B. Harborne, T.J. Mabry, and H. Mabry, Editors. 1975, Academic press: New York. p. 78.
36. Domon, B. and C.E. Costello, *A systematic nomenclature for carbohydrate fragmentations in FAB-MS/MS spectra of glycoconjugates*. Glycoconjugate Journal, 1988. **5**(4): p. 397-409.
37. Stewart, J.J.P., *MOPAC2009*. 2009, Stewart Computational Chemistry: Colorado Springs, CO, USA.
38. Dewar, M.J.S., et al., *Development and use of quantum mechanical molecular models. 76. AM1: a new general purpose quantum mechanical molecular model*. Journal of the American Chemical Society, 1985. **107**(13): p. 3902-3909.
39. Stewart, J., *Optimization of parameters for semiempirical methods V: Modification of NDDO approximations and application to 70 elements*. Journal of Molecular Modeling, 2007. **13**(12): p. 1173-1213.
40. McLafferty, F.W. and F. Turecek, *Interpretation of Mass Spectra*. 4th ed. 1993, Sausalito, California: University Science Books.

41. Karni, M. and A. Mandelbaum, *The 'even-electron rule'*. Organic Mass Spectrometry, 1980. **15**(2): p. 53-64.
42. Williams, J.P., et al., *Collision-induced fragmentation pathways including odd-electron ion formation from desorption electrospray ionisation generated protonated and deprotonated drugs derived from tandem accurate mass spectrometry*. Journal of Mass Spectrometry, 2006. **41**(10): p. 1277-1286.
43. Levsen, K., et al., *Even-electron ions: a systematic study of the neutral species lost in the dissociation of quasi-molecular ions*. Journal of Mass Spectrometry, 2007. **42**(8): p. 1024-1044.

Chapter 6
Lactones linked and fused to sugars

In this chapter, five α,β-unsaturated γ-lactones (butenolides) fused to a pyranose ring, two α,β-unsaturated γ-lactones (butenolides) and two β-hydroxy γ-lactones C-C linked to a furanose ring were investigated using electrospray ionization mass spectrometry, MS^n and CID experiments. For the butenolides fused to a pyranose ring, the behaviour was investigated in the positive and negative ion mode, while for the C-C linked butenolides and β-hydroxy γ-lactones only the positive ion mode was addressed. Fragmentation mechanisms are proposed taking into account MS^n experiments, accurate mass measurements (linked butenolides and β-hydroxy γ-lactones) and semi-empirical calculations using the PM6 hamiltonean.

This chapter was based on two publications:

- *Electrospray ionization mass spectrometric analysis of newly synthesized a,β-unsaturated γ-lactones fused to sugars*, Paulo J. Amorim Madeira, Ana Margarida Rosa, Nuno M. Xavier, Amélia P. Rauter, M. Helena Florêncio, Rapid Communications in Mass Spectrometry 2010, 24, 1049-1058.
- *Furanose C-C-linked γ-lactones: a combined ESI FT-ICR MS and semi-empirical calculations study*, Paulo J. Amorim Madeira, Nuno M. Xavier, Amélia P. Rauter, M. Helena Florêncio, accepted for publication in Journal of Mass Spectrometry.

6 Lactones linked and fused to sugars

6.1 Electrospray Ionization Mass Spectrometry analysis of newly synthesized α,β-unsaturated γ-lactones fused to sugars

6.1.1 Introduction

The α,β-unsaturated γ-lactone moiety is quite a common structural feature in many natural compounds.[1, 2] This moiety confers a wide variety of biological properties such as antifeeding,[3] phytotoxic, antifungal,[4] antibacterial, insecticidal[5] and anti-inflammatory activity, as well as analgesic effects.[6] Compounds with this feature appear throughout the plant kingdom, from the simple metabolites of lichens and fungi to the sesquiterpenes and steroidal glycosides, having also been found in animal species such as sponges, butterflies and insects.[7] Some of these compounds were described as potential anticancer agents, phospholipase A2 and cyclooxygenase inhibitors.[1]

Electrospray ionization mass spectrometry (ESI-MS) is one of the techniques of choice for the analysis of non-volatile and thermally labile compounds. It produces highly abundant protonated molecules, mainly due to the low residual energy of the ionization process.[8] Combining ESI with collision induced dissociation (CID) provides a powerful tool for structure elucidation of non-volatile and thermally labile compounds, especially biological material and carbohydrate derivatives.[9-12] Fragmentation pathways of five-membered ring

lactones using electrospray ionization tandem mass spectrometry have already been reported.[8, 13] The knowledge of the fragmentation mechanisms of lactones and how their behaviour under ESI conditions can be extended to larger and more complex natural products that contain the above mentioned moiety in their structure. Moreover, little is known about the gas-phase behaviour of α,β-unsaturated γ-lactones linked or fused to sugars. [14-17] Nevertheless, and to the best of our knowledge, there are only a few studies on the fragmentation behaviour of monosaccharides.[18]

We decided, therefore, to perform a detailed study using ESI-MS and CID, on five α,β-unsaturated γ-lactones (butenolides) fused to a furanose ring, recently synthesized compounds with potential relevance regarding their biological properties.[1, 19] In this study, we aimed to establish fragmentation mechanisms and to propose ion structures using both mass spectrometric data and semi-empirical calculations. These methodologies have been reported to be successful in mass spectrometry studies, of which an example is the fragmentation study of flavonoids and flavonoid diglycosides using both ESI-MS and semi-empirical calculations.[20, 21] Other reports can be found in the literature where ESI-MS and PM5 semi-empirical calculations were used. Examples of these are the complexation studies of Schiff bases with monovalent cations[22] and monensin A with divalent cations,[23] as well as the evaluation of the interaction strength of non-covalently bound enkephalins in solution.[24] Furthermore, semi-empirical calculations were used for the establishment of fragmentation pathways under EI conditions[25] and in the study of fullerene derivatives.[26] Fragmentation is greatly influenced by the type of the precursor ion and,

moreover, several reports in the literature show that protonated species decompose more readily than metal cationized species (the metal cationization alters the stability of the product ions). Therefore, the fragmentation mechanisms in the negative ion mode (deprotonated molecules) and in the positive ion mode (protonated and sodiated molecules) are also compared.

6.1.2 Results and Discussion

The relative abundance of the protonated, sodiated and deprotonated forms of the compounds under study in the ESI full scan mass spectra are shown in Table 6.1. The sodiated molecules exhibit high abundance for all compounds, even with the addition of formic acid. This observation is in agreement with the literature [27, 28] and shows that these compounds have high sodium affinities that, with the exception of compound **2**, exceed their proton affinities.

Table 6.1. Relative Abundance (%) of the protonated, sodiated and deprotonated forms of compounds **1**-**5** in the full scan mass spectra acquired.

	Relative Abundance (%)		
Compound	**$[M+H]^+$**	**$[M+Na]^+$**	**$[M-H]^-$**
1	20	100	100
2	100	60	100
3	15	100	16
4	<1*	100	<1*
5	<1*	100	80

In order to establish the fragmentation mechanisms, our study focused on the positive ion mode MS^2 spectra of the protonated and

sodiated molecules, as well as on the negative ion mode MS^2 spectra of the deprotonated species. Negative ion mode ESI-MS^2 spectra exhibited less fragmentation than the positive ion mode spectra and will be discussed first.

6.1.2.1 Negative Ion Mode (Deprotonated molecules)

*Compound **1***

The MS^2 spectrum of the deprotonated molecule of compound **1** (*m/z* 171) is depicted in Figure 6.1. This compound shows little fragmentation and, even at 21% collision energy level (CEL), the most abundant ion is still the deprotonated molecule.

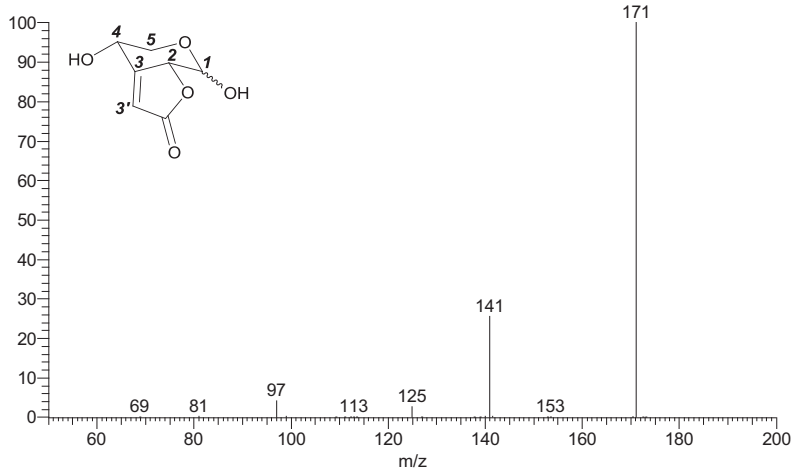

Figure 6.1. Negative ion mode ESI-MS^2 spectra of the deprotonated molecule of compound **1**, CEL: 21%.

The deprotonated molecule of compound **1** can lose 30 Da, which can be attributed to H_2CO, to afford the ion at *m/z* 141. There are, however, three possible fragmentation pathways (Scheme 6.1) that can explain this loss. One involves the abstraction of one hydrogen atom of

C^5 by the oxygen atom at C^4 and the scission of the C^3-C^4 and C^4-C^5 bonds, affording a ^{3,4}A type ion ($\Delta_f H$=-739.2 kJ mol^{-1}), according to the nomenclature proposed by Domon and Costello.[29] The second involves the scission of the O-C^1 and C^1-C^2 bonds, affording a ^{0,1}A type ion ($\Delta_f H$=-653.9 kJ mol^{-1}). The third pathway involves the scission of the O-C^1 and C^4-C^5 bonds, affording a ^{0,4}A type ion ($\Delta_f H$=-634.2 kJ mol^{-1}). Taking into account the semi-empirical estimates of the heats of formation, one might speculate that scission of the C^3-C^4 and C^4-C^5 bonds is the preferred fragmentation pathway. Nevertheless, and to the best of our knowledge, there are no reports in the literature that address the cross-ring cleavages that afford the ^{3,4}A and ^{0,1}A type ions. The ^{0,4}A type ions, however, were detected for a wide variety of compounds, including among others lipopolysaccharides,[30, 31] free and conjugated glycans,[32] N-linked glycans,[28] sialylated glycans[33] and permethylated oligosaccharides.[34] It seems therefore reasonable to assume that this loss occurs through the formation of a ^{0,4}A type ion (structure **c** in Scheme 6.1), that rearranges to afford the structure **a** depicted in Scheme 6.1.

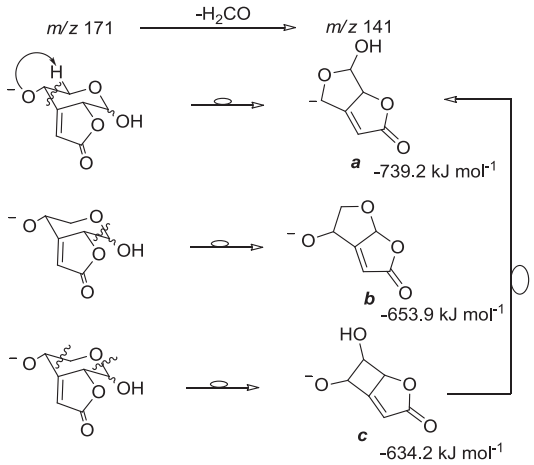

Scheme 6.1. Fragmentation pathway proposals for the formation of the *m/z* 141 ion from the deprotonated molecule of compound **1.**

The deprotonated molecule, m/z 171, can also lose 46 Da, attributed to HCOOH, through the cleavage of the C^5-*O* and C^2-C^1 bonds, to afford the ^{1,5}A type ion at m/z 125 (more details on this fragmentation are presented in Scheme 6.2.

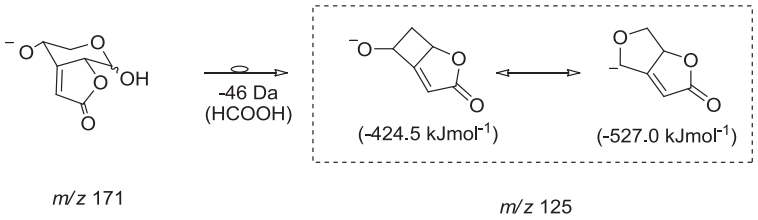

Scheme 6.2. Rearrangement of the *m/z* 125 ion for compound **1.**

The ^{1,5}A type ion has been detected for a wide variety of saccharide derivatives, including steroidal glycosides[35] and permethylated oligosaccharides,[34] as well as glycoproteins[36] and sulfated heparins.[37] The ion at *m/z* 97 could be formed through two distinct fragmentation pathways. One involves the loss of 28 Da (CO) from the *m/z* 125 ion, leading to a calculated $\Delta_f H$ of -242.0 kJ mol^{-1}, and the other involves the loss of 44 Da (CO_2) from the *m/z* 141 ion,

leading to a calculated $\Delta_f H$ of -214.9 kJ mol^{-1}. The calculated $\Delta_f H$ of the resulting ions differs by 27 kJ mol^{-1}. Taking into account that these are semi-empirical estimates for which the average unassigned error is about 34 kJ mol^{-1} (for more details see MOPAC manual[38]), it is reasonable to assume that both species could contribute to the *m/z* 97 ion signal.

The fragmentation proposal for compound **1**, based on all the observations described so far, is depicted in Scheme 6.3.

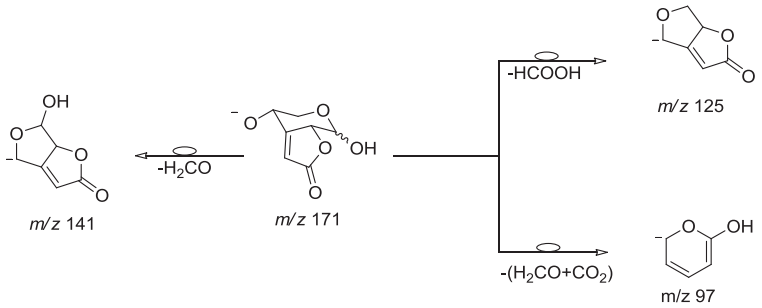

Scheme 6.3. Proposed fragmentation pathway for the deprotonated molecule of compound **1**.

*Compound **2***

The MS^2 spectrum of the deprotonated molecule of compound **2** (*m/z* 201) is depicted in Figure 6.2. Unlike compound **1**, the deprotonated form of **2** shows a greater tendency to fragment, noticeable by its relative abundance (about 26%).

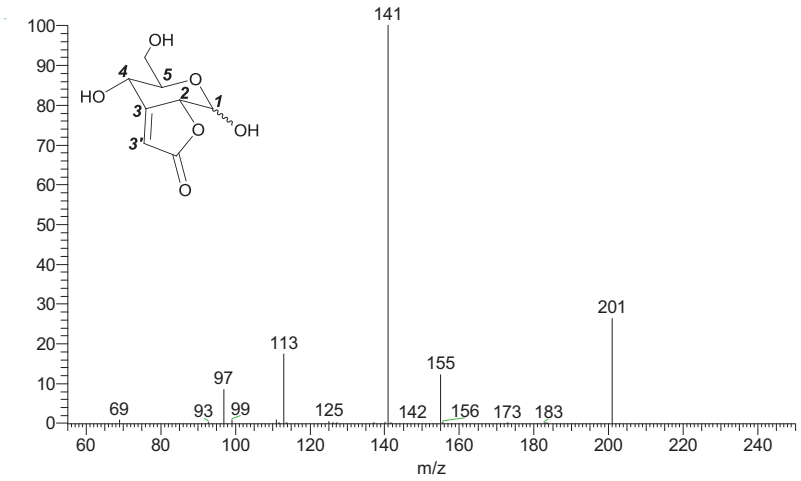

Figure 6.2. Negative ion mode ESI-MS^2 spectra of the deprotonated molecule of compound **2**, CEL: 25%.

The loss of 46 Da from the deprotonated molecule, attributed to HCOOH, is one of the major fragmentation pathways and affords the ^{1,5}A type ion at *m/z* 155 (more details on this fragmentation are presented in Scheme 6.4).

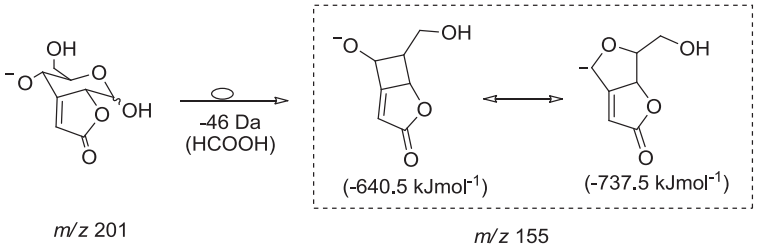

Scheme 6.4. Rearrangement of the *m/z* 155 ion for compound **2.**

There is, however, another fragmentation pathway for compound **2** apart from the ones common to compound **1**. This fragmentation pathway seems to be related to the additional hydroxymethyl group (-CH_2OH) on the sugar ring of compound **2**. The deprotonated molecule of compound **2** (*m/z* 201) can lose 60 Da to afford the ^{0,4}A type ion at

m/z 141. This can be attributed to the loss of hydroxyacetaldehyde, $HOCH_2CHO$, from the sugar ring. This loss has already been reported in the literature for glycosphingolipids containing neutral sugars, using fast atom bombardment.[39] The ion formed by the 60 Da loss has a structure similar to the one proposed for the loss of 30 Da (H_2CO) from the deprotonated molecule of compound **1** (Scheme 6.1). The high abundance of this product ion indicates that it must be extremely stable. Indeed, the proposed ion structure can resonate in order to stabilize the charge of the resulting product ion (Scheme 6.5). The high abundance ion at *m/z* 141 can lose 28 Da, attributed to CO, to afford the ion at *m/z* 113, or it can lose 44 Da, attributed to CO_2, to afford the six-membered ion at *m/z* 97, after rearrangement. All observations reported so far are summarized in Scheme 6.5, which depicts the proposed fragmentation mechanism for the deprotonated molecule of compound **2**.

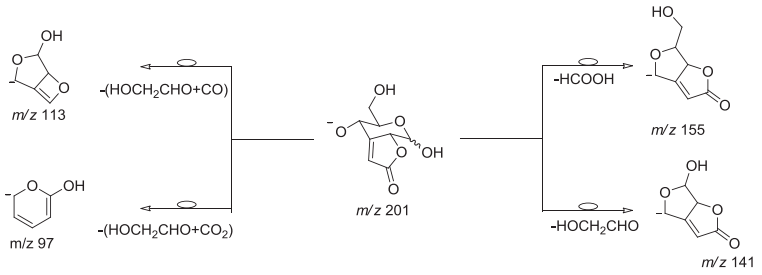

Scheme 6.5. Proposed fragmentation pathway for the deprotonated molecule of compound **2**.

*Compound **3***

The MS^2 spectrum of the deprotonated molecule of compound **3** (*m/z* 285) is depicted in Figure 6.3. The loss of 46 Da from the deprotonated molecule at *m/z* 285 (to afford a $^{1,5}A$ type ion), attributed

to HCOOH for compounds **1** and **2**, can also occur for compound **3**, but is a minor fragmentation pathway for which the relative abundance of the resulting ion (at *m/z* 239) does not exceed 1%.

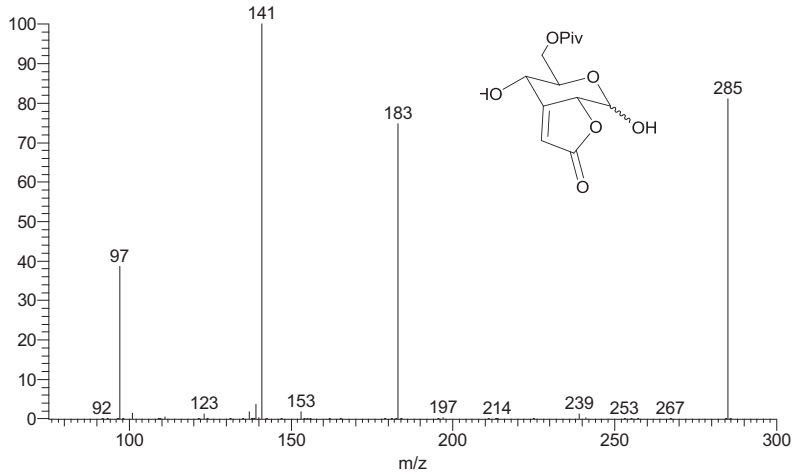

Figure 6.3. Negative ion mode ESI-MS^2 spectra of the deprotonated molecule of compound **3**, CEL: 20%.

The deprotonated molecule of compound **3** can lose 102 Da, attributed to PivOH, affording the abundant ion at *m/z* 183. The abundance of this ion may be attributed to the large volume of the group PivO (i.e. $C_5H_9O_2$). The loss of this group is favoured for steric reasons (substituent's bulkiness). This assumption seems reasonable, since there are reports in the literature correlating the bulkiness of the substituent with the ease of its loss.[40] The deprotonated molecule can also lose 144 Da, attributed to $C_7H_{12}O_3$, affording the ion at *m/z* 141. This loss results from the sugar ring opening at the C^4-C^5 and C^1-sugar ring oxygen bonds. Taking into account the relative abundance of this ion, we should expect it to be extremely stable. The ion at *m/z* 141 can lose 44Da, attributed to CO_2 from the lactone ring, affording, after rearrangement, the six-membered ion at *m/z* 97. These observations are

summarized in the fragmentation mechanism proposal depicted in Scheme 6.6.

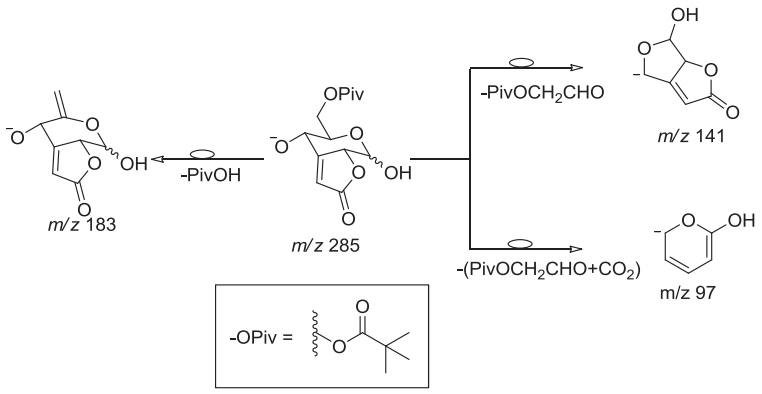

Scheme 6.6. Proposed fragmentation pathway for the deprotonated molecule of compound **3**.

A comparative analysis of the MS^2 spectra of the deprotonated molecules of compounds **1**-**3**, shows that the ions at *m/z* 141 and *m/z* 97 are common to the three compounds. This leads us to suggest that the *m/z* 97 in **1**, which can be explained by two different fragmentation pathways, mainly occurs through the loss of CO_2 (44 Da) from *m/z* 141.

*Compounds **4** and **5***

Compounds **4** and **5** (Scheme 6.7) are isomers that differ in the positions of the lactone moiety and in one of the acetyl groups within the sugar ring. For comparison purposes, the analysis of the ESI-MS^2 spectra of the deprotonated molecules will be performed simultaneously, as presented below. Figure 6.4a and Figure 6.4b depict the ESI-MS^2 spectra of the deprotonated molecules of compound **4** and **5**, respectively.

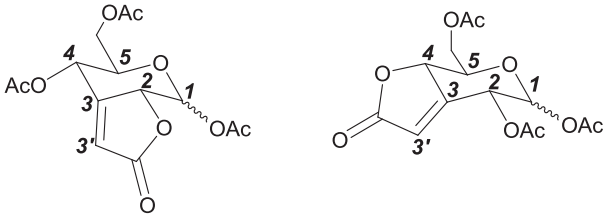

Compound **4** Compound **5**

Scheme 6.7. Structures of compounds **4** and **5**.

The first significant difference in the fragmentation of compounds **4** and **5** is the loss of 42 Da, ketene (H_2CCO), to afford the ion at m/z 285. This loss is more pronounced for compound **5** than for compound **4**, as is evident from the difference in the product ion relative abundance, that is *ca.* 8% for compound **5** whereas for compound **4** it does not exceed 1%. This difference in relative abundance may be related to the different substitution pattern for these two compounds, i.e. the different positions of the lactone moiety and of one of the acetyl groups.

The deprotonated molecules of compounds **4** and **5**, m/z 327, can lose 60 Da, i.e. CH_3COOH, affording the ions at m/z 267. It is noted that this loss is much more pronounced for compound **5** (relative abundance *ca.* 70%) than for compound **4** (relative abundance *ca* 8%). Taking into account that there is no C^2 acetyl group in compound **4**, it seems reasonable to assume that the observed difference is due to the fact that C^2 substituent is much more labile than the others. The second loss of 60 Da from the deprotonated molecule affords a low abundance ion at m/z 207 (~2% for **4** and ~3% for **5**).

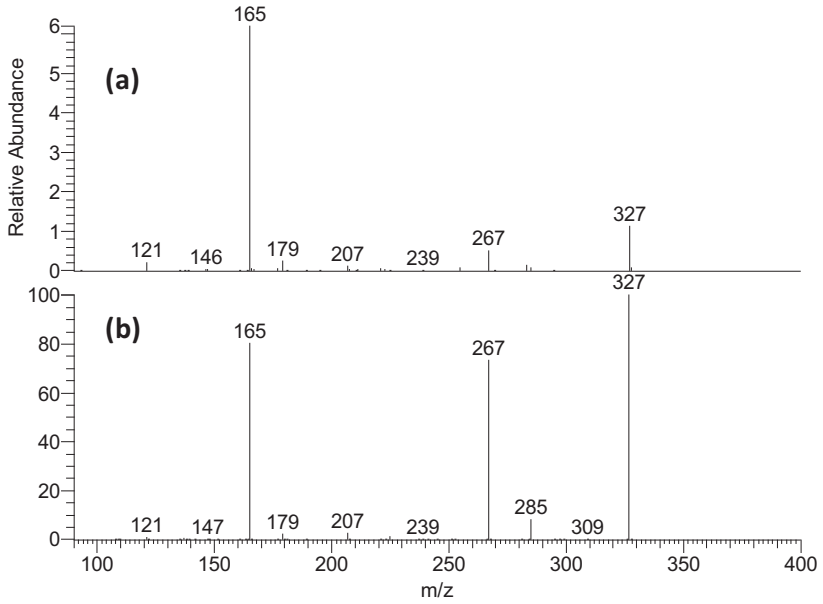

Figure 6.4. Negative ion mode ESI-MS^2 spectra of the deprotonated molecules of: a) compound **4**, CEL: 15%; b) compound **5**, CEL: 15%.

The ion at *m/z* 165 can be formed by the loss of 102 Da from the ion at *m/z* 267. This loss has been reported in the literature for acetylated galactomannans[41, 42] and oligogalacturonides [43, 44] and ascribed to the loss of an acetyl group and a $C_2H_4O_2$ neutral fragment from the sugar ring, affording a ^{0,2}A type ion. Such loss is not possible in the present case, since neither compound **4** nor **5** possess a $C_2H_4O_2$ sugar ring fragment liable to be lost with the acetyl group. It should be noted that the relative abundance of the *m/z* 165 ion is greater for **4** (*ca.* 100%) than for **5** (*ca.* 80%). Moreover, the relative abundance of the *m/z* 267 ion for compound **4** is approximately 8%, while for **5** is 70%. As such, it seems reasonable to argue that for compound **5** the *m/z* 165 ion is formed through the opening of the sugar ring at the C^4-C^5 and C^1-sugar ring oxygen bonds (^{0,4}A type ion) from *m/z* 267, while for **4** the

m/z 165 ion is most probably formed through a concerted loss of CH_3COOH (60 Da) and 102 Da ($C_4H_6O_3$) from the deprotonated molecule. The fragmentation pathways for these two compounds are quite similar to each other and the main differences are related to ion abundance rather than ion structure. The observations described so far are summarized in Scheme 6.8, which depicts the fragmentation proposals for the deprotonated molecules of **4** and **5**.

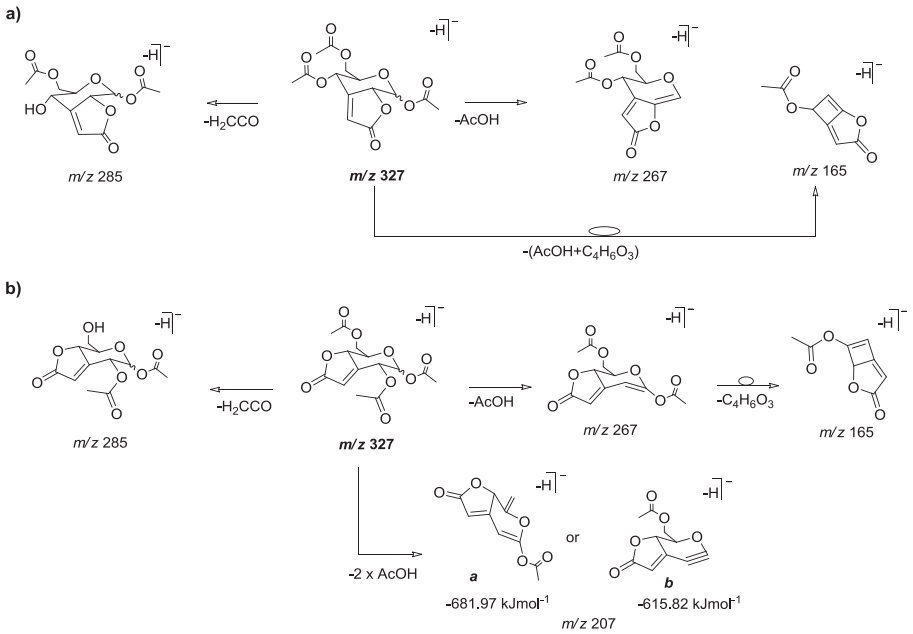

Scheme 6.8. Proposed fragmentation pathway for the deprotonated molecules of: a) compound **4**; b) compound **5**.

In an overall comparison of the fragmentation behaviour under negative ion mode of the compounds studied, several features are noticeable.

The loss of 30 Da (H_2CO) from the deprotonated molecule is only significant (about 26%) for compound **1**.

With respect to the loss of 46 Da, attributed to HCOOH for compounds **1**-**3** (^{1,5}A type ion), this was not detected for **4** and **5**, as expected. This fragmentation appears to be strongly dependent on the degree of substitution of the sugar ring. For compound **1** the loss of HCOOH resulted in a product ion (m/z 125) with a relative abundance of *ca.* 3%. For compound **2** this loss resulted in an ion (m/z 155) with a relative abundance of *ca.* 12%, whereas for compound **3** the resulting ion (m/z 239) had a relative abundance of *ca.* 1%. The energy of the resulting ion may therefore influence the fragmentation. In fact, in accordance with our calculations the $\Delta_f H$ of the m/z 201 → m/z 155 (compound **2**) transition is *ca.* 450 kJ mol^{-1}, whereas for the m/z 171 → m/z 125 (compound **1**) the $\Delta_f H$ is *ca.* 490 kJ mol^{-1}, which is in agreement with our observations.

6.1.2.2 Positive Ion Mode (Protonated and Sodiated molecules)

In order to determine the most probable protonation site, the partial atomic charges for the neutral molecules, presented in Table 6.2, were computed using the Hamiltonian PM6[45] implemented in MOPAC2009.[38] The use of semi-empirical calculations to find the most probable protonation site has already been reported for the particular case of flavonoids.[20]

According to the data presented in Table 6.2, for compounds **1**, **2** and **3**, the most probable protonation site will be the hydroxyl group

linked to the C^4 atom of the sugar ring, whereas for compounds **4** and **5** the most probable site will be the sugar ring oxygen.

Table 6.2. Partial charges for the compounds under study computed using the Hamiltonian PM6[45] implemented in MOPAC2009[38]. (The atom with the greatest negative charge is underlined)

Atom	Charge				
	Comp. **1**	Comp. **2**	Comp. **3**	Comp. **4**	Comp. **5**
O-S.R.	-0.491123	-0.502347	-0.496153	-0.456867	-0.509077
O-1	-0.492247	-0.528708	-0.475928	-0.538113	-0.523169
O-2	-0.411717	-0.410678	-0.443874	-0.464792	-0.487053
O-4	-0.517393	-0.547001	-0.535756	-0.499496	-0.475147
O-6	-	-0.407313	-0.485638	-0.466845	-0.466777
O-Lact	-0.402370	-0.407313	-0.403242	-0.397918	-0.389165
O-Piv	-	-	-0.482565	-	
O-Ac1	-	-	-	-0.421681	-0.425850
O-Ac2	-	-	-	-	-0.424603
O-Ac4	-	-	-	-0.433932	-
O-Ac6	-	-	-	-0.480176	-0.442650

O-S.R.: sugar ring oxygen
O-Lact: lactone carbonyl oxygen
O-x: oxygen linked to carbon x
O-Acx: carbonyl oxygen of the acetyl group linked to carbon x
O-Piv: carbonyl oxygen of the pivaloyl group

It is worth mentioning that the MS^2 spectra of the sodiated molecules exhibited ions 18 Da higher than the m/z values of the precursor $[M+Na]^+$ ions. Those ions, at m/z 213, m/z 243 and m/z 327, were attributed to $[M+Na+H_2O]^+$ for compounds **1**-**3**, respectively. These species are due to ion-molecule reactions occurring in the ion trap during isolation and are consistent with several earlier reports of hydration reactions conducted in ion trap mass spectrometers.[46-52]

*Compound **1***

The MS^2 spectra of the protonated and sodiated molecules of compound **1** are depicted in Figure 6.5a-b, respectively.

Since compound **1** protonates most probably on the hydroxyl group linked to C^4 to afford the ion at m/z 173 (protonated molecule), the loss of water to afford the ion at m/z 155 is straightforward. The protonated molecule (m/z 173) can lose 32 Da, corresponding to CH_3OH, affording the ^{0,4}A type ion at m/z 141. The ion at m/z 173 can also lose 46 Da, attributed to the loss of HCOOH, affording the ^{1,5}A type ion at m/z 127. A concerted loss of HCOOH (46 Da) and H_2O (18 Da) from the protonated molecule at m/z 173 can explain the ion at m/z 109. These observations are summarized in Scheme 6.9, which depicts a possible fragmentation pathway for the protonated molecule of compound **1**.

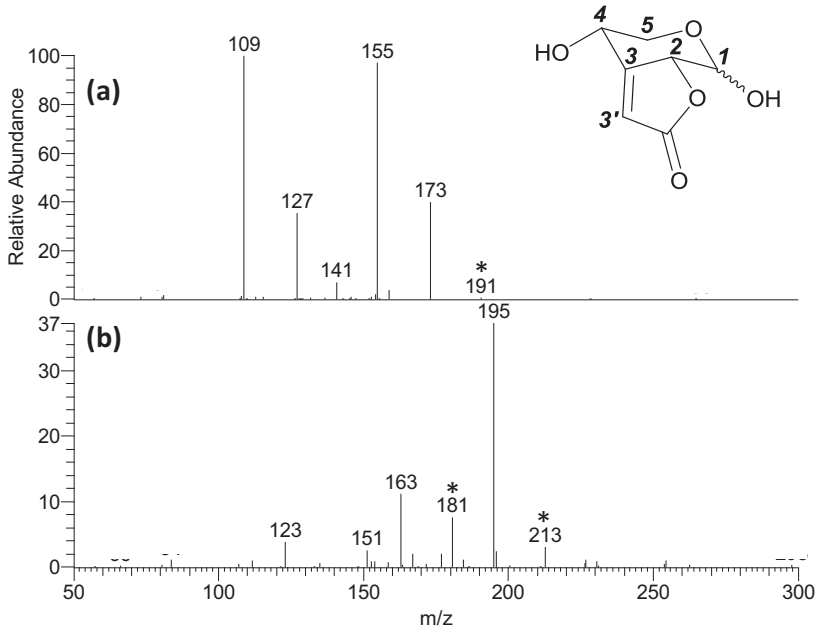

Figure 6.5. Positive ion mode ESI-MS^2 spectra of: a) protonated molecule of compound **1**, CEL: 15%; b) sodiated molecule of compound **1**, CEL: 17%. The ions marked with an asterisk (*) are hydrated species due to ion-molecule reaction within the ion trap.

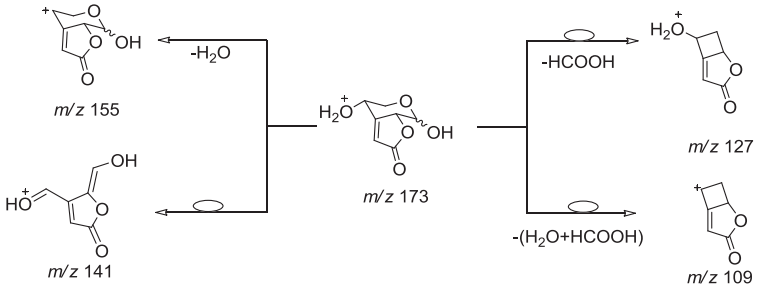

Scheme 6.9. Proposed fragmentation pathway for the protonated molecule of compound **1**.

The sodiated molecule of compound **1** (*m/z* 195), Figure 6.5b, shows two losses common to the ones from the protonated molecule. These are the losses of H_2O (18 Da) and CH_3OH (32 Da) that, in the case of the sodiated molecule, afford the ions at *m/z* 177 and *m/z* 163, respectively. The loss of HCOOH (46 Da) was not detected, which suggests that the cationization may involve the oxygen atoms of the sugar ring, the hydroxyl group linked to C^1 and the oxygen linked to C^2. There are reports in the literature stating that alkali metal ions can undergo coordination with several oxygen atoms simultaneously.[53-55] Our semi-empirical calculations support this assumption and also hypothesize the participation of the lactone moiety oxygen atoms in the cationization. There are, however, some other losses from the sodiated molecule that were not detected in the protonated molecule. These are the direct loss of CO (28 Da) to afford the ion at *m/z* 167 and the loss of 44 Da to afford the ion at *m/z* 151. Although this latter loss might be attributed to CO_2, it seems more probable that it would correspond to CH_2CHOH, lost from the sugar ring since it is suspected that one of the lactone moiety oxygen atoms is involved in the cationization, as supported by our semi-empirical calculations (*vide supra*). The ion at

m/z 123 can be explained by the concerted loss of CH_2CHOH (44 Da) and CO (28 Da) from the sodiated molecule (*m/z* 195). These observations are presented in Scheme 6.10, which depicts a possible fragmentation pathway for the sodiated molecule of compound **1.**

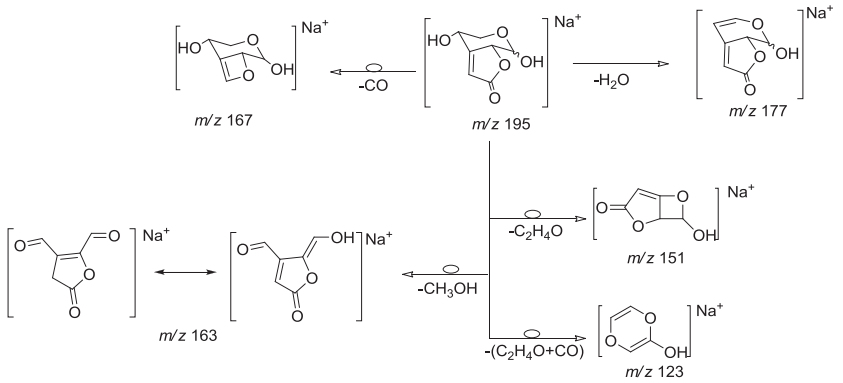

Scheme 6.10. Proposed fragmentation pathway for the sodiated molecule of compound **1**.

*Compound **2***

The MS^2 spectra of the protonated and sodiated molecules of compound **2** are depicted in Figure 6.6a-b, respectively.

Similarly to what was observed for compound **1**, compound **2** protonates at the hydroxyl group linked to the C^4 carbon (Table 6.2). The loss of H_2O, to afford the ion at *m/z* 185, becomes therefore straightforward.

The protonated molecule of compound **2** can lose HCOOH (46 Da), affording the $^{1,5}A$ type ion at *m/z* 157. The proposed structure has a relatively high $\Delta_f H$, 304.2kJ mol^{-1}, which can be indicative of further rearrangement. Indeed, two other structures can be proposed (Scheme 6.11) and their energies were estimated by semi-empirical calculations.

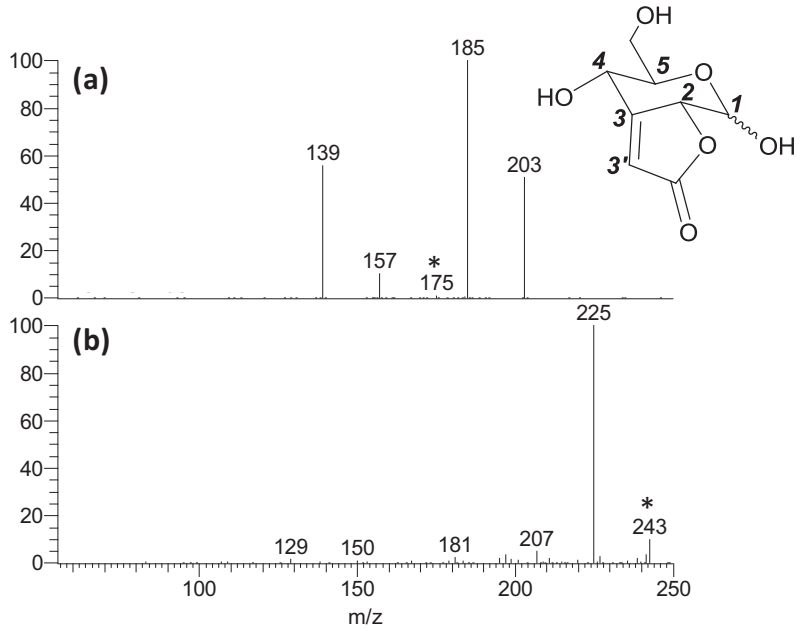

Figure 6.6: Positive ion mode ESI-MS^2 spectra of: a) protonated molecule of compound **2**, CEL: 8%; b) sodiated molecule of compound **2**, CEL: 17%. The ions marked with an asterisk (*) are hydrated species due to ion-molecule reaction within the ion trap.

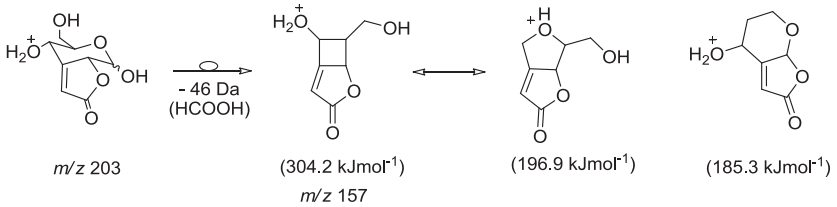

Scheme 6.11. Rearrangement of the *m/z* 157 ion for compound **2.**

The concerted loss of H_2O (18 Da) and HCOOH (46 Da) from the protonated molecule at *m/z* 203 can explain the relatively abundant ion at *m/z* 139. These observations are summarized in Scheme 6.12, which depicts the proposed fragmentation pathways for the protonated molecule of compound **2**.

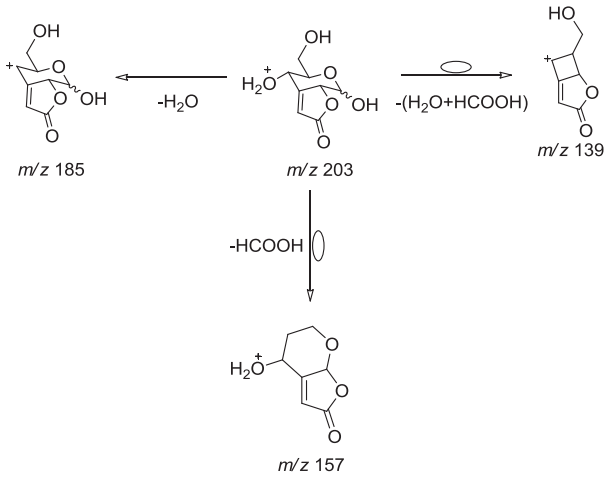

Scheme 6.12. Proposed fragmentation pathway for the protonated molecule of compound **2**.

The sodiated molecule of compound **2** (*m*/*z* 225), Figure 6.6b, shows one loss common to the protonated molecule, that is, the loss of H_2O (18 Da), to afford the ion at *m*/*z* 207. Losses of CO (28 Da) and C_2H_4O (44 Da) from the sodiated molecule, to afford the ions at *m*/*z* 197 and *m*/*z* 181, respectively, were not detected for the protonated molecule. These observations are presented in Scheme 6.13, which depicts the proposed fragmentation pathways for the sodiated molecule of compound **2**.

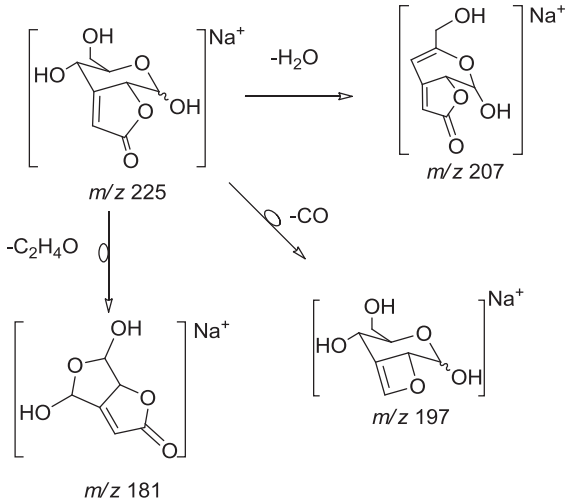

Scheme 6.13. Proposed fragmentation pathway for the sodiated molecule of compound **2**.

*Compound **3***

The MS^2 spectra of the protonated and sodiated molecules of compound **3** are depicted in Figure 6.7a-b, respectively.

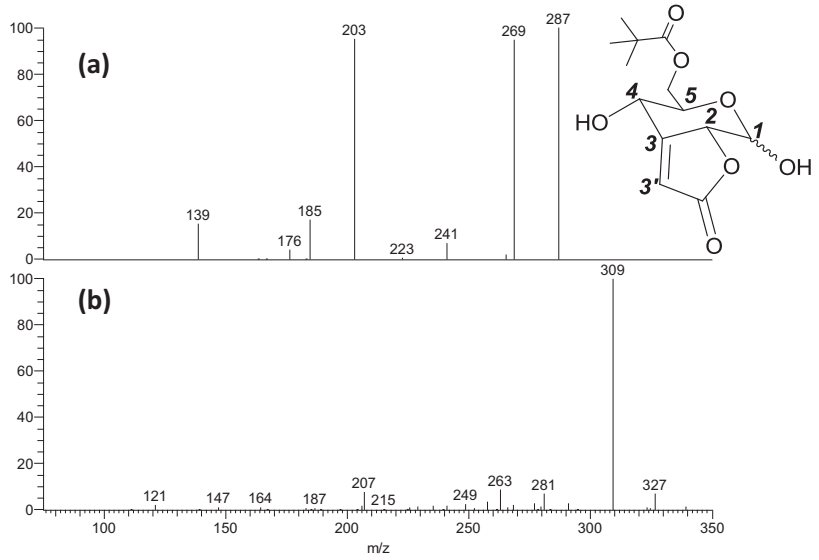

Figure 6.7. Positive ion mode ESI-MS^2 spectra of: a) protonated molecule of compound **3**, CEL: 10%; b) sodiated molecule of compound **3**, CEL: 22%.

The partial atomic charge data presented in Table 6.2 shows that the most probable protonation site is the hydroxyl group at C^4, similarly to what was found for compounds **1** and **2**. The loss of H_2O from the protonated molecule (*m*/*z* 287) to afford the ion at *m*/*z* 269 is, therefore, straightforward.

The protonated molecule can also lose HCOOH (46 Da) to afford the $^{1,5}A$ type ion at *m*/*z* 241, similarly to what was found for compounds **1** and **2**. This ion can undergo additional rearrangements, resulting in more stable structures that are presented in Scheme 6.14.

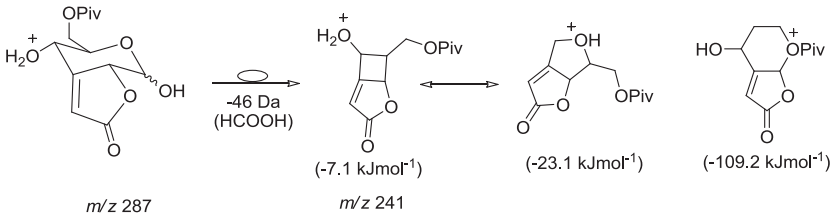

Scheme 6.14. Rearrangement of the *m*/*z* 241 ion for compound **3.**

The loss of 84 Da and 102 Da from the protonated molecule, to afford the ions at *m*/*z* 203 and *m*/*z* 185, respectively, result from the presence of the pivaloyl group at C^5. The concerted loss of PivOH (102 Da) and HCOOH (46 Da) can afford the ion at *m*/*z* 139.

These observations are summarized in Scheme 6.15, which depicts the proposed fragmentation pathways for the protonated molecule of compound **3**.

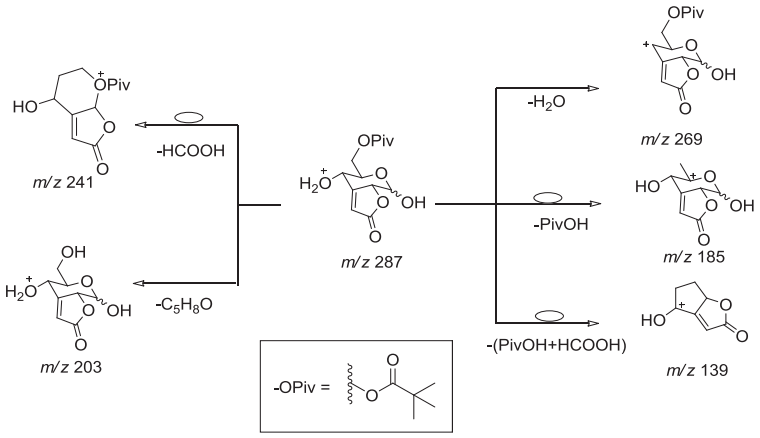

Scheme 6.15. Proposed fragmentation pathway for the protonated molecule of compound **3**.

The sodiated molecule of compound **3** (*m/z* 309), Figure 6.7b, can lose 28 Da, attributed to CO from the lactone ring, affording the ion at *m/z* 281. The ion at *m/z* 263 can be explained by loss of HCOOH (46 Da) from the sodiated molecule. As proposed above, this loss involves the scission of the sugar ring oxygen-C^5 and C^1-C^2 bonds, resulting in a ^{1,5}A type ion. The proposed rearrangement is depicted in the inset of Scheme 6.16.

The ion at *m/z* 207 can be explained by the loss of PivOH (102 Da) from the sodiated molecule, through one hydrogen migration, probably from the C^5. These observations are presented in Scheme 6.16, which depicts a possible fragmentation mechanism for the sodiated molecule of compound **3**.

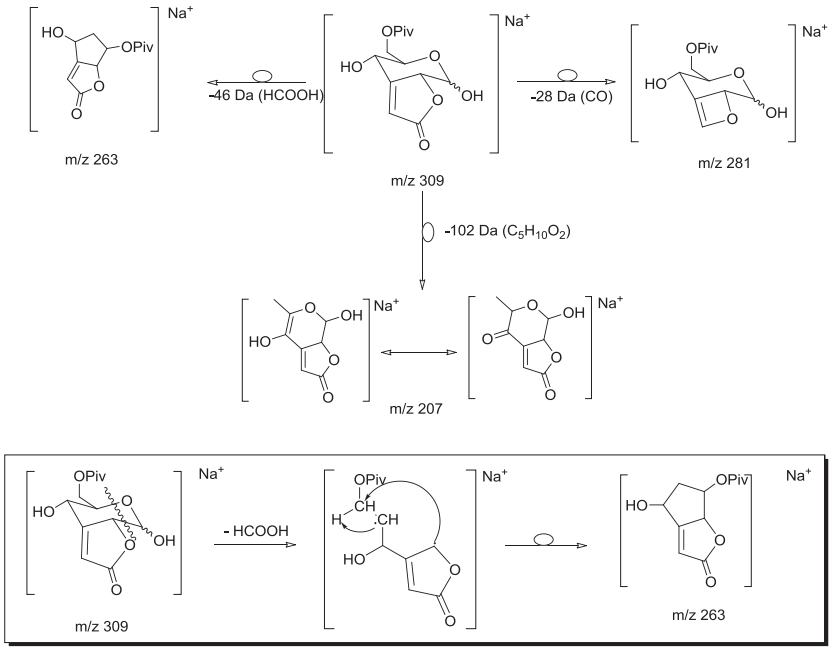

Scheme 6.16. Proposed fragmentation pathway for the sodiated molecule of compound **3**.

*Compounds **4** and **5***

Compounds **4** and **5** are isomers that differ only in the positions to which the lactone moiety is fused to the sugar ring, as mentioned before (Scheme 6.7). For ease of comparison and in an approach similar to the one used for the deprotonated molecule (negative ion mode), the analysis of the MS^2 spectra of the protonated and sodiated molecules will be addressed simultaneously. Figure 6.8a and b depict the ESI-MS^2 spectra of the protonated molecules of compounds **4** and **5**, respectively.

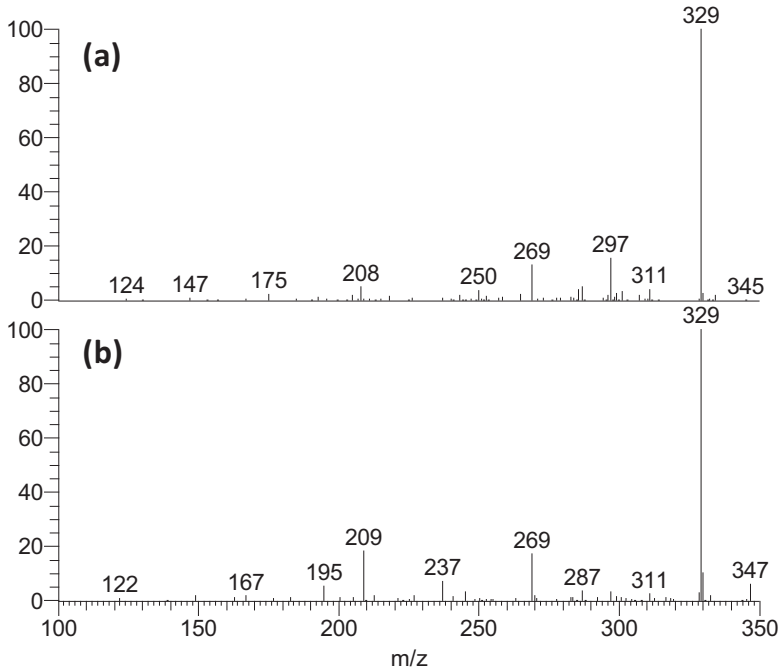

Figure 6.8: Positive ion mode ESI-MS^2 spectra of the protonated molecules of: a) compound **4**, CEL: 20%; b) compound **5**, CEL: 15%.

The partial atomic charge data presented in Table 6.2 show that for compounds **4** and **5** the most probable protonation site is the oxygen attached to the anomeric carbon, i.e. C^1.

The loss of H_2O from the protonated molecules of compound **4** and **5** (*m/z* 329) to afford the ion at *m/z* 311 was detected for both compounds. It is noted that this loss is not as favoured for compound **5** as for compound **4.** Indeed, the relative abundance of the resulting ion (*ca.* 3%) is lower than the one for compound **4** (*ca.* 10%). For compound **4** this loss may occur from an intramolecular aldolic addition, resulting in an eight-membered structure as shown in Scheme 6.17.

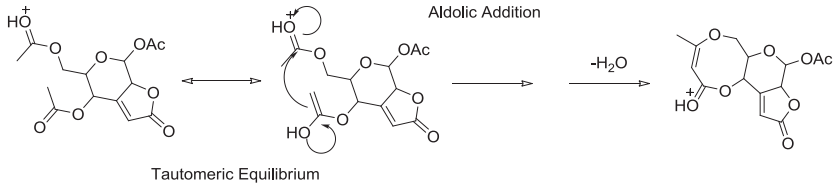

Scheme 6.17. Proposed aldolic addition for the formation of the *m/z* 311 ion from the protonated molecule of compound **4.**

The ion at *m/z* 297, detected for both compounds, can be attributed to the loss of 32 Da (CH_3OH) from the protonated molecule. This loss is more favoured for compound **4** (15.7%) than for compound **5** (3.2%) and it seems therefore to be related to the different position of the lactone moiety.

The ion at *m/z* 287, detected for both compounds in a low abundance (<5%), can be attributed to the loss of ketene (H_2CCO), i.e. 42 Da, from the protonated molecule at *m/z* 329.

The ion at *m/z* 269, also detected for both compounds, is due to the loss of 60 Da (i.e. CH_3COOH) from the protonated molecule. For compound **4**, this loss is probably from the C^6 acetyl group ($\Delta H_f(m/z$ 269) = -433 kJ mol^{-1}). For compound **5**, there are two possible fragmentation pathways, one involves the loss of the C^6 acetyl ($\Delta H_f(m/z$ 269) = -394 kJ mol^{-1}) and the other involves the loss of the C^2 acetyl ($\Delta H_f(m/z$ 269) = -371 kJ mol^{-1}). Both are feasible, taking into account the average unassigned error in these predictions (*vide supra*).

A combined loss of CH_3OH (32 Da) and CH_3COOH (60 Da) from the protonated molecule can explain the ion at *m/z* 237, while the ion at *m/z* 195 can be explained through a combined loss of CH_3OH

(32 Da), CH_3COOH (60 Da) and ketene (42 Da) from the protonated molecule.

The ion at *m/z* 209 shows a significant relative abundance difference for compounds **4** and **5**, being more abundant for the latter. This ion was attributed to the combined loss of two CH_3COOH from the protonated molecule at *m/z* 329. Taking into account that the relative abundances of the *m/z* 269 ion are approximately the same for both compounds, it seems reasonable to assume that this loss is dependent on the substituents position in the precursor ion.

All the observations described so far are summarized in Scheme 6.18, which depicts the possible fragmentation mechanisms for the protonated molecules of compounds **4** and **5**.

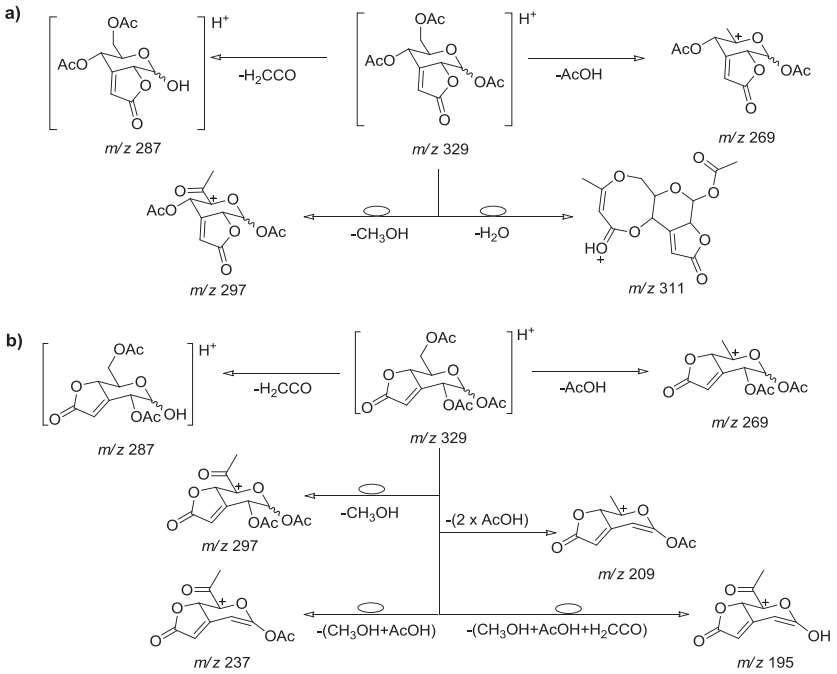

Scheme 6.18. Proposed fragmentation pathway for the protonated molecules of: a) compound **4**; b) compound **5**.

The ESI-MS^2 spectra of the sodiated molecules of compounds **4** and **5** are depicted in Figure 6.9a and b, respectively.

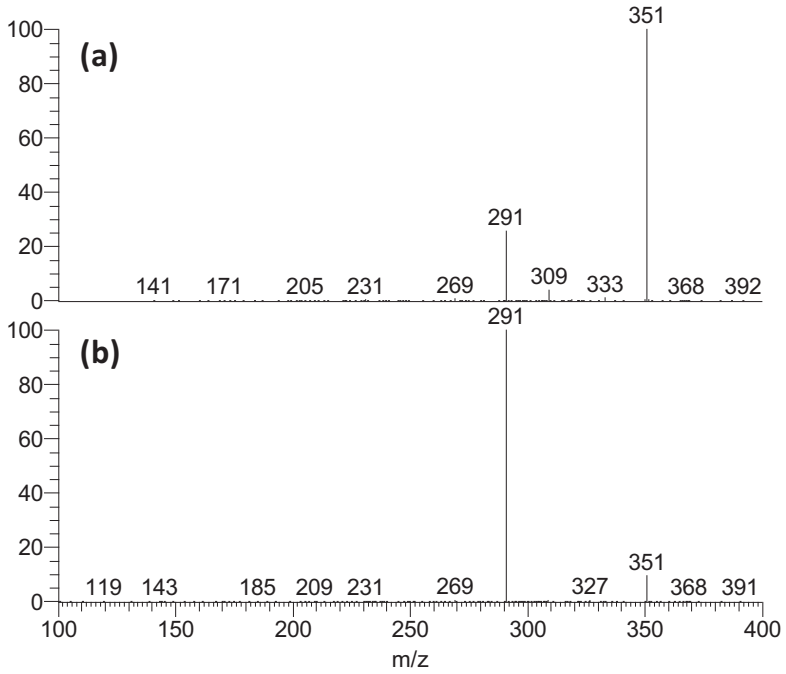

Figure 6.9. Positive ion mode ESI-MS^2 spectra of the sodiated molecules of: a) compound **4**, CEL: 22%; b) compound **5**, CEL: 22%.

Taking into account that the collision energy level is approximately the same for compounds **4** and **5**, the difference in relative abundance of their sodiated molecules suggests that the sodiated molecule of **4** is more stable than the one for compound **5**. This observation is supported by the $\Delta_f H$ estimated using semi-empirical calculations (Table 6.3). Moreover, it is noticeable that, for these two compounds, the fragmentation of their sodiated molecules is, by far, less extensive than for compounds **1**-**3**, as discussed above.

Table 6.3. Most stable structures of the sodiated molecules of compounds **4** and **5** and their $\Delta_f H$ (kJ mol^{-1}) estimated using the Hamiltonian PM6[45] implemented in MOPAC2009.[38]

Structure	$\Delta_f H$ (kJ mol^{-1})
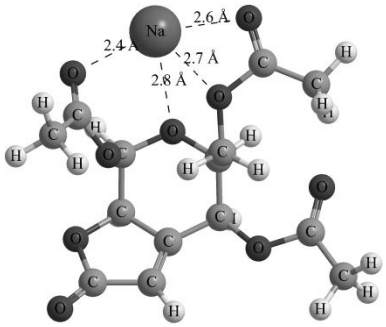 (Compound **4**)	-1259.2
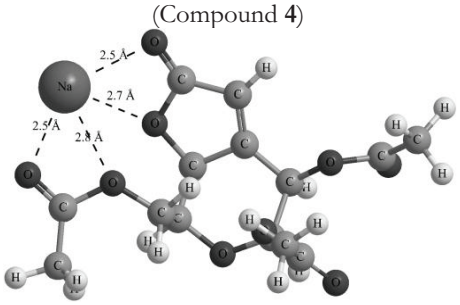 (Compound **5**)	-1233.3

The loss of 42 Da from the sodiated molecule, attributed to ketene (H_2CCO) as in the negative ion mode, to afford the ion at m/z 309, is more favourable for compound **4** than for compound **5**. Taking into account the optimized structure and $\Delta_f H$ of the sodiated molecule of compound **4** (Table 6.3), it is reasonable to assume that this loss most certainly involves the C^4 acetyl group.

The ion at m/z 291, attributed to the loss of CH_3COOH from the sodiated molecules of both compounds, is the base peak in the MS^2 spectrum of compound **5** (Figure 6.9b). This observation, along with the fact that the collision energy given is almost identical, is indicative that

the loss of CH_3COOH is more favoured for compound **5**. This is similar to what was observed for the protonated molecules of both compounds. The semi-empirical data (Table 6.3) allowed us to speculate that this loss will occur from the C^4 acetyl group for compound **4** and, for compound **5**, possibly either from the C^1 or C^2 acetyl groups. A semi-empirical estimate of the $\Delta_f H$ for these two possibilities is presented in Scheme 6.20 and it is clear that the loss of the C^2 acetyl group is preferred.

The observations described so far are summarized in Scheme 6.19 and Scheme 6.20, which depict possible fragmentation pathways for the sodiated molecules of compounds **4** and **5**, respectively.

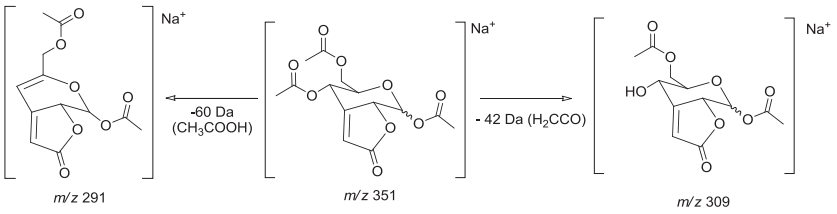

Scheme 6.19. Proposed fragmentation pathway for the sodiated molecule of compound **4**.

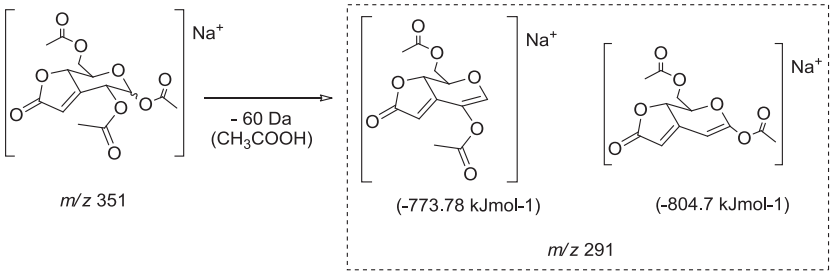

Scheme 6.20. Proposed fragmentation pathway for the sodiated molecule of compound **5**.

In an overall comparison of the fragmentation behaviour under positive ion mode of the protonated and sodiated molecules of the

compounds under study, several features are noticeable as below summarized.

For the protonated molecules, the loss of H_2O is present in all compounds. The resulting ion has always a relative abundance above 90%, with the exception of **4** and **5** for which the relative abundance of the resulting ion is rather low (*ca.* 4% and *ca.* 2%, respectively). The loss of HCOOH (46 Da), leading to a $^{1,5}A$ type ion, was detected for compounds **1**-**3** and not for **4** and **5**.

The loss of the C^6 substituent was detected for compounds **3**, **4** and **5**. Compound **3** loses PivOH, while **4** and **5** lose CH_3COOH.

Regarding the sodiated molecules, the loss of H_2O was detected for compounds **1** and **2** and the loss of CO was detected for compounds **1**-**3**. It is worth mentioning that this latter loss was not detected for the protonated molecules. The loss of 44 Da, attributed to C_2H_4O, was detected only for compounds **1** and **2**. The loss of 46 Da, attributed to HCOOH, was only detected for compound **3**. For the protonated molecules of compounds **1** and **2**, we have attributed this loss to the formation of a $^{1,5}A$ type ion. In addition, and similarly to what was observed for the protonated molecules, the loss of the C^6 substituent was detected for compound **3**, corresponding to the loss of PivOH, and for compounds **4** and **5**, corresponding to the loss of CH_3COOH.

6.1.3 Conclusions

In the negative ion mode, the major fragmentation pathways from the deprotonated molecule correspond to cross-ring cleavages from the sugar ring. All compounds form ^{0,4}A type ions albeit very low abundance species for **4** and **5**.

In the positive ion mode, losses from the substituents are the major fragmentation pathways for the protonated molecules. Loss of water is the most abundant for compounds **1**-**3**. For compounds **4** and **5**, the major fragmentations correspond to the losses of acetic acid and methanol. Nevertheless, for compound **1** a ^{1,5}A type ion can be found with reasonable abundance. The sodiated molecules show little fragmentation, the most abundant corresponding to loss of methanol for compound **1**, and losses of acetic acid for compounds **4** and **5**.

The MS^2 spectra of the deprotonated, protonated and sodiated molecules allow to distinguish the **4** and **5** isomers.

6.2 Furanose C-C-linked γ-lactones: a combined ESIFT-ICR MS and semi-empirical calculations study

6.2.1 Introduction

The α,β-unsaturated γ-lactone moiety is a common structural feature in many natural and synthetic bioactive products.[1, 2] Compounds with lactones of this type appear throughout the plant kingdom, from the simple metabolites of lichens and fungi to the steroidal glycosides, and were even found in animal species such as sponges and insects.[7] This moiety confers a wide variety of biological properties such as cytotoxic,[56-59] antifeeding,[3] phytotoxic and antibacterial,[60] antifungal,[4] insecticidal,[5] anti-inflammatory,[61] and analgesic effects.[6] There are reports in the literature describing the potential use of compounds with this moiety as antitumor agents,[59, 61] phospholipase A2 and cyclooxygenase inhibitors,[60] and antibiotics.[60] The conjugated system can act as a Michael acceptor for the addition of protein functional groups playing a fundamental role in determining bioactivity.[19, 62] Besides the biological properties described above, sugars incorporating such moieties have been used as precursors for the synthesis of many bioactive compounds, *e.g.* branched-chain sugars.[1, 2]

Electrospray ionization mass spectrometry (ESI-MS) is one of the techniques of choice for the analysis of non-volatile and thermally labile compounds.[63-65] It produces highly abundant protonated/cationized molecules, mainly due to the low residual energy of the ionization process.[8] The combination of ESI with collision induced dissociation

(CID) results in a powerful tool for structure elucidation of non-volatile and thermally labile compounds, especially biological material and carbohydrate derivatives.[9-12]

The fragmentation pathways of five-membered ring lactones using electrospray ionization mass spectrometry have already been reported.[8, 13] Recently, we reported the gas-phase behaviour of α,β-unsaturated γ-lactones fused to pyranose rings;[66] nevertheless, studies on the gas-phase behaviour of monosaccharide derivatives of this type are still lacking. In fact, studies that deal with the gas-phase behaviour of monosaccharides are scarce.[14-16, 18, 67]

The knowledge of the fragmentation mechanisms of these sugar lactones and how they behave can be extended to larger and more complex natural products that contain the above mentioned feature in their structure. Hence, we investigated and compared the fragmentation pathways of two butenolides and two β-hydroxy γ-lactones, C-C linked to a furanose ring,[19] using for that purpose electrospray ionization FTICR-mass spectrometry.

The fragmentation pathways were proposed taking into account MS^2 and MS^3 experiments, together with collision induced dissociation (CID) and sustained off-resonance irradiation-collision activated dissociation (SORI-CAD), as well as semi-empirical calculations. These inexpensive computational methodologies have been successfully employed in mass spectrometry studies, for example in the fragmentation of flavonoids and flavonoid diglycosides[20, 21] and, more recently, α,β-unsaturated γ-lactones fused to pyranose units.[66] Furthermore, semi-empirical calculations were used in complexation studies,[22, 23] in the evaluation of the strength of non-covalent

interactions,[24] establishment of fragmentation pathways under EI conditions[25] and in the study of fullerene derivatives.[26] The fragmentation pathways are greatly influenced by the type of precursor ion and several studies have shown that protonated species fragment more readily than metal-cationized ones since the metal cationization alters the stability of the product ions.[14-16] In this study, the behaviour of both protonated and sodiated species is also compared.

6.2.2 Results and Discussion

6.2.2.1 Protonation Site

To establish the most probable protonation site, semi-empirical calculations were performed to determine the ΔH_f of the neutral and possible protonated forms of the compounds under study and $\Delta_r H$ was computed. These results are summarized in Table 6.4. Analysis of the data presented shows that protonation at the O^d atom (atom labelling is given in Chapter 2) gives rise to the lowest energy structure. We shall postulate therefore that all compounds protonate preferentially at the O^d atom.

Table 6.4. $\Delta_f H$, in kJ mol^{-1}, for the protonation reaction of the compounds under study (compounds numbering and atoms labeling are given in Scheme 2.5 (Chapter 2) and the lowest energies obtained are underlined). The energies were computed using the PM6 Hamiltonian[45] as implemented in MOPAC 2009.[38]

	Compound			
Protonation Site	**1**	**2**	**3**	**4**
O^a	726.9	715.7	728.4	711.9
O^b	706.9	694.5	750.0	722.8
O^c	740.9	716.4	736.1	730.7
O^d	695.2	679.3	699.8	684.7
O^e	706.9	719.9	724.3	715.3
O^f	712.4	709.0	727.6	720.3
O^g	-	-	703.2	689.5

6.2.2.2 Mass Spectrometry

The relative abundances of the protonated and sodiated forms of the compounds under study in the full scan mass spectra are shown in Table 6.5. The sodiated molecules exhibit high abundance for all compounds, even with the addition of formic acid. This observation is in agreement with previous reports [27, 28] and shows that these compounds have high sodium affinities.

In order to establish fragmentation pathways, our study focuses on the analysis of the MS^2 spectra of the protonated molecules and on the MS^3 spectra of some key ions in the MS^2 spectra.

Table 6.5: Relative abundance (%) of the protonated and sodiated molecules of compounds **1**-**4** in the full scan mass spectra.

	$[M+H]^+$		$[M+Na]^+$	
Compound	***m/z***	**Rel. Ab. (%)**	***m/z***	**Rel. Ab. (%)**
1	283.12	8	305.10	100
2	333.13	13	355.12	100
3	301.13	16	323.10	100
4	351.14	12	373.13	100

*Protonated Compounds **1** and **2***

The MS^2 spectrum of the protonated molecule of compound **1** is depicted in Figure 6.10a and the MS^3 spectra of the ions at *m/z* 225.08, 167.03 and 139.04, are depicted in Figure 6.10b-d, respectively.

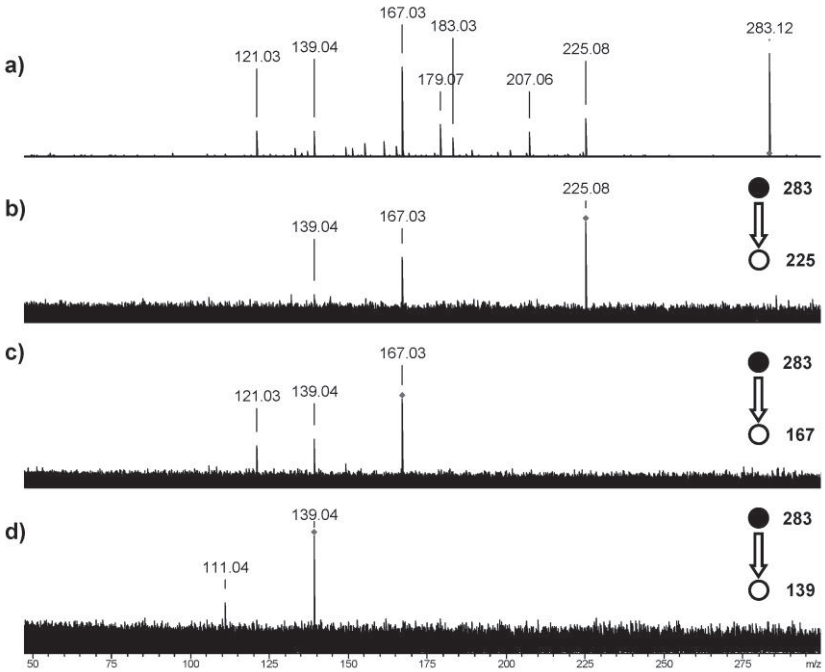

Figure 6.10. Mass spectra acquired for compound **1**: a) MS^2 spectrum of the protonated molecule at *m/z* 283 (E_{col}=-8.0eV); b) MS^3 spectrum of the ion at *m/z* 225 (SORI-CAD, SORI power=0.26%, Frequency Offset=400Hz); c) MS^3 spectrum of the ion at *m/z* 167 (SORI-CAD, SORI power=0.20%, Frequency Offset=400Hz); d) MS^3 spectrum of the ion at *m/z* 139 (SORI-CAD, SORI power=0.17%, Frequency Offset=400Hz).

The MS^2 spectrum of the protonated molecule of compound **2** is depicted in Figure 6.11a and the MS^3 spectra of the ions at *m/z* 275.09, 239.07 and 211.07, are depicted in Figure 6.11b-d, respectively. The high accuracy mass measurements enabled the attribution of ion compositions, with errors below 7 ppm for both compounds (data presented in Table 6.6 and Table 6.7, for **1** and **2**, respectively).

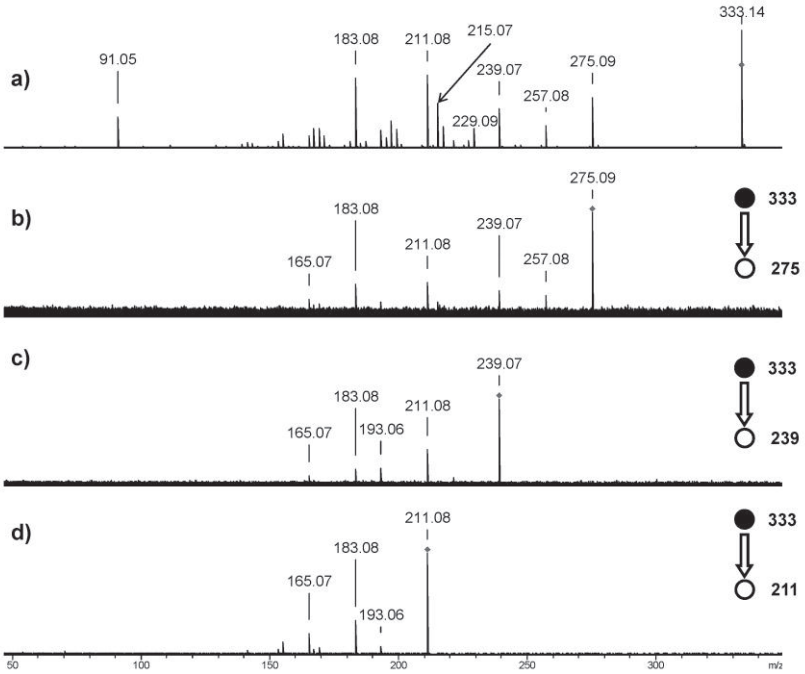

Figure 6.11. Mass spectra acquired for compound **2**: a) MS^2 spectrum of the protonated molecule at *m/z* 333 (E_{col}=-9.0 eV); b) MS^3 spectrum of the ion at *m/z* 275 (SORI-CAD, SORI power=0.38%, Frequency Offset=400 Hz); c) MS^3 spectrum of the ion at *m/z* 239 (SORI-CAD, SORI power=0.35%, Frequency Offset=400 Hz); d) MS^3 spectrum of the ion at *m/z* 211 (SORI-CAD, SORI power=0.25%, Frequency Offset=400 Hz).

Table 6.6. Ion assignment for the fragmentation pattern proposed for the protonated molecule of compound **1**.

Ion		*m/z*	Error (ppm)	Ion Formula
$[M+H]^+$		283.11758	0.1	$C_{14}H_{19}O_6^+$
$[M+H-C_3H_6O]^+$		225.07558	0.8	$C_{11}H_{13}O_5^+$
$[M+H-C_3H_8O_2]^+$		207.06498	1.0	$C_{11}H_{11}O_4^+$
$[M+H-C_5H_8O_2]^+$	$^{0,2}A^+$	183.06492	1.5	$C_9H_{11}O_3^+$
$[M+H-(C_3H_6+C_3H_6O)]^+$		183.02866	0.8	$C_8H_7O_5^+$
$[M+H-C_4H_8O_3]^+$	$^{1,4}A^+$-H	179.07025	0.1	$C_{10}H_{11}O_3^+$
$[M+H-C_5H_8O_3]^+$	$^{2,4}A^+$	167.07044	-1.0	$C_9H_{11}O_3^+$
$[M+H-2C_3H_6O]^+$		167.03385	0.2	$C_8H_7O_4^+$
$[M+H-C_5H_{10}O_3]^+$	$^{2,4}A^+$-2H	165.05465	-0.2	$C_9H_9O_3^+$
$[M+H-2C_3H_6O-CO]^+$		139.03895	0.1	$C_7H_7O_3^+$
$[M+H-2C_3H_6O-CH_2O_2]^+$		121.02847	-0.1	$C_7H_5O_2^+$
$[M+H-2C_3H_6O-2CO]^+$		111.04430	-2.2	$C_6H_7O_2^+$

Table 6.7. Ion assignment for the fragmentation pattern proposed for the protonated molecule of compound **2**.

Ion		*m/z*	Error (ppm)	Ion Formula
[M+H]$^+$		333.13542	-6.5	$C_{18}H_{21}O_6^+$
[M+H-C$_3$H$_6$O]$^+$		275.09068	2.6	$C_{15}H_{15}O_5^+$
[M+H-C$_3$H$_8$O$_2$]$^+$		257.08027	0.6	$C_{15}H_{13}O_4^+$
[M+H-C$_3$H$_8$O$_2$-H$_2$O]$^+$		239.06982	1.9	$C_{15}H_{11}O_3^+$
[M+H-C$_4$H$_8$O$_3$]$^+$	$^{1,4}A^+$-H	229.08560	1.4	$C_{14}H_{13}O_3^+$
[M+H-C$_5$H$_8$O$_3$]$^+$	$^{2,4}A^+$	217.08572	0.9	$C_{13}H_{13}O_3^+$
[M+H-C$_5$H$_{10}$O$_3$]$^+$	$^{2,4}A^+$-2H	215.07008	0.9	$C_{13}H_{11}O_3^+$
[M+H-C$_3$H$_8$O$_2$-H$_2$O-CO]$^+$		211.07522	0.7	$C_{14}H_{11}O_2^+$
[M+H-C$_3$H$_8$O$_2$-H$_2$O-2CO]$^+$		183.08048	0.2	$C_{13}H_{11}O^+$
[M+H-C$_{11}$H$_{14}$O$_6$]$^+$		91.05421	0.2	$C_7H_7^+$

The protonated molecules of these compounds, *m/z* 283.12 for **1** and *m/z* 333.14 for **2**, can lose 58.04 Da to afford the ions at *m/z* 225.08 and *m/z* 275.09, respectively. The high accuracy mass measurements allow us to attribute this loss to C_3H_6O. For compound **2**, this loss is straightforward and was attributed to acetone (CH_3COCH_3) resulting from the *O*-isopropylidene moiety. For compound **1**, however, this loss may be explained by two possible pathways. One of the pathways involves the loss of acetone from the *O*-isopropylidene moiety (ion structure **a** in Scheme 6.24, page 245), similarly to what was proposed for **2**, while the other one involves the loss of propenol from the *C*^{3} substituent (ion structure **b** in Scheme 6.24, page 245). To access which of the two ion structures is indeed the most probable one, semi-empirical calculations were performed. The transition that affords ion structure **a** corresponding to the loss of acetone from the *O*-isopropylidene moiety, has a Δ_rH of *ca.* 389 kJ mol^{-1}, while Δ_rH for the one that affords ion structure **b** is *ca.* 194 kJ mol^{-1}. Hence, it is reasonable to assume that the *m/z* 225.08 ion is due to the loss of propenol from the *C*^{3} substituent of the sugar ring.

The ions at *m/z* 207.07 for **1** and *m/z* 257.08 for **2** were attributed to the loss of $C_3H_8O_2$, corresponding to propane-2,2-diol, which results from the scission of the 1,2-*O*-isopropylidene moiety, from the protonated molecule (*m/z* 283.12 for **1** and *m/z* 333.14 for **2**). The *m/z* 257.08 ion was also detected for compound **2** in the MS^3 spectrum of the *m/z* 275.09 ion and results from the loss of H_2O from this ion (Figure 6.11b). These observations suggest that, for compound **2**, two fragmentation pathways can occur to afford the ion at *m/z* 257.08. One is the loss of H_2O from the *m/z* 275.09 ion, whereas the other is the direct loss of the *O*-isopropylidene moiety from the protonated molecule, as shown in Scheme 6.24. For compound **1**, however, the MS^3 spectrum of the *m/z* 225.08, depicted in Figure 6.10b, does not show the loss of H_2O to afford an ion at *m/z* 207.06. As such, the loss of 58.04 Da (C_3H_6O) from the protonated molecule of **1** may be preferentially attributed to the loss of propenol (structure **b** in Scheme 6.24), rather than acetone (structure **a** in Scheme 6.24). This assumption is supported by the semi-empirical calculations addressed above.

For compound **1**, the ion at *m/z* 183.03 was attributed to the concerted loss of the C^3 substituent, propenol (C_3H_6O), and C_3H_6 from the isopropylidene group of the protonated molecule. The MS^2 spectrum of the protonated molecule of compound **2** also exhibits an ion at *m/z* 183.03, although with a rather low abundance (*ca.* 1%). This ion can be attributed to the loss of phenylmethanol (C_7H_8O) and C_3H_6 (isopropylidene group) from the protonated molecule.

A loss of $C_4H_8O_3$ (i.e. 104.05 Da, 2-hydroxypropan-2-yl formate) from the protonated molecule of compounds **1** and **2** can explain the ions at *m/z* 179.07 and *m/z* 229.09, respectively, since none of them was

detected in the MS^3 spectra acquired. The $C_4H_8O_3$ loss may occur through the scission of the furanose ring at the C^1-C^2 and C^4-O bonds and that of the C^2-O bond, affording a ^{1,4}A-H type ion, according to the nomenclature proposed by Domon and Costello.[29] A possible mechanism for this fragmentation is presented in Scheme 6.21.

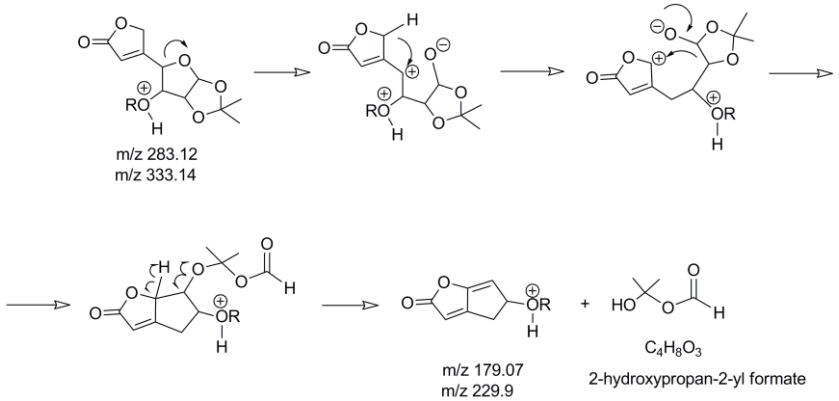

Scheme 6.21. Possible mechanism for the loss of 2-hydroxypropan-2-yl formate ($C_4H_8O_3$, 104.05 Da) from the protonated molecule of compounds **1** and **2** to afford the ions at m/z 179.07 and m/z 229.09, respectively.

For compound **2**, the ions at m/z 217.09 (loss of $C_5H_8O_3$ from $[M+H]^+$) and 215.04 (loss of $C_5H_{10}O_3$ from $[M+H]^+$) can be ascribed to cross-ring cleavages at bonds 2 and 4 (bond labelling is given in Chapter 2) of the furanose ring of the protonated molecule. The m/z 217.09 can be attributed to a $^{2,4}A^+$ ion, while the ion at m/z 215.04 can be ascribed to the $^{2,4}A^+$-2H ion. Interestingly, the abundance of the $^{2,4}A^+$-2H ion (rel. abund. 40%) is higher than that of $^{2,4}A^+$ ion (rel. abund. 18%). The equivalent ions were found for compound **1**, i.e. the $^{2,4}A^+$-2H ion was found at m/z 165.05 and the $^{2,4}A^+$ ion at m/z 167.07, although with lower relative abundance, 5% and 7%, respectively. This difference in behaviour can be ascribed to the different substituent at C^3. For compound **1** another cross-ring cleavage was found, which gave the low

abundance ion (*ca.* 5%) at *m/z* 183.06, attributed to the loss of $C_5H_8O_2$ from the protonated molecule, affording a $^{0,2}A^+$ type ion. Interestingly, such loss was not detected for compound **2** (Scheme 6.24), also probably due to the different substituent at *C*^{3}. For compound **1**, the MS^2 spectrum of the protonated molecule (Figure 6.10a) shows a high abundance ion at *m/z* 167.03 (>80%). The MS^3 spectrum of the *m/z* 225.08 ion (Figure 6.10b) shows that this ion loses 58.04 Da (*i.e.* C_3H_6O) to afford the *m/z* 167.03 ion. For compound **2**, the equivalent fragmentation pathway (i.e. loss of C_3H_6O) from the *m/z* 275.09 ion was not detected (Figure 6.11b).

For compound **1,** the ions at *m/z* 139.04 and *m/z* 121.03, present in the MS^2 spectrum of the protonated molecule, were attributed to the loss of CO and HCOOH, respectively, from the *m/z* 167.03 ion (Figure 6.10c). A possible mechanism for the loss of HCOOH is depicted in Scheme 6.22. The ion at *m/z* 111.04, present in the MS^3 spectrum of *m/z* 139.04 ion, also appears in the MS^2 spectrum (Figure 6.10a), even though with a low abundance (*ca.* 1%), and was attributed to the loss of CO from the *m/z* 139.04 ion (Figure 6.10d).

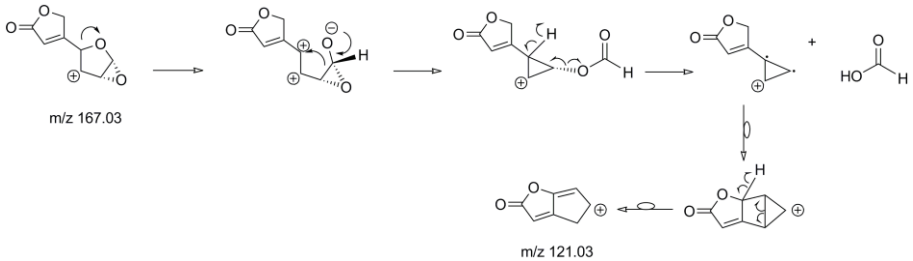

Scheme 6.22. Possible mechanism for the loss of HCOOH from the *m/z* 167.03 ion to afford the *m/z* 121.03 ion.

For compound **2**, the ion at *m/z* 239.07 can be explained by the loss of H_2O from the *m/z* 257.08 ion (Figure 6.12).

A possible mechanism for this loss is presented in Scheme 6.23, and involves the scission of the O-C^1 and O-C^4 bonds and further hydrogen rearrangement. However, the formation of this ion cannot be ruled out from a mixture of other possible fragmentation mechanisms in view of the smaller difference in the protonation reaction energies for compound **2**.

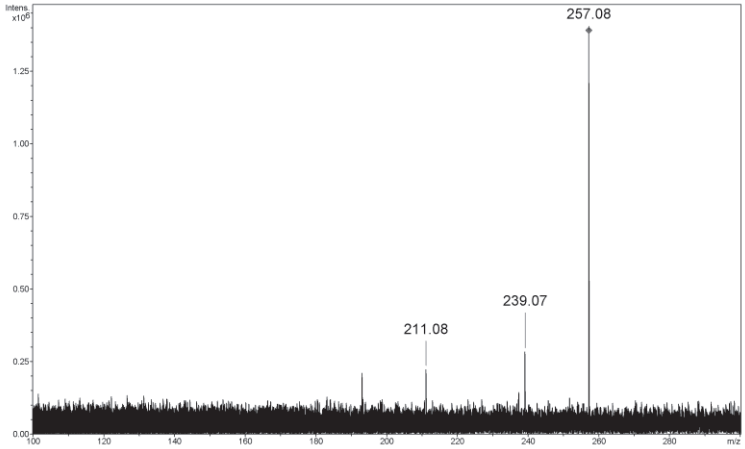

Figure 6.12. MS^3 spectrum of the *m/z* 257.08 ion of protonated compound **2**.

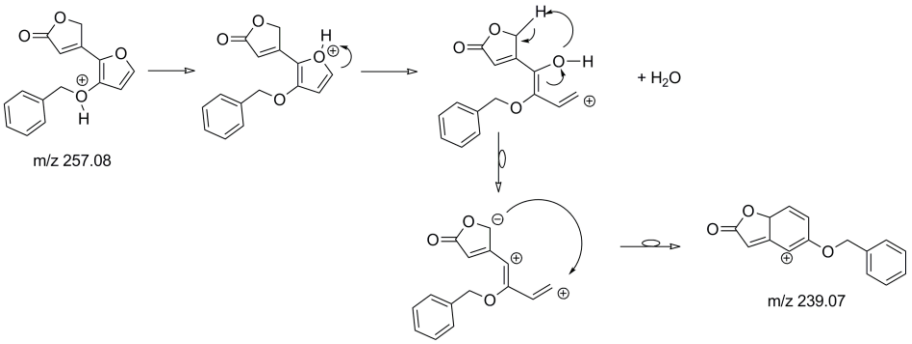

Scheme 6.23. Possible fragmentation mechanism for the loss of water from the *m/z* 257.08 ion affording the *m/z* 239.07 ion.

The MS^3 spectrum of the *m/z* 239.07 (Figure 6.11c) shows that this ion loses CO affording the *m/z* 211.08 ion, which subsequently can

lose another CO (confirmed by MS^3, Figure 6.11d) affording the ion at *m/z* 183.08. The ion at *m/z* 91.05 was attributed to the tropylium ion, formed by direct loss of 242.08 Da from the protonated molecule of **2**. This assignment was made taking into account the accurate mass data and the fact that the *m/z* 91.05 ion was not detected in any of the MS^3 experiments performed.

All these observations are summarized in Scheme 6.24, that depicts the proposed fragmentation mechanism for compounds **1** and **2**.

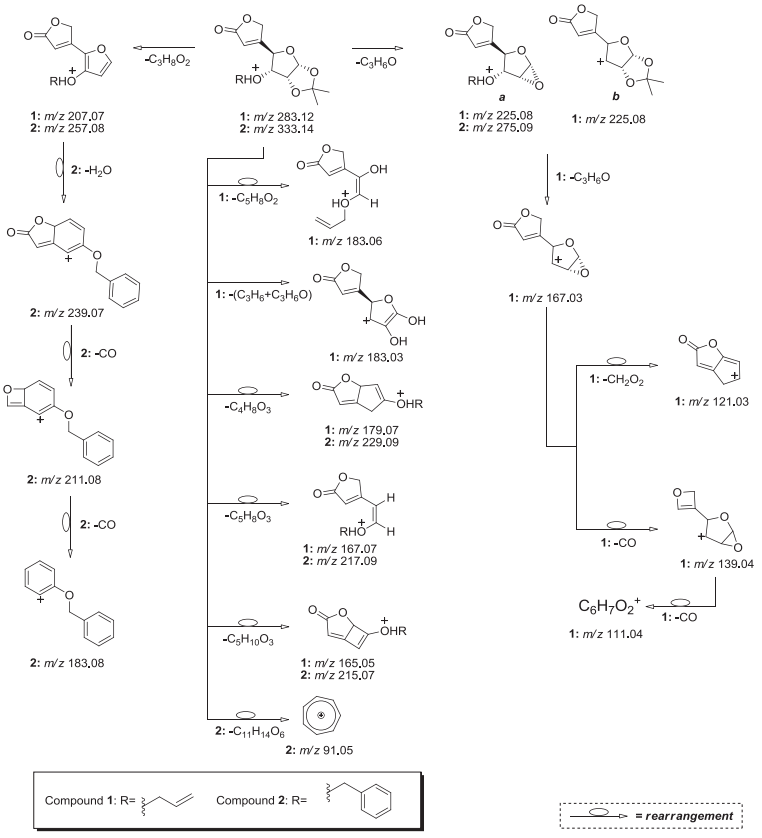

Scheme 6.24. Proposed fragmentation mechanism for the protonated molecules of compounds **1** and **2**.

*Protonated Compounds **3** and **4***

The MS^2 of the protonated molecule of compound **3** and the MS^3 spectra of the ions at *m/z* 283.12, 243.09 and 167.07 are depicted in Figure 6.13.

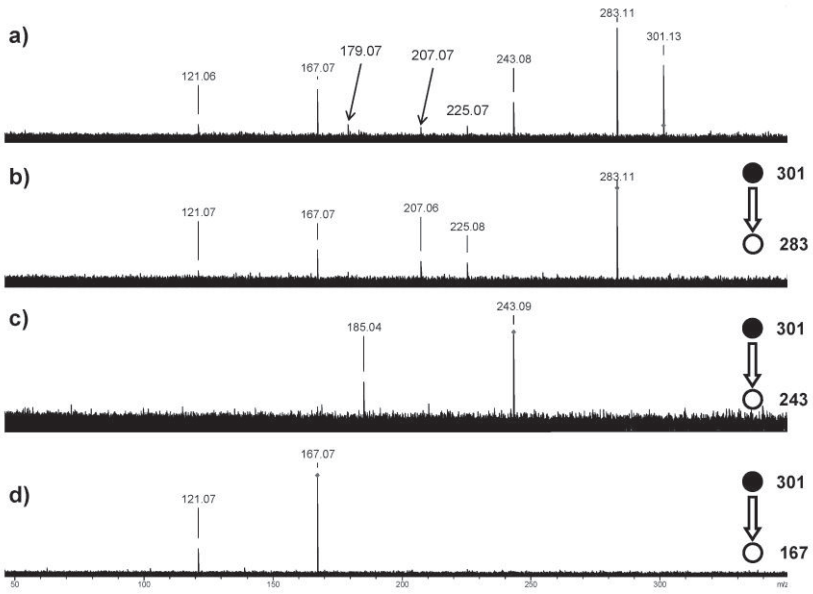

Figure 6.13. Mass spectra acquired for compound **3**: a) MS^2 spectrum of the protonated molecule at *m/z* 301 (E_{col}=-9.0 eV); b) MS^3 spectrum of the ion at *m/z* 283 (SORI-CAD, SORI power=0.30%, Frequency Offset=400 Hz); c) MS^3 spectrum of the ion at *m/z* 243 (SORI-CAD, SORI power=0.25%, Frequency Offset=400 Hz); d) MS^3 spectrum of the ion at *m/z* 167 (SORI-CAD, SORI power=0.20%, Frequency Offset=400 Hz).

Figure 6.14 depicts the MS^2 spectrum of the protonated molecule of compound **4** (Figure 6.14a) and the MS^3 spectra of the ions at *m/z* 275.09, 239.07 and 175.08 (Figure 6.14b-d, respectively). The high accuracy mass measurements enabled the attribution of ion compositions, with errors below 5 ppm, for both compounds and the results are presented in Table 6.8 and Table 6.9, respectively.

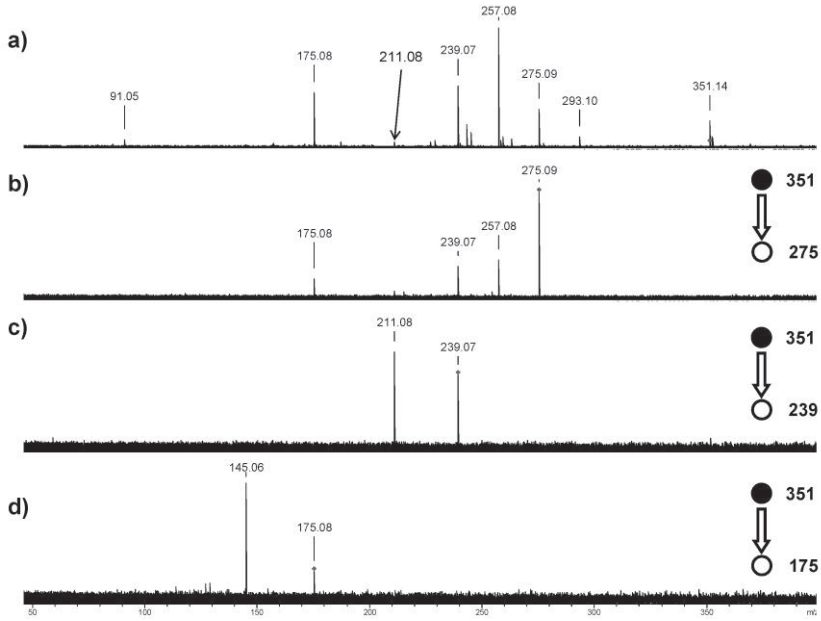

Figure 6.14: Mass spectra acquired for compound **4**: a) MS^2 spectrum of the protonated molecule at *m/z* 351 (E_{col}=-5.0 eV); b) MS^3 spectrum of the ion at *m/z* 275 (SORI-CAD, SORI power=0.25%, Frequency Offset=400 Hz); c) MS^3 spectrum of the ion at *m/z* 239 (SORI-CAD, SORI power=0.35%, Frequency Offset=400 Hz); d) MS^3 spectrum of the ion at *m/z* 175 (SORI-CAD, SORI power=0.25%, Frequency Offset=400 Hz).

Table 6.8. Ion assignment for the fragmentation pattern proposed for the protonated molecule of compound **3**.

Ion		*m/z*	Error (ppm)	Ion Formula
$[M+H]^+$		301.12874	-1.9	$C_{14}H_{21}O_7^+$
$[M+H-H_2O]^+$		283.11821	-2.1	$C_{14}H_{19}O_6^+$
$[M+H-C_3H_6O]^+$		243.08679	-1.9	$C_{11}H_{15}O_6^+$
$[M+H-H_2O-C_3H_6O]^+$		225.07494	3.6	$C_{11}H_{13}O_5^+$
$[M+H-H_2O-C_3H_8O_2]^+$		207.06507	0.6	$C_{11}H_{11}O_4^+$
$[M+H-2C_3H_6O]^+$		185.04408	2.0	$C_8H_9O_5^+$
$[M+H-H_2O-C_5H_8O_3]^+$	$^{2,4}A'^+$ ‡	167.07012	0.9	$C_9H_{11}O_3^+$
$[M+H-H_2O-C_5H_8O_3-CH_2O_2]^+$		121.06488	-0.8	$C_8H_9O^+$

‡ $^{2,4}A'^+$ refers to the cross-ring cleavage of the *m/z* 283.12 ion.

Table 6.9. Ion assignment for the fragmentation pattern proposed for the protonated molecule of compound **4**.

Ion	*m/z*	Error (ppm)	Ion Formula
[M+H]$^+$	351.14328	1.6	$C_{18}H_{23}O_7^+$
[M+H-C_3H_6O]$^+$	293.10193	0.1	$C_{15}H_{17}O_6^+$
[M+H-$C_3H_8O_2$]$^+$	275.09170	-1.1	$C_{15}H_{15}O_5^+$
[M+H-$C_3H_8O_2$-H_2O]$^+$	257.08099	-0.2	$C_{15}H_{13}O_4^+$
[M+H-C_7H_8O]$^+$	243.08638	-0.1	$C_{11}H_{15}O_6^+$
[M+H-$C_3H_8O_2$-2H_2O]$^+$	239.07039	-0.5	$C_{15}H_{11}O_3^+$
[M+H-$C_3H_8O_2$-2H_2O-CO]$^+$	211.07529	0.3	$C_{14}H_{11}O_2^+$
[M+H-$C_3H_8O_2$-$C_4H_4O_3$]$^+$	175.07552	-0.9	$C_{11}H_{11}O_2^+$
[M+H-$C_3H_8O_2$-$C_4H_4O_3$-CH_2O]$^+$	145.06482	-0.2	$C_{10}H_9O^+$
[M+H-$C_{11}H_{16}O_7$]$^+$	91.05444	-2.3	$C_7H_7^+$

The protonated molecule of compound **3**, *m/z* 301.13, loses H_2O affording the ion at *m/z* 283.12. Interestingly, this loss was not detected for compound **4**. As such, it is reasonable to assume that an interaction between the OH group in carbon *C*^{5} and the benzyl group in *C*^{3} may occur. This interaction, reported in the literature as an intramolecular OH···π hydrogen bond,[68] should be much stronger in compound **4** (aromatic ring substituent: benzyl group) than in compound **3** (one double bond substituent: allyl group).

The protonated molecules of both compounds lose C_3H_6O affording the ion at *m/z* 243.08 for compound **3** and *m/z* 293.10 for compound **4**. For compound **4**, this *m/z* 293.10 ion is clearly due to the loss of acetone from the *O*-isopropylidene moiety (ion structure **a** in Scheme 6.25). Nevertheless, for compound **3** not only the loss of acetone from the *O*-isopropylidene moiety (ion structure **b** in Scheme 6.25) but also propenol from the *C*^{3} substituent (ion structure **a** in Scheme 6.25) might afford the *m/z* 243.08 ion. Semi-empirical calculations were performed to access which of the two transitions is the most probable one. The loss of acetone, affording ion structure **a** in

Scheme 6.25, has a $\Delta_r H$ of 409 kJ mol^{-1}, while the loss of propenol, affording ion structure **b** in Scheme 6.25, has a $\Delta_r H$ of 173 kJ mol^{-1}. It seems therefore reasonable to assume that the *m/z* 243.08 ion is preferably formed through the loss of propenol from the protonated molecule, similarly to what was proposed for compound **1**. Nevertheless, in the MS^2 spectrum of protonated **4** (Figure 6.14a), an *m/z* 243.08 ion (structure **b** in Scheme 6.25) was also detected, although with low abundance. This ion was attributed to the loss of phenylmethanol from the C^3 substituent.

For compound **3**, the ion at *m/z* 243.09 can lose another C_3H_6O (Figure 6.13c) to afford the ion at *m/z* 185.04, which was not detected in the MS^2 of the protonated molecule (Figure 6.13a).

The highly abundant ion at *m/z* 283.12, observed in the MS^2 spectrum of compound **3** (Figure 6.13a), was isolated and fragmented by means of SORI-CAD and its spectrum is presented in Figure 6.13b. Similarly to what was found earlier for compound **1**, this ion can lose 58.04 Da to afford the ion at *m/z* 225.08 (to note that the protonated molecule of **2** also loses 58.04 Da). Similarly to compound **1,** two structures can be proposed for this *m/z* 225.08 ion and semi-empirical calculations were employed to access the most probable one. Moreover, since this ion is similar to the ion at *m/z* 225.08 of compound **1**, it is reasonable to assume that the loss of the C^3 substituent will be preferred. The semi-empirical calculations indeed showed that the transition that affords ion structure **c**, loss of acetone, has a $\Delta_r H$ of *ca.* 90 kJ mol^{-1}, while the loss of propenol to afford ion structure **d** has a $\Delta_r H$ *ca.* -35 kJ mol^{-1}, which supports our assumption. The *m/z* 283.12 ion can also lose 76.05 Da, attributed to the loss of propane-2,2-diol due

to the scission of the 1,2-*O*-isopropylidene moiety to form the *m/z* 207.07 ion, as well as 116.05 Da attributed to $C_5H_8O_3$, which is consistent with a cross-ring fragmentation affording *m/z* 167.07, a $^{2,4}A$ type ion, according to the nomenclature proposed by Domon and Costello.[29] This ion was also detected for compound **1**, although with rather low abundance (~7%) when compared with the abundance of the *m/z* 167.07 ion in compound **3** (~47%). To note that these spectra, the MS^2 spectrum of the protonated compound **1** (Figure 6.10a) and the MS^3 spectrum of the $[M+H-H_2O]^+$ ion (*m/z* 283.11) for compound **3** (Figure 6.13b) were taken in slightly different activation conditions. For the MS^2 spectrum, "classic" CID was used; while for the MS^3, Sustained Off-Resonance Irradiation-Collision Activated Dissociation (SORI-CAD) was employed. Nevertheless, the different activation conditions alone do not explain the difference observed in relative abundances. In fact, there are reports in the literature that state that the dissociation pathways are reproducible using both activation techniques [69] and that SORI-CAD has analogies with ion trap CID.[70, 71] Hence, it is reasonable to assume that the stereochemistry of the C^3 might play a crucial role in this fragmentation. A hydrogen migration from the C^3 substituent oxygen to the lactone carbonyl, prior to the fragmentation, could be even considered to occur. Such migration would be easier for compound **3**, for which both the lactone moiety and the C^3 substituent are on the same plane, than for compound **1**, for which these two moieties are on different planes. An interesting observation concerns the fact that there are two ions with the nominal mass 167 in the mass spectra of compounds **1** (Figure 6.10a-c) and **3** (Figure 6.13a-b), that is, the *m/z* 167.03 and *m/z* 167.07 ions. The *m/z* 167.03 ion has its origins

in the sequential loss of two C_3H_6O moieties and its abundance is higher for compound **1**, while the *m/z* 167.07 ion results from the fragmentation of the sugar ring and its abundance is higher for **3**. Taking into account that the stereochemistry may influence the fragmentation pattern,[67, 72] it may be assumed that the difference in the abundances of these two ions could be related with the *C*^{3} stereochemistry of the parent molecule. From the MS^3 spectrum of the ion at *m/z* 167.07 it is noticeable that it loses 46.01 Da, attributed to HCOOH, affording the ion at *m/z* 121.07.

Furthermore, the protonated molecule of compound **4**, *m/z* 351.14, can lose 76.05 Da, attributed to the loss of propane-2,2-diol from the 1,2-*O*-isopropylidene moiety, affording the ion at *m/z* 275.09, as well as 260.09 Da ($C_{11}H_{16}O_7$), affording the ion at *m/z* 91.05 attributed to the tropylium ion. Similarly to what has been proposed for compound **2**, the formation of the latter ion occurs directly from the protonated molecule, since it was not detected in any of the MS^3 experiments performed on the other ions.

The ion at *m/z* 257.08, the most abundant in the MS^2 spectrum of the protonated molecule of compound **4**, can be attributed to the loss of H_2O from the *m/z* 275.09 ion and it seems to possess the same backbone structure of the *m/z* 207.07 ion detected for compound **3**. This H_2O loss was confirmed by the MS^3 spectrum depicted in Figure 6.14b. From the analysis of this MS^3 spectrum it is also possible to attribute the ion at *m/z* 175.08 to the loss of the lactone moiety ($C_4H_4O_3$) from the ion at *m/z* 275.09. The MS^3 spectrum of the ion at *m/z* 257.08 (Figure 6.15) showed that this ion loses H_2O to afford the ion at *m/z* 239.07, with the same structure and by a similar mechanism

as for compound **2** (Scheme 6.24). As mentioned for compound **2**, the formation of this ion cannot be ruled out from a mixture of other possible fragmentation mechanisms, in view of the smaller difference in the protonation reaction energies for compound **4**.

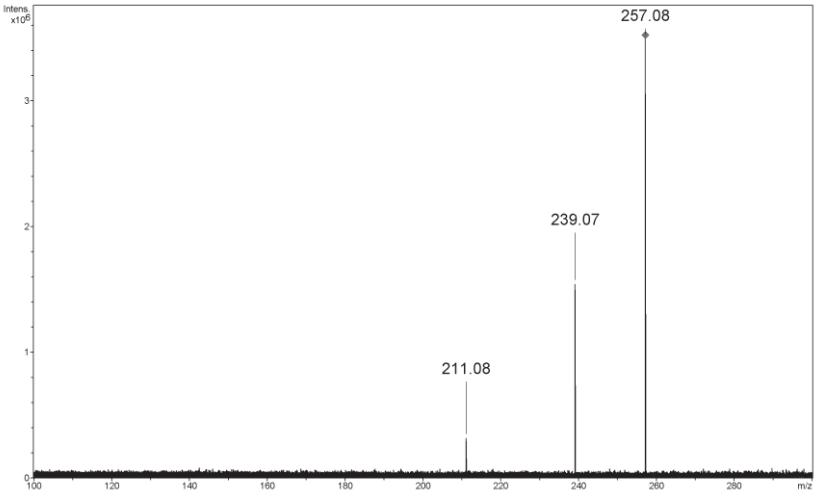

Figure 6.15. MS^3 spectrum of the m/z 257.08 ion of protonated compound **4**.

The MS^3 spectrum of the m/z 239.07 ion, depicted in Figure 6.14c, clearly shows that the m/z 211.08 ion results from the loss of 27.99 Da, attributed to CO. Furthermore, the ion at m/z 175.08 can lose CH_2O, affording the ion at m/z 145.06 (Figure 6.14d) that was not detected in the MS^2 spectrum of the protonated molecule of compound **4** (Figure 6.14a).

To note that ions resulting from cross-ring cleavages of the protonated molecules of compounds **3** and **4** were not detected. For these two compounds such behaviour might be related with the lack of the α,β unsaturated system of the lactone. The delocalization of this system might help in the scission of the C^4-O bond of the furanose.

Nevertheless, for compound **3** the $[M+H-H_2O]^+$, *i.e.* *m/z* 283.12, can suffer cross-ring fragmentations to afford $^{1,4}A^+$-H and $^{2,4}A^+$ type ions.

All these observations are summarized in Scheme 6.25, which depicts the fragmentation mechanism proposed for the protonated molecules of compound **4** and **5**.

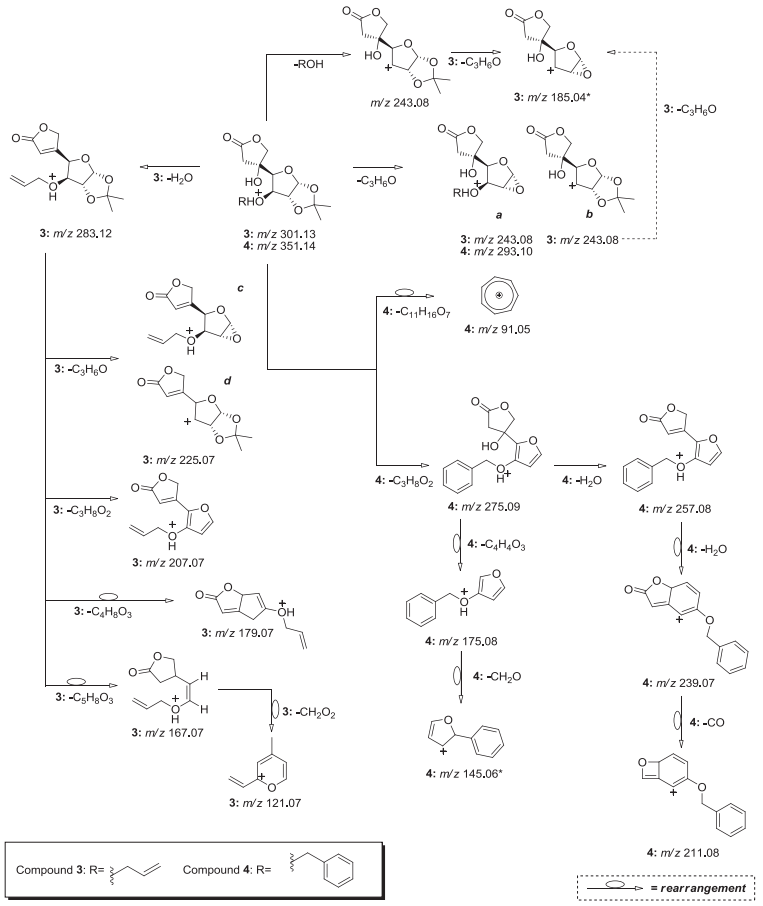

Scheme 6.25. Proposed fragmentation mechanisms for the protonated molecules of compound **3** and **4** (* the ions at *m/z* 185.04 for compound **3** and *m/z* 145.06 for compound **4** were not detected in the MS^2 spectra of the protonated molecules).

*Sodiated forms of Compounds **1-4***

To access the possible cationization site, semi-empirical calculations were performed and the most stable structures (and the corresponding cationization reaction enthalpies, $\Delta_r H$, values in kJ mol^{-1}) are presented in Table 6.10.

Table 6.10. Most stable structure of sodiated compounds **1**-**4** and corresponding $\Delta_r H$ value (kJ mol^{-1}) estimated using the PM6 Hamiltonian implemented in MOPAC2009 (distances in Å)

Compound	Structure	$\Delta_r H$ (kJ mol^{-1})
1	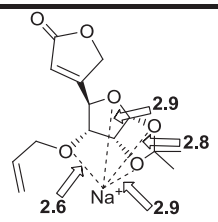	330.05
2	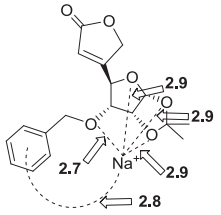	292.44
3	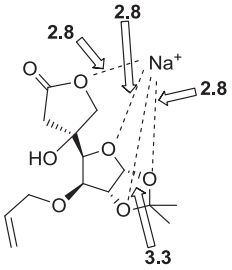	320.47
4	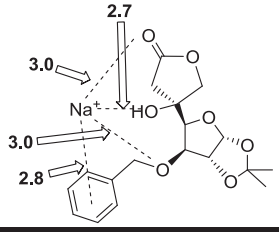	270.10

Of all four compounds studied, compounds **2** and **4** showed the lowest $\Delta_f H$ value. In fact, analyzing their structures (Table 6.10) it is possible to note that cationization of these two compounds involves the benzyl substituent that can account for their low heat of formation. This semi-empirical prediction is in agreement with the literature data where cations are known to bind strongly to aromatic systems.[73, 74]

The relative abundances and attribution errors for the sodiated compounds are presented in Table 6.11.

Table 6.11. Detected product ions of sodiated compounds **1-4**.

Compounds	Collision Voltage (V)	*m/z* (Rel. Abundance; error)
1	-10	$[M+Na]^+$: 305 (100%; 2.6 ppm) $[M+Na-C_3H_6O]^+$: 247 (0.06%; 1.6 ppm)
2		$[M+Na]^+$: 355 (100%; -7.0 ppm) $[M+Na-C_3H_6O]^+$: 247 (0.2%; -9.3 ppm)
3		$[M+Na]^+$: 323 (100%; -5.0 ppm) $[M+Na-H_2O]^+$: 305 (0.2%; -5.5 ppm) $[M+Na-C_3H_6O]^+$: 265 (0.04%; -3.6 ppm)
4		$[M+Na]^+$: 373 (100%; 1.4 ppm) $[M+Na-C_3H_6O]^+$: 315 (0.05%; -1.2 ppm)

As expected, the sodiated compounds are more stable than the protonated ones and their fragmentation is less extensive, which is clearly noticeable by the low relative abundances of the product ions as well as by the small number of product ions formed. Moreover, no new product ions were found when the collision cell voltage was increased, whereas a decrease of the precursor and product ions abundances was observed. The loss of 58 Da is the major fragmentation pathway for all compounds, with the exception of **3** for which the main fragmentation

was attributed to the loss of water. In fact, this behaviour was also observed for protonated compound **3**. Similarly to what was found for the protonated molecules of compounds **1** and **3**, the formation of $[M+Na-C_3H_6O]^+$ ion from their sodiated molecules has two possible pathways: the loss of the C^3 substituent and/or the loss of acetone from the *O*-isopropylidene moiety. From the structure of the sodiated molecules (Table 6.10), it is possible to propose that for compound **3** the C_3H_6O loss occurs from the C^3 substituent since the *O*-isopropylidene moiety is involved in the alkali metal coordination. For compound **1** the C_3H_6O loss is not as straightforward. Nevertheless, taking into account that the sodium is closer to the oxygen atom of the C^3 substituent, it seems reasonable to assume that the C_3H_6O loss shall occur from the *O*-isopropylidene moiety.

6.2.3 Conclusions

A loss of 58.04 Da was detected for all compounds and based on semi-empirical calculations it was possible to attribute it unequivocally to propenol from the C^3 substituent, rather than acetone from the *O*-isopropylidene moiety for compounds **1** and **3**. For compounds **2** and **4** this loss was easily attributed to acetone from the *O*-isopropylidene moiety.

Cross-ring cleavages from the protonated molecule were only detected for compounds **1** and **2**. For compound **3**, the cross-ring cleavages detected were due to the fragmentation of the $[M+H-H_2O]^+$ ion. The lack of cross-ring cleavages from the protonated molecules of

3 and **4** was attributed to the absence of the conjugated α, β unsaturated system of the lactone for these compounds. The delocalization of this system might help the scission of the C^4-O bond. This observation enabled us to conclude that the lactone moiety has indeed a substantial influence on the fragmentation of the sugar ring.

The stereochemistry may have played a crucial role in the fragmentation of compounds **1** and **3**, since the m/z 167.07 ion was formed with higher abundance for the de-hydrated compound **3** than for compound **1**. For these two species the C^3 stereochemistry is the only structural difference.

The sodiated forms of all compounds showed very little fragmentation, the main decomposition pathway being the loss of C_3H_6O and, for compound **3**, also the loss of water.

Semi-empirical calculations proved to be helpful for the proposal of fragmentation pathways and also in the assignment of the probable protonation and alkali metal coordination sites.

6.3 References

1. Xavier, N.M. and A.P. Rauter, *Easy and Stereoselective Approach to α,β-Unsaturated γ-Lactones Fused to Pyranoses from Furanose Scaffolds.* Organic Letters, 2007. **9**(17): p. 3339-3341.
2. Xavier, N.M. and A.P. Rauter, *Sugars containing α,β-unsaturated carbonyl systems: synthesis and their usefulness as scaffolds in carbohydrate chemistry.* Carbohydrate Research, 2008. **343**(10-11): p. 1523-1539.
3. Paruch, E., J. Nawrot, and C. Wawrzenczyk, *Lactones: Part 11. Feeding-deterrent activity of some bi- and tricyclic terpenoid lactones.* Pest Management Science, 2001. **57**(9): p. 776-780.
4. Staunton, J. and K.J. Weissman, *Polyketide biosynthesis: a millennium review.* Natural Product Reports, 2001. **18**(4): p. 380-416.
5. Justino, J., et al., *Sugar derivatives containing oxiranes and α,β-unsaturated γ-lactones as potential environmentally friendly insecticides.* Pest Management Science, 2005. **61**(10): p. 985-990.
6. Borsato, M.L.C., et al., *Analgesic activity of the lignans from Lychnophora ericoides.* Phytochemistry, 2000. **55**(7): p. 809-813.
7. Rauter, A.P., et al., *Efficient synthesis of α,β-unsaturated γ-lactones linked to sugars.* Tetrahedron: Asymmetry, 2001. **12**(8): p. 1131-1146.
8. Crotti, A.E.M., et al., *The fragmentation mechanism of five-membered lactones by electrospray ionisation tandem mass spectrometry.* International Journal of Mass Spectrometry, 2004. **232**(3): p. 271-276.

9. Desaire, H. and J.A. Leary, *Differentiation of Diastereomeric N-Acetylhexosamine Monosaccharides Using Ion Trap Tandem Mass Spectrometry.* Analytical Chemistry, 1999. **71**(10): p. 1997-2002.

10. Penn, S.G., M.T. Cancilla, and C.B. Lebrilla, *Collision-Induced Dissociation of Branched Oligosaccharide Ions with Analysis and Calculation of Relative Dissociation Thresholds.* Analytical Chemistry, 1996. **68**(14): p. 2331-2339.

11. Banoub, J., et al., *Electrospray Tandem Mass Spectrometry of a Novel Series of Amphipathic Functionalized Ether-linked Di- and Trisaccharides and Cyclic Oligosaccharides.* Journal of Mass Spectrometry, 1997. **32**(1): p. 109-121.

12. Young, M.K., N. Dinh, and D. Williams, *Analysis of <I>N</I>-acetylated hexosamine monosaccharides by ferrocenyl boronation and tandem electrospray ionization mass spectrometry.* Rapid Communications in Mass Spectrometry, 2000. **14**(16): p. 1462-1467.

13. Yin, W., Y. Ma, and Y. Zhao, *The fragmentation mechanism of β-(N-alkyl/arylamino)-a,β-unsaturated carboxylates under electrospray ionization conditions.* Amino Acids, 2006. **31**(3): p. 333-336.

14. Madhusudanan, K.P., et al., *Effect of metal cationization on the tandem mass spectra of glycosyl dithioacetals.* Journal of Mass Spectrometry, 2005. **40**(1): p. 25-35.

15. Madhusudanan, K.P., et al., *Tandem mass spectra of ammonium ion, metal ion and ligated metal ion adducts of acyclic sugar derivatives.* Rapid Communications in Mass Spectrometry, 2003. **17**(8): p. 816-824.

16. Madhusudanan, K.P., B.A. Bhat, and S.N. Suryawanshi, *Collision-induced dissociation of MCl^+ adducts (M = Mg, Mn, Zn, Co, Ni and Cu) and Cu^+ and Ag^+ adducts of dithioalkyl ketene acetals.* Rapid

Communications in Mass Spectrometry, 2001. **15**(10): p. 788-798.

17. Eller, K. and H. Schwarz, *Organometallic chemistry in the gas phase.* Chemical Reviews, 1991. **91**(6): p. 1121-1177.
18. Beneito-Cambra, M., et al., *Study of the Fragmentation of D-Glucose and Alkylmonoglycosides in the Presence of Sodium Ions in an Ion-Trap Mass Spectrometer.* Analytical Letters, 2009. **42**(6): p. 907 - 921.
19. Xavier, N.M., et al., *Synthesis and Biological Evaluation of Sugars Containing α,β-Unsaturated γ-Lactones.* European Journal of Organic Chemistry, 2008. **2008**(36): p. 6134-6143.
20. Justino, G.C., C.M. Borges, and M.H. Florêncio, *Electrospray ionization tandem mass spectrometry fragmentation of protonated flavone and flavonol aglycones: a re-examination.* Rapid Communications in Mass Spectrometry, 2009. **23**(2): p. 237-248.
21. Franski, R., et al., *Electrospray mass spectrometric decomposition of some glucuronic acid-containing flavonoid diglycosides.* Phytochemical Analysis, 2003. **14**(3): p. 170-175.
22. Przybylski, P., et al., *ESI MS and PM5 semiempirical studies of gossypol schiff base with (R)-tetrahydrofurfurylamine complexes and monovalent cations.* Journal of Molecular Structure, 2004. **693**(1-3): p. 95-102.
23. Huczynski, A., B. Brzezinski, and F. Bartl, *Structures of complexes of benzyl and allyl esters of monensin A with Mg^{2+}, Ca^{2+}, Sr^{2+}, Ba^{2+} cations studied by ESI-MS and PM5 methods.* Journal of Molecular Structure, 2008. **886**(1-3): p. 9-16.
24. Ishikawa, K., T. Nakamura, and Y. Koga, *Cross-checking of nanoelectrospray ionization mass spectrometry and computer simulation for*

the evaluation of the interaction strength of non-covalently bound enkephalins in solution. Journal of Mass Spectrometry, 2001. **36**(8): p. 937-942.

25. Zayed, M.A., et al., *Mass spectrometric investigation of buspirone drug in comparison with thermal analyses and MO-calculations*. Spectrochimica Acta, Part A: Molecular and Biomolecular Spectroscopy, 2007. **67**(2): p. 522-530.
26. Khairallah, G. and J.B. Peel, *Cyano Adduct Anions of C70: Electrospray Mass Spectrometric Studies*. Journal of Physical Chemistry A, 1997. **101**(36): p. 6770-6774.
27. Kazmaier, T., et al., *Quantitative analysis of malto-oligosaccharides by MALDI-TOF mass spectrometry, capillary electrophoresis and anion exchange chromatography*. Fresenius' Journal of Analytical Chemistry, 1998. **361**(5): p. 473-478.
28. Harvey, D.J., *Matrix-assisted laser desorption/ionization mass spectrometry of carbohydrates*. Mass Spectrometry Reviews, 1999. **18**(6): p. 349-450.
29. Domon, B. and C.E. Costello, *A systematic nomenclature for carbohydrate fragmentations in FAB-MS/MS spectra of glycoconjugates*. Glycoconjugate Journal, 1988. **5**(4): p. 397-409.
30. Kussak, A. and A. Weintraub, *Quadrupole ion-trap mass spectrometry to locate fatty acids on lipid A from Gram-negative bacteria*. Analytical Biochemistry, 2002. **307**(1): p. 131-137.
31. Schilling, B., et al., *Characterization of Lipid A Acylation Patterns in Francisella tularensis, Francisella novicida, and Francisella philomiragia Using Multiple-Stage Mass Spectrometry and Matrix-Assisted Laser*

Desorption/Ionization on an Intermediate Vacuum Source Linear Ion Trap. Analytical Chemistry, 2007. **79**(3): p. 1034-1042.

32. Vakhrushev, S.Y., A. Zamfir, and J. Peter-Katalinic, *0,2An cross-ring cleavage as a general diagnostic tool for glycan assignment in glycoconjugate mixtures*. Journal of the American Society for Mass Spectrometry, 2004. **15**(12): p. 1863-1868.
33. Mechref, Y., P. Kang, and M.V. Novotny, *Differentiating structural isomers of sialylated glycans by matrix-assisted laser desorption/ionization time-of-flight/time-of-flight tandem mass spectrometry*. Rapid Communications in Mass Spectrometry, 2006. **20**(8): p. 1381-1389.
34. Zhao, C., et al., *Collisionally Activated Dissociation and Electron Capture Dissociation Provide Complementary Structural Information for Branched Permethylated Oligosaccharides*. Journal of the American Society for Mass Spectrometry, 2008. **19**(1): p. 138-150.
35. Tai, Y., et al., *Identification of C-21 steroidal glycosides from the roots of Cynanchum chekiangense by high-performance liquid chromatography/tandem mass spectrometry*. Analytica Chimica Acta, 2006. **572**(2): p. 230-236.
36. Sandra, K., et al., *The Q-Trap mass spectrometer, a novel tool in the study of protein glycosylation*. Journal of the American Society for Mass Spectrometry, 2004. **15**(3): p. 413-423.
37. Tissot, B., et al., *Towards GAG glycomics: Analysis of highly sulfated heparins by MALDI-TOF mass spectrometry*. Glycobiology, 2007. **17**(9): p. 972-982.
38. Stewart, J.J.P., *MOPAC2009*. 2009, Stewart Computational Chemistry: Colorado Springs, CO, USA.

39. Hemling, M.E., et al., *Fast atom bombardment mass spectrometry of glycosphingolipids. Glycosphingolipids containing neutral sugars.* Biochemistry, 1984. **23**(24): p. 5706-5713.

40. Ari, J.B., I. Navon, and A. Mandelbaum, *The effect of steric hindrance on the relative rates of anchimerically assisted alcohol eliminations from MH+ ions of 2-substituted 1,4-dialkoxybutanes upon CI and CID: Experiment and theory.* International Journal of Mass Spectrometry, 2006. **249-250**: p. 433-445.

41. Nunes, F.M., M.R. Domingues, and M.A. Coimbra, *Arabinosyl and glucosyl residues as structural features of acetylated galactomannans from green and roasted coffee infusions.* Carbohydrate Research, 2005. **340**(10): p. 1689-1698.

42. Simões, J., et al., *Structural features of partially acetylated coffee galactomannans presenting immunostimulatory activity.* Carbohydrate Polymers, 2010. **79**(2): p. 397-402.

43. Quéméner, B., et al., *Assignment of acetyl groups to O-2 and/or O-3 of pectic oligogalacturonides using negative electrospray ionization ion trap mass spectrometry.* Journal of Mass Spectrometry, 2003. **38**(6): p. 641-648.

44. Ralet, M.-C., et al., *Mapping sugar beet pectin acetylation pattern.* Phytochemistry, 2005. **66**(15): p. 1832-1843.

45. Stewart, J.J.P., *Optimization of parameters for semiempirical methods V: Modification of NDDO approximations and application to 70 elements.* Journal of Molecular Modeling, 2007. **13**(12): p. 1173-1213.

46. Guan, Z. and J.M. Liesch, *Solvation of acylium fragment ions in electrospray ionization quadrupole ion trap and Fourier transform ion*

cyclotron resonance mass spectrometry. Journal of Mass Spectrometry, 2001. **36**(3): p. 264-276.

47. Perera, B.A., et al., *Influence of a ring substituent on the tendency to form H_2O adducts to Ag^+ complexes with phenylalanine analogues in an ion trap mass spectrometer*. Journal of Mass Spectrometry, 2002. **37**(4): p. 401-413.
48. Somogyi, Á., S.P. Pasilis, and J.E. Pemberton, *Electrospray ionization of uranyl-citrate complexes: Adduct formation and ion-molecule reactions in 3D ion trap and ion cyclotron resonance trapping instruments*. International Journal of Mass Spectrometry, 2007. **265**(2-3): p. 281-294.
49. Groenewold, G.S., et al., *Secondary Ion Mass Spectrometry of Zeolite Materials: Observation of Abundant Aluminosilicate Oligomers Using an Ion Trap*. Analytical Chemistry, 2001. **73**(2): p. 226-232.
50. Scott, J.R., et al., *Experimental and Computational Study of Hydration Reactions of Aluminum Oxide Anion Clusters*. Journal of Physical Chemistry A, 2000. **104**(30): p. 7079-7090.
51. Wu, H.-F. and J.S. Brodbelt, *Gas-Phase Chelation Reactions of Monopositive Cations with Heteroaromatic Ligands*. Inorganic Chemistry, 1995. **34**(3): p. 615-621.
52. Seymour, J.L. and F. Turecek, *Distinction and quantitation of leucine-isoleucine isomers and lysine-glutamine isobars by electrospray ionization tandem mass spectrometry (MS^n, n = 2, 3) of copper(II)-diimine complexes*. Journal of Mass Spectrometry, 2000. **35**(4): p. 566-571.
53. Cancilla, M.T., et al., *Coordination of Alkali Metals to Oligosaccharides Dictates Fragmentation Behavior in Matrix Assisted Laser Desorption*

Ionization/Fourier Transform Mass Spectrometry. Journal of the American Chemical Society, 1996. **118**(28): p. 6736-6745.

54. Cancilla, M.T., et al., *Fragmentation Reactions in the Mass Spectrometry Analysis of Neutral Oligosaccharides*. Analytical Chemistry, 1999. **71**(15): p. 3206-3218.

55. Park, Y. and C.B. Lebrilla, *Application of Fourier transform ion cyclotron resonance mass spectrometry to oligosaccharides*. Mass Spectrometry Reviews, 2005. **24**(2): p. 232-264.

56. Li, D., et al., *Four butenolides are novel cytotoxic compounds isolated from the marine-derived bacterium, Streptoverticillium luteoverticillatum 11014*. Archives of Pharmacal Research, 2006. **29**(8): p. 624-626.

57. Oh, S., et al., *Synthesis and biological activity of (+)-hedychilactone A and its analogs from (+)-sclareolide*. Bioorganic & Medicinal Chemistry Letters, 2006. **16**(6): p. 1656-1659.

58. El-Subbagh, H.I., et al., *Synthesis and Biological Evaluation of Certain α,β-Unsaturated Ketones and Their Corresponding Fused Pyridines as Antiviral and Cytotoxic Agents*. Journal of Medicinal Chemistry, 2000. **43**(15): p. 2915-2921.

59. Cateni, F., et al., *Synthesis and biological properties of new α-methylene-γ-butyrolactones and α,β-unsaturated δ-lactones*. European Journal of Medicinal Chemistry, 2006. **41**(2): p. 192-200.

60. Ma, S., Z. Shi, and Z. Yu, *Synthesis of β-halobutenolides and their Pd(0)-catalyzed cross-coupling reactions with terminal alkynes and organozinc reagents. A general route to β-substituted butenolides and formal synthesis of cis-whisky lactone*. Tetrahedron, 1999. **55**(41): p. 12137-12148.

61. Rüngeler, P., et al., *Inhibition of transcription factor NF-kB by sesquiterpene lactones: a proposed molecular mechanism of action.* Bioorganic & Medicinal Chemistry, 1999. **7**(11): p. 2343-2352.

62. Favier, L.S., et al., *Anti-ulcerogenic activity of xanthanolide sesquiterpenes from Xanthium cavanillesii in rats.* Journal of Ethnopharmacology, 2005. **100**(3): p. 260-267.

63. Kebarle, P. and U.H. Verkerk, *Electrospray: From ions in solution to ions in the gas phase, what we know now.* Mass Spectrometry Reviews, 2009. **28**(6): p. 898-917.

64. Covey, T.R., B.A. Thomson, and B.B. Schneider, *Atmospheric pressure ion sources.* Mass Spectrometry Reviews, 2009. **28**(6): p. 870-897.

65. Cech, N.B. and C.G. Enke, *Practical implications of some recent studies in electrospray ionization fundamentals.* Mass Spectrometry Reviews, 2001. **20**(6): p. 362-387.

66. Madeira, P.J.A., et al., *Electrospray Ionization Mass Spectrometry analysis of newly synthesised α,β-unsaturated γ-lactones fused to sugars.* Rapid Communications in Mass Spectrometry, 2010. **24**: p. 1049-1058.

67. March, R.E. and C.J. Stadey, *A tandem mass spectrometric study of saccharides at high mass resolution.* Rapid Communications in Mass Spectrometry, 2005. **19**(6): p. 805-812.

68. Kowski, K., W. Lüttke, and P. Rademacher, *Evidence for intramolecular OH...π hydrogen bonding in unsaturated alcohols from UV photoelectron spectroscopy.* Journal of Molecular Structure, 2001. **567-568**: p. 231-240.

69. Solouki, T., et al., *Electrospray Ionization and Matrix-Assisted Laser Desorption/Ionization Fourier Transform Ion Cyclotron Resonance Mass Spectrometry of Permethylated Oligosaccharides.* Analytical Chemistry, 1998. **70**(5): p. 857-864.

70. McLuckey, S.A. and D.E. Goeringer, *Slow Heating Methods in Tandem Mass Spectrometry.* Journal of Mass Spectrometry, 1997. **32**(5): p. 461-474.

71. Douglas, E.G. and A.M. Scott, *Evolution of ion internal energy during collisional excitation in the Paul ion trap: A stochastic approach.* The Journal of Chemical Physics, 1996. **104**(6): p. 2214-2221.

72. Starke, I., et al., *Mass spectra of tetrahydroisoquinoline-fused 1,3,2-O,N,P- and 1,2,3-O,S,N-heterocycles: influence of ring size and fusion, of present heteroatoms, substituent effects and of the stereochemistry on fragmentation.* Rapid Communications in Mass Spectrometry, 2008. **22**(10): p. 1519-1527.

73. Lacey, D., et al., *Aspirin revealed: A cationization strategy for detecting acetylsalicylic acid by MALDI mass spectrometry.* International Journal of Mass Spectrometry, 2007. **261**(2-3): p. 192-198.

74. Ma, J.C. and D.A. Dougherty, *The Cation-π Interaction.* Chemical Reviews, 1997. **97**(5): p. 1303-1324.

Chapter 7
Conclusions and Future Work

7 General Conclusions and Future Work

7.1 General Conclusions

The results presented in this thesis cover a wide range of mass spectrometry application in the area of low molecular weight analytes with environmental and biological interest: from the classical establishment of fragmentation mechanisms to gas-phase thermochemistry, passing through the development of new MALDI matrices for the analysis of small molecules.

Using nanosized TiO_2 anatase phase, it was possible to ionise several compounds of different classes with high efficiency and with the absence of interfering matrix peaks. Interestingly, radical ions were found for some of the analytes and the preliminary results show that the electrochemical properties of the analytes, together with the surface properties of the photo-catalyst, might be responsible for this behaviour. A comparative study using two common organic matrices clearly showed that the inorganic matrix is more suitable for the analysis of small molecules. To note that quercetin mass spectra using 2,5-DHB showed a large number of interfering peaks that were subsequently identified as matrix-analyte clusters. This identification led us to expand the investigation to the study of flavonoid-2,5-DHB interaction. To this respect, we performed experiments to study the behaviour of the 2,5-DHB either alone or in the presence of analyte (flavonoids). We found evidences for the formation of multimeric species based on dehydrated

2,5-DHB moieties, as well as tetramers, pentamers, hexamers and heptamers which were reported, for the first time, in this study. All flavonoids were found to form cluster ions with the dehydrated 2,5-DHB moiety and for two of the flavonoids studied (luteolin and kaempferol) we found evidence for the formation of cluster ions with retro Diels-Alder fragments. Interestingly, the size of the cluster ions formed is strongly dependent on the flavonoid structure.

Regarding the investigation of aniline derivatives, all studies were performed with the purpose to distinguish isomers. All compounds studied showed little fragmentation and in most cases (haloanilines in particular) the fragmentation was not helpful in distinguishing the various isomers. The exceptions were 2-chloroaniline, 2-bromoaniline and the nitroaniline isomers. Competitive fragmentation of proton-bound dimers was used to distinguish the various isomers by pairing them with 4-nitroaniline and it was found that the branching ratio value can indeed be useful to distinguish isomers. Preliminary Electron Capture Dissociation (ECD) results were included in this thesis, mainly because signals corresponding to doubly- and triply-charged analytes were detected in the mass spectra. To access the origin of these multiply-charged species more experiments are still required.

Five isoflavones were studied and their fragmentation mechanisms were proposed taking into account MS^n experiments, accurate mass measurements and semi-empirical calculations. The semi-empirical calculations allowed proposing the C^4 keto group as the probable protonation site. Losses of $^{\bullet}CH_3$ and CH_3OH were only detected in compounds with the methoxy group attached to the B-ring. As such, the resulting species can be considered as diagnostic ions and

were useful in distinguishing two isomers included in this study (prunetin and biochanin A). The semi-empirical calculations were also useful in the establishment of fragmentation mechanism. For example, the retro Diels-Alder $^{1,3}A^+$ and $^{1,3}B^+$ ions were detected; nevertheless, the $^{0,4}B^+$ ions were not detected for any of the isoflavones under study. Semi-empirical calculations showed that energetic factors might be responsible for the absence of the $^{0,4}B^+$ ion in these isoflavones. A comparison of the fragmentation of isoflavones (genistein and biochanin A) with their flavone counterparts (apigenin and acacetin) clearly shows that the position of the B-ring greatly influences fragmentation.

Several newly synthesized lactones, either fused or C-C linked to sugars, were studied in this thesis. The fused lactones were studied in the negative and positive ion mode. In the negative ion mode, it was found that the main fragmentation pathways involve cross-ring cleavages, whereas in the positive ion mode, particularly for the protonated molecules, the main fragmentation pathways are those involving the substituents. The sodiated molecules showed little fragmentation. The fragmentation pattern alone allowed the distinction of two isomers included in this study.

Regarding the study of C-C linked lactones, cross-ring cleavages from the protonated molecule were only detected for two of the compounds studied. The lack of cross-ring cleavages in the fragmentation of the protonated molecules, for some of the compounds, was attributed to the absence of the conjugated α, β unsaturated system of the lactone for these compounds. The delocalization of this system might help the scission of the C^4-O bond.

Hence, the lactone moiety has indeed a substantial influence on the fragmentation of the sugar ring. Influence of the stereochemistry on the fragmentation pattern was also observed for these compounds. The sodiated forms of all compounds showed very little fragmentation, the main decomposition pathway being the loss of C_3H_6O and water for one of the compounds. Semi-empirical calculations again proved to be helpful for the proposal of fragmentation pathways and also in the assignment of the probable protonation and alkali metal coordination sites.

7.2 Future Work

In order to improve and develop the work here presented, some suggestions can be made:

- Regarding the MALDI analysis of small molecules using TiO_2 anatase phase as matrix, the study of the influence of the electrochemical properties on the formation of radical ions can be extended to other analytes;
- Regarding the analysis of aniline derivatives, particularly their behaviour under ECD conditions, further experiments are needed such as varying the irradiation time as well as using higher electron energies;
- Regarding the study of newly synthesized lactones, it is planned to extend the study to thiosugars and determine the influence of the sulphur on the fragmentation.

Appendix

A. Mass spectra of substituted anilines (Chapter 4)

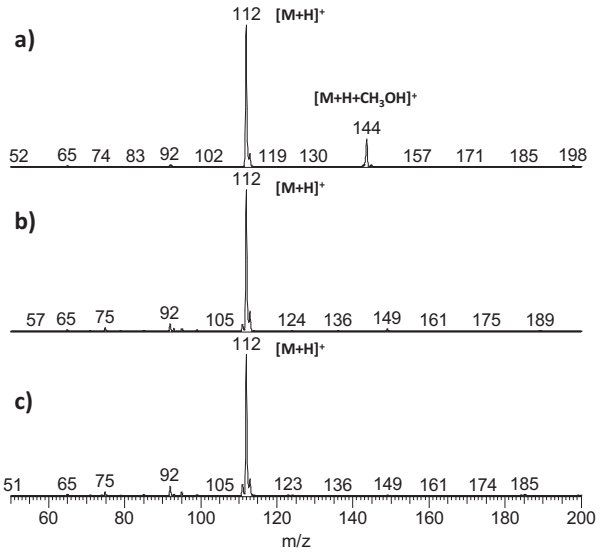

Figure A.1. ESI mass spectra of: a) 2-fluoroaniline; b) 3-fluoroaniline; c) 4-fluoroaniline.

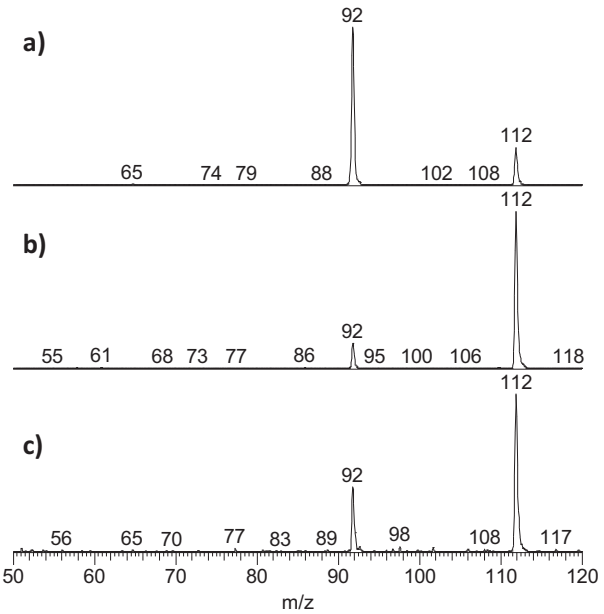

Figure A.2. ESI-MS^2 spectra **at** CEL=30% of the protonated molecules of: a) 2-fluoroaniline; b) 3-fluoroaniline; c) 4-fluoroaniline.

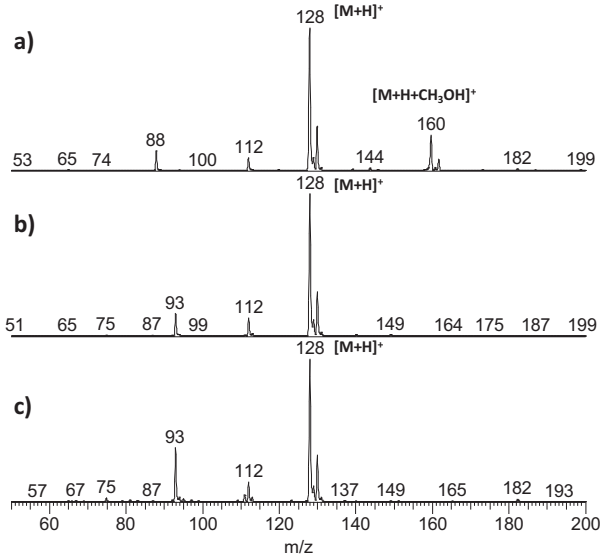

Figure A.3. ESI mass spectra of: a) 2-chloroaniline; b) 3-chloroaniline; c) 4-chloroaniline.

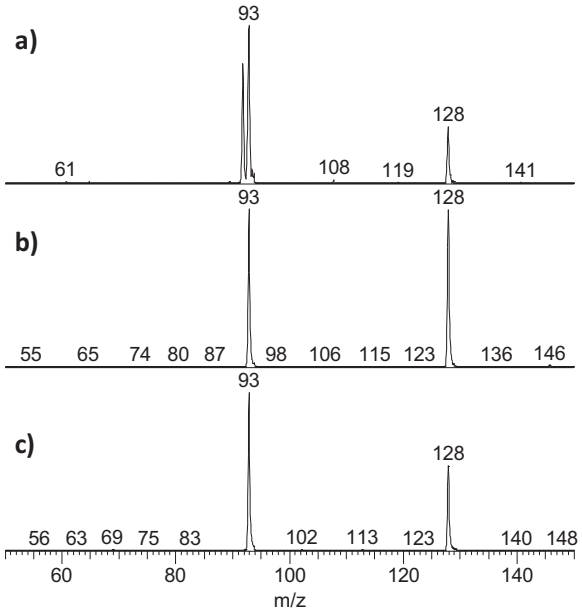

Figure A.4. ESI-MS^2 spectra at CEL=30% of the protonated molecules of: a) 2-chloroaniline; b) 3-chloroaniline; c) 4-chloroaniline.

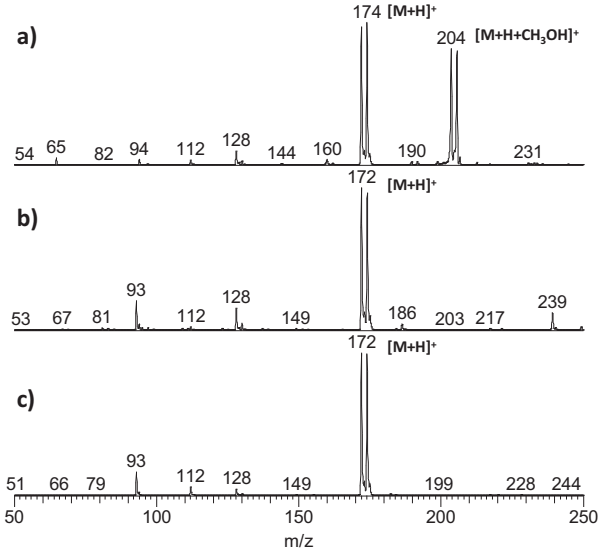

Figure A.5. ESI mass spectra of: a) 2-bromoaniline; b) 3-bromoaniline; c) 4-bromoaniline.

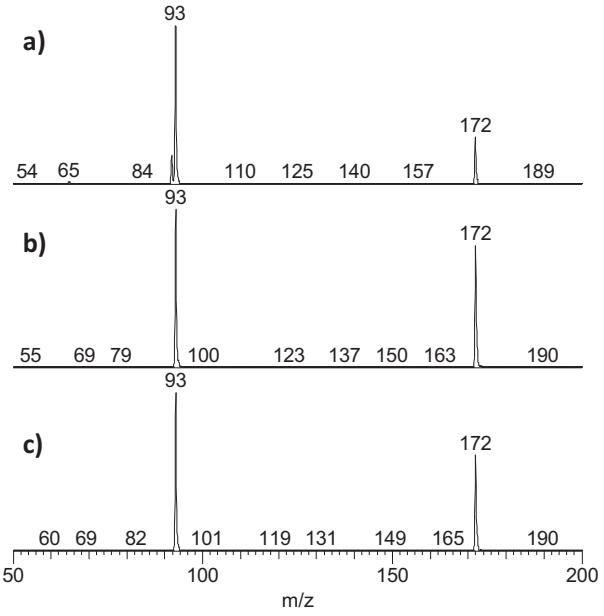

Figure A.6. ESI-MS^2 spectra at CEL=30% of the protonated molecules of: a) 2-bromoaniline; b) 3-bromoaniline; c) 4-bromoaniline.

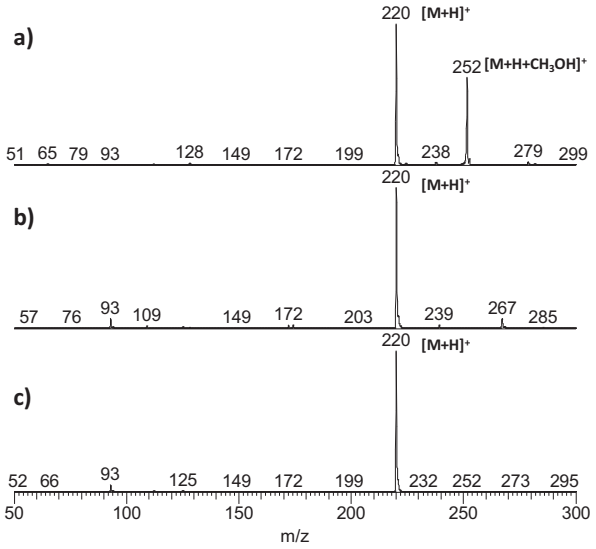

Figure A.7. ESI mass spectra of: a) 2-iodoaniline; b) 3-iodoaniline; c) 4-iodoaniline.

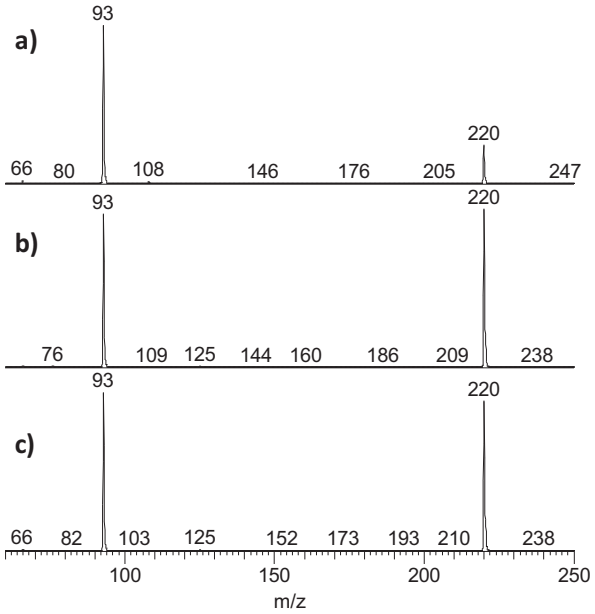

Figure A.8. ESI-MS^2 spectra at CEL=30% of the protonated molecules of: a) 2-iodoaniline; b) 3-iodoaniline; c) 4-iodoaniline.

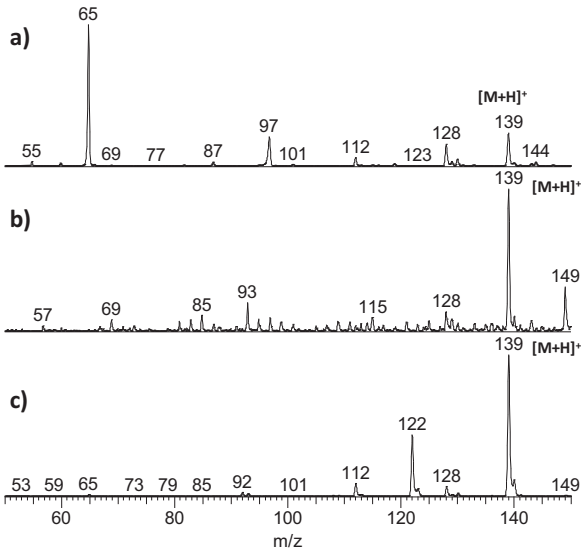

Figure A.9. ESI mass spectra of: a) 2-nitroaniline; b) 3-nitroaniline; c) 4-nitroaniline.